CRANFIELD UNIVERSITY

AMINU MUSA CHINDO

Towards a CubeSat relevant mission payload for demonstrating aspects of In-Situ Resource Utilisation (ISRU) on a C-type Near-Earth Asteroid (NEA)

School of Aerospace, Transport & Manufacturing (SATM)

PhD in Aerospace

Report Submitted for the award of PhD. Degree

Academic Year: 2016 - 2021

Supervisors: Prof David C. Cullen and Dr Joan Pau Sanchez Cuartielles

January 2022

CRANFIELD UNIVERSITY

School of Aerospace, Transport, and Manufacturing (SATM)
PhD in Aerospace

Report Submitted for the award of PhD degree

Academic Year 2016 - 2021

Aminu Musa Chindo

Towards a CubeSat relevant mission payload for demonstrating aspects of In-Situ Resource Utilisation (ISRU) on a C-type Near-Earth Asteroid (NEA)

Supervisors: Prof David C. Cullen and Dr Joan Pau Sanchez Cuartilles
January 2022

© Cranfield University 2022. All rights reserved. No part of this publication may be reproduced without the written permission of the copyright owner.

ABSTRACT

Nearly 50 years ago, humankind long dreamed of colonizing or exploiting the neighbouring planets Mars, the Moon, comets, and asteroids in our Solar System for technological and profit-oriented purposes. The concept of *In-Situ* Resource Utilisation (ISRU) is likely to be a means to achieving those dreams. High cost and the possibilities of failure associated with the development of full-size ISRU spacecraft, early use of CubeSat payloads for ISRU technology demonstration would serve as a technology readiness level (TRL) driver and a de-risking technology. Mars Oxygen In-Situ Resource Utilization Experiment (MOXIE) is the only small size ISRU demonstration payload currently flown and on Mars to demonstrate oxygen extraction from the Martian atmosphere. The regolith/soils present in smaller bodies are identified to be rich in minerals resources such as precious metals, volatiles, organic and non-organic materials that can be harnessed for the good of humankind. This PhD research work aimed to advance an initial CubeSat-like payload design to demonstrate an *ISRU* process on a C – type near-earth asteroid (NEA).

The result of the literature review performed was, the project background was elaborated. From the trade-off studies carried out for the selection process of the potential destinations and the ISRU process, C-type NEA 162173 Ryugu JU3, and hydrometallurgical sulphuric acid leaching experiment on olivine minerals have emerged as the winners. System requirements are generated, and for the proposed CubeSat payload system architecture comprising of sample acquisition subsystem, reaction chamber subsystems, acid solution delivery and extraction subsystem, the electroplating/wining subsystem, and analytical subsystem, an initial overall payload system design was achieved. This project has been focused on the re-design and manufacturing of the reaction chamber subsystems and top-plate system, and the design and manufacture of the leaching and the liquid handling sub-system (LHS). The result of laboratory hydrometallurgical sulphuric acid leaching experiments carried out found the optimal condition to achieve higher metal extraction from the reaction mixture occurs at 5M H_2SO_4 acid concentration, 1:5 mineral to acid volume ratio (1g/5ml), and in a state of

agitation. The inclusion of bromophenol blue (BPB) dye in the leaching experiment to eliminate the initial use of litmus paper, detect the loss of acid concentration by providing a real-time visual colour transition from yellow to blue, within the required acid pH range and would expect to be compatible with future flight implementation. Using the 5M H_2SO_4 acid concentration, the BPB dye solution was observed to degrade and change to colourless. Sourcing an alternative dye that is stable in 5M H_2SO_4 acid to mitigate against this looming challenge was suggested for future work. The payload system design together with the optimal leaching condition generated, informed the Breadboard (BB) payload prototype system design, component selection, and manufacture. A version of the Reaction Chamber Subsystem (RCS) oven implemented in a co-running CubeSat relevant payload design (ISRU water extraction), and based on the initial size and volume, appears to be suitable for this project. The RCS is manufactured from a material that is sulphuric acid-resistant and was re-designed to allow for interfacing to the LHS. The top plate implemented on CubeSat based ISRU water extraction project was adapted, re-designed, and manufactured from a material that is sulphuric acid-resistant to enable the accommodation of the LHS and the associated system that will ensure efficient interaction between acid solution and the collected olivine regolith. The LHS subsystem is comprised of valves, pumps, manifolds, reservoirs, tubing connectors, and fittings. These components are interconnected, and they interact to establish the LHS that will allow for efficient liquid handling in microgravity. The LHS is operated to deliver H_2SO_4 acid solution from the reservoir into the RCS and the extraction of the leachate from the RCS respectively.

In the conclusion, the manufactured BB payload system was operated to simulate hydrometallurgical leaching and aspects of liquid handling processes. The result indicates the usefulness of the process and its feasibility for CubeSat implementation. Additional tests need to be performed to further validate the BB payload system's usefulness. Also, various future works are presented that will increase the technology readiness level of the design concept to further validate the usefulness of the ISRU BB payload system.

Keywords:

CubeSat, ISRU, Hydrometallurgy, NEA, Ryugu, Leaching, Extraction

ACKNOWLEDGEMENTS

All Praise is due to Allah (SWT) who has made it possible for me to come this far during this study. My sincere appreciation goes to Prof David Cullen for his patience and guidance during my Ph.D. sojourn at Cranfield University; not left out are the members of the Cranfield Space Research Group, I say a big thank you for the memorable time we have shared.

I would like to especially thank Mr. Elioenai Sitepu a co-researcher and fellow Ph.D. student within the Cranfield Space Research Group. We have a point of overlap in our individual research work, and I acknowledge the use of some of his design work components comprising the Reaction Chamber Sub-system (RCS) and the top-plate sub-system as the initial basis for re-designing these components to suit my design implementation.

To my sponsors the Nigerian Petroleum Technology Development Fund (PTDF), I wish to say a big thank you to the fund for sponsoring me to pursue a Ph.D. in Aerospace with a bias in the concept of In Situ Resource Utilisation *(ISRU*). I remain indebted to the fund for this kind and rare opportunity.

To my employer the National Space Research Development Agency (NASRDA) of Nigeria; I wish to express my sincere gratitude for allowing me to further my Ph.D. study in Aerospace.

To my beloved parents, wife, children, and other family members too numerous to mention here, I say a big thank you for your support, patience, and prayer. My sincere appreciation also goes to my friends.

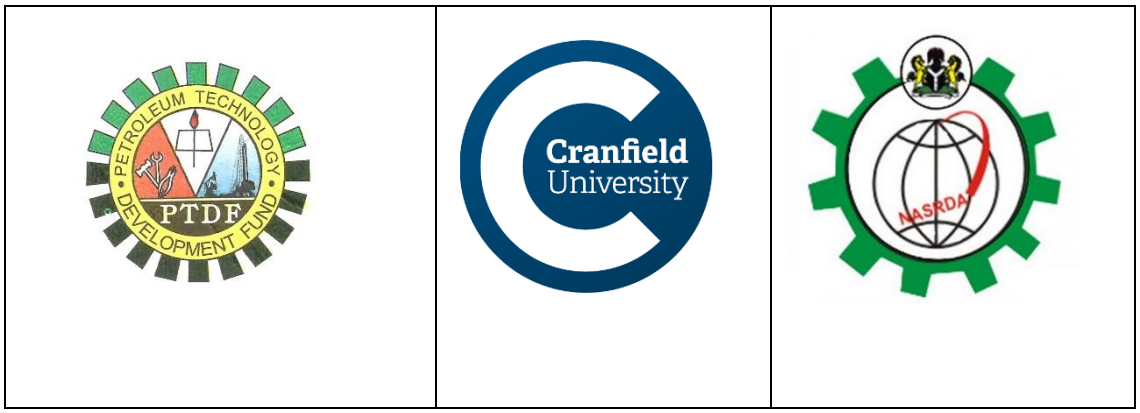


TABLE OF CONTENTS

ABSTRACT i
LIST OF FIGURES xiv
LIST OF TABLES xviii
LIST OF EQUATIONS xxi
LIST OF ABBREVIATIONS xxii
1 INTRODUCTION 1
1.1 RESEARCH BACKGROUND 1
1.2 RESEARCH GAP AND RESEARCH QUESTIONS 2
1.3 RESEARCH CONTRIBUTION TO KNOWLEDGE 6
1.4 RESEARCH AIM AND OBJECTIVES 7
1.4.1 AIM OF THE PROJECT: 7
1.4.2 THE PROJECT OBJECTIVES 7
1.5 RESEARCH METHODOLOGY 8
1.6 THESIS ORGANISATION 11
2 LITERATURE SURVEY AND PROJECT BACKGROUND 13
2.1 INTRODUCTION 13
2.2 LITERATURE RESOURCES 13
2.2.1 SCOPUS 13
2.2.2 NASA TECHNICAL REPORTS SERVER (NTRS) 14
2.2.3 PRIVATE INDUSTRIES 14
2.2.4 USING THE COMPILED SOURCES OF LITERATURE IN THE CONTEXT OF THIS RESEARCH 16
2.3 RESULT AND ANALYSIS OF PROJECT COMPONENTS 17
2.3.1 OVERVIEW OF THE SOLAR SYSTEM IN OFASTEROID STUDIES 17
2.3.2 GENERAL REVIEW OF THE POTENTIAL LOCATIONS FOR DEMOSTRATION OF ISRU PROCESS 18
2.3.3 ASTEROID FORMATION 19
2.3.4 OVERVIEW OF AN ASTEROID 20
2.3.5 ASTEROID TAXONOMY 23
2.4 ASTEROID MINERAL COMPOSITION 25
2.4.1 THE METEORITE 26
2.4.2 MINERAL COMPOSITION OF THE METEORITES 26
2.5 ANALYSIS OF THE METEORITE MINERAL COMPOSITION 28
2.5.1 SPECTROSCOPY 28
2.5.2 LABORATORY ANALYSIS OF METEORITES 31
2.5.3 GROUND BASED DEEP SPACE NETWORK (DSN) REMOTE SENSING 33
2.5.4 NEW SAMPLE RETURN MISSIONS TO C-TYPE NEA 35
2.6 RESULT OF ASTEROID/METEORITE ANALYSIS 37

2.6.1 CI CARBONACEOUS CHONDRITE METEORITE 37
2.6.2 CM CARBONACEOUS CHODRITE METEORITE.....37
2.6.3 OVERVIEW OF ISRU TECHNOLGY.....38
2.7 OVERVIEW OF CUBESAT TECHNOLOGY.....43
2.7.1 CUBESAT RELEVANT TO INTERPLANETARY MISSIONS 46
2.7.2 RESULT OF THE LITERATURE REVIEW BASED ON CUBESAT TECHNOLOGY.....47
2.7.3 OVERALL SUMMARY OF THE LITERATURE REVIEW.....47
2.9 CONCLUSION.....49
3 C-type NEA DOWN SELECTION PROCESS 51
3.1 INTRODUCTION 51
3.2 REASON FOR SELECTING THE C-TYPE NEA FAMILY AS POTENTIAL DESTINATION FOR DEMOSTRATION OF THE ISRU PROCESS 51
3.3 REQUIREMENT FOR SELECTING POTENTIAL C-TYPE NEA 52
3.3.1 C-TYPE-NEA_R1 (ASTEROID SIZE IN TERMS OF DIAMETER)....52
3.3.2 C-TYPE-NEA_R2 (PROJECTED PROFIT DUE TO MINERAL ABUNDANCE) 52
3.3.3 C-TYPE-NEA_R3 (C-TYPE NEA NEXT CLOSE APPROACH).....52
3.3.4 C-TYPE-NEA_R4 (SEMI MAJOR AXIS (SMA)).....53
3.4 OBSERVATIONAL DATABASES AS INFORMATION SOURCE FOR C-TYPE NEA SELECTION.....53
3.5 FILTERING PROCESS TO REDUCE THE POTENTIAL C-TYPE NEA..57
3.6 TRADE-OFF STUDY TO SELECT THE C-TYPE NEA AS A PRIMARY TARGET 59
3.6.1 WEIGHTING AND SCALING OF PARAMETER.....59
3.6.2 SCORING OF THE RAW RESULT AND THE TRADE-OFF STUDIES RESULT INCLUDING THE WEIGTHING.....61
SENSITIVITY ANALYSIS 63
3.7.....63
3.7.1 MAKING THE WEIGHTING VALUE ORDER USED IN THE TRADE-OFF STUDIES UNIFORM 64
3.7.2 A SMALL INCREASE TO THE SCORES LESS THAN 10% OF THE ORIGINAL SCORED VALUES FOR EACH OF THE POTENTIAL C-TYPE NEA EXCLUDING THE HIGHEST AND THE LOWEST SCORE 64
3.7.3 A SMALL INCREASE TO THE SCORES LESS THAN 10% OF THE ORIGINAL SCORED VALUES FOR EACH OF THE POTENTIAL C-TYPE NEA AND A SMALL DECREASE OF LESS THAN 10% OF THE WINING C-TYPE NEA EXCLUDING THE HIGHEST AND LOWEST SCORE 66
3.8 DISCUSSION 67

3.9 CONCLUSION 68
4 ISRU SELECTION PROCESS FOR IMPLEMENTION IN THE CONTEXT OF CUBESAT TECHNOLOGY 69
4.1 INTRODUCTION 69
4.2 THERMAL REDUCTION PROCESSES 70
4.2.1 CARBOTHERMAL REDUCTION PROCESS WITH METHANE 71
4.2.2 THERMAL REDUCTION WITH HYDROGEN (H_2) 74
4.2.3 CARBOTHERMAL REDUCTION WITH CARBON MONOXIDE (CO) 75
4.2.4 VAPOUR PHASE PYROLYSIS 77
4.2.5 SULPHURIC ACID TREATMENT OF METALLIC OXIDE 79
4.2.6 MOLTEN OXIDE ELECTROLYSIS/MAGMA ELECTROLYSIS 81
4.3 INCLUSION OF THE 7th ADDITIONAL PROCESS 82
4.4 IDENTIFICATION AND DESCRIPTION OF PARAMETER FOR TRADE-OFF STUDY TO DOWN SELECT POTENTIAL ISRU PROCESS 83
4.4.1 BENEFICIATION STAGE 83
4.4.2 CORE PROCESSING STAGE 83
4.4.3 MATERIAL HANDLING AND STORING STAGE 84
4.4.4 PROCESS POWER REQUIRMENT 84
4.4.5 PROCESS TEMPERATURE REQUIREMENT 84
4.4.6 PROCESS TECHNOLOGY READINESS LEVEL (TRL) 84
4.4.7 PROCESS SOURCE OF REACTANT/CONSUMABLE 85
4.4.8 PROCESS CONTROL MECHANISM 85
4.4.9 PROCESS MONITORING MECHANISM 85
4.4.10 PROCESS SUITABILITY WITH ANOTHER FEEDSTOCK 85
4.4.11 DEFINATION OF THE SEVEN POTENTIAL ISRU PROCESSES UNDER CONSIDERATION 86
4.5 TRADE-OFF STUDY TECHNIQUES SELECTIONS 86
4.5.1 APPLYING MULTI-CRITERIA DECISION ANALYSIS (MCDA) MODEL IN THE ISRU PROCESS SELECTION 87
4.6 SENSITIVITY ANALYSIS 97
4.6.1 SENSITIVITY METHODS 97
4.6.2 SMALL INCREASE TO THE SCORES LESS THAN 10% OF THE ORIGINAL SCORED VALUES FOR EACH CRITERION UNDER THE PROCESSES P1 – P7 EXCLUDING HIGHEST AND LOWEST SCORE (1 AND 0) 98
4.7 CONCLUSION 100
5 OVERALL PAYLOAD SYSTEMS LEVEL DESIGN 102
5.1 INTRODUCTION 102
PAYLOAD SYSTEM TOP LEVEL REQUIREMENT CAPTURE AND CLASSIFICATION 103
5.2 103

5.2.1 TOP LEVEL PAYLOAD SYSTEM REQUIREMENT CAPTURE AND CLASSIFICATION....104
5.3 THECONCEPT OF CUBESAT COMPATICLE PAYLOADS FOR EARLY ISRU DEMOSTRATION WITHIN THE CRANFIELD SPACE GROUP....129
5.3.1 EXTRACTION AND DIOXYGEN AND DIHYDROGEN PRODUCTION FROM WATER-ICE CONTAINING REGOLITH....129
5.4 LEAD TO THE OVERALL PAYLOAD SYSTEM DESIGN....130
5.4.1 OVERVIEW OF THE PAYLOAD SUBSYSTEM....131
5.5 OPERATION CONCEPT FOR THE PAYLOAD SYSTEM DESIGN....135
5.6 CONCLUSION....136
6 LABORATORY HYDROMETALLURGICAL SULPHURIC ACID LEACHING OF OLIVINE MINERAL AS THE SIMULANT FOR THE C-TYPE NEAR EARTH ASTEROID (NEA) RYUGU....138
6.1 INTRODUCTION....138
6.2 AIMS OF THE EXPERIMENTS....141
6.3 OBJECTIVES OF THE EXPERIMENT....141
6.4 MATERIAL, RE-AGENTS AND THE EQUIPMENT....142
6.4.1 OLIVINE MINERAL....142
6.4.2 SULPHURIC ACID....143
6.4.3 EQUIPMENT USED....143
6.5 DESIGN OF HYDROMETALLURGICAL SULPHURIC ACID LEACHING EXPERIMENT OF OLIVINE REGOLITH SIMULANT USING TRIAL EXPERIMENT....144
6.5.1 TRIAL HYDROMETALLURGICAL SULPHURIC ACID LEACHING EXPERIMENT OF OLIVINE REGOLITH SIMULANT....144
6.5.2 FURTHER TRIAL HYDROMETALLURGY SULPHURIC ACID LEACHINGEXPERIMENTUSING 0.090 – 0.259MM GRAIN PARTICLES SIZE....145
6.6 DESIGN METHOD FOR THE LABORATORY HYDROMETALLURGAL SULPHURIC ACID INITIAL LEACHING EXPERIMENT ON OLIVINE MINERAL SIMULANT....147
6.6.1 INTRODUCTION....147
6.6.2 DESCRIPTION OF THE EXPERIMENT PROCEDURE....147
6.6.3 IMPLEMENTATION OF THE INITIAL LABORATORY HYDROMETALLURGICAL SULPHURIC ACID LEACHING EXPERIMENT ON THE OLIVINE MINERAL SIMULANT....149
6.6.4 IMPLEMENTATION OF THE REPEAT LABORATORY HYDROMETALLURGICAL SULPHURIC ACID LEACHING EXPERIMENT OF OLIVINE MINERAL SIMULANT....159

6.7 SULPHURIC ACID LEACHING EXPERIMENT OF OLIVINE MINERAL AND USING BPB PH DYE INDICATOR TO MONITOR PH CHANGE AS THE ACID CONCENTRATION REDUCES 168
6.7.1 INTRODUCTION 168
6.7.2 AIMS OF THE EXPERIMENT 168
6.7.3 OBJECTIVES OF THE EXPERIMENT 168
6.7.4 DESCRIPTION OF THE EXPERIMENT PROCEDURE 168
6.7.5 PH DYE INDICATOR SELECTION PROCESS 169
6.7.6 PREPARATION OF THE BPB DYE INDICATOR SOLUTION 171
6.7.7 INITIAL TESTING OF THE BPB PH DYE SOLUTION 171
6.7.8 IMPLEMENTATION OF THE LABORATORY HYDROMETALLURGICAL SULPHURIC ACID LEACHING EXPERIMENT ON THE OLIVINE MINERAL SIMULANT AND USING 8.8mM CONCENTRATION BPB pH DYE INDICATOR TO MONITOR COLOUR CHANGE AS THE ACID CONCENTRATION REDUCES 173
6.8 EXPERIMENT TO INVESTIGATE THE EFFECT OF 1M AND 5M SULPHURIC ACID CONCENTRATION AND DISTILLED WATER ONLY ON 8.8mM BPB DYE INDICATOR 176
6.8.1 INTRODUCTION 176
6.8.2 PROCEDURE TO INVESTIGE THE EFFECT OF DIFFERENT CONCENTRATIONS OF SULPHURIC ACID (1M&5M) AND DISTILLED WATER ONLY ON THE BPB DYE INDICATOR 176
6.8.3 RESULT AND DISCUSSION FOR THE EXPERIMENT USING BPB DYE INDICATOR WITH ONLY SULPHURIC ACID (1M&5M) AND DISTILLED WATER ONLY 178
6.9 LEACHING INERT SAND (SILICATE MINERAL) USING SULPHURIC ACID (1M AND 5M) AND DISTILLED WATER TOGETHER WITH 8.8mM BPB DYE INDICATOR TO MONITOR THE COLOUR CHANGE 178
6.9.1 INTRODUCTION 178
6.9.2 PROCEDURE FOR THE EXPERIMENT TO INVESTIGATE THE EFFECT OF DIFFERENT CONCENTRATIONS OF SULPHURIC ACID (1M&5M) AND DISTILLED WATER ONLY ON THE BPB DYE INDICATOR USING INERT SAND AND SILICATE MINERAL IN PLACE OF OLIVINE MINERAL 179
6.9.3 RESULT AND DISCUSSION FOR THE LEACHING EXPERIMENT USING 1M&5M SULPHURIC ACID, DISTILLED WATER AND INERT SAND AND SILICATE MINERAL AND 8.8mM OF THE BPB DYE INDICATOR SOLUTION TO MONITOR THE COLOUR TRANSISTION 179
6.9.4 CONCLUSION IN RESPECT OF LEACHING EXPERIMENT USING 1M&5M SULPHURIC ACID, DISTILLED WATER AND INERT

SAND AND SILICATE MINERAL AND 8.8mM OF THE BPB DYE INDICATOR SOLUTION TO MONITOR THE COLOUR TRANSITION ... 180
6.9.5 DISCUSSION IN RESPECT OF THE INITIAL AND REPEAT EXPERIMENT AND THOSE USING BPB DYE SOLUTION. ... 180
6.10 CONCLUSION ... 181
7 BREADBOARD (BB) PAYLOAD PROTOTYPE DESIGN AND COMPONENTS SELECTION, ASSEMBLY, TESTING AND OPERATIONS ... 182
7.1 INTRODUCTION ... 182
7.2 BREADBOARD (BB) PROTOTYPE PAYLOAD DESIGN PROCESS ... 182
7.3 AIMS OF THIS CHAPTER ... 183
7.4 OBJECTIVES OF THIS CHAPTER ... 183
7.5 OVERVIEW OF THE BREADBOARD (BB) PROTOTYPE PAYLOAD SYSTEM ... 184
7.6 BB PAYLOAD PROTOTYPE SYSTEM DESIGN AND COMPONENTS SELECTION ... 186
7.6.1 REACTION CHAMBER SUB-SYSTEM (RCS) DESIGN AND MATERIAL SELECTION ... 186
7.6.2 TOP PLATE MODIFICATION AND MATERIAL SELECTION ... 188
7.6.3 PLUNGER SYSTEM DESIGN AND MATERIAL SELECTION ... 189
7.6.4 MOTORISED LEAD SCREW LINEAR ACTUATOR SYSTEM DESIGN AND MATERIAL SELECTION ... 191
7.6.5 DESIGN OF SEALING MECHANISM AND MATERIAL SELECTION ... 199
7.6.6 ACID RESERVOIR DESIGN AND MATERIAL SELECTION cid reservoir design and material selection ... 202
7.6.7 MANIFOLD SELECTION ... 203
7.6.8 SOLENOID VALVE (SV) SELECTION ... 204
7.6.9 PUMP SELECTION ... 206
7.6.10 TUBING AND FITTING MATERIAL SELECTION ... 207
7.7 ELECTRICAL/ELECTRONIC SUPPORT SYSTEM IN THE BREADBOARD (BB) PROTOTYPE PAYLAOD SYSTEM DESIGN ... 208
7.8 OVERVIEW OF THE DRIVE CIRCUIT FOR THE CONTROL OF THE SV AND THE STEPPER MOTOR CONTROL FOR THE ACTUATION OF THE PLUNGER ... 209
7.8.1 THE DRIVE CIRCUIT FOR THE CONTROL OF THE SV ... 209
7.8.2 TRANSISTOR SWITCHING CIRCUIT DESIGN AND COMPONENTS SELECTION ... 210
7.8.3 SIMPLE TRANSISTOR CIRCUIT CONCEPT OF OPERATION ... 213
7.8.4 GROUND TESTING OF THE SV SWITCHING CONTROL USING THE IRF640N TRANSISTOR SWITCHING CIRCUIT ... 215
7.8.5 STEPPER MOTOR CONTROL FOR THE LINEAR ACTUATION OF THE PLUNGER IN/OUT OF THE RCS ... 217

7.8.6 CODE WRITING, CODE UPLOADING, AND THE SYSTEM TESTING 221
7.8.7 STEPPER MOTOR STEPPING USING ARDUINO IDE TO CONTROL THE PLUNGER LINEAR TRANSLATION TO A PRE-DETERMINE HEIGHT/DEPTH AND CORRESPONDING TO DISPLACED VOLUME 223
7.8.8 MICRO-STEPPING THE BIPOLAR STEPPER MOTOR 224
7.8.9 GROUND DEMOSTRATION OF THE STEPPER MOTOR MOTION IN FORWARD AND REVERSE DIRECTION 224
7.9 OVERALL BB PROTOTYPE SYSTEM ASSEMBLY, TESTING AND DEMOSTRATION OF OPERATION 225
7.9.1 BB PROTOTYPE SYSTEM ASSEMBLY 226
7.10 CONCLUSION 228
8 USING THE DESIGNED AND MANUFACTURED BREADBOARD PAYLOAD PROTOTYPE TO SIMULATE DEMOSTRATION OF THE HYDROMETALLURGY SULPHURIC ACID LEACHING OF THE OLIVINE MINERAL AND ASPECT OF LIQUID HANDLING 230
8.1 INTRODUCTION 230
8.2 AIMS OF THE EXPERIMENT 232
8.3 OBJECTIVES OF THE EXPERIMENT 232
8.4 MATERIAL, RE-AGENT AND EQUIPMENT USED 233
8.4.1 OLIVINE MINERAL 233
8.4.2 DISTILLED WATER 233
8.4.3 EQUIPMENT USED 234
8.5 EXPERIMENT DESIGN METHODOLOGY TO SIMULATE THE DEMOSTRATION OF THE EXTRACTION OF THE BPB SOLUTION FROM THE BPB DYED OLIVINE MINERAL DISSOLVED IN WATER 234
8.5.1 PREPARATORY STEPS FOR CREATING THE BPB DYED OLIVINE REGOLITH 236
8.6 EXTRACTION EXPERIMENT PROCESS OF THE BPB SOLUTION USING THE BB PAYLOAD PROTOTYPE WITH NO AGITATION 237
8.6.1 MEASURING THE MAXIMUM ABSORBANCE FOR THE EXTRACTED BPB SOLUTION USING THE BB PAYLOAD PROTOTYPE 239
8.6.2 COMPUTING THE CONCENTRATION OF THE BPB USING THE BEER'S LAMBERT EQUATION 240
8.6.3 EXPERIMENT1 RESULT USING BB PAYLOAD PROTOTYPE FOR THE BPB SOLUTION EXTRACTION IN A STATIONARY/NON-AGITATED STATE 243
8.7 EXTRACTION EXPERIMENT PROCESS OF THE BPB SOLUTION USING 15ML PLASTIC CENTRIFUGE TUBE WITH NO AGITATION 245

8.7.1 MEASURING THE MAXIMUM ABSORBANCE FOR THE EXTRACTED BPB SOLUTION USING THE 15MLS PLASTIC CENTRIFUGE TUBE WITH NO AGITATIONBB PAYLOAD PROTOTYPE....246
8.7.2 COMPUTING THE CONCENTRATION OF THE BPB USING THE BEER'S LAMBERT EQUATION....247
8.7.3 EXPERIMENT2 RESULT USING THE 15MLS CENTRIFUGE TUBES FOR THE BPB SOLUTION EXTRACTION IN A NON-AGITATED STATE....250
8.8 EXTRACTION EXPERIMENT PROCESS OF THE BPB SOLUTION USING 15ML PLASTIC CENTRIFUGE WITH AGITATION USING THE VERTICAL ROTARY MIXER....252
8.8.1 MEASURING THE MAXIMUM ABSORBANCE FOR THE EXTRACTED BPB SOLUTION USING THE 15MLS PLASTIC CENTRIFUGE TUBE WITH WITH AGITATION USING THE VERTCAL ROTARY MIXER....253
8.8.2 COMPUTING THE CONCENTRATION OF THE BPB USING THE BEER'S LAMBERT EQUATION....254
8.8.3 EXPERIMENT3 RESULT USING THE 15MLS CENTRIFUGE TUBES FOR THE BPB SOLUTION EXTRACTION IN AN AGITATED STATE USING THE VERTCAL ROTARY MIXER....256
8.9 COMPARISON OF THE EXPERIMENTS RESULT....258
8.9.1 COMPARING THE RESULT OF EXPERIMENT1 USING THE BB PAYLOAD PROTOTYPE IN NON-AGITATED STATE TO THOSE OF EXPERIMENT2 USING 15MLS CENTRIFUGE TUBE IN NON-AGITATED STATE....258
8.9.2 COMPARING THE RESULT OF EXPERIMENT1 USING THE BB PAYLOAD PROTOTYPE IN NON-AGITATED STATE TO THOSE OF EXPERIMENT2 USING 15MLS CENTRIFUGE TUBE IN NON-AGITATED STATE....259
8.9.3 COMPARING THE RESULT OF EXPERIMENT2 USING THE 15MLS CENTRIFUGE TUBE IN NON-AGITATED STATE TO THOSE OF EXPERIMENT3 USING 15MLS CENTRIFUGE TUBE IN AGITATED STATE....259
8.10 DISCUSSION OF THE BPB SOLUTION EXTRACTION EXPERIMENTS RESULT BASED ON THE THREE (3) DIFFERENT EXPERIMENT CARRIED OUT....262
8.11 CONCLUSION....264
9 SUMMARY AND DISCUSSION, CONCLUSIONS, AND FUTURE WORK..267
9.1 IINTRODUCTION....267
9.2 SUMMARY AND DISCUSSION....267
9.3 FINAL CONCLUSION....279

9.4 FUTURE WORKS 280
9.4.1 IMMEDIATE TERM FUTURE WORK 280
9.4.2 MEDIUM TERM FUTURE WORK 283
9.4.3 LONG TERM FUTURE WORK (TOWARD PAYLOAD FLIGHT IMPLEMENTATION) 284
REFERENCES 285
Appendix 1. Representation of Photographic evidence of the sulphuric acid leaching experiment 296
Appendix 2. Present Iteration to estimate the sizing of the leadscrew by relaxing the CubeSat envelope to increase by 20% 311
Appendix 3. Represent Iteration to estimate the plunger and the O ring specifications/dimension 313
Appendix 4. Represent the leaching experiment using the BPB dye indictor 315

LIST OF FIGURES

Figure 2-1: The sun and its planet from (John & Alex, 2014) 18

Figure 2-2: Showing millions of asteroid floating in the asteroid belt (John & Alex, 2014) 20

Figure 2-3: Near earth asteroid classification (NASAJPL, n.d.) 22

Figure 2-4: Main belt asteroid (MBA) from (Briggs, 2021).....23

Figure 2-9: Comparison of the mineral and water composition of CI and CM2.38

Figure 2-5: MOXIE Instrument for the Mars 2020 rover mission from (Gotame, 2020) 40

Figure 2-6: RESOLVE rover payload from (ROOMSJA, 2016).....42

Figure 2-7: Sample 1U CubeSat from (Michalevsky & Winetraub, 2017) 43

Figure 2-8: Showing the running total of nanosatellite and CubeSat launch from 1999 to date (Nanosatsdatabase, 2022).....45

Figure 3-1: Chart showing the distribution of NEA discovered as of 7th March 2017 54

Figure 4-1: comparison of the mineral composition in C-type NEA and Lunar regolith.....70

Figure 4-2: reaction flow of carbo-thermal reduction process with methane.....72

Figure 4-3: Hydrogen reduction process to produce iron and oxygen.....75

Figure 4-4: Reaction flow of carbo-thermal reduction with carbon monoxide....76

Figure 4-5: vapour phase pyrolysis.....78

Figure 4-6: Sulphuric acid electrolysis process 80

Figure 4-7: Molten oxide electrolysis process 82

Figure 5-1: CAD design for the sample acquisition subsystem comprising counter rotating brushes/paddles and Archimedes screws, extended scissor mechanism and rotatable carousal of five reaction oven (Sitepu, 2020). .130

Figure 5-2:. Block diagram representation of the subsystems of the proposed CubeSat compatible ISRU demonstration payload for metal extraction...132

Figure 6-1: setup for the initial leaching experiment 144

Figure 6-5: Experimental result of the repeat hydrometallurgical H_2SO_4 acid leaching of olivine mineral. 161

Figure 6-6: the BPB dye indicator test result 172

Figure 6-7: result for the sulphuric acid leaching experiment using BPB dye indicator solution to monitor the colour transition.....175

Figure 6-8: Result for the effect of 1M&5M acid concentration and distilled water on the 8.8mM BPB dye indicator.....177

Figure 7-1: From the left the Liquid Handling Sub-system (LHS) architecture and to the right is the designed and manufactured LHS using a combination of polymer and CNC machined parts 186

Figure 7-2*:* To the left and a CNC machined printed version of the RCS, to the right is the PLA 3D printed version of the RCS and in the centre is a Catia V5 designed version of a single open-ended RCS.....187

Figure 7-3: To the left represents the initial top plate used in the CubeSat based ISRU water extraction project, middle is the modified top view and to the right is the modified bottom view of the top plate respectively.....188

Figure 7-4: Modified top-plate showing the design plunger support position and inlet dimensions.....189

Figure 7-5: Left to the right the Catia V5 designed plunger, PLA 3D printed versions of the plunger and CNC machined version of the plunger. 190

Figure 7-6: Designed plunger, the plunger arm support and plunger head dimensions.....191

Figure 7-7: Left to right the Catia model of the stepper motor assembly, physical version of the stepper motor with mounted plunger attached to the support arm.....192

Figure 7-8: left to right showing *catia V5 model and the PLA 3D printed version of the plunger arm support*.....196

Figure 7-9: Designed plunger arm support showing the dimension of the screw lead support, screw lead nut screwing position and the plunger support .196

Figure 7-10: Left to right showing the stepper motor-based support assembled with the flange ball bearing and the designed base support showing the dimensions.....198

Figure 7-11: Left to right showing the stepper motor designed vertical support with the various dimensions.....199

Figure 7-12: a chart for elastomer material hardness and pressure selection (ORD5700, n.d.).....201

Figure 7-13*:* Left to right showing images of the designed and selected Elastomer O ring and the one implemented in the production of dioxygen project....202

Figure 7-14: showing the collapsible reservoir assembled with a double ended fitting MINISTAC tubing.....203

Figure 7-15: Left to the right is the PLA 3D printed version of the manifold, a Catia V5 model of the manifold and the physical manifold assembled with valves control.....204

Figure 7-16: showing the LFN flange type solenoid valves mounted on a manifold (leeco, n.d.).....205

Figure 7-17: IRF640N MOSFET transistor (Apogeeweb, n.d.).....212

Figure 7-18 : 7805 dc voltage regulator (components101, n.d.).....213

Figure 7-19: Breadboard components mounting showing the circuit driving components MOSFET transistor and the voltage regulator.....213

Figure 7-20: An assembly of the transistor circuit together with the SV and the collapsible reservoir.....215

Figure 7-21: On the left is the transistor switch with no load current induced, in the middle with load current induced to operate a single SV and to the right with induced load current to operate two SV. 216

Figure 7-22: An Arduino Uno board (spiceman, n.d.).....218

Figure 7-23: An easy driver board (Sparkfun, n.d.).....219

Figure 7-24: Physical breadboard interconnection between the Arduino board and the Easy driver board.....221

Figure 7-25: written code to control the linear transition of the stepper motor into RCS and out of the RCS.....222

Figure 7-26: Assembly of Arduino and Easy driver board interfacing other components (the Dc voltage power source, and the laptop).....225

Figure 7-27 : To the left is 3D machined, in the centre is designed model and to the right is 3D printed and built BB prototype.....226

Figure 8-1: To the left is the wet version of the BPB dyed olivine regolith and to the right is the dry version of the BPB dyed olivine regolith.....236

Figure 8-2: sample simulation of the BB payload system extraction experiment 238

Figure 8-3: Represent sample extraction experimental result for Replica1-1..240

Figure 8-7: Experiment1 BPB extraction result based on using the BB payload prototype and including the replicas.....244

Figure 8-4: Represent sample extraction experimental result for Replica2-1..247

Figure 8-8: Experiement2 BPB extraction result using 15mls centrifuge tubes in non-agitated state.....251

Figure 8-5: plastic centrifuge tubes agitated using the vertical rotary mixer....253

Figure 8-6: Represent sample extraction experimental result for Replica1-1..254

Figure 8-9: Experiement3 BPB extraction result using 15mls centrifuge tubes in agitated state.....257

Figure 8-10: Experiment1-3 average BPB extraction result 260

LIST OF TABLES

Table 3-1: Summary of potential candidate C-type NEA based on their physical, Engineering and Economic values 55

Table 3-2: Reduced potential C-type NEA for demonstration of the ISRU process 58

Table 3-3: Parameter weighting scaling that will be used used for the trade-off study of the potential locations.....61

Table 3-4: Raw scoring result for the potential C-type NEA 61

Table 3-5: Overall result of the trade-off study.....62

Table 3-6: Comparing the result of the sensitivity analysis by making the weighting value order uniform to those of the original result based on initial trade-off studies.....64

Table 3-7: Present a comparison of the result of the sensitivity analysis based on small increase to the scores less than 10% of the original scored values to those of the original result based on initial trade-off studies 66

Table 3-8: Present a comparison of the result of the sensitivity analysis based on small increase to the scores less than 10% of the original scored values and a small decrease to the scores less than 10% of the winning candidate C-type NEA to those of the original result based on initial trade-off studies...67

Table 4-1: A performance matrix table describing the performance of the options against the criteria 88

Table 4-2: Performance matrix result converted into raw numbers for ease of scoring.....89

Table 4-3: Raw scoring for the potential ISRU processes.....90

Table 4-4: The preference scores, weighting of the criteria and overall weighted scores.....93

Table 4-5: A combination of the scoring and weighting of each criterion to get the overall weighted score for each of the options.....96

Table 4-6: result of making the weighted value order uniform and comparing with the result of the initial trade-off studies 98

Table 4-7: Showing the result of small positive change across all the processes 99

Table 4-8: Showing the result of small increase for P1 to p6 and small decrease change for P7.....100

Table 5-1: ISRU payload top level system requirement.....105

Table 5-2: RCS ISRU Payload sub-system level requirement.....111

Table 6-1: Chemical analysis of Olivine (Mg rich) mineral (scangrit, 2021) 142

Table 6-2: showing the measure olivine mineral +void volume and the measured masses 145

Table 6-3: *Showing the acid to mineral volume ratio used for the experiment* 147

Table 6-4: Summary of design parameters used for the initial hydrometallurgical leaching process.....150

Table 6-5: Showing Maximum liquid depletion in percentage across the four experiments for the initial laboratory leaching experiment 154

Table 6-6: showing the mass losses corresponding to each sample in each experiment 156

Table 6-7: Showing the Maximum liquid depletion in percentage based on the four different experiments for the repeat leaching experiment 163

Table 6-8: showing a comparison of mineral % loss and mineral swelling across all sample of the experiment.....167

Table 6-9: summary of dye indicators used in the selection process 170

Table 6-10: Showing the volume of ethanol and mass of BPB salt used and the resultant concentration of the BPB solution.....171

Table 7-1*: showing the three different NEMA11 motorised lead screw linear actuator stepper motor* 194

Table 7-2*: the chosen lead screw specification* (Thomson, n.d.).....195

Table 7-3: Ball bearing specification and the lead screw machining data.....197

Table 7-4: showing the specifications of the designed elastomer O ring 200

Table 7-5: Listing the specification of the LFN SV (leeco, n.d.) 205

Table 7-6: specification of different types of pumps for selection.....207

Table 7-7: List of different types of driver controllers for a selection process..218

Table 7-8: Showing the pins cross connections between the Arduino and Easy driver boards (Sparkfun, n.d.) 220

Table 7-9: Truth table showing the combination of micro-step state (Sparkfun, n.d.).....224

Table 8-1: Parameters for the experiment.....235

Table 8-2: A summary result for the extraction experiments in three replicas using the BB payload prototype 242

Table 8-5: Interpreting the codes along the x-axis of the bar plot 244

Table 8-3: A summary result for the extraction experiments using the 15ml centrifuge tubes in three replicas and non-agitated 249

Table 8-4: A summary result for the extraction experiments using the 15ml centrifuge tubes in three replicas and agitated 255

Table 8-6: Showing the average amount of BPB solution extracted, the average extraction efficiency and the corresponding difference of the BPB solution extracted and the average extraction efficiency across the experiment1-3 261

Table 8-7: Showing the significant differences in the extraction result and the corresponding equivalent in percentage 265

LIST OF EQUATIONS

Equation 1: Present the Methane reduction of metallic oxide 73

Equation 2: Represent Methane reformation or methanation using nickel catalyst with additional hydrogen from the water electrolysis process 73

Equation 3: Represent the water electrolysis producing hydrogen and oxygen 73

Equation 4 and Equation 5: Represent the hydrogen step reduction chemical reaction of metal oxide and the water electrolysis to produce hydrogen and oxygen.....74

Equation 6: Represent CO chemical reduction reaction of metal oxide.....77

Equation 7: Represent the carbon dioxide decomposed to form carbon monoxide and oxygen. 77

Equation 8: Represent the decomposition of the metallic 78

Equation 9: Represent metal oxide reaction with concentrated sulphuric acid..79

Equation 10: Represent the hydrolysis of iron sulphate to produce iron, oxygen, and sulphuric acid.....79

Equation 11, Equation 12 and Equation 13: Represent the decomposition of FeO into molten regolith, Oxygen evolvement at the anode and metal deposition at the cathode 81

Equation 14: Represent the linear summation of the product of weight by the scores of each criterion 95

Equation 15: Represent the motor torque equation.....192

LIST OF ABBREVIATIONS

AIM	Asteroid Impact Mission
AU	Astronautical Unit
BLEO	Beyond Low Earth Orbit
CC	Carbonaceous Chondrite
CI	Ivuna Chondrite
CM	Mighei Chondrite
COPINS	CubeSat Opportunity Inter-Satellite Network Sensors
COTS	Commercial Off the Shelf
DC	Direct Current
DLR	German Aerospace Centre
DSI	Deep Space Industry
DSN	Deep Space Network
EDL	Entry Decent and Landing
EM	Explorer Mission
EMPA	Electro Microprobe Analysis
ESA	European Space Agency
FoM	Figure of Merit
HCCL	Hydrated Carbonaceous Chondrite Lithologies
HOC	High Ordinary Chondrite
IAU	International Astronautical Union
IRTF	Infra-Red Telescope Facility
ISRU	In-Situ Resource Utilisation
IT	Information Technology
JAXA	Japanese Aerospace Exploration Agency
JPL	Jet Propulsion Laboratory
JSC	Johnson Space Centre
LAVA	Luna Advance Volatile Analysis
LEO	Low Earth Orbit
LLOC	Low Low Ordinary Chondrite
LOC	Low Ordinary Chondrite
LRPM	Lunar Resource Prospector Mission
MarCO	Mars Cube One

MBA	Main Belt Asteroid
MID	Mid Infra-Red
MOXIE	Mars Oxygen ISRU Experiment
MPL	Minor Planet Centre
NASA	National Aeronautics and Space Administration
NEA	Near Earth Asteroid
NEAR	Near Earth Asteroid Rendezvous
NEO	Near Earth Object
NEODyS	Near Earth Object Dynamic Site
NIR	Near Infra-Red
NIRS	Near Infra-Red Spectral
NTRS	NASA Technology Reporting System
NTRS	NASA Technical Report Server
OC	Ordinary Chondrite
OVEN	Oxygen and Volatile Extraction Node
PhD	Doctor of Philosophy
PILOT	Precursor In-Situ Lunar Oxygen Testbed
PISCES	Pacific International Space Centre for Exploration System
PRI	Planetary Resource Industry
PSD – XRD	Position Sensitive Detector – X-Ray Diffraction
RELAB	Reflectance Laboratory
RESOLVE	Regolith and Environment Science and Oxygen and Lunar Volatile Extraction
SAS	Sample Acquisition System
SHC	Specific Heat Capacity
SLS	Space Launch System
SMASS	Small Main Belt Asteroid Spectroscopic Survey
SOXE	Solid Oxide Electrolysis
SSA	Space System Awareness
TRL	Technology Readiness Level
UV	Ultra-Violent
VIR	Visible Infra-Red

1 INTRODUCTION

The background of the research, research gap and research questions, research contribution to knowledge, the aim and objectives of the research, the research methodology, and research thesis structure are presented in this chapter.

1.1 RESEARCH BACKGROUND

In Situ Resource Utilisation (ISRU)/space mining is a subject of immense interest in recent times, several planets in our Solar System such as Mars, the Moon, asteroids, and comets are identified to be rich in minerals resources such as precious metals, volatiles, organic and non-organic materials that can be harness for the good of humankind. Today all space mission physical materials and components are supplied from the Earth; the mass penalty is one of the major challenges, the more mass you carry on the spacecraft, the more fuel that is required to compensate for the additional mass, making space-related missions very expensive. The terrestrial resources (fossil fuel, precious metals) depletion rate is on the increase, and humanity is paying heavily for this depletion in the form of higher prices for manufactured goods. ISRU/ space mining is an emerging research area that entails the collection and processing of space materials into their end products for the use of humankind (Crawford, et al., 2014). The development of ISRU technology has the potential to significantly reduce the number of supplies that need to be imported from Earth; key products are produced on the destination surface, such as metals to be used for space manufacturing, oxygen for astronaut use, and propellant used for space transportation and thereby increasing self-sustainability in space. This technology will also serve as a means of economic earning and a steppingstone for deep space ISRU to Mars and beyond. In the long term, the mined space resources can be transported to Earth to complement the depleting terrestrial resources, the process called "space mining."

The Near Earth Asteroids (NEA) appear to be the least expensive source of raw materials to be exploited as compared to other deep space solar system bodies such as Mars and the Moon. The NEAs relative to the Mars has a proximity of

0.3 Astronautically Unit (AU) translating to 44,879,361km or less within the Earth orbit which has shortened the duration to arrive at the destination (NASA-Mars, 2020); guarantee a low delta-V budget and, by extension, low fuel penalty. The National Aeronautics and Space Administration (NASA) Mars 2020/Perseverance rover is one of the missions to Mars to demonstrate key aspects of future ISRU systems

Until recently, the CubeSat spacecraft have been limited to Low Earth Orbit (LEO) operations; CubeSat's have high potential to reach other celestial bodies. CubeSat's are low cost, are low power, are low mass, have less risk and shorter development period, and have miniaturized Commercial Off-The-Shelf (COTS) components. Examples of successful Beyond Low Earth Orbit (BLEO) CubeSat missions include Mars Cubet One (MarCO) (Chahat, et al., 2020), a secondary CubeSat payload in the InSight flight mission. MarCO CubeSats is the twin's technology demonstration payload that provides an experimental communications relay to let scientists on Earth to know about InSight's spacecraft landing (NASA-JPL, 2018).

This PhD research work aims at advancing the study of *ISRU* on a C – type NEA and their reduction to practical demonstration and implementations compatible with CubeSat like payloads to produce payload design and supporting evidence that can be used to propose their inclusion on upcoming flight opportunities. It is worthy to note that the research work does not cover trajectories analysis, communication, and other related mission design concept, it focuses on payload design considerations.

1.2 RESEARCH GAP AND RESEARCH QUESTIONS

The planetary regolith and the atmosphere are the potential resources that would be used for the demonstration of the ISRU processes. Most of the existing ISRU studies are aimed to be implemented on a full-sized scale, they require large-scale infrastructure, they will consume a lot of power and as a result, such a mission would cost millions to billions of dollars and would take a longer period to implement (10years and above).

The development of a technology demonstrator needed to test the ISRU process before they are built and launched on a large scale will increase the Technology Readiness Level (TRL), reduce the risk, cost, development time and ensure that the concept would work at the desired location. So far Mar Oxygen ISRU Experiment (MOXIE) is the only ISRU technology demonstration experiment currently operational on Mars to validate the TRL of an ISRU concept to harness oxygen from the Martian atmosphere using Solid Oxide Electrolysis (SOXE) techniques. SOXE is a well-established Earth-based concept operating at a relatively high temperature of approximately 500°C - 850°C (Peter, et al., 2015). Within the Cranfield Space Research Group, a similar study to extract oxygen using the space regolith was carried out to implement the SOXE techniques on a small-sized CubeSat like ISRU demonstration payload.

This PhD research work would attempt to scale down a conventional Earth-based ISRU techniques into a miniature ISRU demonstration payload in CubeSat form factor that will use the regolith to extract metal as a de-risking technology. To the best knowledge of the researcher, this miniaturised payload system in the form of a CubeSat form factor to extract metal from the asteroid regolith resource is the first ISRU technology demonstrator. This research work would attempt to answer the following research question.

- "Which is the possible Earth-based ISRU techniques that will be compatible working within CubeSat form factor to demonstrate the ISRU process on the identified target location?".

ISRU studies have existed for the last 60 years and diverse feedstock such as asteroid regolith, Martian atmosphere and Martian regolith and Lunar/Moon regolith are the potential resources for the demonstration of the ISRU process. The Lunar and the asteroid regolith; they both are composed of silicate minerals such as the olivine. The oxides of the olivine mineral are mainly iron oxide (FeO), silicon dioxide (SiO_2), aluminium oxide (Al_2O_3), magnesium oxide (MgO), calcium oxide (CaO), and other minerals such as sodium oxide (Na_2O), potassium oxide (K_2O), manganese oxide (MnO) present in minute quantities (Ruzicka, et al., 2001). Several ISRU processes

namely, chemical reduction with Hydrogen, methane or carbon monoxide, vapour phase pyrolysis, sulphuric acid treatment, and molten oxide electrolysis have been considered for the extraction of oxygen as the primary product and metal waste from the Lunar regolith (Schwandt, et al., 2012). Due to similarities in the mineral composition among the Lunar and the asteroid, this research work will consider scaling down these conventional ISRU processes for the extraction of oxygen as the primary product and metal waste from the Lunar regolith for implementation on the asteroid regolith for the extraction process to give priority to metal production as the primary product and where possible oxygen as a secondary product. Further literature studies on the ISRU processes are presented in Chapter 2 and the ISRU selection process for implementation on a CubeSat based payload is presented in Chapter 4.

- "Is it possible to scale down well-established Earth-based ISRU techniques into a miniature demonstration payload in the CubeSat form factor?".

MOXIE payload is a miniaturised version of a well-established Earth based concept the SOXE presently, operational on Mars to demonstrate the process of oxygen extraction from the Martian atmosphere. MOXIE is designed to occupy a small volume of (23.9 cm x 23.9 cm x 23.9 cm) with a corresponding mass of 15 Kg (Hoffman, et al., 2015). The current volume and mass of the MOXIE payload and the rate at which the conventional payload system is miniaturised is an indication that the development of a much small-sized ISRU demonstrator payload in the CubeSat form factor is feasible. The small-sized ISRU demonstration CubeSat payload is intended to be accommodated in a maximum of 6U form factor with corresponding mass equivalent to approximately 9 Kg. Further studies on the CubeSat for interplanetary missions is presented in Chapter 2. The CubeSat based relevant components payload design and manufacture is presented in Chapter 7 and the demonstration of the leaching process and the aspect of liquid handling using the designed and manufactured payload is presented in Chapter 8.

- "Where will be a suitable location in which to perform an ISRU experiment via CubeSat mission demonstration payload and what is the potential resource?"

Studies related to the concept of ISRU suggest that the Lunar/Moon, Mars, asteroids and Comets are potential locations for the demonstration of ISRU studies (Josephine, et al., 2022). These locations are described towards selecting a potential location for ISRU CubeSat implementation studies in this project.

The Lunar/Moon due to the available information regarding its composition as obtained during the Apollo mission appears to be the most favoured location as compared to other locations (Mars and Asteroid). Several planned returns missions to the Moon such as NASA Artemis planned Humans return to the Moon 2024 (NASA, 2020), the Russia Luna 27 lander mission 2025 (ESA, n.d.) etc. have further burst the potential of the Lunar missions. In terms of proximity, the Lunar/Moon is the closest planetary body to the Earth as compared the Mars and the Asteroids. The Lunar/Moon body has a relatively deep surface gravity well of 1.62m/s^2 (NASA-Moon, n.d.), which will endanger the landing of a free-flying CubeSat payload on its surface.

the Mars exploration missions have long been in existence. NASA Viking program is the first US mission to successfully land two identical spacecraft (Viking 1 and 2) on the surface of Mars (NASA-Mars, n.d.). The knowledge of the abundant resources available on the Mars regolith and atmosphere has further burst the potential of Mars as destination for the demonstration of the ISRU process. Presently, MOXIE payload is operational on Mars to demonstrate an ISRU process for the extraction of oxygen using the SOXE techniques. The Mars surface just like the Moon have an existence of deeper surface gravity, greater than double those on the Moon surface, approximately 3.7m/s^2 (NASA-Mars, n.d.), this might pose a bigger challenge for the CubeSat payload in terms of landing on the Mars surface.

The third potential location for demonstration of the ISRU process is the asteroids as it is believed that it stores plenty of beneficial materials and are scattered around the entire solar system (Shepard, 2015). NASA's vision for

the exploration of asteroids was realised in 2001 when NEA-Rendezvous (NEAR) Shoemaker landed on 433 Eros NEA (NASA-Solarsystem, n.d.). Scientists believe that asteroids record the most primitive molecular compounds of the solar system and has also increase the study of asteroids (Shepard, 2015). Studies related to ISRU from asteroid bodies started to occur in the late 1990s. ISRU in the asteroid context is mostly concentrated on the extraction of its precious/platinum metal, the concept known as Asteroid mining (Kargel, 1996). The asteroid surface gravity as compared to those of the Mars and the Moon are quite insignificant (for instance C-type NEA Ryugu has surface gravity field in the range of 10^{-4} ms^{-2}). This scenario of having an insignificant gravity field on the asteroid surface is not likely to pose a challenge in landing a CubeSat like payload on the surface of the asteroid.

A review of the Mars, Moon, and the asteroids as potential locations for ISRU CubeSat implementation studies in this project, the asteroid appears not to have a significant surface gravity, landing of a CubeSat spacecraft on an asteroid requires less energy. Whereas on the Mars and the Moon, due to relatively higher surface gravity compared to the asteroid, higher energy is required to achieve the landing of the CubeSat spacecraft on these planetary bodies (Mars and the Moon). This scenario might impede the CubeSat payload operations. The C-type NEA was selected as the target destination for the demonstration of the ISRU process. These three research questions presented above will constitutes the drivers for this PhD research work.

1.3 RESEARCH CONTRIBUTION TO KNOWLEDGE

This PhD research work output has achieved the initial design, manufacture, and testingof key subsystems in the form of breadboard (BB) ISRU payload for the extraction of acid metal solution as a de-risking technology that will increase the TRL. The early-stage ISRU simulation of the leaching process and an aspect of liquid handling process using the designed and manufactured BB ISRU payload has been accomplished. The design and the manufacture of the BB

ISRU payload and using same to simulate the leaching process and the aspect of liquid handling has indicates the feasibility of the research work.

1.4 RESEARCH AIM AND OBJECTIVES

1.4.1 AIM OF THE PROJECT**:**

To design and manufacture a CubeSat based payload system that will demonstrate a scalable implementation of ISRU process on a C-type NEAs using the regolith materials to extract metal as a de-risking technology.

1.4.2 THE PROJECT OBJECTIVES

- To develop a focused literature review relevant to ISRU process, the asteroid mining technologies, and CubeSat like payloads. The development of a focused literature review based on the three key components (ISRU process, asteroid and CubeSat) can be achieved by first studying relevant and published literatures to understand the current state of the relevant knowledge.
- To identify locations for ISRU demonstration and their available resources. Identifying the locations/destinations for ISRU demonstration and their available resources, several asteroids' databases, various asteroid missions, asteroid observations, and other relevant literature sources were reviewed and documented
- To identify one or more ISRU processes/techniques based on the heritage that will be compatible with CubeSat-like payloads. Identifying one or more ISRU process compatible working with the CubeSat based form factor will be achieved via the literature review of both the well-known Earth-based processes and those processes proposed to be implemented on the Moon/Lunar bodies.
- To produce a payload design to demonstrate the selected technology on a suitable asteroids mission. The payload design will inform the production of the model of the technology that will be eventually translated into 3D printed version

- To produce a model of the technology and its implementation to guide further studies and justifications. After producing the payload design, the model of the technology was produced using CATIA V5 software tool to enable the initial 3D printing of the modelled part using polymer material as a de-risking approach and towards justifying the CNC machine production.
- To identify subsystems and components of the design to implement appropriate experiments and testing. The outcome of the 3D printed version of the model as a de-risking approach, the subsystem components are identified that will inform the BB assembly for the implementation of the appropriate experiments and testing.
- To disseminate study findings with the objectives of getting the payload selected for inclusion on future missions.
- To publish peer-reviewed technical papers and produce a Ph.D. thesis.

1.5 RESEARCH METHODOLOGY

- Review the up-to-date state-of-the-art technology for ISRU process, Asteroid mining, and the CubeSat payload to form a coherent background and the basis for subsequent PhD work.

ISRU processes, asteroid mining technologies and the CubeSat like payloads constitutes the three major element that form the basis of this PhD research work. Up to date literatures related to these three elements (ISRU technology, asteroids, and CubeSat payload) were reviewed and a coherent background story was established and would be used to form the basis for the subsequent PhD research work (methodology relevant to objectives 1).

- Identify and justify the choice of one or more target/candidate asteroids to be used as case studies to aid in the establishment of a requirement for the development of ISRU/Asteroid mining approaches using the CubeSat relevant experiment.

A review of the Mars, Moon, and the asteroids as potential locations for ISRU CubeSat implementation studies in this project, the asteroid appears not to have

a significant surface gravity, landing of a CubeSat spacecraft on an asteroid requires less energy. Whereas on the Mars and the Moon, due to relatively higher surface gravity compared to the asteroid, higher energy is required to achieve the landing of the CubeSat spacecraft on these planetary bodies (Mars and the Moon). This scenario might impede the CubeSat payload operations. The C-type NEA was selected as the target destination for the demonstration of the ISRU process.

From the on-set of this research a review of the Mars, Moon, and the asteroids as potential locations for ISRU CubeSat implementation, the asteroids has been identified as the target destination for the demonstration of the ISRU process using the CubeSat technology. Due to the presence of abundant natural resources such as mixture of organic matter, volatiles, metals and rocks on the C-type NEA, their availability in the neighbourhood to the Earth, the C-type NEA has been identified as a potential destination for other space missions. The sample return missions from Ryugu and Bennu asteroids has further burst future mission opportunities to the C-type NEA. Literature studies was carried out based on several NEO databases such as NASA NEO, Aerospace centre NEA, NEODyS, minor planet centre and Asterank database. 15764 NEA including (Amor, Aten, Apollo and Atira) were identified towards choosing one or two target/candidate asteroids to be used as case studies. At the time, out of the 15764 NEA discovered, only 314 NEAs have been classified and only 9% of the classified NEAs translating to 28 are C-type NEA. A trade-off studies was conducted on the 28 identified C-type NEA toward selecting a potential destination for the demonstration of the ISRU process.

C-type NEA Ryugu has outperformed the other C-type NEA in the trade-off studies and has emerged as the target destination for the demonstration of the ISRU process. A further Sensitivity Analysis (SA) performed to validate the result of the initial trade-off studies has further confirmed C-type NEA Ryugu as the destination for the demonstration of the leaching process (methodology relevant to objectives 2).

- To identify one or more ISRU processes/techniques based on the heritage that will be compatible working with CubeSat-like payloads.

Via literature review six (6) existing Lunar ISRU processes namely (chemical reduction with Hydrogen, methane or carbon monoxide, vapour phase pyrolysis, sulphuric acid treatment, and molten oxide electrolysis) allows to produce oxygen and metal as both primary and secondary product were identified (Schwandt, et al., 2012). These 6 existing Lunar ISRU processes were considered to give priority to metal production on the C-type NEA as the primary product and where possible oxygen as secondary product. Multi-Criteria Decision Analysis (MCDA) techniques, a subset of the Multi – Criteria Analysis (MCA) was considered in the selected process, the MCDA tools is easy to be used and good at analysing complex tasks. The MCDA model was used to implement a trade-off study on the potentially identified techniques to down select to one or two technologies to be considered. A further Sensitivity Analysis (SA) was performed to validate the process selection ranking that results from the trade-off studies. Hydrometallurgical Sulphuric acid leaching process on olivine mineral selected as the outcome of the initial trade-off studies was further confirmed as the ISRU technology process to be implemented and compatible with the CubeSat form factor (methodology relevant to objectives 3).

- Produce a model of the chosen ISRU/Asteroid mining processes to guide subsequent stages of the project.

A model of the chosen design concept was developed using the CAD software (CATIA V5) to enable the initial 3D printing of the modelled part using the polymer material as a de-risking approach to justify the CNC machine part production. The manufactured components were physically assembled to validate the intended breadboard (BB) prototype payload system. software code (Arduino sketches produced in the Arduino IDE) was developed and uploaded onto the hardware components to drive the operational sequence of the BB prototype payload system. The modelled parts were tested for fitting together and the parts detected not to fit together are adjusted in the CAD software (CATIA V5), printed iteratively and test again and again until the best fits was identified. The tested/acceptable

modelled parts/components are finally manufactured using the CNC machined techniques and assembled into the BB payload system that would be tested for the demonstration of the leaching and the aspect of liquid handling processes. (Methodology relevant to objectives 4, 5 and 6).

- To publish peer-reviewed technical papers and produce a PhD thesis

Finally, the finding of these research work has resulted to the production of a PhD thesis document. The completion of the identified future work will increase the TRL of the CubeSat-like ISRU payload system and would also lead to the formation of an elegant system that will inform the flight model design, manufacture, testing, and validation. The accomplished PhD document has the potential for the appropriate communities to consider the payload/experiment design for inclusion in future missions (methodology relevant to objectives 7 and 8)

1.6 THESIS ORGANISATION

Chapter 1. This chapter introduces the background of the research, research gap and the research question, research contribution to knowledge, the aim and objectives of the research, the research methodology, and research thesis structure that form a guide for the PhD implementation.

Chapter 2. In this chapter, a literature survey was conducted, and information related to the key element that constitutes the research topic, the Asteroid as potential locations and their resources, ISRU technologies, and CubeSat technology were obtained. Also, the asteroid mineralogy and mission to Ryugu, Bennu, and other classes of Asteroid were reviewed. This information will be used to develop a background story for this PhD research work.

Chapter 3. The asteroid selection criteria are discussed in this Chapter towards identifying the potential C-type Near-Earth Asteroid (NEA) candidate for the demonstration of the ISRU process. Parameters are generated for conducting a trade-off study, and the result of the trade-off study is obtained.

Chapter 4. In this chapter potential, ISRU processes that will be suitable to the CubeSat technology were identified. Parameters were generated based on the engineering, economic, and resource availability, a trade-off study was conducted based on the generated parameters, and the result was obtained to down select the processes to one or two.

Chapter 5. In this Chapter the general overview of the Cranfield CubeSat relevant payload for the demonstration of the ISRU process has been introduced and discussed

Chapter 6. Laboratory leaching experiment performed, this will help generate a requirement for implementation in the bread-board demonstration and eventually in the flight model payload development.

Chapter 7. This Chapter is concerned with the design, development, and manufacture of the bread-board system for the demonstration of an aspect of the ISRU process

Chapter 8. This Chapter entails using the designed and manufactured Breadboard (BB) payload prototype to simulate demonstration of the hydrometallurgy sulphuric acid leaching of the olivine mineral and aspect of liquid handling.

Chapter 9. Summary and discussion, conclusions, and future work are presented in this Chapter

2 LITERATURE SURVEY AND PROJECT BACKGROUND

2.1 INTRODUCTION

In this Chapter, a literature survey was conducted to review studies related to the three main components that constitute this research work (the concept of ISRU technology, destination for demonstration of the ISRU process, and interplanetary CubeSat technology) that are available in the public domain. The information's obtained through the review process can form a basis for tailoring the choice of an appropriate ISRU process that can be demonstrated on the identified destination asteroid that will be compatible with the interplanetary CubeSat technology.

Literature sources such as the Scopus, NASA technical Reports Server (NTRS), NEA databases and many more were reviewed to populates relevant up to date information in the context of this PhD work that will help inform the research process. In the end of this chapter, discussions related to the process and results findings are presented, along with a summary and conclusion.

2.2 LITERATURE RESOURCES

Considering the broad nature of the Ph.D. research topic that spanned across aerospace (both engineering and astronomy), chemical engineering, and other related sciences, choosing appropriate sources of information is key. In this regard, several databases in the public domain are considered, such as Scopus, NASA technical Reports Server (NTRS), Google scholars, NEA databases. Other sources are the private industries that are interested in the ISRU studies focusing on asteroid mining, these industries are Planetary Resources, and Deep Space Industries all are registered companies in the United States of America.

2.2.1 SCOPUS

Scopus is the largest abstract and citation database of peer-reviewed literature such as scientific journals, books, and conference proceedings. The diverse inter-disciplinary information available in the Scopus database, cutting across the field

of engineering and technology, astronomy, sciences, medicine, social science, and a lot more, prompted the choice of Scopus as the primary source of information for this research work. https://www.scopus.com

2.2.2 NASA TECHNICAL REPORTS SERVER (NTRS)

The NTRS is a database sponsored by NASA that provides access to NASA technology and sciences research activities. The NTRS database is used to compliment Scopus because most of the NTRS information is not available in the Scopus database and other sources of information. Update information that is not necessarily available in the Scopus is checked through the NASA-TRS. https://www.sti.nasa.gov/

2.2.3 PRIVATE INDUSTRIES

Other private industries are interested in the ISRU studies focusing on asteroid mining; a periodic check for information on the industry's website will also avail the researcher with an update on their progress. Among these industries are Planetary Resources and Deep Space Industries, all registered companies they reside in the United States of America.

2.2.3.1 PLANETARY RESOURCE INDUSTRY (PRI)

The planetary Resource industry is an American private investor in asteroid mining. Their vision is to expand the economy of the world into deep space by harnessing the asteroid resources. https://www.planetaryresources.com/

2.2.3.2 DEEP SPACE INDUSTRY (DSI)

This is another American Asteroid mining company, with a mission to change the economics of the space industry by prospecting, harvesting, processing and manufacturing the asteroid resources. Deep Space Industries

2.2.3.3 NEA DATABASES

As one of the types of solar system bodies of interest, NEA has several databases set up by government and private agencies to archive information about the NEA for reference purposes. Some of these databases are NASA NEO database, German Aerospace center NEA database, Minor planet center database, ESA

sponsored NEODyS database, and Asterank: a scientific and economic database.

2.2.3.4 NASA NEO DATABASE

This database is sponsored and managed by NASA near-Earth object-Jet Propulsion Laboratory (NASA NEO-JPL) and provides information about the physical and dynamical properties of all NEO. https://cneos.jpl.nasa.gov/ca/

2.2.3.5 ASTERANK DATABASE

This is a scientific and economic database of over 600,000 asteroids at the time of compiling this report. Important data such as the asteroid mass, type, composition, and orbital information are collected from multiple scientific sources such as the Minor Planet Centre (MPC) and NASA-JPL. With this information, the cost and rewards of mining asteroids are estimated. https://www.asterank.com/

2.2.3.6 NEODyS DATABASE

NEODyS is an acronym that stands for Near-Earth Object Dynamic Site sponsored by ESA on one side and the Department of Mathematics, University of Pisa. The NEODyS provides information and services for all NEA. Each NEA has its own dynamically generated home page providing information and services. NEODyS-2 is an improved version of the NEODyS https://newton.spacedys.com/neodys/

2.2.3.7 GERMAN AEROSPACE CENTRE NEA DATABASE (DLR NEA-DB)

The DLR NEA- database is sponsored within the ESA- Space Situation Awareness (ESA-SSA) fund. It is a database of physical and dynamical properties of NEAs that contains published data on all known NEAs. German Aerospace Center (DLR) - Space Foundation

2.2.3.8 NHATS ACCESABLE NEA DATABASE

This database is compiled by the Centre for NEO Studies and containing the results of the NEO Human Space Flight Accessible Targets Study (NHATS). They

are simple to understand, and they allow easy download of NHATS data. https://cneos.jpl.nasa.gov/nhats/.

2.2.3.9 MINOR PLANET CENTRE DATABASE (MPC-database)

The MPC-database is a subset of the International Astronomical Union (IAU); they are responsible for collecting observational data for minor planets such as asteroids and comets, calculating their orbits, and publishing the information via the Minor Planet Circular. The database is sponsored by NASA. https://www.minorplanetcenter.net/iau/

2.2.4 USING THE COMPILED SOURCES OF LITERATURE IN THE CONTEXT OF THIS RESEARCH

This section described the methodology the compiled sources of literature are used in the context of this research work to produce relevant information related to ISRU-CubeSat development.

2.2.4.1 FORMULATING A SEARCH METHOD FOR THE LITERATURE REVIEW

In this section a search method is formulated to search for the relevant literatures focusing on the primary source of information (Scopus). A combination of relevant keywords/search terms such as (ISRU, CubeSat, NEA) are formulated. The formulated search words/terms are then combined into a search string and are used to retrieve the search results. To check the relevance of the search results, random sample of the searched document are taken to see how they are related to the ISRU concept. Where most of the result are not relevant to the ISRU context, a reconstruction of the search string is required. Finally, the relevant search results of the literature review are catalogued and could be used for the development of specific ISRU techniques of interest.

2.2.4.2 REFINEMENTS TECHNIQUES

Th refinements techniques help the researcher to keep updated with current areas of studies related to ISRU concept. Two main areas are considered: keeping updated from journal publications and other general information sources. In Scopus a feature update set up allows for an automatic weekly or bi-weekly notification via email to the researcher to provide new publications update.

Information from secondary databases (NTRS, private companies' website and the NEA DB) are manually checked weekly or bi-weekly to get update on new publications.

2.3 RESULT AND ANALYSIS OF PROJECT COMPONENTS

The results and analysis of the project components covering the overviews of the solar system, ISRU technologies, and the CubeSat technology is presented in this section.

2.3.1 OVERVIEW OF THE SOLAR SYSTEM IN OF ASTEROID STUDIES

In this subsection of the PhD research work, the overview of the solar system was presented. The asteroid mineralogy was reviewed. The literature based on the meteorites were reviewed to establish the general postulation that the asteroids are the presumed parent's bodies of the meteorite. Finally, the mineral composition of the meteorite was reviewed to establish the commonest meteorites suitable for the project implementation.

The solar system or the Sun system comprises the Sun and all the objects that orbit around it. It is made up of the eight major planets, namely Mercury, Venus, Earth, Mars, Jupiter, Saturn, Uranus, Neptune, and the ninth planet called Pluto; Pluto has renamed a dwarf planet because of its small size as compared to the earth-moon. The Near Earth Object (NEO) that is near the Earth comprising of the comet and asteroids (Ahrens, 2013). The solar system is as shown in Figure 2-1

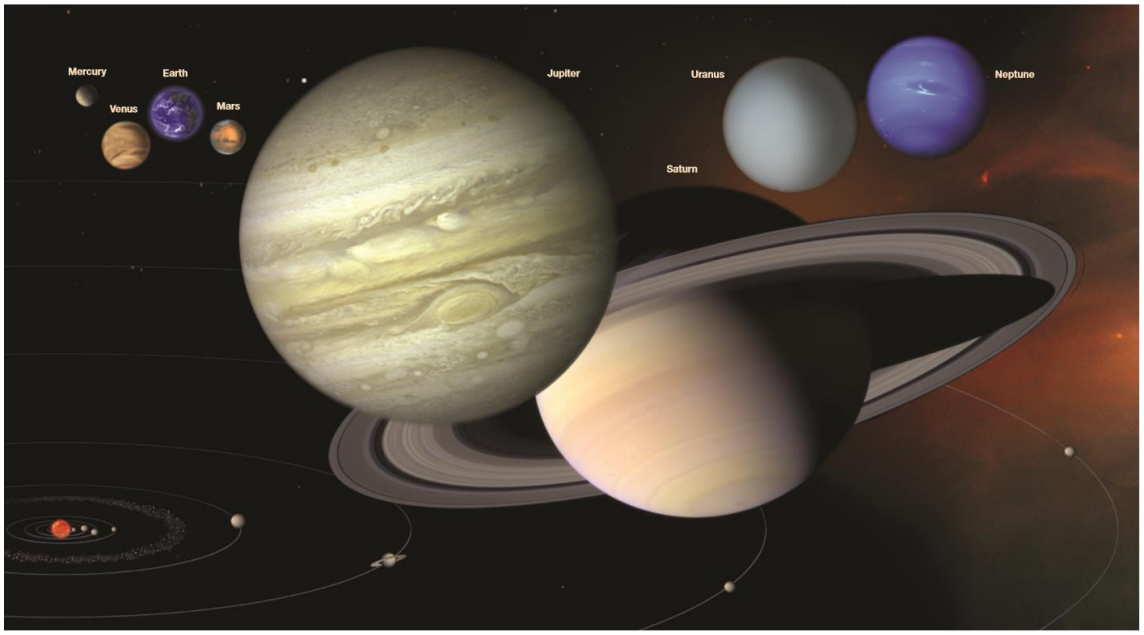


Figure 2-1: The sun and its planet from (John & Alex, 2014)

2.3.2 GENERAL REVIEW OF THE POTENTIAL LOCATIONS FOR DEMOSTRATION OF ISRU PROCESS

The outcome of the literature studies carried out based on the various potential locations for demonstration of the ISRU process. The Lunar, Mars, and the Asteroids appear to be the favoured locations for ISRU process demonstration. The Lunar regolith, Martian atmosphere, Martian regolith and the asteroid regolith are the potential feedstock that can be used in the demonstration of the ISRU process to extract useful materials.

2.3.2.1 ANALYSIS OF THE POTENTIAL LOCATIONS FOR DEMOSTRATION OF ISRU PROCESS

The Lunar location due to their heritage, since the Apollo era, samples of the Lunar material have been successfully brought to Earth. There exists abundance of knowledge regarding the composition of the Lunar material when compared to other locations (Mars and Asteroid), they are the most favoured for demonstration of the ISRU process. The increase in the study of Mars and the current idea of sending humans to Mars from various space agencies, the Mars has been identified as the second most favoured destination for the demonstration of the ISRU process. Due to the abundance volatiles, metals and other relevant

resources on the asteroids, the asteroid family are assumed to be potentially the third most favoured location for the demonstration of the ISRU process.

The Lunar bodies despite been the closest one to Earth, it has a relatively deep gravity well of 1.62m/s^2, which might engender the CubeSat landing process on their surfaces. Similarly, the Mars has deeper gravity than Lunar, 3.7m/s^2, which might generate a bigger challenge if a CubeSat landing on their surfaces is required. The asteroids in addition to the abundant resources present there in, they do not have a significant surface gravity as compared to the Lunar and Mars. Therefore, landing a spacecraft on an asteroid requires less energy when compared to other bodies; the spacecraft does not require high energy to slow down to have safe touch down at the surface of the asteroid. In the case of the Mars and Lunar, due to the relative deeper gravity field, higher energy is required to slow down the spacecraft. Due to these challenges associated with the Lunar and Mars surface landing in the context of the CubeSat like payload for ISRU demonstration, the asteroid was selected as the potential destination for the demonstration of the ISRU process using the CubeSat form factor.

2.3.3 ASTEROID FORMATION

The asteroid formation fits neatly into the solar nebula hypothesis that explains the formation of the entire solar system. The theory postulate that about 4.5 to 5billion years ago, the solar system developed out of a huge cloud of gases and dust floating through space (John & Alex, 2014). Due to gravitational pull, these gases and dust move slowly toward one another to form a core; the core grows and increases in mass and generates a more powerful gravitational field. The material in the initial cloud formed a flattened disk that continued moving around the Sun, and from this disk, material such as the planets, moons, comets, and asteroids are formed (John & Alex, 2014). Due to the gravitation effect, the particles accreted into larger particles called the planetesimals. The planetesimal close to the Sun becomes harder and they constitute part of the inner planets. Those lying near the outer edge of the inner solar system, just beyond Mars, due to their proximity to Jupiter and the effect of the Jupiter gravitational force they were unable to accrete into a planet , they are constantly pulled , keeping them

away from accreting into a planet (John & Alex, 2014), they remain separate as shown in Figure 2-2



Figure 2-2: Showing millions of asteroid floating in the asteroid belt **(John & Alex, 2014)**

The largest planetesimals become the planets and moons, while the smallest one becomes the Asteroid and the comets. The Mars, moon, and asteroids are potentially relevant for the ISRU technology demonstration (Grier & Rivkin , 2018). Each of these solar system bodies on its own is endowed with natural resources; the Martian atmosphere is approximately 95% carbon dioxide, the moon is rich in the lunar regolith, and the asteroids are believed to contain a mixture of organic matter, volatiles, metals, and rocks materials (Lefèvre, et al., 2008; Kronrod, et al., 2018; DeMeo & Carry, 2014).

2.3.4 OVERVIEW OF AN ASTEROID

Asteroids were the last class of bodies in the solar system to be discovered; they are now thought to be potentially rich in varied materials within the solar system (Nelson , et al., 1993). It has been estimated that the mineral wealth in the belt of asteroids between Mars and Jupiter would be equivalent to about a 100billion dollars for every person on Earth today (Wong, 2018). The projected benefit on the mineral wealth in the asteroid belt in terms of profit accrued to every person on Earth is best described by the law of supply and demand. There is an inverse relationship between the supply and prices of goods and services while demand is unchanged (Boyle, 2021). To ensure the attainment of the projected benefit a balance has to be in place, a decrease in supply of the material when demand remain the same, the prices tend to rise to higher equilibrium and,

hence ensuring maximum profit. The asteroids relative to their orbital position are classified into a NEA; those near the Earth and relatively easy to access (Amor, Apollo, Aten, and Atira NEA) and the Main Belt Asteroid (MBA) those found between Mars and Jupiter and the Trojan asteroid those found in the same orbit with planets (John & Alex, 2014). Relative to their mineral composition the asteroids are classified into carbonaceous (C-type), stony (S-type) and metallic (M-type) asteroid (John & Alex, 2014).

2.3.4.1 NEA OR EARTH APPROACHING ASTEROID

The NEA are believed to be originally from the Main Belt Asteroid (MBA) before they are being expelled from the belt by disturbing resonances with Jupiter and Mars (Bojan , 2013). The NEA/Earth approaching asteroids, they are the type of asteroids relative to their orbital position has the shortest distance (perihelion) to the Sun, less than 1.3 AU, they cross the earth orbit around the Sun or approaches the earth orbit. The NEA is divided per their Aphelion, perihelion, and semi-major axis into Aten, Apollo, Amor, and Atira (NASAJPL, n.d.).

2.3.4.1.1 AMOR NEA

The Amor are asteroids whose orbits approach but do not cross the Earth's orbit; their orbit is further from the Sun than the Earth's orbits. Some of the Amor asteroids have their orbit residing entirely between the Earth and Mars orbit; they are economically attractive in the near term because of their proximity to earth orbit. This family of NEA has their orbit exterior to Earth and interior to Mars, the semi-major axis a > 1AU with Aphelion $1.017<q<1.3$AU. Asteroid (1221) Amor is an example of an Amor asteroid (NASAJPL, n.d.).

2.3.4.1.2 APOLLO NEA

The Apollo asteroids orbit cross the earth orbit, they spend most of their time outside earth orbit, they have a wider orbit than the Earth. They are economically attractive in the near term because of their proximity to the Earth's orbit. This family of asteroids has semi-major axis a > 1AU and the aphelion $q < 1.017$. Asteroid (1862) Apollo is an example of an Apollo asteroid (NASAJPL, n.d.).

2.3.4.1.3 ATEN NEA

The Aten asteroid orbit also crosses the earth orbit; they spend most of their time inside the Earth's orbit. They are equally economically attractive in the near term because of their proximity to Earth's orbit. This family of asteroids has semi-major axis a < 1AU and the aphelion q > 0.983. Asteroid (2062) Aten is an example of an Aten asteroid (NASAJPL, n.d.).

2.3.4.1.4 ATIRA NEA

The Atira asteroid has its orbit entirely contained within the Earth's orbit; they stay closer to the Earth and never cross the earth orbit. The semi-major axis a < 1AU and the aphelion q < 0.983. Asteroid (163693) Atira is an example of Atira NEA (NASAJPL, n.d.). The NEA are divided per their Aphelion, perihelion and semi major axis into Aten, Apollo, Amor and Atira is as shown in Figure 2-3

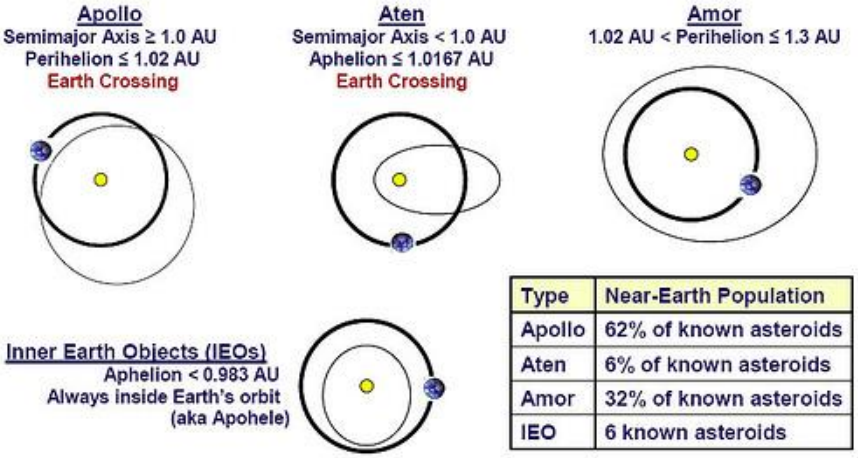


Figure 2-3: Near earth asteroid classification (NASAJPL, n.d.)

2.3.4.2 MAIN BELT ASTEROID (MBA)

The Asteroid lying between the orbits of Mars and Jupiter are described as the main belt asteroids and reside at a distance between 2.12 and 3.3AU from the Sun (Briggs, 2021). The MBA constitute most of the asteroid family. Ceres and Vesta are some examples of the main belt asteroid. The image of the MBA is as shown in Figure 2-4

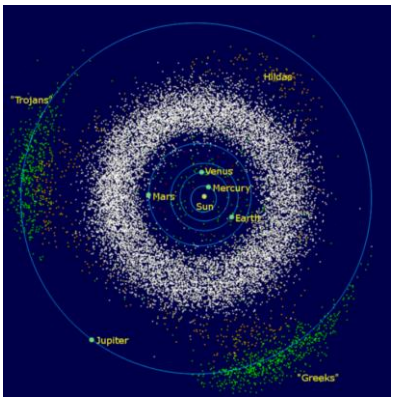


Figure 2-4: Main belt asteroid (MBA) from (Briggs, 2021)

2.3.4.3 TROJAN ASTEROID

The Trojans asteroids move in the same orbits as Jupiter, they do not collide with it because they orbit in one of the langrage points of stability L4 and L5 (Moore, 2005). Jupiter Trojan is the most significant populations of Trojans.

2.3.5 ASTEROID TAXONOMY

Asteroids are taxonomically classified based on some observable optical properties independent of specific mineralogical interpretations such as their albedo. The albedo is a measure of the reflectivity of the asteroids; a white, perfectly reflecting surface has a high albedo of 1.0, and a black, perfectly absorbing surface has a low albedo of 0.0 (Lucy, 2018). There are three primary categories of asteroid depending on their mineral composition.

2.3.5.1 S – TYPE ASTEROID

The S – Type asteroid constitutes 17% of known asteroids; they are composed of metallic iron mixed with iron and magnesium silicates; relatively brighter albedo in the range of 0.1 – 0.22, they inhabit the inner asteroid belt (John & Alex, 2014)

2.3.5.2 M – TYPE (METALLIC) ASTEROID

Constitutes the rest of the known asteroid, dominated by metals, particularly iron and nickel; relatively brighter with an albedo in the range of 0.10 – 0.13, they inhabit the main belt middle region (John & Alex, 2014).

2.3.5.3 C – TYPE (CARBONACEOUS) ASTEROID

The C – type asteroid constitutes over 75% of known asteroids; they are characterized by a mixture of lightweight carbon-rich minerals. Their albedo is in the range of 0.03 – 0.09; they are so dark that they absorb most of the light incident on them, and the reason why they are difficult to be dictated, they inhabit the main belt's outer region (John & Alex, 2014). Based on the resource extraction standpoint, the carbonaceous C-type asteroids are the most desirable; as they contain a mixture of volatiles, organic molecules, rock, and metals (Badescu, 2013). The C – type NEA asteroid is the asteroid of interest in this PhD research work, even though the research targets the production of metals, the C-type NEA they are preferred to the M-type NEA asteroid for the abundance of organic material in addition to rock and minerals there in, making it a potential source for other resources and a target for other missions. The C - group/complex are further expanded and classified into Thelon and Small Main – Belt Asteroid Spectroscopic Survey (SMASS).

2.3.5.3.1 THOLEN CLASSIFICATIONS

The Tholen C – group classification is further expanded into B – type, G – type, F – type and C – type, generally they share common properties with certain variation in terms of albedo, absorption characteristics and mineral composition. For example, the B – type asteroid is like the C – type asteroids; B – type asteroid albedo tends to be greater, the spectrum is bluish and has ultraviolent absorption properties compare to the C – type asteroids.

2.3.5.3.2 SMALL MAIN – BELT ASTEROID SPECTROSCOPY SURVEY (SMASS)

The SMASS group is made of the following classifications C – type having the most spectra in the group, B – type which correspond to the Thelon B and F - type, C_g and C_{gh} – type correspond to the Thelon G – type and C_b – type which correspond to transition object between the SMASS C and B – type asteroid.

In this Ph.D. research work, the C-type NEA is target as the destination for demonstration of the ISRU process using the CubeSat technology. The C-type

NEA is believed to be economically more viable for the ISRU processes demonstrations in the nearest future for the following reasons:

- Abundance of natural resources such as mixture of organic matter, volatiles, metals, and rocks materials present therein. A 7m C-type NEA weighing approximately 500 tonnes may contain up to 200 tonnes of volatiles such as water and carbon rich compounds (100 tonnes each), 90 tonnes of metals (83 tonnes iron, 6 tonnes nickel and 1 tonne cobalt) and 200 tonnes of silicate residue (Zacny, et al., 2013).
- Due to the abundance of other natural resources, the C-type NEA are identified as potential target/destination for other space missions
- Its availability in the immediate neighbourhood to the earth which makes it easily accessible.
- The sample return missions from the Ryugu and Bennu will further burst future missions' opportunities and
- Low gravitational pull on the surface of the C-type NEA as compared to the Moon and Mars is a specific feature that will aid the mission using the CubeSat technology

2.4 ASTEROID MINERAL COMPOSITION

The knowledge of the asteroid mineral composition is based on deduction from the meteorites find or fall and other observations such as ground-based deep space network remote sensing and In-flight spectroscopy (Shepard, 2015). The C-type NEA based on their chemical composition contained organic and non-organic molecules and volatiles. The target product for this research is metal resource for the manufacture of infrastructure In Situ; the candidate C-type NEA must have the presence of metal resource such as iron (Fe), Platinum group metals (PGM) and rare metals in its mineral composition.

In this section a study of the mineral composition of the meteorites are reviewed to establish a clue to its originality with the asteroid within the solar system.

2.4.1 THE METEORITE

The meteorite is believed to be progeny of the asteroids that undergo transmutation on their way through the earth atmosphere to the earth surface. They are part of meteors that survive flight through the atmosphere and fall on the ground and are categories into falls and finds. The meteorite falls are the kind of meteorite that are observed to fall and then collected and are believed to be more valuable because they are more likely to be fresh and less altered by exposure to the climate. The meteorite finds, their entry is not observed, they are stumbled upon and constitutes bulk of meteorite collection and most likely altered due to exposure to the climate effect. The study of the mineral composition of the meteorites will give a clue to its origin within the solar system (Shepard, 2015). The meteorites are classified based on the presence of Iron-nickel metal into achondrites (iron and stony iron) meteorite and chondrite (stony) meteorites. The chondritic meteorites represent the largest family of the meteorites and are believed to retain much of their original structure. They are divided into ordinary chondrite (OC) and carbonaceous chondrite (CC) meteorites. The OC meteorite based on their iron content are further classified into High (H), low (L) and low-low (LL) OC meteorite (Shepard, 2015). The CC meteorites comprises of six normal group (CI, CM, CO, CV, CK and CR) arranged in the order of reducing aqueous alteration and two unusual groups (CH and CB) (Choe, et al., 2010)

2.4.2 MINERAL COMPOSITION OF THE METEORITES

Most of the metals in the meteorite are not found in their free form; they exist in compound state such as silicate compound (pyroxene, olivine, and feldspar), oxides compound (magnetite, wustite and ilmenite), sulphides compound (iron sulphide) and carbides compound (silicon carbide). The silicate minerals pyroxene, Olivine and feldspar are the most abundant mineral in meteorites, they dominate the stony class of meteorites (Weisberg M.K, 2018). These minerals when they undergo aqueous alteration, they are depleted from their mafic silicate state with increase in magnesium and decrease in the iron and transmute into phyllosilicate matrix.

2.4.2.1 OLIVINE $(Mg,Fe)_2SiO_4$

Olivine is predominantly made of two end members the fayalite (Fe_2SiO_4) and the forsterite (Mg_2SiO_4). The mineral olivine can be pure forsterite, pure fayalite, or any combination of the two (iron and magnesium are interchangeable). They are represented in terms of molecular percentages, for instance If we say that the olivine is 50 moles% fayalite (also written Fa_{50}), it means that for every 50 iron atoms there are 50 magnesium atoms in a ratio of 1:1 (50 + 50 = 100). The fayalite Fe_2SiO_4 is the iron end member and Forsterite Mg_2SiO_4 is the magnesium end member of the olivine solid solution series. In meteorite, the olivine mineral is usually forsterite, having more magnesium than iron in the carbonaceous chondrite (Weisberg M.K, 2018).

2.4.2.2 PYROXENE $(Ca,Mg,Fe)SiO_3$.

The pyroxene is classified in terms of three end members namely $CaSiO_3$, $MgSiO_3$, and $FeSiO_3$. These end members correspond to the minerals wollastonite (Wo), enstatite (En), and ferrosilite (Fs) and are reported in terms of molecular percentages (e.g., $Wo_{42}En_{54}Fs_4$). A more complex pyroxene called the clinopyroxene that combined all the three end members exist with the molecular formula $(Ca,Mg,Fe)SiO_3$ (Weisberg M.K, 2018).

2.4.2.3 FELDSPAR $[(K,Na,Ca)(Si,Al)_4O_8]$

Feldspar is an aluminum silicate mineral with various amounts of sodium, calcium, and potassium. It is made up of plagioclase $(Na,Ca)(Si,Al)_3.O_8$ and orthoclase $KAlSi_3O_8$. Plagioclase can further be divided into calcium rich anorthite and sodium rich albite (Weisberg M.K, 2018).

2.4.2.4 ILMENITE $(FeTiO_3)$

The ilmenite is a mineral compound containing iron, titanium and oxygen and are commonly found in the achondrite family of the meteorite, they also exist in the lunar basalts and the Martians basalts (Weisberg M.K, 2018)

2.4.2.5 MAGNETITE (Fe_2O_3)

The magnetite is an iron and oxygen compound commonly found in a reasonable quantity in the matrix of carbonaceous chondrites such as the Murchison

chondrite (CM) and in lesser amounts in ordinary chondrites and some achondrites (Weisberg M.K, 2018)

2.4.2.6 IRON SULPHIDES (FeS)

The sulphide mineral exists in nearly all meteorites. It is found as nodules in iron meteorites. In chondritic meteorites, it is usually found as small blebs or grains in both chondrules and matrix averaging about 6 wt% (Weisberg M.K, 2018). The FeS is much more present in the CI-type carbonaceous chondrite up to (9wt%) than in the CM-type carbonaceous chondrite which is up to 7wt% (Jarosewich, 1990).

2.4.2.7 SILICON CARBIDE (SiC)

The compound silicon carbide Occurs as interstellar dust grains in the Murchison CM carbonaceous chondrite and other chondrites (Weisberg M.K, 2018)

2.5 ANALYSIS OF THE METEORITE MINERAL COMPOSITION

The deduction based on the meteorites find or fall and other observations are used to establish the knowledge of the asteroid mineral composition. The sources of these meteorites are still a subject for debate and several spectroscopic analyses both ground base (laboratory analysis of meteorite and using the ground based deep space network (DSN) to perform remote sensing) and in-flight spectroscopy on asteroids to show agreement with the meteoritic records have been carried out.

2.5.1 SPECTROSCOPY

Spectroscopy is an analytical method for qualitative and quantitative estimation by use of light. UV-spectroscopy (190 – 400nm), Visible spectroscopy (400 – 800nm) and infrared spectroscopy (800 – 1000nm) are examples of spectroscopy methods. These techniques are adapted and widely used in the planetary sciences to identify ice and hydrated minerals at the surface of asteroids and planets from solar reflectance spectroscopy (Berk p., et al., 2010).

2.5.1.1 IN SPACE SPECTROSCOPY

To establish and consolidate on the asteroid mineralogy and their link with meteorites collection several spacecraft missions near the asteroid were studied. These missions/asteroids flyby and rendezvous will enable a direct comparison between the telescopic observation from the ground DSN, the laboratory analysis of the meteorite and what is learned in proximity with the planetary body (asteroid) towards establishing a common ground on the relationship between the asteroids and meteorites. Some of these missions are discussed thus:

2.5.1.2 GALILEO SPACECRAFT MISSIONS

The Galileo spacecraft mission is a NASA mission, launched on the 18th of October 1989 on board space shuttle Atlantis on a mission STS – 34 to Jupiter and was the first spacecraft mission to flyby an asteroid in proximity and the first to discover the moon of an asteroid. The spacecraft flew by an S-type asteroid 951 Gaspra in October 1991 within 1601km and at a speed of 8km/s. The asteroid was observed to be irregular in shape, heavily cratered having some magnetic effect and a dimension of 19 x 12 x 11km in diameter (John & Alex, 2014).

In August 1993, Galileo flew by the second asteroid 243 Ida, which is another S-type asteroid, Ida was also found to be irregular in shape and heavily cratered with dimension almost twice that of Gaspra (54 x 24 x 15km). Ida was discovered to have a moon called Dactyl, the bulk density of Ida was estimated to be 2.6g/cm^3 which is consistent with chondritic composition and modest porosities of around 30 – 40%. Most CC meteorites have density in the range 2.5 – 3.0g/cm^3. Gaspra and Ida are both main belt asteroids (MBA) (Shepard, 2015).

2.5.1.3 ROSETTA SPACECRAFT MISSIONS

Rosetta spacecraft mission is an ESA science program to planetary bodies, launched in March 2004 by an Ariane-5 Vehicle from Kourou in France. The primary objectives of the mission are to rendezvous with comet 67P/Churyumov-Gerasimenko. In September 2008, Rosetta flew by an E-type main belt asteroid 2867 Steins. Images taken of the asteroids Steins with the OSIRIS (Optical, Spectroscopic, and Infrared remote imaging system) cameras within 803km and at a relative speed of 8.6km/s, show that steins have a spherical diameter of

5.3km, with a very large crater more than 2.1km in diameter. The albedo of steins at a wavelength of 632nm, was obtained to 0.4, Steins is not solid rock but a rubble pile with a conical appearance (Keller, et al., 2010).

In July 2010, Rosetta flew by the second M-type main belt asteroid the 21 Lutetia. Images taken of the asteroid Lutetia with the OSIRIS cameras within 3162km and at relative speed of 15km/s reveals that Lutetia has an estimated dimension of 132 x 101 x 76km, an estimated bulk density in the range 3.98 – 5.0g/cm^3 with albedo of 0.22 (Rosetta, 2021). Burucci et al., (2008) suggest the closest analogue to asteroid (21) Lutetia are the carbonaceous chondrite meteorites the CO-CV type.

2.5.1.4 NEAR-SHOEMAKER SPACECRAFT MISSIONS

Near Earth Asteroid Rendezvous Shoemaker spacecraft mission (NEAR – Shoemaker) was the first NASA discovery mission and the first mission to a NEA. The mission was launched on the 17th of February 1996 on board Delta II launch vehicle at Cape Canaveral LC-17B. The primary objectives of the mission were to rendezvous and achieve orbit around the NEA Eros and study the size, shape, mass, composition, magnetic field and surface and internal structure of Eros (NEARShoemaker, 1996).

On the 14th of February 2000, the NEAR-Shoemaker spacecraft enter orbit with the S-type NEA Eros. The spectra data from the spacecraft has shown spectral features of Eros to be consistent with the ordinary chondrite meteorites without pinning it down to specific OC subtypes. Eros has a dimension of 13 x 13 x 33km in size and has also exhibited different geology including ridges, grooves, craters, and boulders. The Eros has a bulk density of 2.7g/cm^3, the bulk density of typical OC meteorites is 3.5 g/cm^3, suggesting that Eros has about 20% empty pore (Shepard, 2015).

On the 27th of June 1997 the NEAR-Shoemaker spacecraft en-route to NEA Eros, flew by the C-type NEA 253 Mathilde. The spectra data from the spacecraft at a relative distance 1200km of the asteroid reveals that Mathilde was a porous rubble pile with roundish shape and an average diameter of 53km with gigantic

impact crater 20km wide. The very dark nature of Mathilde asteroid made them to absorb 96% of the sunlight and reflecting only 4%. The most likely meteorite analogs for Mathilde are CI and CM meteorites (Shepard, 2015).

The spacecraft change in velocity due interaction between the spacecraft and the asteroid allowed for an estimate of the mass, coupled with the diameter, a bulk density of 1.3g/cm^3 was estimated. Most CC meteorites have density in the range 2.5 – 3.0g/cm^3, this suggest that Mathilde has about 50% pore space (Shepard, 2015).

2.5.1.5 DAWN SPACECRAFT MISSIONS

The Dawn spacecraft mission is yet another NASA space mission launched on the 27th September 2007 on board Delta II 7929H launch vehicle. The mission aimed at the two largest main belt asteroids the Ceres and Vesta.

On the 18th July 2011, the spacecraft enter orbit with the first asteroid to be discovered 4 Vesta, the spectra data from the spacecraft at 542km show that the asteroid has diverse color, they show albedo as low as 0.1 in one region and as high as 0.67 at other regions, over 220km in diameter. A V-type asteroid, the gravity measurement by Dawn determined Vesta's mass and revealed its bulk density to be 3.5g/cm3, like Lutetia (Shepard, 2015).

On 6th March 2015, the spacecraft enter orbit with 1 Ceres. Spectral observation suggest that the Ceres surface is composed of clay-silicate changed by the presence of water, Ceres is almost twice in size of the Vesta and does not seem to have a family of asteroids that appear to have been derived from it (Shepard, 2015).

2.5.2 LABORATORY ANALYSIS OF METEORITES

To establish the mineralogy of asteroids, the meteorite falls and find are analysed in the laboratory through several spectroscopy techniques such as Electro Microprobe Analysis (EMPA), Position Sensitive Detector X-Ray Diffraction (PSD-XRD) and Visible/Near Infrared Red and Mid Infrared reflectance spectra.

2.5.2.1 RESULT OF THE LABORATORY ANALYSIS OF METEORITES

Report on publication based on the laboratory results measurement carried out on a suite of 15CM carbonaceous meteorites and one CI carbonaceous meteorites powder using bidirectional spectrometer in the Visible/Near Infrared (VIR-NIR) and Mid Infrared (MIR) band. The reflectance spectra of the meteorite sample were acquired at Brown University using NASA/Keck Reflectance laboratory (RELAB) facility. The result findings show the presence of a 0.7µm band in the meteorite sample, an indication of aqueous alteration. Due to the aqueous alteration reaction, the anhydrous phases of the carbonaceous chondrites (CC) meteorites transmute into hydrated phyllosilicates ranging in abundance from approximately 60 – 90vol. %. The asteroids that formed CM/CI meteorites were initially composed of anhydrous components chondrules and the matrix silicates; the chondrules are typically composed of Mg-rich olivine (forsterite), Fe-Ni metal and some glassy mesostasis and on the other hand, the matrix silicates tend to contain more Fe-rich olivine (fayalite) (McAdam, et al., 2015).

This study group attempt to determine the total phyllosilicate abundance in the CC meteorites powder using the Position Sensitive Detector X-Ray Diffration (PSD-XRD) techniques. 38 Samples of the CC meteorite were acquired, of which 10 belongs to the CR chondrite meteorite, 25 belongs to the CM chondrite meteorite and 3 belongs to the ungrouped CC meteorite family. The result findings among the CR and the CM CC meteorites clearly show depletion of mafic silicate (iron and magnesium rich silicate) and the resulting increase in the phyllosilicate abundance in the CM CC meteorites as the aqueous alteration rate increases (Howard, et al., 2015).

This research group study the progressive alterations of cronstedstite (iron rich phyllosilicate) to Mg-serpentine across the CM carbonaceous chondrites members. The chemical analysis of the CM CC meteorite was obtained using Cameca CAMEBAX electron microprobe at the NASA Johnson Space Center. The study group could establish the increasing aqueous alteration trend across the CM chondrite meteorites from Murchison-Bells < Pollen-Murray < Mighei <

Nogoya < Cold Bokkeveld. This alteration trend in the CM CC meteorite suggests a constant rate of production of new phyllosilicate relative to the mineralogical transition from cronstedstite to Mg- serpentine an indication of the depletion of iron rich cronstedtite to Mg rich serpentine in the production of new phyllosilicates compound (Browning, et al., 1996).

2.5.3 GROUND BASED DEEP SPACE NETWORK (DSN) REMOTE SENSING

To strengthen on the laboratory analysis findings and those of the inflight spectroscopy on the relationships between the meteorite and the asteroid, six publications related to the ground based DSN remote sensing were reviewed further to determine and establish a relationship between the asteroids and meteorites. All the six papers but one seems to agee with one another that the C-type asteroids are the presumed parents' bodies of carbonaceous chondrite and the commonents meteorites are Ivuna (CI) and Mighei chondrite (CM).

2.5.3.1 RESULT OF THE GROUNDS BASED DEEP SPACE NETWORK REMOTE SENSING

This research group carried out a DSN telescopic investigation of C-type asteroids dominated region in the main belt between 2.2 to 3.6AU, with an aim to study the aqueous alteration process, and to compare the spectra of these hydrous objects with those of CM2 carbonaceous chondrites meteorite. The data have been obtained during several observational runs at the Asiago Observatory with the 1.8m telescope and at ESO-Lasilla with the 1.5m telescope (Fornasier, et al., 1999). The result of the investigation seems to indicate that aqueous altered asteroids could be the parent's body of the CM2 meteorites, this result corroborate Vila's report of (1994), which has earlier revealed that a zone of the outer main belt seems to be dominated by objects which have undergone aqueous alteration process by liquid water which dissolved and produces materials like phyllosilicates, sulphates, oxides, carbonates, and hydroxides. The region dominated by these hydrated minerals fall between 2.6 and 3.5 AU and they essentially belong to the C, G, F and B complexes taxonomic classes (

Fornasier, et al., 1999).In the final analysis of the result findings, the research term has obtained visible spectroscopy of 34 asteroids belonging to C, G, B and P classes between 2.2AU and 3.9AU which revealed that more than 65% of the investigated asteroids show the presence of absorption bands due to aqueous alteration products (0.6, 0.7, and 0.8 – 0.9µm). A comparison of the observed hydrated asteroids with those of 7 members of the Murchison (CM2) carbonaceous chondrite meteorites, has revealed a good match (differences ≤ 3%) between the meteorites and most of the observed asteroids, suggesting that the hydrated asteroids might be the parent bodies of the CM2 meteorites (Fornasier, et al., 1999).

This research group carried out a study to establish the relationship between 22B-type asteroids spectra (assembled from 13 new object observations and 9 objects from the published literature) with meteorites spectra of 15,000 samples obtained from the NASA Reflectance Experiment Laboratory library (NASA-RELAB). The B-type asteroid spectra fall into 3 groups; the Pallas, Themis, and everything else as specified by the research group. The Pallas group object show a trend of analog from the CV, CO, CK meteorites groups, the Themis group object show a trend of analogs from the CI, CM, CR, CI-Unusual, and CM-Unusual meteorite corroborating the work of Hiroi et al. (1996) (Clark, et al., 2010). The B-type asteroids are consistent with CM, CI, and CM/CI Unusual carbonaceous chondrites. The Pallas group object are not consistent with the previous work, the Pallas group can be matched with CK, CO or CV meteorite (Clark, et al., 2010).

This research group carried out spectroscopy studies on Bennu asteroid (191955) 1999 RQ36 and compared them with variety of meteorite samples from all the major carbonaceous chondrite groups (CI, CM, CV, CO, CR, and CK) obtained from the NASA Reflectance Experiment Laboratory (NASA – RELAB) database. Their findings point to CI and CM as the most likely meteorites analog for RQ36 and CO and CR as the least likely meteorites. They further compare their studies with other B-type asteroids, RQ36 was discovered to be more like the Themis group B-types than the Pallas group B-types (Clark et al. 2010). RQ36

falls on the border between Pallas and Themis group asteroid spectral (Clark, et al., 2011). The asteroid 24 Themis was recently discovered to have water ice on the surface (Campins et al. (2010a) and Rivkin and Emely (2010).). In the final analysis of the result findings, the research term speculates that RQ36 may in fact be composed of CM1 like materials/minerals (Clark, et al., 2011)

This study compares 13 near infra-red (0.8 – 2.4µm) spectra of two primitive C complex asteroids broken into 7 Themis family members and 6 Veritas family members. The research finding shows that many of the Themis and Veritas family group object are a match to the CM2 carbonaceous chondrite which is consistent with the previous work (Fornsier et al., (1999), Clark et al., (2010). The researcher found a reasonable match between the asteroid spectra and the individual carbonaceous meteorites, also the spectra diversity between the Themis and the Veritas families is also present in the meteorite collections (Ziffer, et al., 2011) This study group carried out a study to determine the compositions and relationship with meteorites and the asteroids complexes, the study group obtained spectra for 17C and X complexes using NASA Infrared Telescope Facility (NASA - IRTF) and SpeX infrared spectrometer. The research team in their conclusion suggest that for the C complex kaolinite and montmorillonite are possible precursor phyllosilicates, they ruled out kaolinite because it suggests a nonchondritic precursor and has never been observed in chondrites. For the X complex, they suggest that precursor phyllosilicates were montmorillonite or serpentines, these minerals have been observed in CM chondrites (Ostrowski, et al., 2011).

2.5.4 NEW SAMPLE RETURN MISSIONS TO C-TYPE NEA

Other new sample return missions to NEA includes the Hayabusa spacecraft sample return mission to S-type NEA, Hayabusa 2 spacecraft mission to C-type NEA Ryugu and the OSIRIS-Rex a NASA spacecraft mission to a C-type NEA Bennu.

2.5.4.1 HAYABUSA SPACECRAFT SAMPLE RETURN MISSION TO S-TYPE NEA

In May 2003 the Japanese space agency (JAXA), launched a sample return mission spacecraft (Hayabusa spacecraft mission) to an S-type Apollo NEA 25143 Itokawa, aimed at characterizing its size, shape, rotation period and composition. The Near Infrared Spectral (NIRS) onboard the Japanese Hayabusa spacecraft obtained more than 80,000 spectra of asteroid Itokawa during mapping operations at the asteroid from September to November 2005. The spectral absorption band indicates that the surface of the asteroid has an olivine-rich mineral assemblage potentially like LL ordinary chondrites meteorites. The first spectrum from Itokawa was obtained by NIRS on 10/9/2005 at 50km from the asteroid. During the second mapping phase in October 2005, the spacecraft hovered at 3.5 to 7km above the asteroid (Fujiwara, et al., 2006). Itokawa was so small with a diameter of 500m, its gravity much weaker than Eros, based on the slight gravitational tug of Itokawa on Hayabusa, the mass was measured and used to calculate the bulk density of 1.9g/cm^3. OC meteorites have bulk densities of 3.5g/cm^3, so Itokawa is 40 – 50% pore space, translating into some rubble pile asteroids. Itokawa surfaces appear rugged and jumbled (Shepard, 2015).

2.5.4.2 HAYABUSA2 MISSION TO C-TYPE NEA RYUGU

Hayabusa2 is a JAXA sample return mission to a C-type NEA 1999 JU3 (Ryugu) a less than 1km diameter asteroid. The mission was lunched on 3rd March 2014 and has arrived the destination on the 27th June 2018, the mission has stayed at the target asteroid (Ryugu) for 18months. After touchdown and sample collection, the mission has since return to earth with the samples in the year 2020 (Yutchi, et al., 2019).

2.5.4.3 OSIRIS-REX MISSION TO B-TYPE NEA 101955 (BENNU)

OSIRIS-REx is a NASA sample return mission to a B-type NEA 101955 (Bennu), about 500m in size and roughly spherical. The mission was launched on 8th September 2016 and has arrived the destination in the year 2018 (NASA, 2019). The mission has successfully performed touch-and-go sample collection on 20th

October 2020 and has commenced earth return in March 2021, the mission is scheduled to deliver the sample return capsule (SRC) to earth on 24th September 2023 (NASA, 2019)

2.6 RESULT OF ASTEROID/METEORITE ANALYSIS

The overall result of the laboratory analysis of meteorite, the ground based remote sensing and the in - flight spectroscopy have consistently agreed with one another on the general postulation that the asteroids are the presumed parent's bodies of the meteorite, and the commonest meteorites are the CI and the CM Carbonaceous Chondrites Meteorite (CCM), dominated by the phyllosilicate minerals. CI and CM CCM are among the 8-carbonaceous chondrite group (CI, CM, CO, CV, CR, CH, CB, and CK) whose classification are based on their mineralogical and petrographic characteristic. They are believed to contain diverse mixture of minerals such as hydrated and anhydrous silicates, oxides, sulphides, and organic material (Edward, 2007).

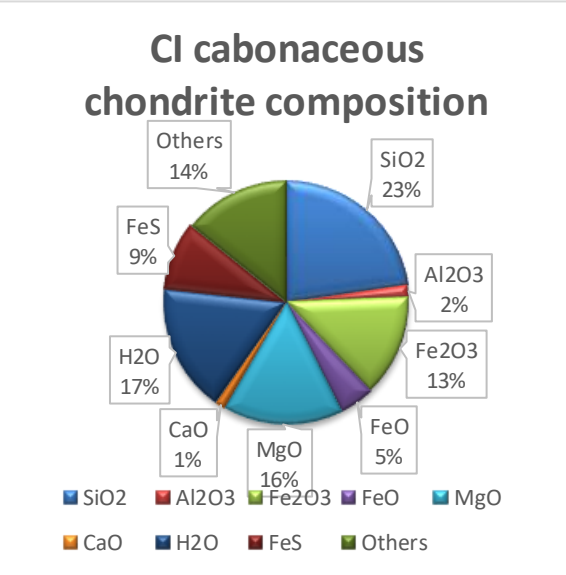
2.6.1 CI CARBONACEOUS CHONDRITE METEORITE

The CI group of carbonaceous chondrite meteorite are named after the Ivuna meteorites. All the CI chondrites are of petrologic type 1, indicating that they are heavily hydrated meteorites consisting of fine grained, phyllosilicate-rich matrix with minor magnetite, sulfides, sulfates, and carbonates, and rare isolated olivine and pyroxene fragments (Weisberg, et al., 2006). The CI chondrite meteorite are extremely fragile and highly susceptible to weathering and do not survive long on the earth surface after they fall. Orgueil and Ivuna are example of CI chondrites.

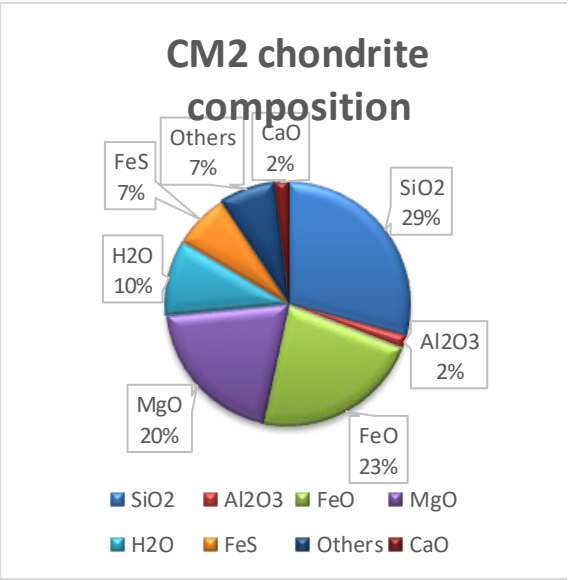
2.6.2 CM CARBONACEOUS CHODRITE METEORITE

The CM group of carbonaceous chodrite meteorite are named after the Mighei chondrite meteorite. All CM chondrite meteorite are type2 petrologic group, they experience extensive aqueous alteration, unlike the CI chondrite they retain recognisable chondrules and its matrix has un-altered olivine and/or pyroxene, with higher presence of magnetite and less sulphides (Eugene, 1990). Murchison and Mighei are example of CM chondrite.

This PhD research work is interested in the extraction of metal as primary product. The prevalence of metal oxide (Iron oxide) content in the CM2 CCM family, about 23vol% FeO as against CI CCM with about 5vol% FeO, the CM2 CCM have been selected as a preferred candidate for this research work. CM2 CCM is selected as the source of the resources for this research work. Chemical analysis of the carbonaceous chondrite CI CC and CM2 CCM showing the various mineral and the water content is as shown in the **Error! Reference source not found.**.



Orgueil CC meteorite (Braukmüller, et al., 2018)



Murchison CC meteorite (Braukmüller, et al., 2018)

Figure 2-5: Comparison of the mineral and water composition of CI and CM2

2.6.3 OVERVIEW OF ISRU TECHNOLGY

The general overview of the relevant ISRU technologies is presented in this section of the PhD research work towards identifying a suitable ISRU technology for its implementation in the context of the CubeSat ISRU payload.

ISRU technologies have been studied for several years to achieve the extraction of space resources. Literatures relevant to the ISRU technology such as Mars Oxygen ISRU Experiment (MOXIE) and Regolith and Environmental Science and Oxygen and Lunar Volatile Extraction (RESOLVE) payloads) has been identified and reviewed. Mars Oxygen ISRU Experiment (MOXIE) is the only ISRU process

flown in the Mars rover 2020 and presently, in the Mars environment, demonstrating the ISRU process for the production of oxygen using the Martian carbon dioxide via Solid Oxide Electrolysis process (SOXE) and the Regolith and Environmental Science and Oxygen and Lunar Volatile Extraction (RESOLVE) which is a demonstration of Lunar Resource Prospector Mission (LRPM) in a lunar analog at Hawaii on the slope of Mauna kea.

2.6.3.1 MARS OXYGEN ISRU EXPERIMENT (MOXIE) MARS 2020 INSTRUMENT

The MOXIE is one of the seven scientific instruments carried in the NASA Mars 2020 mission to demonstrate in situ production of oxygen from the Martian atmosphere, which contains approximately 95% carbon dioxide. The oxygen can be used to support the crew breathing needs and can also be used as fuel oxidizer for a Mars ascent vehicle. MOXIE uses a solid oxide electrolysis (SOXE) stack for converting carbon dioxide to oxygen (Gotame, 2020)

The SOXE stark consisted of a supported electrolyte cell, with thin printed electrodes that are coated with catalytic cathode on one side and an anode on the other. The carbon dioxide flows over the catalysed cathode surface under an applied electrical potential, a reaction occurs, and it is electrolyzed. The carbon monoxide is exhausted, and the oxygen ion electrochemically driven through the SOXE to an anode where it is oxidized. The oxygen atoms combined to produce the gaseous oxygen (Gotame, 2020)

Study has suggested that the MOXIE instrument can produce consumable grade (99.6%) oxygen at a rate of 20g/hr. On April 20, 2021, in the first operation, MOXIE produced about 5 grams oxygen from the carbon dioxide in the Martian atmosphere by using the SOXE equipment and this is equivalent to about 10 minutes' worth of breathable oxygen for an astronaut (NASA, 2021)

The MOXIE instrument for the Mars 2020 rover mission is as shown in Figure 2-6



Figure 2-6: MOXIE Instrument for the Mars 2020 rover mission from (Gotame, 2020)

2.6.3.2 RESOLVE PAYLOAD

RESOLVE is an acronym that stand for "Regolith and Environmental Science and Oxygen and Lunar Volatile Extraction" carried on a rover and designed as an analogue mission to demonstrate ISRU process on a terrestrial location on the slope of Mauna Kea which is identified based on their physical similarities with the lunar bodies. The payload is designed to find, extract, and process the resources available at the lunar poles. To achieve this mission objectives, the RESOLVE payload consists of several subsystems, such as the Neutron spectrometer and Near Infrared (NS-NIR) spectrometer, Oxygen and Volatile Extraction Node (OVEN) and the Lunar Advance Volatile Analysis (LAVA) (Paz, et al., 2013)

The rover system weight 260kg, the RESOLVE payload has a total mass of 150kg, it is 1.5m long and 1.6m wide with ground clearance of 0.13m. The rover solar array is the primary source of power to the system that are connected directly to the RESOLVE payload. Two rechargeable lithium-ion battery (2 x 48VDC) provide the on-board power. Each battery provides 2.57Kwh of energy, the total combined energy capacity of the battery system amount to 5.14Kwh (Paz, et al., 2013).

2.6.3.2.1 NEUTRON SPECTROMETER AND NEAR INFRARED SPECTROMETER (NS-NIR)

The NS-NIR constitutes the prospecting subsystems on the RESOLVE payload, they are to locate the volatiles and identify the minerals in the regolith. Once the location of interest has been identified the sample acquisition system are deployed (Paz, et al., 2013)

2.6.3.2.2 SAMPLE ACQUISITION SYSTEM (SAS)

The Sample Acquisition System incorporates an auger and a coring drill system. The auger performs evaluation of the regolith mechanics, and the coring drill is used to acquire one-meter core of the sample, which is then transferred to the Oxygen Volatile Extraction Node (OVEN) (Paz, et al., 2013)

2.6.3.2.3 OXYGEN VOLATILE EXTRACTION NODE (OVEN) SUBSYSTEM

The OVEN reactor received the sample and baked it to 423K to separate volatile of interest from the core sample. The released volatiles are sent to the Lunar Advanced Volatile Analysis (LAVA) subsystem for characterisation. Once the volatile characterisation portion of the experiment is complete, the OVEN subsystem can raise the temperature of the sample segment to more than 1173K in the presence of hydrogen gas (H_2) to extract oxygen from the iron oxide (Fe_2O_3) in the lunar regolith (Paz, et al., 2013). Water released from the volatiles or produced in the hydrogen reduction reaction can be further separated and imaged with the water droplet demonstration in the LAVA subsystem

2.6.3.2.4 LUNAR ADVANCED VOLATILE ANALYSIS (LAVA) SUBSYSTEM

The LAVA subsystem is the point where the volatiles are characterised, by identifying the type and quantity of volatile present. The characterisation of the volatile is achieved with the help of mass spectrometer and gas chromatograph (MS/GC). The mass spectrometer and gas chromatograph are designed to sense volatiles such as hydrogen, carbon, nitrogen, and compounds such as water, carbon monoxide, methane, or ammonia (Paz, et al., 2013). The image of the RESOLVE rover payload is as shown in Figure 2-7



Figure 2-7: RESOLVE rover payload from (ROOMSJA, 2016)

Several other well established Lunar ISRU methods namely, chemical reduction with Hydrogen, methane or carbon monoxide, vapour phase pyrolysis, sulphuric acid treatment, and molten oxide electrolysis have been studied for the extraction of Oxygen as the primary product and metal waste (Schwandt, et al., 2012). Due to the similarities in the mineral composition existing among both the lunar regolith and the asteroid regolith. In this research work, these identified and well established Lunar ISRU technologies, might be considered in Chapter 4 as baseline from among which to select the most convenient ISRU techniques for CubeSat implementation in the asteroid context to give priority to metal production as the primary product.

2.6.3.3 CHALLENGES ASSOCIATED WITH THE CURRENT ISRU TECHNOLOGIES

The current ISRU studies requires large mass, high power, they very expensive to implement with possible risk of failure and they take longer period to implement. For instance, the NASA-LRPM rover system targeted for launch in the year 2018; weight 260kg, has power requirement up to 5kw, might take 10 years or more toimplement and will consume about a quarter of a billion dollar to be implemented (space news, 2014). The CubeSat shall serve as a technology demonstration and de-risking payload with capability to cheaply perform the proof-of-concept demonstration of the ISRU technology on the potential C-type

NEA that then allows for investment that will lead to larger scale industrial implementation.

2.7 OVERVIEW OF CUBESAT TECHNOLOGY

In this section of the PhD research work the overview and the analysis of the CubeSat technology is presented.

The whole idea about the CubeSat stated in the year 1999 as a collaborative effort between Professor Jordi Puig – Suari of the California polytechnic state university (CalPoly) and Professor Bob Twigs of the Stanford university space systems development laboratory. The CubeSat project was started to provide a standard for design of picosatellites to reduce cost, mass and size, and also to have shorter development time, sustain frequent launches and increase accessibility to space as compared to the larger spacecraft mission (Heid H, et al., 2000). The current CubeSat performance is limited to volume, power, travel range within LEO, they are relatively cheaper to manufacture with a shorter development period as compared the conventional spacecraft. A Sample CubeSat is as shown in Figure 2-8

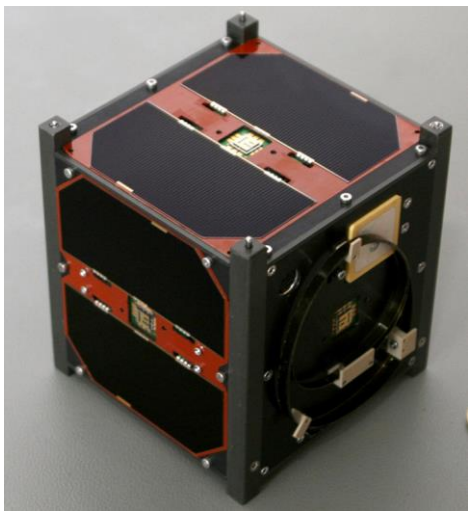


Figure 2-8: Sample 1U CubeSat from (Michalevsky & Winetraub, 2017)

The CubeSat is a subset of the Nanosatellites family with a mass range of 1 – 10kg; a standard unit (1U) has a volume of 1litre (10cm x 10cm x 10cm) with a corresponding mass up to 1.33kg. Depending on the design configurations,

CubeSat can be scaled up into higher form factor in the order 3U, 6U, 12U and up to 27U (Heid H, et al., 2000). The typical power budget of various CubeSat is size specific, for instance 1 – 2.5W for U, 2 – 5W for 2U and 7 – 20W for 3U CubeSat (Heidt H, et al., 2000).

As at the 12th December 2021 a total of 1766 CubeSat has been launched successfully (Nanosatsdatabase, 2022), the annual CubeSat launch distribution from 1999 to date is shown Figure 2-9

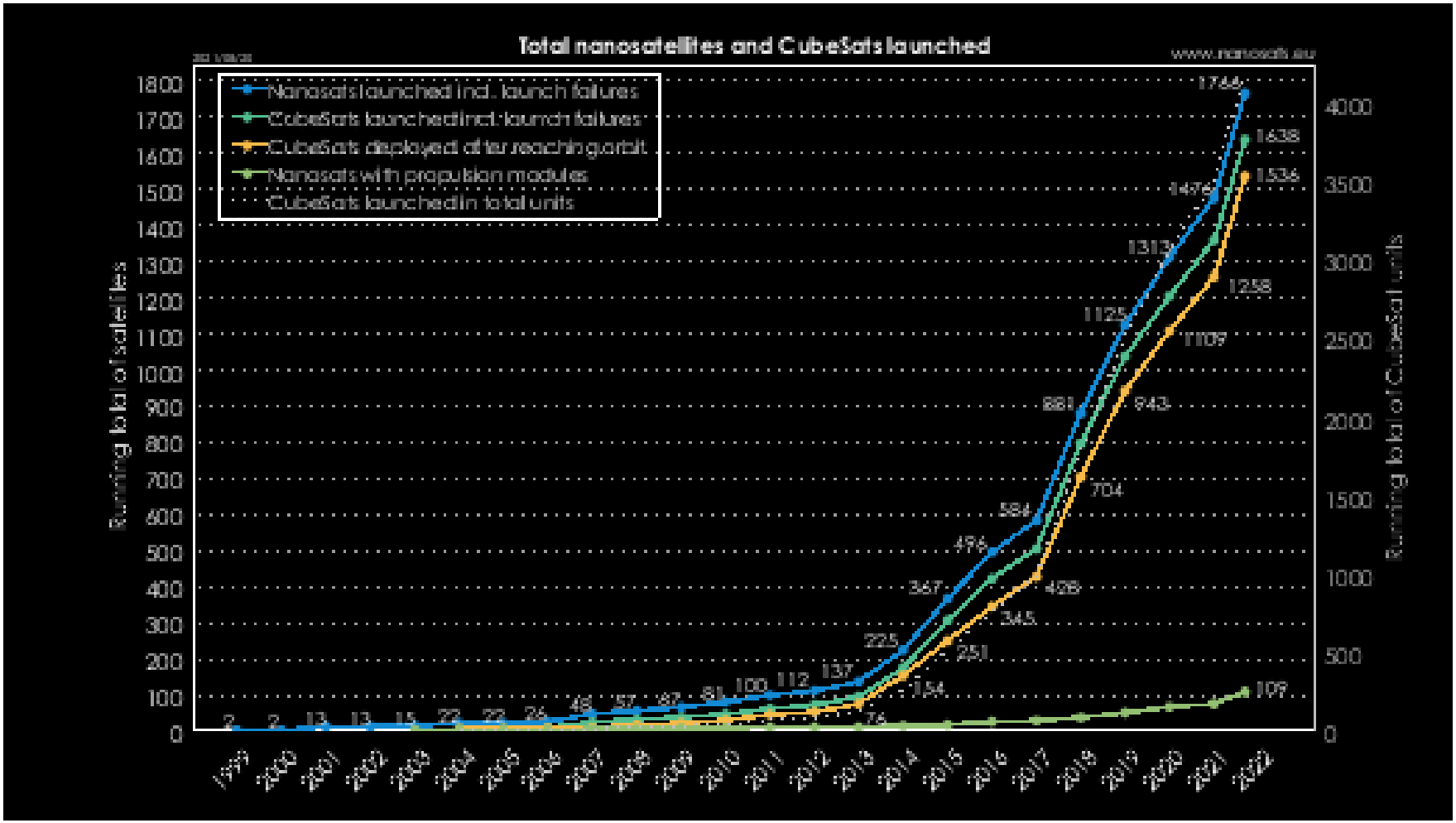


Figure 2-9: Showing the running total of nanosatellite and CubeSat launch from 1999 to date **(Nanosatsdatabase, 2022)**

2.7.1 CUBESAT RELEVANT TO INTERPLANETARY MISSIONS

In the past CubeSat has been limited to Low Earth Orbit (LEO) operations. Currently, the inclusion of spacecraft having the CubeSat specifications are planned in the next generation of interplanetary missions. Some of the successful CubeSat missions includes:

2.7.1.1 MARS CUBE ONE (MarCO)

MarCO is CubeSat mission developed by NASA-JPL and accompanied the InSight (Interior Exploration using Seismic Investigations, Geodesy and Heat Transport) Mar's mission lander in 2018 as a secondary payload. The primary objective of the mission is to autonomously fly to Mars to monitor the InSight lander Entry, Descent, and Landing (EDL) phase and transmit the status information about the main spacecraft after it lands on Mars to the earth (Schoolcraft, et al., 2016). MarCO is a 6U and twin spacecraft built on the heritage of Interplanetary Nano-Spacecraft Pathfinder in Relevant Environment (INSPIRE). The twins CubeSat payload have successfully completed their missions on November 26, 2018 (NASA, n.d.).

2.7.1.2 BIO-SENTINEL CUBESAT

Bio-sentinel is one of 10 low-cost CubeSats mission selected as secondary payloads that will be launched aboard Artemis I formally Explorer Mission One (EM-1). The primary objectives of the mission are to develop a biosensor that will be used to detect and measure the impact of space radiation to living organisms over an extended period in deep space environment (Lewis, et al., 2014). The mission having completed assembly and battery testing gets a step closer to flight (NASA, 2021)

2.7.1.3 HERA-EUROPEAN SPACE AGENCY (ESA) MISSION MINIATURE CUBESATS

The Hera - ESA mission along with NASA's Double Asteroid Redirect Test (DART) spacecraft in an international planetary defence collaboration called the Asteroid Impact & Deflection Assessment (AIDA). The AIDA aimed to assess the feasibility of deflecting the heliocentric path of an NEA binary system (Ferrari, et al., 2015). NASA-DART is the mission impactor, and the Hera-ESA is the mission

observer. The NASA-DART spacecraft launched in July 2021 will perform a kinetic impact on the smaller asteroid (Dimorphos) of the binary asteroids in September 2022 is expected to alter its orbit around Didymos as well as create a substantial crater (ESA, n.d.). The Hera-ESA mission is due to be launched in October 2024, Hera will travel to a binary NEA pair and deploy miniature CubeSats for a detailed post-impact survey to gather crucial scientific data to help scientists and future mission planners better understand asteroid compositions and structures (ESA, n.d.).

2.7.2 RESULT OF THE LITERATURE REVIEW BASED ON CUBESAT TECHNOLOGY

The outcome of the literature survey based on the CubeSat technology, relevant interplanetary CubeSat mission such as (MarCO, HERA-ESA etc.) have emerged. The miniaturisation of MOXIE payload to occupy a small volume of (23.9 cm x 23.9 cm x 23.9 cm) with a corresponding mass of 15 Kg (Hoffman, et al., 2015) is an indication that the development of a much small-sized ISRU demonstrator payload in the CubeSat form factor is feasible. This project will consider the design and manufacture of an ISRU-CubeSat compatible payload in a maximum of 6U form factor to harness regolith material for metal extraction. The CubeSat limitation (power and volume) are considered as the design driver for this project implementation.

2.7.3 OVERALL SUMMARY OF THE LITERATURE REVIEW

The overall summary of the literature reviewed is presented in this section.
In terms of asteroid as the potential destination for the demonstration of the ISRU process and using a CubeSat form factor:

- The knowledge relevant to the physical characteristic, orbital parameters and trajectory information of the NEA has been sought and will be used in the future section of this thesis document toward the selection of a potential C-type NEA.
- The knowledge of the asteroid mineral composition has been sought and the relationship between the asteroid and the meteorite was confirmed.

Reviewed literature on the analysis of meteorite has further confirmed the postulation that the C-type NEAs are the presumed parent body meteorite and CI and CM CCM are confirmed to be the commonest meteorite

- Since the PhD is about the extraction of metal for infrastructure development In Situ, higher presence of FeO about 23vol% in the CM CCM as compared to CI CCM has informed the choice of CM2 CCM as the preferred candidate material.

In terms of ISRU technology as the process for demonstration on the destination C-type NEA and using a CubeSat form factor:

- General knowledge of the existing ISRU processes has been sought
- MOXIE appears to be the only miniaturised ISRU demonstration payload currently available and operational in Mars to harness the Martian atmosphere.
- So far performing miniaturised ISRU process using the regolith material from asteroid to extract metal appears to be non-existing and hence these studies.
- Other matured ISRU studies surveyed based on the extraction of oxygen as the primary product and metal waste from the Lunar regolith.
- Similarities in the mineral composition existing among both the lunar regolith and the asteroid regolith has prompted the selection of these matured Lunar ISRU processes as potential ISRU process implementable in the CubeSat form factor for metal extraction using the asteroid regolith.

In terms of using the CubeSat form factor as the technology for demonstration on the destination C-type NEA:

- General knowledge of the existing CubeSat technology (both LEO and interplanetary) has been sought
- Power and volume were identified as the design limitations for the interplanetary CubeSat implementation and will be considered during the design and manufacture of the ISRU based CubeSat
- Miniaturisation of MOXIE designed to occupy a small volume of (23.9 cm x 23.9 cm x 23.9 cm) with a corresponding mass of 15 Kg is an indication

that the development of a much small-sized ISRU demonstrator payload in the CubeSat form factor is feasible.

- The small-sized ISRU demonstration CubeSat payload is intended to be accommodated in a maximum of 6U form factor with corresponding mass equivalent to approximately 9 Kg.

2.9 CONCLUSION

The literature review on the three components that entails the PhD research work (the asteroid, ISRU technology and inter-planetary CubeSat technology) has been concluded.

- The relationship between C-type asteroids to the carbonaceous chondrite (CC) meteorite has been established, the general postulation that the C-type NEA asteroids are the presumed parent's bodies of the meteorite, and the commonest meteorites are the CI and the CM CC meteorite. CM2 CC meteorite is selected as the source of the resources for this research work.
- Several well established Lunar ISRU methods has been identified and due to their similarities in the mineral composition with the asteroid regolith. The well-established Lunar ISRU technologies, might be considered as baseline techniques from among which to select the most convenient ISRU techniques for CubeSat implementation in the asteroid context to give priority to metal production as the primary product.
- The miniaturisation of MOXIE payload to occupy a small volume of (23.9 cm x 23.9 cm x 23.9 cm) with a corresponding mass of 15 Kg has made the development of a much small-sized ISRU demonstrator payload in the CubeSat form factor is feasible. The CubeSat limitation (power and volume) are considered as the design driver for this project implementation.

All the information's obtained in this chapter will form the basis for developing the project background and subsequently, tailoring the choice of an ISRU process that can be demonstrated on a C-type NEA that will be compatible with the

interplanetary CubeSat technology. In the coming two chapters a trade studies will be conducted on the different types ISRU technology and the possible destination C-type NEA asteroids identified and toward down selecting one or two potential ISRU process and potential C-type NEA destination.

3 C-TYPE NEA DOWN SELECTION PROCESS

3.1 INTRODUCTION

In the previous chapter an overview of the potential destination, the ISRU process and the CubeSat technology was presented. It is pertinent, therefore, to select a destination for ISRU demonstration that is compatible for CubeSats performance and limitations before implementing the payload design. In this section the C-type NEA down selection process was carried out/achieved through a trade-off study method. Selecting and justifying the choice of suitable C-type NEA candidate for this PhD research work; the scientific importance of the candidate asteroids, the design considerations and including the CubeSat constraint are the components considered to derive the C-type NEA requirement. These NEA requirements are defined and must be reasonably satisfied by the potential candidate asteroid. Following the selection of the location for the ISRU process demonstration, chapter 4 will focus on the ISRU process selection that is CubeSat compatible.

3.2 REASON FOR SELECTING THE C-TYPE NEA FAMILY AS POTENTIAL DESTINATION FOR DEMOSTRATION OF THE ISRU PROCESS

Several reasons for selecting the C-type NEA Family as the potential destination for demonstrating the ISRU process was introduced in section 2.3.5.3.2. The C-type NEA relative to their location within the solar system, they appear to be the best option for the CubeSat mission. The C-type NEA stay closer to both the Earth and the Sun compared to the Trojan and the MB asteroids. The missions duration to reach the NEA resident within <1.3 AU compared to the Trojan or MB asteroid resident within a maximum of 5.35 and 3.2 AU respectively is small, a low delta-V is required to reach them. A maximum of 2.5 Kms^{-1} low thrust delta-V is required to land on the NEA as against 7.6 Kms^{-1} and 8 – 10 Kms^{-1} high thrust delta-V to land on the Trojan and MB asteroid respectively (Carroll, 2017). The C-type NEA is also endowed with abundant resources that include hydrocarbon, volatiles, and metals among others and these will trigger flight opportunities to the C-type NEA (Zacny, et al., 2013)+. Fewer rendezvous missions to NEA that have been accomplished include NEAR Shoemaker a

NASA mission to NEA Eros an S-type NEA, Hayabusa1 JAXA sample return mission to S-type NEA and the recently concluded sample return missions to C-type NEA Bennu and Ryugu respectively tagged Osiris-Rex and Hayabusa2 missions.

3.3 REQUIREMENT FOR SELECTING POTENTIAL C-TYPE NEA

Towards selecting the potential C-type NEA candidate for the mission, the defined requirements shall be reasonably satisfied by each of the potential candidate C-type NEA in the selection process.

3.3.1 C-TYPE-NEA_R1 (ASTEROID SIZE IN TERMS OF DIAMETER)

Asteroid with diameter greater than 200m are ideal for exploration, their spin rates are low compared to the smaller asteroid with diameter far <200m (Chang, et al., 2017). The asteroid due to smaller diameter <200m, they spin so rapidly and in the context of the CubeSat spacecraft it is difficult to match the rotation of a rapidly rotating asteroid with a CubeSat spacecraft, making landing on the asteroid very challenging. The C-type NEA diameter size to be considered shall fall in the range of greater than (>) 200m and less than or equal to () 1000

3.3.2 C-TYPE-NEA_R2 (PROJECTED PROFIT DUE TO MINERAL ABUNDANCE)

Due to the abundant resources on the C-type NEA, a projection was made in respect of the profit against the initial value of the resources available in the C-type NEA. The C-type NEA that record the highest profit will take the lead and will be recorded higher scores.

3.3.3 C-TYPE-NEA_R3 (C-TYPE NEA NEXT CLOSE APPROACH)

This is the point at which the C-type NEA come closest to the earth. The concept of close approach brings the C-type NEA closer to the earth, creating a launch opportunity such that the distance covered by the spacecraft to rendezvous with the asteroid is shorten. All C-type NEA with the closest approach to earth that fall

within the range below 0.1AU are convenient for the mission and will attract the highest score.

3.3.4 C-TYPE-NEA_R4 (SEMI MAJOR AXIS (SMA))

This is the average of the summation of the longest distance (Aphelion) and the shortest distance (Perihelion) of a planetary body away from the Sun (Kambezidis, 2012). The semi-major axis of the earth is 1AU approximately 150million Km from the sun (Kambezidis, 2012). The C-type NEA with semi major axis equal to or below 1.3AU is chosen. Considering the concept of inverse law, the solar irradiation is inversely proportional to the square of the distance from the sun to the target planetary body within the solar system (Martins, 2017). For instance, beyond the 1.3AU, the reduce solar irradiation will significantly influence the CubeSat power subsystem. C-type NEA with semi major axis equal to or below 1.3AU will attract the highest score.

3.4 OBSERVATIONAL DATABASES AS INFORMATION SOURCE FOR C-TYPE NEA SELECTION

As of the 7th March 2017, 15764 NEA were discovered including (Amor, Aten, Apollo and Atira) from observational databases. Refer to section 2.1.1 of the literature review section, several NEA databases have been compiled and reviewed; these databases are considered as the sources for populating the candidate C-type NEA. A combination of the NHATS database and the Asterank database were considered for the selection of Potential C-type NEA. The NHATS database, it is interactive in terms of the information search, they provide the physical and orbital characteristics of the NEA which are not provided using the Asterank database. The Asterank database was given preference over the NEODyS-2 database, it contains detailed information about the total delta-V, launch date, flight duration and calculated trajectory. Using the combined databases (NHATS and the Asterank) the NEA physical characteristics such as (diameter, absolute magnitude, and the gravity well), trajectory data including the (delta-V and launch date and next close approach) and the orbital parameters which include (semi-major axis, eccentricity, inclination, and orbital period) are generated for the potential C-type NEA and are used in the selection process.

Figure 3-1 below shows the distribution of the NEA discovered from the observational databases as of the 7th March 2017.

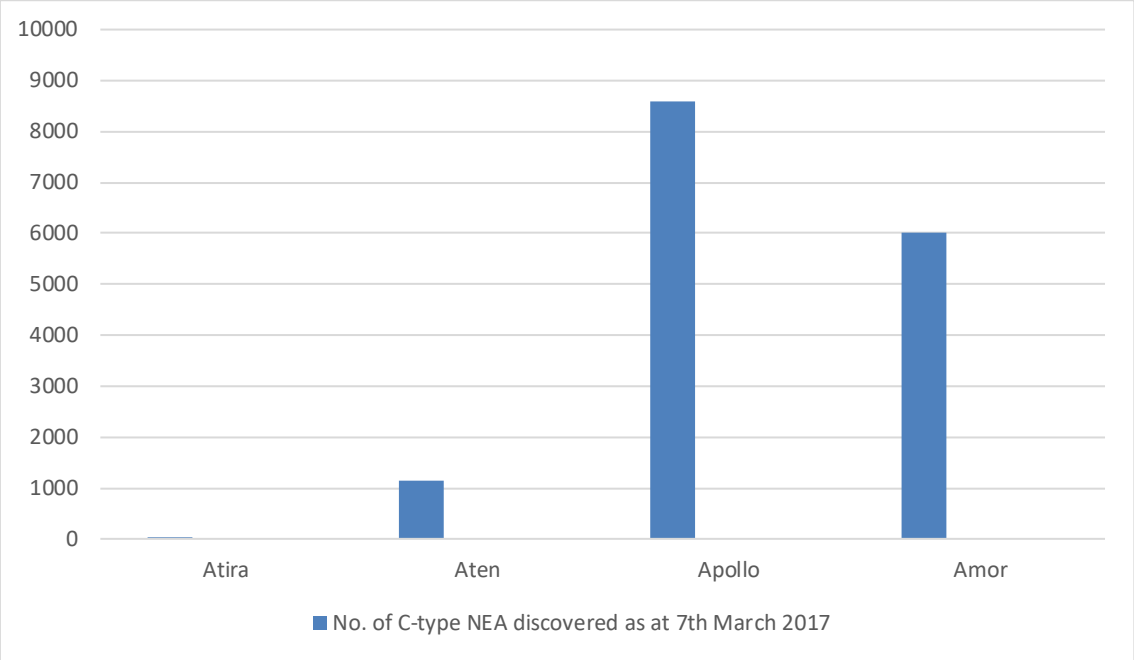


Figure 3-1: Chart showing the distribution of NEA discovered as of 7th March 2017

Out of the 15764 NEA discovered as distributed in Figure 3-1, only 314 NEAs have been classified at the time and only 9% of the classified NEAs translating to 28 are C-type NEA. This is largely because the C-type Asteroid generally has the lowest albedo, they are hard to discover, they are only observable during close approaches to Earth. Out of the 28 C-type NEA classified and based on the identified requirement only 20 selected potential C-type NEA are presented in Table 3-1.

Table 3-1: Summary of potential candidate C-type NEA based on their physical, Engineering and Economic values

Asteroid Name/Designation	Type	Albedo	diameter (km)	Apelion (AU)	Perihelion (AU)	Semi major axis (AU)	Earth proximity (AU)	Next close Approach (AU)	Next close Approch date	Eccentricity (e)	Value ($)	Estimated profit ($)	Comments
(101955) Bennu	B	0.05	0.48	1.3554	0.8967	1.1261	0.1261	0.0987	2/11/2037	0.2037	9.05B	2.50B	OSIRIS Rex mission intended to return sample to earth in 2023 for analysis
(10302) 1989ML	C (E)	0.51	0.25	1.4456	1.0987	1.2722	0.2722	0.0995	2/7/2022	0.1364	13.94B	4.38B	
(136793) 1997AQ18	C	TBD	1.20	1.6808	0.6133	1.1471	0.1471	0.1882	14/12/2050	0.4653	286.95B	25.10B	
(162173) Ryugu 1999 JU3	C	0.05	0.87	1.4158	0.9633	1.1896	0.1896	0.0605	29/12/2020	0.1902	82.76B	30.08B	Hayabusa2 mission intended to return sample to earth in 2020 for analysis
(175706) 1996FG3	Ch	0.04	2.34	1.4227	0.6853	1.0540	0.0540	0.0783	3/5/2022	0.3498	1.33T	181.33B	
(276049) 2002CE26	C	0.03	3.33	3.4852	0.9808	2.2330	1.2330	0.1793	11/9/2024	0.5608	33.39T	1.70T	
(285263) 1998QE2	Ch	0.06	2.70	3.8090	1.0376	2.4233	1.4233	0.0392	31/5/2013	0.5718	TBD	TBD	
(308635) 2005YU55	C	0.07	0.31	1.6552	0.6590	1.1571	0.1571	0.1214	31/10/2036	0.4305	49.84B	6.23B	
(341843) 2008EV5	C (X)	0.10	0.40	1.0383	0.8783	0.9583	-0.0417	0.0423	20/12/2023	0.0835	11.2B	1.20B	
(4660) Nereus	C (E)	0.39	TBD	2.0246	0.9527	1.4887	0.4887	0.0263	11/12/2021	0.3600	4.71B	1.39B	
(52381) 1993HA	TBD	0.14	0.34	1.4625	1.0942	1.2784	0.2784	0.1697	19/11/2028	0.1441	TBD	TBD	
(5496) 1973NA	C (X)	TBD	3.40	3.9838	0.8865	2.4352	1.4352	0.1523	26/6/1992	0.6360	TBD	TBD	
(65679) 1989UQ	C (B)	0.06	0.72	1.1574	0.6728	0.9151	-0.0849	0.1559	15/10/2024	0.2647	TBD	TBD	
(7350) 1993VA	C(X)	0.05	2.36	1.8862	0.8257	1.3560	0.3560	0.1294	14/11/2023	0.3911	TBD	TBD	
(85989) 1999 JD6	Cg	0.08	1.84	1.4419	0.3242	0.8831	-0.1170	0.1308	20/7/2020	0.6328	TBD	TBD	

Asteroid Name/Designation	Type	Albedo	diameter (km)	Apelion (AU)	Perihelion (AU)	Semi major axis (AU)	Earth proximity (AU)	Next close Approach (AU)	Next close Approch date	Eccentricity (e)	Value ($)	Estimated profit ($)	Comments
1999SF10	TBD	TBD	0.06	1.6015	0.9549	1.2782	0.2782	0.0210	10/12/2025	0.2529	TBD	TBD	
2007EF	C	0.07	0.26	1.1567	0.4839	0.8203	-0.1797	0.1380	4/3/2033	0.4101	TBD	TBD	
2009UX17	C	0.01	0.54	1.2883	1.0900	1.1892	0.1892	0.1985	6/12/2022	0.0834	TBD	TBD	
2009UY19	C	0.06	0.11	1.0551	0.9921	1.0236	0.0236	0.0760	2/11/2038	0.0308	TBD	TBD	
3200 Phaethon	B	0.11	5.10	2.4025	0.1399	1.2712	0.2712	0.0826	11/12/2050	0.8899	100T	5.30T	

3.5 FILTERING PROCESS TO REDUCE THE POTENTIAL C-TYPE NEA

From the 20 potential C-type NEA listed in Table 3-1, four filters generated in section 3.3 were applied to reduce the possible C-type NEA contenders. The four filters listed below are applied to ensures that the C-type NEA meet the requirement defined in Section 3.2.

Filter 1: The minimum diameter ≥ 200m, this filter is determined by the spin rate of the target body for the demostration of the ISRU process. Asteroid with smaller diameter <200m, they spin so rapidly and in the context of the CubeSat spacecraft it is difficult to match the rotation of a rapidly rotating asteroid with a CubeSat spacecraft during landing/touchdown. Filter 2: Semi major axis ≤ 1.3AU, this filter is determined by the distance from the sun to the target planetary body within the solar system. The distance beyond the 1.3AU, the reduce solar irradiation will significantly influence the CubeSat power subsystem and also the duration a given astronomical object takes to completes one orbit around another object

Filter 3: projected profit, this filter is determined due to the abundance of valuable resources on the potential destination which can project the value of the resources contained therein and the projected profit. For instance, a 7m C-type NEA weighing approximately 500 tonnes may contain up to 200 tonnes of volatiles such as water and carbon rich compounds (100 tonnes each), 90 tonnes of metals (83 tonnes iron, 6 tonnes nickel and 1 tonne cobalt) and 200 tonnes of silicate residue

Filter 4: Next close approach ≤ 0.1AU, this filter is determined by how closest the potential body is to the Earth. This scenario creates a launch opportunity such that the distance covered by the spacecraft to rendezvous with the asteroid is shorten.

The C-type NEA presented in Table 3-1, they are subjected to initial filtering process to satisfy the outlined requirement in Section 3.2. 20 C-type NEA are reduced to five and they include C-type NEA 101955 Bennu, 162173 Ryugu JU3,

2008EV5, (10302) 1989ML and 2005YU55, they all pass the five of the initial filters, they are carried forward as shown in Table 3-2 for further trade-off.

Table 3-2: Reduced potential C-type NEA for demonstration of the ISRU process

C-type NEA name	C-type NEA type	Semi major axis (AU)	Next closest approach (AU)	Diameter in (m)	Projected profit ($)
Ryugu	C	1.1819	0.0605	870	30.08B
Bennu	B	1.1261	0.0987	480	2.5B
1989ML	C	1.2722	0.995	250	4.38B
2005 YU55	C	1.1571	0.114	310	6.23B
2008 EV5	C_x	0.9583	0.0423	400	1.2B

The reduced potential C-type NEA as presented in Table 3-2, they meet a combination of the following requirement

- All the identified C-type NEA have orbital period below 500days corresponding to 1.37 earth years. Considering the operational lifetime of the CubeSat components between 2-3years, C-type NEA with orbital period equal to or below 2 years will be appropriate for the mission.
- All the identified C-type NEA have semi major axis below 1.3AU. Beyond the 1.3AU and due to reduced solar irradiation the CubeSat power subsystem will be affected.
- All the identified C-type NEA have diameters greater than 200m. Those with diameter >200m have minimal spin rate and those <1000m are expected to maintain relatively low gravity field.
- All the identified C-type NEA appears to have next close approach distances (AU) <0.1AU. The concept of close approach brings the C-type NEA closer to the earth such that the distance covered by the spacecraft to rendezvous with the asteroid is shorten
- All the identified C-type NEA they all have recorded level of projected profit

- All the identified C-type NEA they seem to belong to different C-type complexes (Thelon and SMASS)

The five identified potential C-type NEA presented in Table 3-2, they are observed to share different values in terms of their surface semi major axis, next close approach, projected profit, and the diameter size. In performing the trade-off studies over the selected criteria some range of scores are defined and allocated to the potential C-type NEA based on these different values.

3.6 TRADE-OFF STUDY TO SELECT THE C-TYPE NEA AS A PRIMARY TARGET

Four parameters namely, SMA, NCA, asteroid diameter and the projected profit as presented in Table **3**-**2** are considered for doing the trade-off study to determine the potential C-type NEA as the primary target for the demonstration of the ISRU process. Each parameter is scored using a certain scale (from 1 – 5). Where 5 represent the highest scale for the most preferred case and 1 represent the least scale for the least preferred case.

3.6.1 WEIGHTING AND SCALING OF PARAMETER

The CubeSat payload is required to land on the surface of the destination C-type NEA and safely secured to perform the ISRU processes. Parameters such as the asteroid diameter that influences the asteroid spin rate is the most important parameter. The Semi Major Axis (SMA) and the Next Close Approach (NCA) that influences ease of access to the destination asteroid are the second most important parameters toward achieving the safe and secured landing on the destination asteroid. The least important parameter is the projected profit. The projected profit is considered the least important parameter because it is only achievable when an ISRU process was successfully performed. The success of the ISRU process hinges on a safe and secured landing. Based on this analysis, the weighting and scaling of each parameter is presented in Table 3-3. The values for each potential C-type NEA presented in Table **3**-**2** are converted to a measurable scale for the trade-off study as presented in Table 3-3

The asteroid diameter influences the asteroid spin rate, high spin rate is attributed to planetary bodies with diameter much <200m and will affect a safe and secured landing on the potential C-type NEA using the CubeSat payload. Those asteroid with diameter >200m has lower spin rate are less complicated at landing Therefore, the asteroid with higher diameter they score higher (5) and those with lower diameter they score the least (1), while the remaining are scored in-between 1 – 5.

Destination C-type NEA with lower SMA in Astronomic Unit (AU) have shorter distance to arrive at and they score higher (5) and those with higher SMA have longer distance to arrive at and they score the least value (1) while the remaining are scored in-between 1 – 5.

Destination asteroid with shorter NCA in AU have shorter distance to arrive at and they score higher (5) and those with higher NCA in AU have longer distance to arrive at and they score the least value (1) while the remaining are scored in-between 1 – 5.

Destination asteroid with higher profit is score higher (5) and those with lower profit they score least valure (1) while the remaining are scored in-between 1 – 5.

Table 3-3: Parameter weighting scaling that will be used used for the trade-off study of the potential locations

Parameters	Weighting of parameters (%)	Parameter scaling
Asteroid diameter	30% (0.3)	Least Asteroid diameter= 1
		Most Asteroid diameter = 5
Semi-major axis	25% (0.25)	Least SMA = 5
		Most SMA = 1
Next close approach	25% (0.25)	Least NCA = 5
		Most NCA = 1
Projected profit	20% (0.2)	Most profit = 5
		Least profit = 1
Total	100%	

3.6.2 SCORING OF THE RAW RESULT AND THE TRADE-OFF STUDIES RESULT INCLUDING THE WEIGTHING

The result of the raw scoring for the potential locations based on the scaling in the range of 1 – 5 is presented Table 3-4

Table 3-4: Raw scoring result for the potential C-type NEA

Parameter	Ryugu	Bennu	2005YU55	2008EV5	1989ML
Diameter	4	3	2	2	1
SMA	2	3	2	5	1
NCA	4	3	1	5	3
Profit	5	1	2	1	1

The overall trade-off studies based on the scaling and weighting value of each of the parameters is presented in Table 3-5

Table 3-5: Overall result of the trade-off study

Parameter	Weight (%)	Scale	Ryugu	Bennu	2005YU55	2008EV5	1989ML
Diameter	30	1	24	18	12	12	6
		5					
SMA	25	1	10	15	10	25	5
		5					
NCA	25	1	20	15	5	25	15
		5					
Profit	20	1	20	4	8	4	4
		5					
Total	100		74	52	35	66	30

The raw scoring and the overall result of the trade-off studies are presented in Table 3-5 and Table 3-5 respectively, from the results it is obvious C-type NEA Ryugu has emerged the prepared candidate for the mission with C-type NEA 2008EV5 and Bennu emerging as the second and third best alternatives respectively.

C-type NEA Ryugu, 2008EV5 and Bennu, they emerged the first, second and third in the trade-off studies. In terms of proximity to Earth, the most accessible C-type NEA is the 2008EV5, it has the least semi-major axis (SMA) of 0.9583AU as compared to the Ryugu and Bennu each having SMA of 1.1261AU and 1.1819AU respectively. In terms of economic value and projected profit, Ryugu is the highest with an estimated value of 82.76B and profit of 30.08B, followed by

Bennu and 2008EV5 each with 2.5B and 1.2B profit respectively. Ryugu and Bennu share the same albedo value of 0.05 and they belong to the same Tholen C-type group each as against 2008EV5 with an albedo value of 0.07 and belonging to C_x group; the lower albedo is an indication that Ryugu and Bennu are more pristine and are likely to contain more valuable materials. In terms of size (diameter), Ryugu is the largest of the five C-type NEA considered and followed by Bennu and then 2008EV5. Missions to both Ryugu and Bennu are earth samples return missions, Hayabusa2 mission has long returned the Ryugu samples to Earth in late 2020 and the OSIRIS REx mission is expected to return the Bennu samples to Earth in 2023. The Earth samples return missions will provide the ground truth information about the composition of Ryugu and Bennu asteroid, and richer data set will be obtained that will further strengthen their choice. In spites of the fact that 2008EV5 has outperformed Bennu C-type NEA in the trade-off studies and has emerged as the second-best target destination for the demonstration of the ISRU process. Bennu with lower albedo, larger diameter, has more profit and is an Earth sample return mission as against the second best alternative 2008EV5, preference is given to Bennu C-type NEA to occupy the second position and 2008EV5 as the third-best alternative. The new order of the ranking is Ryugu, Bennu and 2008EV5 as the first, second and third respectively.

3.7 SENSITIVITY ANALYSIS

The trade-off studies have been performed and the potential destination for the demonstration of the ISRU process using the CubeSat base payload system was established. To validate the process selection order's ranking that results from the trade-off studies a sensitivity Analysis is performed. A small change that does not alter the scale significantly is performed on the numerical scores or the defined weight factors to observe the overall effect of these changes to the ranking order. If the sensitivity check reveals that small changes could significantly reverse a decision, the decision process must be adjusted to its insensitive state. To ensure the robustness of the selected process obtained through the trade-off studies carried out, three methodologies are applied; these methods include:

3.7.1 MAKING THE WEIGHTING VALUE ORDER USED IN THE TRADE-OFF STUDIES UNIFORM

In this methodology, all weighting values are set to a uniform value, assuming 25 for each of the parameter under the processes and resulting in 100 total weighting values. Applying these new changes, the scoring order is consistent with result of the trade-off studies, and the differences are in-significant. Applying a uniform score across the parameters. C-type NEA Ryugu recorded the highest score of 75%, followed by 2008EV5 with 65% and the third position was occupied by Bennu with 50%, then 2005YU55 with 35% and finally 1989ML with 30%. Presented in

Table 3-6 is a comparison of the trade-off studies result and those of the sensitivity analysis carried based on making the weighting value order used in the trade-off studies uniform.

Table 3-6: Comparing the result of the sensitivity analysis by making the weighting value order uniform to those of the original result based on initial trade-off studies

Potential C-type NEA	**Ryugu overall scores in %**	**Bennu overall scores in %**	**2005YU55 overall scores in %**	**2008EV5 overall scores in %**	**1989ML overall scores in %**
Original result based on the initial trade-off studies	74.00	52.00	35.00	66.00	30.00
Scores due to uniform weighted value for each parameter	75.00	50.00	35.00	65.00	30.00

3.7.2 A SMALL INCREASE TO THE SCORES LESS THAN 10% OF THE ORIGINAL SCORED VALUES FOR EACH OF THE POTENTIAL

C-TYPE NEA EXCLUDING THE HIGHEST AND THE LOWEST SCORE

A small increase in the scored values for the trade-off studies parameters less than 10% and excluding the highest and lowest score has been implemented to observe how those small changes will affect the ranking order of the trade-off studies result. The implementation of the small changes is in step order of 1% through 10% for each of the scored value for the initial trade-off studies excluding the highest and lowest score. Presented in Table 3-7 is the comparison of the trade-off studies result and those of the sensitivity analysis carried based a small increase to the scores less than 10% of the of the original scored values for each of the potential C-type NEA excluding highest and lowest score. The order of the scoring with range of the changes between 1 – 10% remain consistent, C-type NEA Ryugu still remain in the lead, followed by C-type NEA 2008EV5 in the second position and the C-type NEA Bennu maintaining the third position. The margin across all the winning alternatives is insignificant, below 1% of the total score for each of the alternatives with a 1% increase. As the order of the small changes below 10% continue to increase the overall new scores increase for each of the potential C-type NEA as illustrated in Table 3-7.

Table 3-7: Present a comparison of the result of the sensitivity analysis based on small increase to the scores less than 10% of the original scored values to those of the original result based on initial trade-off studies

Potential C-type NEA	Ryugu overall scores in %	Bennu overall scores in %	2005YU5 overall scores in %	2008EV5 overall scores in %	1989ML overall scores in %
Original result based on the initial trade-off studies	74.00	52.00	35.00	66.00	30.00
A small increase to the scores less than 10% of the of the original scored values for each of the potential C-type NEA excluding highest and lowest score					
5% small change	76.70	54.4	36.50	66.60	30.75
4% small change	76.16	53.92	36.20	66.48	30.60
3% small change	75.62	53.44	35.90	66.36	30.45
2% small change	75.08	52.96	35.60	66.24	30.30
1% small change	74.54	52.48	35.30	66.12	30.15

3.7.3 A SMALL INCREASE TO THE SCORES LESS THAN 10% OF THE ORIGINAL SCORED VALUES FOR EACH OF THE POTENTIAL C-TYPE NEA AND A SMALL DECREASE OF LESS THAN 10% OF THE WINING C-TYPE NEA EXCLUDING THE HIGHEST AND LOWEST SCORE

In this scenario a small increase to the scores less than 10% of the of the original scored values for each of the potential C-type NEA and small decrease of less than 10% to the winning C-type NEA excluding highest and lowest score has been implemented to observe how those small changes will affect the ranking order of the trade-off studies result. The implementation of the small changes is in step order of 1% through 10% for each of the scored value for the initial trade-off studies excluding the highest and lowest score. Presented in Table 3-8 is the comparison of the trade-off studies result and those of the sensitivity analysis carried out. The order of the scoring with range of the changes between 1 – 10% remain consistent, C-type NEA Ryugu still remain in the lead, followed by C-type NEA 2008EV5 in the second position and C-type NEA Bennu maintaining the third position. The margin across all the winning alternatives is insignificant, below

1% of the total score for each of the alternatives with a 1% increase. As the order of the small changes below 10% continue to increase the overall new scores increase for each of the potential C-type NEA and decreases for the winning C-type NEA as the small decrease of less than 10% continues as illustrated in Table 3-8.Table 3-8: Present a comparison of the result of the sensitivity analysis based on small increase to the scores less than 10% of the original scored values and a small decrease to the scores less than 10% of the winning candidate C-type NEA to those of the original result based on initial trade-off studies

Potential C-type NEA	**Ryugu overall scores in %**	**Bennu overall scores in %**	**2005YU5 overall scores in %**	**2008EV5 overall scores in %**	**1989ML overall scores in %**
Original result based on the initial trade-off studies	74.00	52.00	35.00	66.00	30.00
A small increase to the scores less than 10% of the of the original scored values for each of the potential C-type NEA and a small decrease of less than 10% of the wining C-type NEA excluding highest and lowest score					
5% small change	71.30	54.40	36.50	66.60	30.75
4% small change	71.84	53.92	36.20	66.48	30.60
3% small change	72.38	53.44	35.90	66.36	30.45
2% small change	72.92	52.96	35.60	66.24	30.30
1% small change	73.46	52.48	35.30	66.12	30.15

3.8 DISCUSSION

In this section the reason for selecting the C-type NEA family as the potential destination for the demonstration of the ISRU process has been outline and the selection process was performed. The requirement for the selection process were generated from a combination of NHATS and Asterank databases. 15764 NEA were generated from the databases and only 314 NEA have been classified and only 20 are C-type NEA. A four-stage initial filtering process was applied to the 20 C-type NEA to lower the number of the potential target. Five C-type NEA namely (Ryugu, Bennu, 2005YU55, 2008EV5 and 1989ML) has been identified as the potential destination and are subjected to a further trade-off study. The result of the further trade-off study, C-type NEA 162173 Ryugu has emerged the

best performing candidate followed by 2008EV5 and finally Bennu. The sensitivity analysis was also performed to validate the trade-off studies performed.

3.9 CONCLUSION

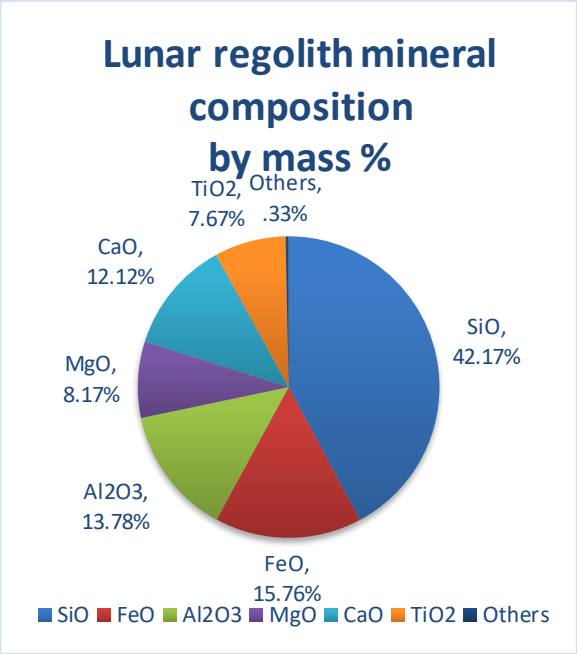
In the conclusion, C-type NEA 162173 Ryugu emerged as the leading candidate in both the trade-off study and the sensitivity analysis ranking and as the target destination for the demonstration of the ISRU process in this research work. The choice of Ryugu is envisaged not to affect rest of the PhD work. Due to shallow gravity well on the surface of Ryugu and unlike the Moon, a small amount of force is required to counter the effect of the shallow gravity well on the CubeSat during descent and landing. The asteroids and the Moon missions both are focused on regolith resources. Currently, mission opportunities to asteroids with the successful return of the sample return missions by Hayabusa 2 back to earth and the expected return of the recently concluded OSIRIS-REx missions to Bennu in 2023 are beginning to become popular. In the next chapter the *ISRU* technology selection process would be perform.

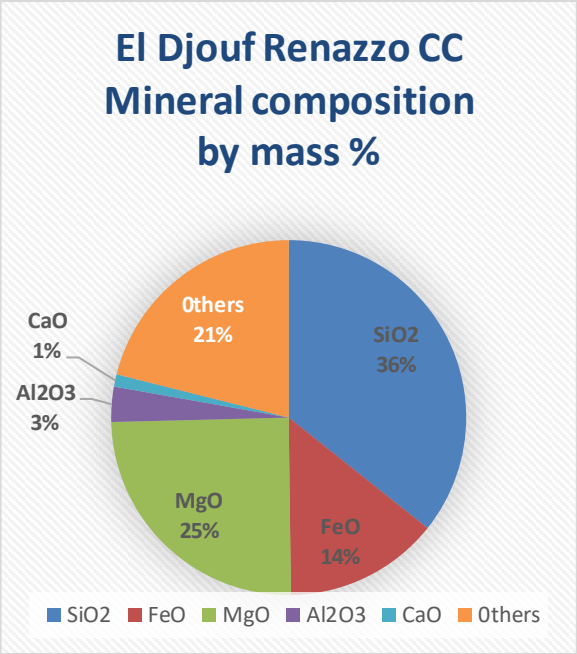
4 ISRU SELECTION PROCESS FOR IMPLEMENTION IN THE CONTEXT OF CUBESAT TECHNOLOGY

4.1 INTRODUCTION

This section of the thesis will discuss the ISRU selection process to down select an ISRU method for implementation in the context of CubeSat payload. Several processes for the extraction of Oxygen as the primary product and metal waste from lunar regolith, have been under consideration, namely, chemical reduction with Hydrogen, methane or carbon monoxide, vapour phase pyrolysis, sulphuric acid treatment, and molten oxide electrolysis (Schwandt, et al., 2012). Mineral compositional similarities exist among both the lunar regolith and the asteroid regolith; they both are composed of silicate minerals such as (olivine), the oxide of these olivines is mainly iron oxide (FeO), silicon dioxide (SiO_2), aluminium oxide (Al_2O_3), magnesium oxide (MgO), calcium oxide (CaO) and other minerals such as sodium oxide (Na_2O), potassium oxide (K_2O), manganese oxide (MnO) present in minute quantities (Ruzicka, et al., 2001). The production of Oxygen from the Lunar materials so that human life can be sustained In situ is the most important (Taylor A & Carrier D, 1993). The listed Lunar ISRU processes (chemical reduction with Hydrogen, methane or carbon monoxide, vapour phase pyrolysis, sulphuric acid treatment, and molten oxide electrolysis) allows the production of Oxygen and metal, and the production of metal from the lunar materials will enable the establishment of Lunar infrastructures (Schwandt, et al., 2012).

In the same vein, these 6 Lunar ISRU processes listed earlier will be conveniently considered on the asteroid regolith extraction process to give priority to metal production as the primary product, where possible Oxygen as secondary product. The chemical analysis of Apollo 14 soil 12070b and that of the C-type NEA analogue carbonaceous chondrite El Djouf Renazzo to illustrate the mineral compositional similarities are as shown in the Figure 4-1





High Ti Basalt Apollo 11 (Fagan & Neal, 2016)

C-type NEA analogue El Djouf CR (Bischoff, et al., 1993)

Figure 4-1: comparison of the mineral composition in C-type NEA and Lunar regolith

The result of the literature studies on the asteroid/meteorite analysis in section 2.6 has established that the asteroids are the presumed parent's bodies of the meteorite, and the commonest meteorites are the CI and the CM Carbonaceous Chondrites Meteorite (CCM). Furthermore, in subsection 2.4.2 the olivine mineral present in the meteorites is usually forsterite, having more magnesium than iron in the CCM. This aspect of the research work is more interested in the use of the primary product (Metal) and the likely metal of interest could be Magnesium, Iron, or both.

In this section of the PhD research work, the ISRU process that will allow the production of metals' products from the C-type NEA as the primary outcome are reviewed toward selecting a method or two that can be implemented.

4.2 THERMAL REDUCTION PROCESSES

These processes are based on the reduction of metal compounds (such as metallic oxide) to the corresponding metals by more active metals or non-metals in the activity

series through the application of heat. The process operates at elevated temperatures in the range of 1000 – 1600^{o}C and is accompanied by the evolution of heat. Methane, Carbon monoxide and Hydrogen are used as reducing agents in the thermal reduction process of metal oxide to liberate the Oxygen forming a free metal.

4.2.1 CARBOTHERMAL REDUCTION PROCESS WITH METHANE

The carbothermal reduction process is a carbon base reduction process that has been used terrestrially to produce high-purity silicon from the silicon compound; it can also be used to produce iron metal from the asteroid regolith through carbon reduction of iron oxide compounds. The process requires a temperature above 1600^{o}C, and the products are iron and Oxygen as primary and secondary products respectively (Carsten, et al., 2012).

The process earned the name carbothermal because the methane compound is unstable at the operating temperature and decomposes into carbon and Hydrogen, with the carbon serving as the actual reductant. The process has three basic steps; namely, carbon reduction of metallic oxide, methane reformation and water electrolysis; all these steps are illustrated in Figure 4-2.

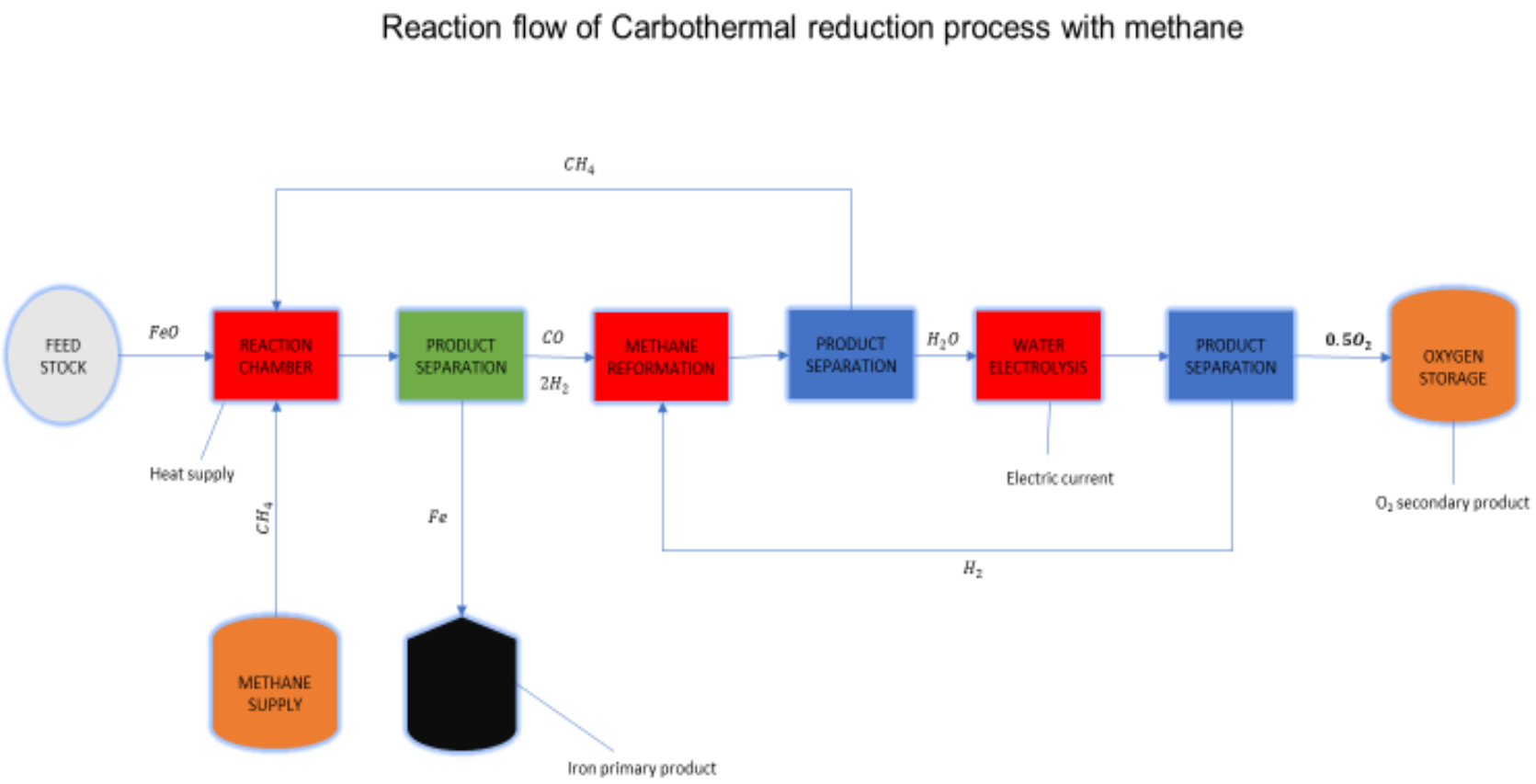


Figure 4-2: reaction flow of carbo-thermal reduction process with methane

The chemical reaction equation illustrating the three basic steps are as shown below using iron oxide compound as the feedstock from the CM CC meteorite regolith:

Equation 1: Present the Methane reduction of metallic oxide

$$FeO + CH_4 \rightarrow Fe + CO + 2H_2 \quad Step\ I \qquad \textbf{Equation 1}$$

Equation 2: Represent Methane reformation or methanation using nickel catalyst with additional hydrogen from the water electrolysis process

$$CO + 3H_2 \rightarrow CH_4 + H_2O \qquad Step\ II \qquad \textbf{Equation 2}$$

Methane formed from the methanation process is recycled to the initial process and the water is electrolysed producing hydrogen and oxygen. The hydrogen is feed into step II as addition to the methane reformation process and the oxygen stored as secondary product. The iron product can be used for infrastructure development in space and the oxygen used for breathing by astronaut and as a source of fuel.

Equation 3: Represent the water electrolysis producing hydrogen and oxygen

$$H_2O \rightarrow H_2 + {}^{1}/_{2}\,O_2 \qquad Step\ III \qquad \textbf{Equation 3}$$

The carbothermal reduction process was demonstrated in 2010 at the analogue test site on Mauna kea on the big island of Hawaii using JSC-1A simulant (Tephra melt); concentrated solar energy was used as the source of power-producing 600 - 700w that was used to heat 26g of JSC-1A simulant over a period of 80minutes; 11.5g of water was collected yielding 9.6g of Oxygen (Gustafson, et al., 2011). As shown above the same process can operate well on simple metal oxide such as (FeO) which is available in the CM CC meteorite matrix to produce iron as the primary product.

4.2.2 THERMAL REDUCTION WITH HYDROGEN (H_2)

This process uses Hydrogen for the reduction of iron oxide. The iron oxide in the required grain size is feed into the reaction chamber, where it chemically reacts with hydrogen gas under an operating temperature of 900^{o}C. Iron (Fe) and water (H_2O) are produced. The Hydrogen can be sourced from the earth for the initial reaction with the iron oxide; the water electrolysis in the second stage of the reaction will produce Hydrogen and Oxygen; the Hydrogen can be recycled to sustain the initial process/reaction. The system will consider outsourcing the Hydrogen in situ from the volatile minerals. The iron oxide content of the asteroid feedstock determines the efficiency of the reaction process. Murchison carbonaceous chondrite (CM CC) meteorite with about 23% FeO content is best suited for this process (Jarosewich, 1990)

Equation 4 and Equation 5: Represent the hydrogen step reduction chemical reaction of metal oxide and the water electrolysis to produce hydrogen and oxygen

$$FeO + H_2 \rightarrow Fe + H_2O$$ Step reduction reaction **Equation 4**

$$H_2O \rightarrow H_2 + {}^{1}/_{2}\, O_2$$ Step for electrolysis of water Error! Reference source not found.

The process is a straightforward process with minimum of two steps involved: thermal reduction of metallic oxide using hydrogen and water electrolysis. The thermal reduction with Hydrogen of the FeO is as demonstrated in the Figure 4-3 below:

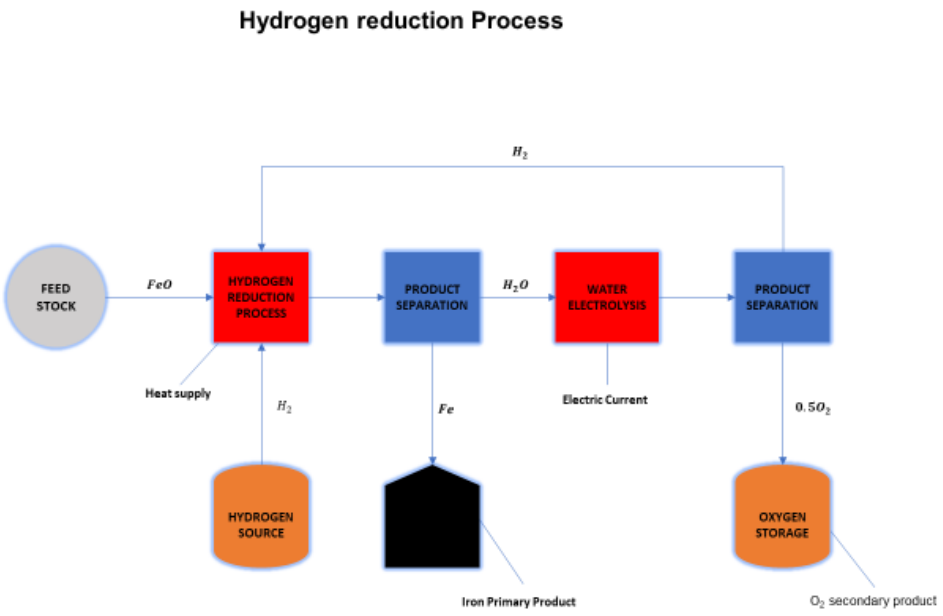


Figure 4-3: Hydrogen reduction process to produce iron and oxygen

The hydrogen reduction process was demonstrated using both tephra material and JSC-1A lunar soil simulant, and the reactant inside the reactor is heated at a stepwise controlled rate of 10°C/minutes, through 90minutes duration to attain 900°C. In a sampled process, a total of nearly 4hrs was required to conclude the processes of heat up (96minutes), hydrogen reduction (90minutes) and cool down (45minutes). This excludes the time for beneficiation (Clark L, et al., 2009). Field test result of the Precursor in Situ Lunar Oxygen Testbed (PILOT) Hydrogen Reduction reactor performed by Lockheed Martins and NASA in Pacific International Space Center for Exploration Systems (PISCES) at Hawaii. 11.6kg sample of JSC-1A simulant was used to produces 110ml of water (Clark L, et al., 2009).

4.2.3 CARBOTHERMAL REDUCTION WITH CARBON MONOXIDE (CO)

This is one of the carbothermal mechanisms of iron oxide reduction through gaseous intermediates carbon monoxide (CO) at a temperature up to 1000°C with the formation of solid iron and carbon dioxide (CO_2) (L'vov, 2000).

Elevated temperature level and the CO concentration in the reaction determine the efficiency of the metallic oxide reduction process (Lalvani, et al., 2004). In comparison

to hydrogen reduction of FeO; it was estimated that the reaction rate of iron oxide reduction with CO was 2 – 3 times lower than that with H_2, the activation energy for the reduction reaction in CO was estimated to be 19.8KJ/mol in pure CO stream, the activation energy in H_2 atmosphere was found to be 42.1KJ/mol (Lalvani, et al., 2004). The experiment carried out on Iron oxide of 99% purity, both fine and coarse grade particles with 1.22 and 58.6 µm particles sizes respectively were used. The solid samples were preheated to the desired temperature under an inert gas atmosphere of nitrogen, followed by the introduction of CO at a temperature between 800-900^{o}C.

The products of the reaction are suspected to be an iron oxide (FeO), iron (Fe) and iron carbide (FEC). Various concentration of CO was used in the reaction; the result indicates that the rate of CO disintegration and carbide formation is significantly slower at lower CO concentration. The CO partial pressure was sampled for 30%, 40% and 50%; no Fe_3C phase was observed in the product obtained from experiment conducted at CO partial pressure less than 50% (Lalvani, et al., 2004). The carbothermal reduction with carbon monoxide, iron (Fe) and carbon dioxide (CO_2) are produced as demonstrated in the Figure 4-4:

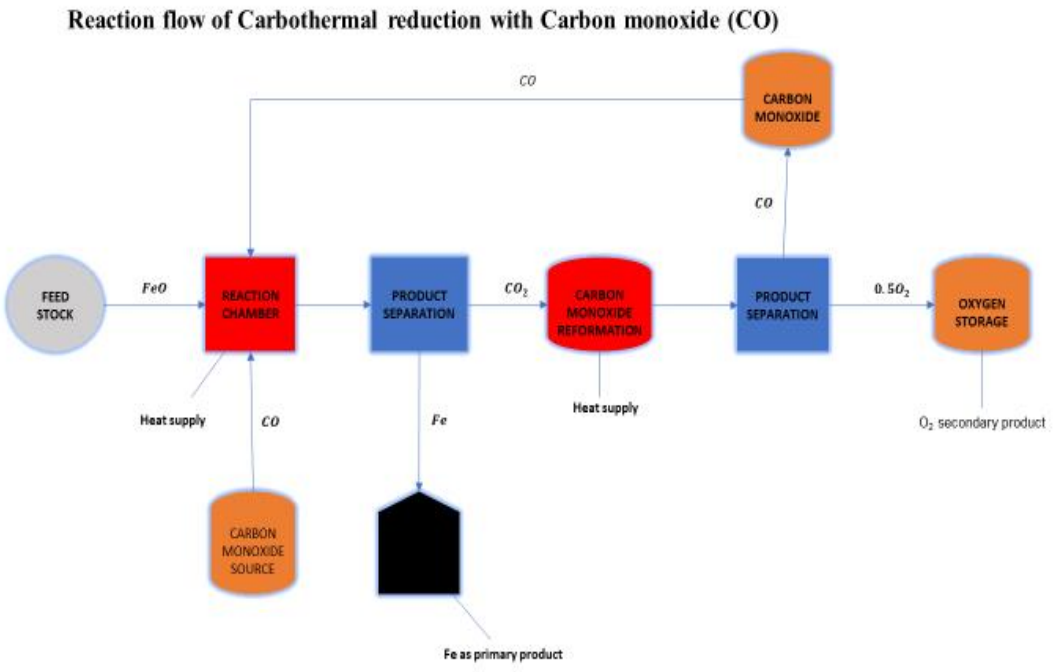


Figure 4-4: Reaction flow of carbo-thermal reduction with carbon monoxide

Equation 5: Represent CO chemical reduction reaction of metal oxide

$$FeO + CO \rightarrow Fe + CO_2$$ **Equation 5**

Equation 6: Represent the carbon dioxide decomposed to form carbon monoxide and oxygen.

$$CO_2 \rightarrow CO + \frac{1}{2} O_2$$ **Equation 6**

The CO is recycled as feed-in to the initial process, Fe and O_2 are the primary and secondary product respectively. The reduction reaction of iron ore by CO shares features like reduction by Hydrogen, and many mechanisms are common to both. Reduction with Hydrogen is endothermic, whereas it is exothermic with CO; conversely, thermodynamics is more favourable with Hydrogen than with CO above 800^{o}C (Wagner, et al., 2006). The main disadvantage of the CO reduction process is the formation of iron carbide at the high concentration level of the CO; the formation of iron carbide will require additional purification steps.

4.2.4 VAPOUR PHASE PYROLYSIS

The process was first proposed by Steurer and Nerad in 1983, but the most significant experiment was carried out by Senior in 1991. This ISRU process is based on a partial decomposition of metal oxide such as (FeO) which is associated with vaporisation. The metal oxide is decomposed into Oxygen at a temperature between 2000^{o}C and 2600^{o}C (John, 2006).

The pyrolysis technique is quite simple and applicable on a wide range of feedstocks such as the silicate compound, ilmenite, and metallic oxide. The vapour phase pyrolysis of the iron oxide is as demonstrated in Figure 4-5:

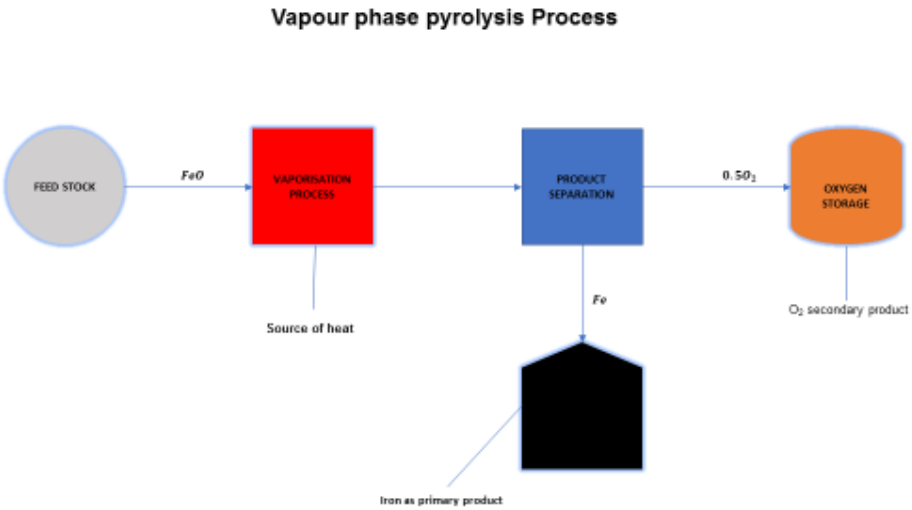


Figure 4-5: vapour phase pyrolysis

Equation 7: Represent the decomposition of the metallic

$$FeO \rightarrow Fe + 1/2O_2$$

Equation 7

The ISRU process has a potential efficiency of between 6.3% - 21% and require no imported chemicals for the reaction process (Eric, et al., 2007). The major drawback of the process is its very high operating temperature.

The pyrolysis experiment demonstration uses a 1m Fresnel lens and a 3.8m parabolic reflector as the heat concentrators; the selected feedstock is ilmenite, enstatite and MLS-1A simulant. The vacuum pyrolysis: depending on the input material, is predicted to yield 11wt% to 20wt% of Oxygen at an operating pressure level under 0.001Torr. Considering the vaporisation process of one net gram of MLS-1A simulant at 1747k over a period of 52minutes and solar intensity of 1005w/m^2 and 0.01Torr, the process yield 10wt% Oxygen (Eric, et al., 2007)

4.2.5 SULPHURIC ACID TREATMENT OF METALLIC OXIDE

This research was conducted by Sullivan in 1992, ilmenite is used as the main feedstock, and three steps are involved in the entire process. Other types of feedstocks such as FeO from CM CC meteorite matrix can also be used. The FeO reacted with concentrated sulphuric acid (H_2SO_4), forming iron sulphate ($FeSO_4$), and water (H_2O).

Equation 8: Represent metal oxide reaction with concentrated sulphuric acid

$$FeO + H_2SO_4 \rightarrow FeSO_4 + H_2O$$ **Equation 8**

Equation 9: Represent the hydrolysis of iron sulphate to produce iron, oxygen, and sulphuric acid

$$FeSO_4 + H_2O \rightarrow Fe + \frac{1}{2}O_2 + H_2SO_4$$ **Equation 9**

The process drawback is associated to its complexity, the schematics of the sulphuric acid treatment/reduction process on FeO feedstock is as demonstrated in the Figure 4-6:

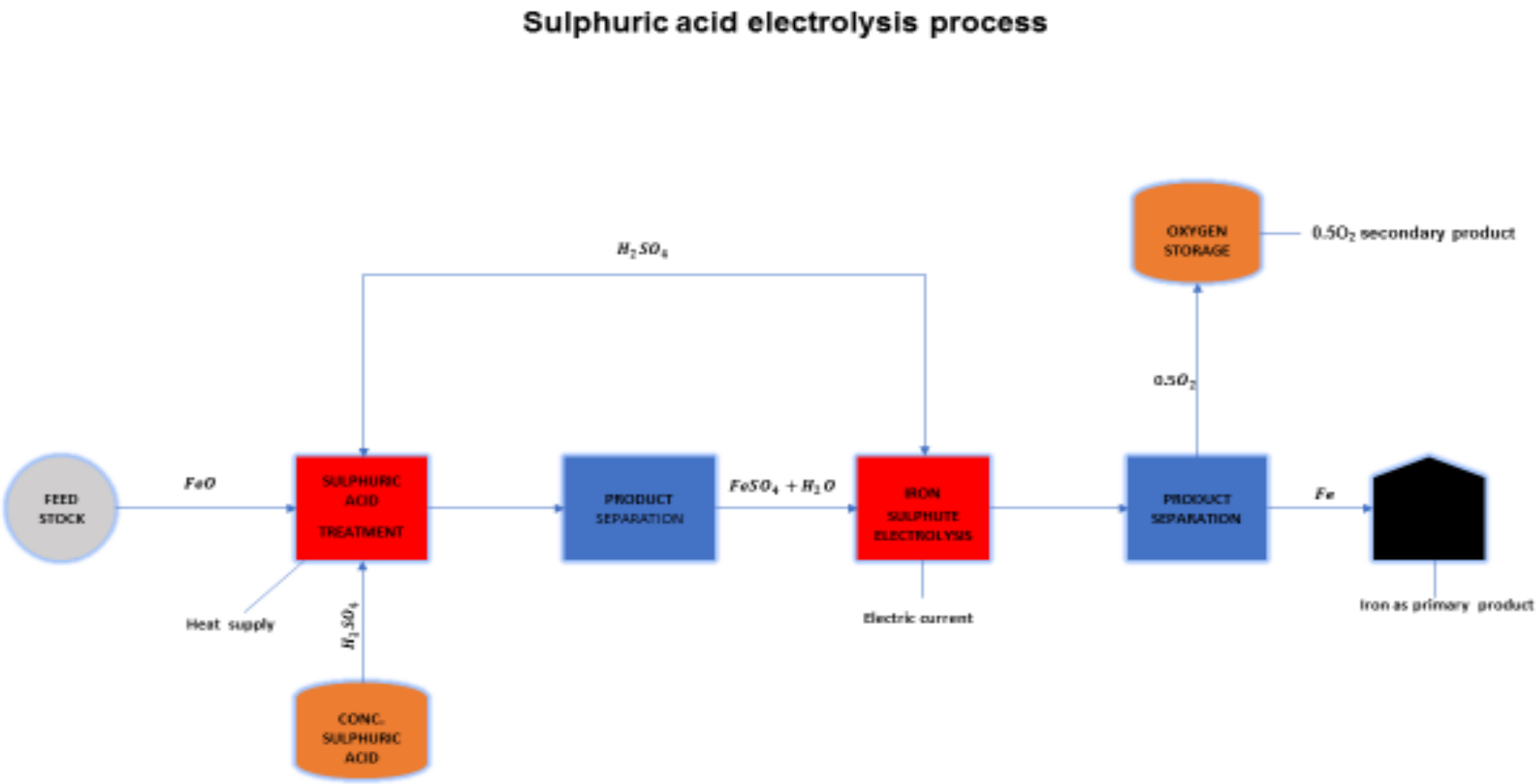


Figure 4-6: Sulphuric acid electrolysis process

4.2.6 MOLTEN OXIDE ELECTROLYSIS/MAGMA ELECTROLYSIS

This ISRU process is one of the straightforward approaches to producing Oxygen and metal by electrolysis demonstrated on molten lunar regolith at an operating temperature of up to 1600°C (Sibille L, et al., 2010). This process can as well work with FeO from the CM CC meteorite matrix. The raw material (FeO) is feed into the reaction chamber and heated to molten regolith, potential source is then applied to the molten regolith such that oxygen evolves at the anode and metal is deposited at the cathode. Ionically, the electrolysis of a metallic compound rich in iron metal and the evolution of oxygen to the anode and iron metal deposit at the cathode is as shown in:

Equation 10, Equation 12 and Equation 13: Represent the decomposition of FeO into molten regolith, Oxygen evolvement at the anode and metal deposition at the cathode

$$FeO \rightarrow Fe + \frac{1}{2}O_2 \qquad \textbf{Equation 10}$$

$$O^{2-} \rightarrow \frac{1}{2}O_2 + 2e^- \qquad \textbf{Equation 101}$$

Cathode:

$$Fe^{2+} + 2e^- \rightarrow Fe \qquad \textbf{Equation 102}$$

The molten oxide electrolysis of the iron oxide is as demonstrated in the Figure 4-7 below:

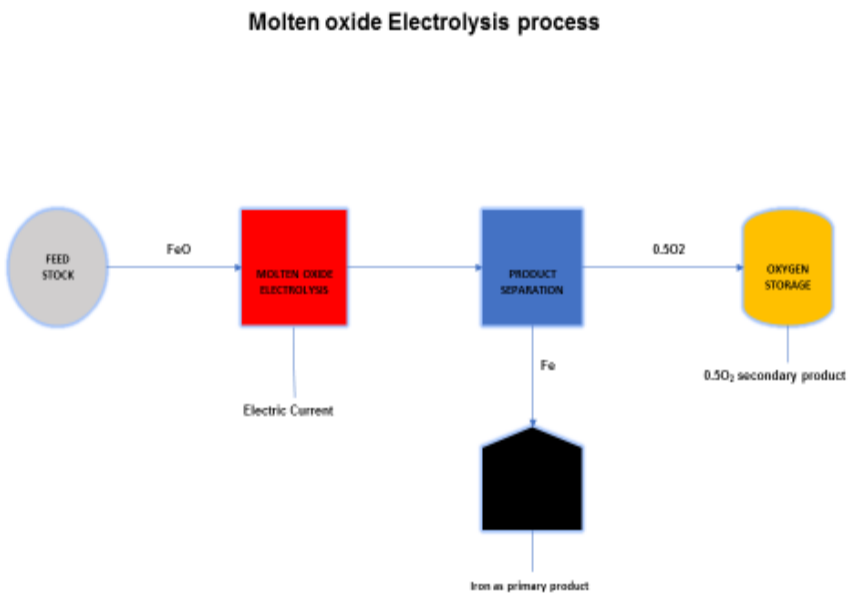


Figure 4-7: Molten oxide electrolysis process

This process has some advantages; it does not require beneficiation, little or no reagent is required from earth and selective winning of metals according to their oxides stabilities is feasible through control of the applied potential. The drawback of this process is that it requires a high operating temperature and the use of expensive platinum metal as electrodes (Curerri, et al., 2006).

4.3 INCLUSION OF THE 7th ADDITIONAL PROCESS

The first step of the sulphuric acid treatment requires the use of hot and concentrated sulphuric acid, concentrated sulphuric acid is very destructive to the skin, eyes etc., severe exposure to hot concentrated sulphuric acid can also result in death (NIOSH, n.d.). Sulphuric acid, having been identified as a better option in the metal extraction process using the inorganic acids family (HCL, HNO_3 and H_2SO_4), sulphuric acid performed effectively on the leaching process (Ha, et al., 2020). Hydrometallurgy sulphuric leaching of metal oxide has been identified as an additional process to be included among the list of the processes to be considered for selection/trade study. The Hydrometallurgy sulphuric acid leaching of metal oxide uses diluted sulphuric acid at room temperature and

share similar system complexity/architecture to the sulphuric acid treatment of the metal oxide.

A 7th additional process the hydrometallurgical sulphuric acid leaching of metal oxide shall be designed to include the electrochemical system that will enable the recovery of the metal contained inside metal-acid solution and quantify it.

4.4 IDENTIFICATION AND DESCRIPTION OF PARAMETER FOR TRADE-OFF STUDY TO DOWN SELECT POTENTIAL ISRU PROCESS

After a review of the various ISRU processes identified, set of parameters related to each of the processes is generated. These parameters will be used as tools to evaluate the multiple processes identified to down select candidate ISRU process that will be implemented in this PhD research work. The Standard ISRU process has four main stages: raw material/resource acquisition, beneficiation, core processing/handling, and storing. The ISRU system complexity can affect the system efficiency and reliability and increase power consumption, and this would form part of the bases for the parameters selection.

4.4.1 BENEFICIATION STAGE

This stage involves crushing, grinding and in some cases, heating of the raw materials to remove impurities to improve the concentration of the ore. The more the number of these stages, the more complex the system can be. The method with fewer beneficiation steps or does not require beneficiation will attract the highest score in the selection process.

4.4.2 CORE PROCESSING STAGE

This is the stage where all the chemical reactions occur; some processes require several steps to accomplish the chemical reaction. For instance, the carbo-thermal reduction process with methane requires three core steps to be accomplished; namely, the metal oxide reaction with methane to liberate the metal from the oxide, methane reformation that will produce methane and water electrolysis that will split the water into Hydrogen and Oxygen. The system with

fewer core processing stages will attract the highest score in the selection process.

4.4.3 MATERIAL HANDLING AND STORING STAGE

The product of the core stage process can be in a solid, liquid, and gaseous state; the state of these materials can affect the handling and storing mechanism. Handling and storing gas material are the most difficult than handling liquid and solid materials because of their compressed nature, low density, and low boiling point. More hardware mass is required to handle gas material than liquid and solid materials, which attracts a mass penalty. The system with fewer processing hardware will attract the highest score in the selection process.

4.4.4 PROCESS POWER REQUIRMENT

Each ISRU process comprises the core system and other subsystems (raw material/resource acquisition, beneficiation and the handling and storing). The power requirement of the process depends on the number of the core system and the subsystems. The combination of the systems and subsystem used at a given time and, in each process, will be the determining factor. Using greater number of the core system and subsystems, more power will be required. The system with a smaller number of the core system and subsystems will attract the highest score in the selection process.

4.4.5 PROCESS TEMPERATURE REQUIREMENT

Based on the ISRU processes studied, they all seem to have a different operating temperature. For instance, the vapour phase pyrolysis required a temperature up to 2600^{o}c. Considering the CubeSat size and volume, the system with the least operating temperature will attract the highest score in the selection process.

4.4.6 PROCESS TECHNOLOGY READINESS LEVEL (TRL)

The TRL is a scale/indicator that estimates the maturity level of technology development. Most of the identified ISRU processes have attained some TRL level of development at both the field and laboratory demonstrations. For instance, the carbo-thermal reduction process is a mature terrestrial technology

that achieved the TRL6. The process that has attain the highest TRL level will attract the highest score in the selection process.

4.4.7 PROCESS SOURCE OF REACTANT/CONSUMABLE

Some of the processes, such as the carbo-thermal reduction process require importing methane consumable from the earth; this will attract a penalty in term of additional weight. Considering the constraint with the CubeSat mass, size and volume, the process that does not require importing consumables from the earth will attract the highest score in the selection process.

4.4.8 PROCESS CONTROL MECHANISM

Some processes, such as the Hydrogen reduction process, requires the use of some control mechanism that triggers and control the Hydrogen gas inlet manifold to allow the inflow of Hydrogen gas into the reactor chamber to initiate the Hydrogen reduction reaction process. the control mechanism adds to the complexity of the system. The process that does not require or has minimal need for the use of the control mechanism will attract the highest score in the selection process.

4.4.9 PROCESS MONITORING MECHANISM

Some processes such as the hydrogen reduction process require a monitoring mechanism that monitors the pressure build-up in the reactor and containment vessel do not exceed 2Psi before introducing the hydrogen gas into the reactor chamber to initiate the hydrogen reduction process. The monitoring mechanism add to the complexity of the system; the process that does not require or has minimal need for the use of monitoring mechanism will attract the highest score in the selection process.

4.4.10 PROCESS SUITABILITY WITH ANOTHER FEEDSTOCK

Some processes are feedstock specific while some others are not; for instance, the Carbo-thermal reduction process is a flexible process that can efficiently process feedstock from other locations. The process suitable with another kind of feedstock will attract the highest score in the selection process.

4.4.11 DEFINATION OF THE SEVEN POTENTIAL ISRU PROCESSES UNDER CONSIDERATION

- P1 – Carbo-thermal reduction process using methane on Iron oxide from C-type NEA regolith to produce Iron (Fe) as the primary product
- P2 – Hydrogen reduction process on Iron oxide from C-type NEA regolith to produce Iron (Fe) as the primary product
- P3 – Carbon monoxide reduction process on Iron oxide from C-type NEA regolith to produce Iron (Fe) as the primary product
- P4 – Vapour phase pyrolysis process on Iron oxide from C-type NEA regolith to extract/produce Iron (Fe) as the primary product
- P5 – Concentrated sulphuric acid treatment on Iron oxide from C-type NEA regolith to produce Iron (Fe) as the primary product
- P6 – Electrolysis on molten Iron oxide from C-type NEA regolith to produce Iron (Fe) as the primary product
- P7. Hydrometallurgical sulphuric acid leaching of olivine mineral as the simulant for C-type NEA with electrowinning and electrochemistry

4.5 TRADE-OFF STUDY TECHNIQUES SELECTIONS

Trade studies are a method or technique through which multiple alternatives based on certain criteria are subjected to a down selection process. The best alternative emerges and will be implemented to achieve a given task (Bahill & Madni, 2017). The trade-off studies involve human numerical judgement and therefore are susceptible to human biases (Bahill & Madni, 2017). The trade-off techniques selection in this research will take cognisance of these biases in allotting scores to the generating criteria upon which the finals selection process is based.

The concept of Multi criteria analysis (MCA) adapted in this research work to evaluate the performances of the identified process or alternative with respect to the defined criteria to select the processes favoured by the criteria in a scoring order of preference. This process does produce an outcome, based on the new outcome a sensitivity analysis can be performed to down select the preferred option among the processes.

In this section the multi-criteria decision analysis model will be used for the performance of the trade-off studies to select the potential process to be implemented in this research work.

4.5.1 APPLYING MULTI-CRITERIA DECISION ANALYSIS (MCDA) MODEL IN THE ISRU PROCESS SELECTION

MCDA is one of the Multi-Criteria Analysis (MCA) techniques used to shortlist or select a limited number of alternative/options with the highest score according to a set of evaluation criteria for subsequent detailed appraisals (Irhoma & Sansom, 2017). The MCDA technique was selected because it is easy to use and good at analysing complex tasks. Our process selection appears to be a complex one, and all the decision-making process/steps as listed below are applied:

4.5.1.1 IDENTIFYING AND DEFINING HIGH-LEVEL CRITERIA AND SUB-CRITERIA

The CubeSat limitation and the ISRU processes are identified as the high-level criteria. Ten performance sub-criteria/parameters are generated from the high-level criteria and would be used for the performance of the trade-off studies; three are specific to the CubeSat limitations, and the remaining seven are particular to the ISRU processes. The seven processes are evaluated against the ten identified performance sub-criteria/parameters. A performance matrix describing the performance of the options/processes against each sub-criteria/parameters is shown in Table 4-1

Table 4-1: A performance matrix table describing the performance of the options against the criteria

High level criteria (HLC)	Sub-Criteria	Processes/Options						
		P1	**P2**	**P3**	**P4**	**P5**	**P6**	**P7**
CubeSat related	Power (w)	10	4	5	36	3	29	1
	Energy (KJ)	35	15	16	123	8	106	2
	Temperature (k)	1873	1173	1173	2873	673	1873	273
ISRU process related	Reactant sourced	Methane	Hydrogen	Carbon monoxide	Not required	Sulphuric acid	Not required	Sulphuric acid
	Process efficiency	0.64	0.76	0.56	0.78	0.33	0.78	0.33
	No. of core processes	3	2	2	1	3	1	3
	No. of material handling	10	8	9	5	8	5	8
	Reaction TRL	TRL5-6	TRL5-6	TRL5-6	TRL3-4	TRL3-4	TRL3-4	TRL3-4
	No. of process monitoring	4	5	5	4	4	4	4
	Process beneficiation	Not required	Required	Required	Not required	Not required	Not required	Not required

The performance of the options/processes against the sub-criteria described in Table 4-1are converted into raw numbers for ease of scoring as presented in **Table 4-2**

Table 4-2: Performance matrix result converted into raw numbers for ease of scoring

Parameters	P1	P2	P3	P4	P5	P6	P7
Average power (W)	10	4	5	36	3	29	1
Total energy (J)	35	15	16	123	8	106	2
Working temperature (^{O}C)	1873	1173	1273	2873	673	1873	298
Reagent sources	0	0	0	1	0	1	0
Process chemical reaction efficiency	0.64	0.76	0.56	0.78	0.33	0.78	0.64
Number of core processes	3	2	2	1	3	1	3
Number of material handling	10	8	9	5	8	5	10
Process TRL level	5.5	5.5	5.5	3.5	3.5	3.5	3.5
Number of process monitoring	4	5	5	4	4	4	4
Process beneficiations	2	3	2	1	1	1	2

4.5.1.2 SCORING OF THE OPTIONS BASED ON THE CRITERIA

After identifying the processes/option and the criteria/requirement and constructing the performance matrix table, the performance of each of the seven possibilities is assessed against the ten sub-criteria to down select several feasible options. A scoring scale is constructed on the strength of preference for each option; a scoring scale of 1 – 5 is used in scoring each sub-criteria/parameter. The most preferred choice is assigned 5, and the least selected option is assigned 1. All other options fall between 1 and 5. The result of the raw scoring for the potential ISRU process based on defined threshold and a scaling in the range of 1 – 5 is presented **in Table 4-3**

Table 4-3: Raw scoring for the potential ISRU processes

Parameter/sub- Criteria	Scaling	P1	P2	P3	P4	P5	P6	P7
Power requirement	Least power required =5	5	5	5	2	5	3	5
	most power required =1							
Energy requirement	Least energy required =5	4	5	5	1	4	2	5
	most energy required =1							
Temperature requirement	Least temperature reqd = 5	2	3	3	1	4	2	5
	most temperature reqd =1							
Reactant source from earth	Reactant not required = 5	1	1	1	5	1	5	5
	Reactant required =1							
Process efficiency	Most efficient system = 5	3	4	2	4	1	4	3
	Least efficient system = 1							
No. of core processes	Most core system = 1	1	3	3	5	1	5	1
	Least core system = 5							

Parameter/sub- Criteria	Scaling	P1	P2	P3	P4	P5	P6	P7
No. of material handling	Least material handling = 5	1	2	1	4	2	4	1
	Most material handling = 1							
Process TRL level	Least TRL level = 1	4	4	4	1	1	1	1
	Most TRL level = 5							
No. of process monitoring	Least monitoring = 5	2	1	1	2	2	2	2
	Most monitoring =1							
Beneficiation requirement	Not required = 5	3	1	3	5	1	5	3
	Required = 1							

4.5.1.3 CRITERIA WEIGHTING

Weighting is done based on the sub-criteria generated from the high-level criteria; 100 point is the weighted point allocated to the whole sub-criteria. The high-level CubeSat criteria have three sub criteria (power, energy, and temperature); they appear to be the most critical and are considered the most important parameters, followed by Technology Readiness Level (TRL) and the reactant outsourcing and finally the least important parameters including the number of material handling, number of core processes, process beneficiation, number of material handling and the chemical reaction efficiency.

Using judgement, 45-point weighting values out of the total of 100 point was allocated to the three most important parameters/sub-criteria related to the CubeSat limitation, and 15point for each of the criteria. The high-level criteria related to the ISRU process have seven sub-criteria/parameters and are allocated the remaining 55point of the 100point. The point is distributed across the sub-criteria/parameters based on preference; the process Technology Readiness Level (TRL) and the reactant outsourcing are considered the second most important parameter and are allocated weighted value of 10 to each. The least important parameter includes the number of material handling, number of core processes, process beneficiation, number of material handling and the chemical reaction efficiency and are allocated weighted value of 7 to each. The description of the preferred scores, weighting of the criteria and overall weighted scores is shown in Table 4-4

Table 4-4: The preference scores, weighting of the criteria and overall weighted scores

High level criteria (HLC)	Point allocation to HLC	Criteria (sub-criteria)	Weighting of each criterion	Scaling
CubeSat related	45	Power requirement	15	Least power required =5
				most power required =1
		Energy requirement	15	Least energy required =5
				most energy required =1
		Temperature requirement	15	Least temperature reqd = 5
				most temperature reqd =1
ISRU process related	55	Reactant source from earth	10	Reactant not required = 5
				Reactant required =1
		Process efficiency	7	Most efficient system = 5
				Least efficient system = 1
		No. of core	7	Most core system = 1

High level criteria (HLC)	Point allocation to HLC	Criteria (sub-criteria)	Weighting of each criterion	Scaling
		processes		Least core system = 5
		No. of material handling	7	Least material handling = 5
				Most material handling = 1
		Process TRL level	10	Least TRL level = 1
				Most TRL level = 5
		No. of process monitoring	7	Least monitoring = 5
				Most monitoring =1
		Beneficiation requirement	7	Not required = 5
				Required = 1
Total weighted scores	**100**		**100**	

4.5.1.4 AMALGAMATION

The Amalgamation step combines the scoring and weighting of each criterion, aimed at getting the overall weighted score for each of the options. Mathematically, the linear summation model was applied where the product of weight by the scores of each criterion are summed.

Equation 11: Represent the linear summation of the product of weight by the scores of each criterion

$$S_i = w_1 S_{i1} + w_2 S_{i2} + \cdots + w_n S_{in} = \sum_{j=1}^{n} w_j S_{IJ} \qquad \textbf{Equation 11}$$

Where,

- n = number of criteria
- S_{ij} = the preferred score for option i on criteria j
- w_j = weight for each criterion
- S_i = the overall score for each option

The summary result of the amalgamation steps combining the raw scoring and weighting of the criteria is as shown in Table 4-5:

Table 4-5: A combination of the scoring and weighting of each criterion to get the overall weighted score for each of the options

High level criteria	Sub-Criteria	Processes/Options							Weight
		P1	P2	P3	P4	P5	P6	*P7*	
CubeSat related	Power (w)	15	15	15	6	15	9	15	15
	Energy (KJ)	12	15	15	3	15	3	15	15
	Temperature (^{0}c)	6	9	9	3	12	6	15	15
ISRU process related	Reactant source	2	2	2	10	2	10	10	10
	Process efficiency	4.2	5.6	2.8	5.6	1.4	5.6	4.2	7
	No. of core processes	1.4	4.2	4.2	7	1.4	7	1.4	7
	No. of material handling	1.4	2.8	1.4	5.6	2.8	5.6	1.4	7
	Reaction TRL	8	8	8	2	2	2	2	10
	No. of process monitoring	2.8	4.2	1.4	2.8	2.8	2.8	2.8	7
	Process beneficiation	4.2	2.8	4.2	7	1.4	7	4.2	7
Overall weighted scores		**57.00**	**64.40**	**63.00**	**52.00**	**55.80**	**58.00**	**71.00**	**100**

4.5.1.5 EXPLANATION OF THE SELECTION/SCORING CRITERIA FOR THE POTENTIAL PROCESS

The overall result for the trade-off studies is presented in Table 4-5, the selection criteria is based on the higher score outcome. It is obvious from the result, process P7 (Hydrometallurgical sulphuric acid leaching of olivine mineral as the simulant for C-type NEA with electrowinning and electrochemistry) has emerged first with 71.00% overall weighted scores, followed by process P2 (Hydrogen reduction process on Iron oxide from C-type NEA regolith to produce Iron (Fe) as the primary product) with 64.40% and in the third position is process P3 (Carbon monoxide reduction process on Iron oxide from C-type NEA regolith to produce Iron (Fe) as the primary product) 63.00%

In the subsequent section the Sensitivity Analysis (SA) is performed to validate the process selection order's ranking that results from the trade-off studies.

4.6 SENSITIVITY ANALYSIS

The trade-off studies have been performed; the ranking of the design alternative has been achieved. The Sensitivity Analysis is performed to validate the process selection order's ranking that results from the trade-off studies by demonstrating that small changes do not alter the scale significantly (Smith, et al., 2008). These changes can be performed on the numerical scores or the defined weight factors to observe the overall effect of these changes to ranking order (Smith, et al., 2008). If the sensitivity check reveals that small changes could significantly reverse a decision, the decision process must be adjusted to its insensitive state. The outcome of the initial trade-off studies showing the various scores for the criteria, weighting values and the overall weighted scores is summarized and illustrated in Table 4-5.

4.6.1 SENSITIVITY METHODS

To these studies, three methodologies are applied towards ascertaining the robustness of the selected processes; the methods are described below:

4.6.1.1 MAKING THE WEIGHTING VALUE ORDER UNIFORM

In this methodology, all weighting values are set to a uniform value, assuming 10 for each of the sub-criteria/parameters under the processes and resulting in 100 total weighting values. Applying these new changes, as shown in Table 4-6. , a new score order emerged as against the against the initial scoring order of the trade-off studies. P6 emerged the leading process, followed by P7 and then P4 in the third position. As presented in Table 4-6 the weighted margin between P6 and P7 the new first and second selected process/option and between P7 and P4 the new second and third selected process/option is two (2) which quite insignificants.

Table 4-6: result of making the weighted value order uniform and comparing with the result of the initial trade-off studies

Item's column	**p1**	**p2**	**p3**	**p4**	**p5**	**p6**	**p7**
Initial score based on the trade-off study	57.00	64.40	63.00	52.00	55.80	58.00	71.00
Result using uniform weighted values	52.00	58.00	56.00	60.00	46.00	64.00	62.00

4.6.2 SMALL INCREASE TO THE SCORES LESS THAN 10% OF THE ORIGINAL SCORED VALUES FOR EACH CRITERION UNDER THE PROCESSES P1 – P7 EXCLUDING HIGHEST AND LOWEST SCORE (1 AND 0)

This process examined how small changes in the raw scores less than 10% of the scored values for each sub-criteria/parameters under a process will affect the ranking order of the selection process. The implementation of the process is in step order of 1% through a range below 10%. Implementing a small change between 1 – 10%, the order of the scoring obtained in the Initial scores based on the trade-off study is maintained. The order of the scoring for a small change between 1 – 5% as presented in Table **4**-**7**, P7, P2 and P3 maintained the lead as the first, second and third position.

Table 4-7: Showing the result of small positive change across all the processes

Item's column	P1	P2	P3	P4	P5	P6	P7
Original/initial scores	57.00	64.40	63.00	52.00	55.80	58.00	71.00
1% small change	57.32	64.64	63.23	52.35	56.04	58.34	71.16
2% small change	57.78	64.89	63.46	52.70	56.28	58.68	71.32
3% small change	57.96	65.13	63.69	53.05	56.51	59.02	71.48
4% small change	58.28	65.38	63.92	53.40	56.75	59.36	71.64
5% small change	58.60	65.62	64.15	53.75	56.99	59.70	71.80

4.6.2.1 SMALL INCREASE TO THE SCORES LESS THAN 10% OF THE ORIGINAL SCORED VALUES FOR EACH CRITERION UNDER THE PROCESSES P1 – P6 AND SMALL DECREASES OF LESS THAN 10% TO PROCESS (P7) EXCLUDING HIGHEST AND LOWEST SCORE (1 AND 0)

This scenario entails making small increase below 10% across all the raw scores under alternatives P1 – P6 and a small decrease below 10% for the winning alternative P7 and excluding raw scores with the highest and the lowest (1 and 0). Implementing the changes in step order of 1% and between 1 – 10%, the order of the scoring obtained in the Initial scores based on the trade-off study is maintained. The order of the scoring for a small change between 1 – 5% as presented in Table 4-8, P7, P2 and P3 maintained the lead as the first, second and third position.

Table 4-8: Showing the result of small increase for P1 to p6 and small decrease change for P7

Item's column	P1	P2	P3	P4	P5	P6	P7
original scores	57.00	64.40	63.00	52.00	55.80	58.00	71.00
1% small change	57.32	64.64	63.23	52.35	56.04	58.34	70.84
2% small change	57.78	64.89	63.46	52.70	56.28	58.68	70.68
3% small change	57.96	65.13	63.69	53.05	56.51	59.02	70.52
4% small change	58.28	65.38	63.92	53.40	56.75	59.36	70.36
5% small change	58.60	65.62	64.15	53.75	56.99	59.70	70.20

4.7 CONCLUSION

Seven well established terrestrial ISRU processes were identified as potential processes for considerations. The multi criteria analysis techniques was use as a suitable tool for the selection process. Trade study was conducted to compare the 7 selected ISRU processes namely (Carbo-thermal reduction with methane (CR-M), Molten oxide electrolysis (MOE), thermal reduction process with hydrogen (TR-H), carbo-thermal reduction with carbon monoxide (CR-CO), sulphuric acid treatment of metallic oxide (SAT-MO), vapour phase pyrolysis (VPP), and including hydrometallurgy sulphuric acid leaching on regolith minerals and using electroplating techniques to deposit the extracted metal and also to identify, and quantify the metals to limit the number of options that has the highest score according to set of evaluation criteria for subsequent detailed appraisals. The result outcome has shown process P7 (the hydrometallurgical Sulphuric acid leaching process on olivine mineral) emerged as the most suitable method to extract metal at C-type NEA and compatible with the CubeSat mission scenario with the highest overall weighted score of 68.62 point. A sensitivity check was conducted to validate the ranking order, and three methodologies were applied.

The result of the sensitivity check based on method 2&3 was consistent, and the initial winning sequence P7, P6 and P5 was maintained and the margin across all the winning alternatives is insignificant. The sensitivity check based on the method1; the order of the scoring was observed to conflict with those of method 2&3, the winning sequence was P6, P5 and P7.

Some of the traded technologies even though they are the most popular and advanced technologies, they have higher energy requirement, higher temperature requirement $\geq 800^0$C and complex step and this might impede the CubeSat functionality. The selected method requires lower operational temperature, lower energy and power requirement and suitable working with the CubeSat. In the conclusion sulphuric acid leaching of the regolith mineral in a low temperature RCS oven and the liquid handling aspect will be implemented in this research work. The leaching process take place in a room temperature and have the least power, energy, and temperature requirement with the following corresponding values 4.6KJ, 2.56w and 298.15k.

5 OVERALL PAYLOAD SYSTEMS LEVEL DESIGN

5.1 INTRODUCTION

This chapter aims to achieve a payload system-level design that will meet the following payload design objectives: Enable the extraction of metal through the hydrometallurgical sulphuric acid leaching of mineral, perform the metal electroplating and electrochemical analysis, that will be CubeSat compatible using a cost-effective budget and able to be operational in the microgravity environment. Designing a payload system that will meet the said payload design objectives, the payload objectives are transformed to generate quantitative requirements and constraints. The generated quantitative requirement and constraint will, in turn, be used to establish the design concept that will meet the payload objectives. This chapter will produce the overall payload systems-level design compatible with the CubeSat form factor.

Over the years, within the Cranfield University Space Research Group in the United Kingdom series of activities have been ongoing concerning the concept of *In Situ* Resource Utilisation *(ISRU*). The main activities in the research group include the development of a CubeSat-compatible payload capable of performing the *ISRU* concept as a de-risking process for future scale-up into a full *ISRU* technology. The water electrolysis to separate (oxygen and hydrogen) and metal extraction from suitable regolith feedstock available on Near-Earth Object (NEO) and planetary surfaces and compatible with CubeSat are some of the critical options under consideration. The general overview of the proposed payload system is discussed, followed by the description of the payload system operation sequence and finally, the conclusion section is presented.

This chapter aims to produce a payload system design that will enable the extraction of metal through the hydrometallurgical sulphuric acid leaching of mineral, perform the metal electroplating and electrochemical analysis, that will be compatible with the CubeSat form factor and able to be operational in the microgravity environment.

PAYLOAD SYSTEM TOP LEVEL REQUIREMENT CAPTURE AND CLASSIFICATION

This section of the thesis would deliver on the generation of the overall top-level payload system requirements, sub-system requirements. To produce the top-level system requirement, and the design concept for the ISRU payload system several assumptions and limitations associated to the CubeSat technology, the location for demonstration of the ISRU process and the ISRU method were identified and discussed. These assumption and limitation include:

Assumption 1: Due to the ISRU CubeSat payload limitation in terms of volume and mass, an upper limit of the amount of regolith that could be reasonably processed to extract the metal material through the leaching process and using acid reagent is considered. Therefore, it can be assumed that 10g of the regolith samples can yield to the extraction of approximately 2g of the Iron metal using the ISRU demonstration payload system.

- Forsterite olivine mineral is the type of mineral present in the C-type NEA and the result of asteroid/meteorite analysis presented in section 2.6, confirmed that Mighei carbonaceous chondrite meteorite (CM CCM) and the Ivuna carbonaceous chondrite meteorite (CI CCM) are the commonest meteorites.
- CM2 CCM family with higher prevalence of FeO about 23% as against 5% FeO present in CI CCM family is considered as the most preferred candidate. The 23% of FeO present in the olivine mineral represent 35.26g of the total mass of the olivine mineral of 153.31g. Therefore, the amount of Fe metal present in the FeO correspond to 27.42g.
- 10g of olivine mineral regolith is expected to produce 2.3g of FeO compound. The FeO compound is expected to produce 1.8g of Fe metal, therefore, the ISRU system should be able to accept at most 10g of olivine mineral regolith to yield approximately 2g of Fe metal

Assumption 2: Power usage should be in accordance with the CubeSat powers system requirement, for example a standard 3U CubeSat has a maximum power budget in the range of 7 – 20W and therefore, a standard 3U CubeSat power consumption shall not be >20W

Assumption 3: The CubeSat is expected to land and anchor in a proper orientation on the surface of a destination C-type NEA. The surface of the destination C-type NEA Ryugu is relatively smooth and covered with granular soil and not rocks. Therefore, at this early stage of the system development, a soil material particle size of <5mm in diameter is considered as the selected baseline diameter.

Assumption 4: A minimum of 6U and 8U CubeSat in the upper limit is considered in the implementation of the overall ISRU payload system mission (including the ISRU payload, power system, avionics system etc.). The ISRU payload system design would incorporate five sub-systems. Assuming each of these sub-system takes a maximum of 1U, then 5U has been used and leaving behind minimum of 1U or maximum of 3U for the other systems.

Assumption 5: This project would focus on the design of two components of the overall ISRU payload system the (RCS and the LHS). As illustrated in fourth assumption, if each of the sub-system would take 1U, then this work target to use 2U CubeSat form factor at the minimum.

5.1.1 TOP LEVEL PAYLOAD SYSTEM REQUIREMENT CAPTURE AND CLASSIFICATION

In this sub-section, the top-level ISRU payload system requirements are captured and classified into functional and non-functional, including operations, design, and scientific requirements. The top-level requirement of the ISRU payload system are categories into (1) the system that supply in-situ material to a processing system, (2) the system that process in-situ material and produce the desired primary product such as metal in leachate form (metal-acid solution) and (3) the system that recover the metal from the leachate and finally (4) the system that analyse the primary product in terms of detecting and quantification. As we progress into the later section of this chapter, the top-level requirements are decomposed down to generate the sub-system requirement. The summary of the top-level payload requirements is as shown in Table 5-1.

Description of requirement ID components as illustrated in Table 5-1 and for instance Top_Func_1 (Top denote top level requirement, and FUNC_1 denote the type of requirement.

Table 5-1: ISRU payload top level system requirement

Requirement ID	Requirement	Requirement descriptions	Requirement types
Top_Func_1	The payload system shall demonstrate the ability to perform the hydrometallurgical H_2SO_4 acid leaching of the regolith material present on the C-type NEA.	The result of a trade study carried out in Chapter 3 and Chapter 4 has led to the selection of the C-type NEA as a potential location for the demonstration of a CubeSat ISRU mission and the selection of the hydrometallurgical H_2SO_4 acid leaching process as the most compatible technique suitable with the CubeSat form factor. The payload shall demonstrate the leaching of the regolith material as the simulant present on the C-type NEA using the H_2SO_4 acid reagent at room temperature to achieve the extraction of metal that would be used in-situ for infrastructure development.	Scientific/Functional
Top_Func_2	The payload shall demonstrate the ability to perform the aspect of liquid handling process.	The supply of the liquid acid to achieve the leaching of the regolith and the extraction of the leachate (metal-acid solution) is a very critical component in the metal extraction process. The ISRU payload shall demonstrate the capability to supply the leaching reagent before the leaching process and extract leachate after the leaching process.	Scientific/Functional

Requirement ID	Requirement	Requirement descriptions	Requirement types
Top_Func_3	The payload shall demonstrate the ability to perform the electro-wining process.	After the demonstration of a successful leaching process, the recovery of the metal from the leachate (metal-acid solution) through the electro-wining process would allow for the quantification and identification of the recovered metal. The ISRU payload shall demonstrate the capability to perform the electro-wining process.	Scientific/Functional
Top_Func_4	The payload shall demonstrate the ability to perform the electrochemical analysis.	The result of achieving a successful metal recovery through the electro-wining process the recovered metal need to be identified and quantified. The identification and quantification of the recovered metal is a necessary requirement and therefore, the ISRU payload system shall demonstrate the capability to perform the electrochemistry analysis	Scientific/Functional
Top_Func_5	Payload shall be able to supply in-situ material to the ISRU system.	The in-situ material is a key ingredient used in the leaching process to achieve the extraction of metal using the acid reagent. The ISRU payload shall demonstrate the ability to	Scientific/Functional

Requirement ID	Requirement	Requirement descriptions	Requirement types
		collect and supply the in-situ material into the ISRU payload system	
Top_Ops_1	Payload shall work under a microgravity environment.	Extreme low gravity exists in the potential destination for the demonstration of ISRU process (the C-type NEA). The ISRU payload system shall demonstrate the ability operate under a microgravity environment.	Performance
Top_Desg_1	The ISRU payload system considered in this project shall be designed to be compatible within 2U CubeSat form factor and with an equivalent mass ≤ 3Kg	The expected CubeSat configuration to perform the overall mission on the lower scale is 6U and 8U on the upper scale. The ISRU payload would use 2U CubeSat volume minimum and 3U on the upper scale	Design/constraint

Requirement ID	Requirement	Requirement descriptions	Requirement types
Top_Desg_2	Based on CubeSat standard a typical 3U payload power requirement range should not be > 20 W.	Considering the upper scale, a 3U ISRU payload power requirement is considered. A 3U CubeSat power ranges from 7 to 20W and therefore, the ISRU payload power range should not exceed 20W	Design/constraint

5.1.1.1 PAYLOAD SUB-SYSTEM LEVELREQUIREMENT GENERATION

As illustrated in section 5.2.1, the top-level ISRU payload system are categories into four systems including the system that process in-situ regolith material. The system that processes in-situ (regolith) material is further broken into the leaching system that leached the metal from the regolith using an acid re-agent to form the leachate (metal-acid solution), and the liquid handling system that supply liquid acid re-agent into the leaching system to leach the regolith material and extract the resultant leachate liquid out of the leaching system to the next level of the process. From the top-level ISRU payload system, five payload sub-systems are classified that would be used to supply the regolith material into the leaching process, liquid re-agent supply and the leachate (metal-acid solution) extraction out of the leaching process, achieving the leaching process, perform the deposition of the metal onto an electrode through electroplating, and the detection and quantification of the deposited metal through electrochemistry process. The overall payload system top-level requirement generated and presented on **Table 5-1** are further decomposed to generate the payload sub-system requirement that will finally be narrow down to components identification and selection for the implementation of the ISRU payload system design**.** The description of requirement ID components is as illustrated; thus, for instance Sub_A_Func_1 (Sub denote subsystem level requirement, A denote that the requirement is sub-system specific and FUNC denote the type of requirement.

5.1.1.1.1 REQUIREMENT GENERATION FOR THE REACTION CHAMBER SUB-SYSTEM (RCS)

The acid re-agent leaching of the regolith materials takes place inside the RCS. The bottom side of the RCS has inlet connection to the Sample Acquisition Sub-system (SAS) through which the regolith material is feed into the RCS and on the topside a connection for the Liquid Handling Sub-system (LHS) through which liquid acid re-agent are supplied into the RCS before the commencement of the leaching process and the leachate is extracted out of the RCS after the leaching process. The top-level requirement with requirement ID (Top_Func_1) presented in Table 5-1 are decomposed to generate the RCS payload sub-system requirement as presented Table 5-2.

Table 5-2: RCS ISRU Payload sub-system level requirement

Requirement ID	Requirement	Requirement source	Requirement type	Requirement description
Sub_R_Func_1	The Reaction Chamber Subsystem (RCS) shall demonstrate the ability for the leaching of the regolith material to achieve metal extraction	Top_Func_1	Functional	The RCS is a critical subsystem in which the leaching process occur, and the leachate is extracted from after the leaching duration has expired. The RCS requirement to show the ability for the leaching of the regolith material shall be demonstrated via physical testing with a 20% minimum of the metal mass extraction efficiency
Sub_R_Desgn_1	The RCS shall be designed to be compatible with the CubeSat form factor	Top_Func_1	Design	Considering the constraint in the volume/size associated with the CubeSat form factor, the RCS shall be designed to occupy 1U CubeSat form factor. This requirement shall be demonstrated initially via design and would finally be implemented physically to fit into the 1U CubeSat form factor
Sub_R_Desgn_2	The RCS shall be made from material that can be compatible working with selected acid reagent.	Top_Func_1	Design	Sulphuric acid is the reagent used for the leaching process and therefore, the material used in making the RCS shall be compatible working with sulphuric acid reagent. This requirement shall be demonstrated initially via design through the selection process from the existing materials compatibility tables and later by testing. The selected material shall be tested to

Requirement ID	Requirement	Requirement source	Requirement type	Requirement description
				observe the effect of corrosion and material degradation when exposed to the acid reagent for the duration of the experiment to determine the unacceptable level.
Sub_R_Desgn_3	The RCS shall be designed to have a maximum of 15ml internal volume to accommodate the reaction mixture (a mixture of acid reagent and 10g regolith material) and also allow space for mounting other components for demonstration of leaching process.	Top_Func_1	Design	This requirement shall be demonstrated via design and would then be implemented via practically demonstration to allow for the accommodation of the reaction mixture and other components.
Sub_R_Desgn_4	The RCS should be able to accept maximum of 10g of regolith material for the leaching process demonstration.	Top_Func_1	Design	This requirement results from the desire to extract 2g of metal from the regolith mixture and shall be demonstrated via a practical means toward achieving the minimum of 20% metal mass extraction efficiency.

Requirement ID	Requirement	Requirement source	Requirement type	Requirement description
Sub_R_Desgn_3	For each set of the leaching reaction process the RCS should be used to demonstrate a minimum of three replicates for the metal production.	Top_Func_1	Design	This requirement shall be used to achieve three demonstrations of the leaching process as a minimum requirement to produce a reliable and acceptable number of replicable results.
Sub_R_Desgn_4	The RCS components shall be designed to fit on to the top-plate mounting position with ease	Top_Func_1	Design	This requirement shall be demonstrated via design implementation and physical testing to show that the RCS fit on to the top-plate mounting position

5.1.1.1.2 REQUIREMENT GENERATION FOR THE LIQUID HANDLING SUBSYSTEM (LHS)

Liquid Handling Sub-system (LHS) serve the dual purpose of liquid acid re-agent supply into the RCS before the commencement of the leaching process and the extraction of leachate (metal-acid solution) out of the RCS after the leaching process. The top-level requirement with requirement ID (Top_Func_2) presented in **Table 5-1** are decomposed to generate the LHS payload sub-system requirement as presented Table 5-2

Table 5 – 3: LHS ISRU Payload sub-system level requirement

Requirement ID	Requirement	Requirement source	Requirement type	Requirement description
Sub_L_Func_1	Constrained by using a maximum of 15ml internal volume of the RCS, the liquid handling subsystem (LHS) shall demonstrate the ability to pump/deliver a maximum of 5ml of sulphuric acid re-agent into the RCS before the commencement of leaching reaction	Top_Func_2	Functional	The 5ml of acid reagent pumped into the RCS added to the volume occupied by the regolith material will allow room for attaching other components. This requirement shall be demonstrated via the design of a fluid flow control circuit and the physical assembly and testing of the system to monitor and regulate the volume of the sulphuric acid re-agent flow into the RCS
Sub_L_Func_2	The LHS shall demonstrate the ability to pump out above 80% of the leached acid-metal solution from RCS after the leaching reaction.	Top_Func_2	Functional	Pumping out above 80% of the leached acid-solution is an indication of the leachate extraction efficiency. This requirement shall be demonstrated via using the designed fluid flow control circuit and the physical assembly and testing of the system.
Sub_L_Func_3	The LHS using plunger mechanism shall demonstrate the	Top_Func_2	Functional	This requirement shall be demonstrated via the design of a linear control

Requirement ID	Requirement	Requirement source	Requirement type	Requirement description
	ability to linearly extend into the RCS the plunger mechanism through a predetermined depth of 10mm to achieve the leached liquid extraction from the RCS			mechanism and the physical assembly and testing of the system to control the extension of the plunger mechanism into the RCS to achieve an efficient leachate extraction out of the RCS
Sub_L_Func_4	The LHS using plunger mechanism shall demonstrate the ability to linearly retract out of the RCS the plunger mechanism through a predetermined height 0f 10mm to achieve the liquid supply into the RCS	Top_Func_2	Functional	This requirement shall be demonstrated via the design of a linear control mechanism and the physical assembly and testing of the system to control the retraction of the plunger mechanism out of the RCS to achieve an efficient sulphuric acid re-agent delivery into the RCS
Sub_L_Desgn_1	The LHS shall demonstrate the ability to isolate the liquid flow control into the RCS when the predetermine 5ml volume of the sulphuric acid solution has been pumped into the RCS	Top_Func_2	Design	This requirement shall be demonstrated via design implementation and physical assembly and testing of the system to achieve the isolation of liquid flow control into the RCS

Requirement ID	Requirement	Requirement source	Requirement type	Requirement description
Sub_L_Desgn_2	The LHS shall demonstrate the ability to isolate the liquid flow control out of the RCS when greater than 80% leachate extraction efficiency was achieve	Top_Func_2	Design	This requirement shall be demonstrated via design implementation and physical assembly and testing of the system to achieve the isolation of liquid flow control out of the RCS
Sub_L_Desgn_3	The LHS shall provide a sealing mechanism to ensure a leakage-free system during the liquid handling process	Top_Func_2	Design	This requirement shall be demonstrated via physical assembly and testing of the system to ensure leakage-free LHS
Sub_L_Desgn_4	The LHS components shall be designed to fit on to the top-plate mounting position with ease	Top_Func_2	Design	This requirement shall be demonstrated via design implementation and physical assembly and testing of the system to show that the LHS fit on to the top-plate mounting position

5.1.1.1.3 REQUIREMENT GENERATION FOR THE METAL RECOVERY SUB-SYSTEM THROUGH ELECTRO-WINING SUB-SYSTEM (EWS) PROCESS

The metal recovery is achieved in this sub-system using the leached metal-acid solution (leachate) obtained from leaching process. through the electro-wining process the metal is recovered from the leachate and deposited onto the electrode. The top-level requirement with requirement ID (Top_Func_3) presented in **Table 5-1** are decomposed to generate the EWS payload sub-system requirement as presented Table 5-2

Table 5 – 4: EW ISRU Payload sub-system level requirement

Requirement ID	Requirement	Requirement source	Requirement type	Requirement description
Sub_E_Func_1	The Electro-Plating and Electro-Wining Subsystem (EP/WS) shall demonstrate the ability to extracted metal inside the leachate (acid-metal solution) and deposit same onto an electrode to achieve greater than 20% metal recovery.	Top_Func_3	Functional	As leaching process result in the production of a leachate (acid-metal solution). Through the EP/WS the metal present in the leachate shall be extracted and deposited onto an electrode to achieve greater than 20% metal recovery. This requirement shall be demonstrated via a practical testing/process.
Sub_E_Desgn_1	The EP/WS shall be made from material that can be compatible working with sulphuric acid	Top_Func_3	Design	Sulphuric acid is the reagent used for the leaching process and therefore, the material used in making the EP/WS shall be compatible working with sulphuric acid reagent. This requirement shall be demonstrated initially via design through the

Requirement ID	Requirement	Requirement source	Requirement type	Requirement description
				selection process from the existing materials compatibility tables and later by testing. The selected material shall be tested to observe the effect of corrosion and material degradation when exposed to the acid reagent for the duration of the experiment to determine the unacceptable level.
Sub_E_Desgn_2	The EP/WS components shall be designed to fit on to the top-plate mounting position with ease	Top_Func_3	Design	This requirement shall be demonstrated via design implementation and physical assembly and testing of the system to show that the EP/WS fit on to the top-plate mounting position
Sub_E_Desgn_3	The electrode used in the EP/WS shall be made from an inert material	Top_Func_3	Design	The inert electrode does not participate in the chemical reaction, they conduct electricity by transferring electrons with the solution (in this regard the leachate) and help in depositing the metal composition of the leachate onto the anode (the positively charge electrode). This

Requirement ID	Requirement	Requirement source	Requirement type	Requirement description
				requirement can be demonstrated via practical demonstration.

5.1.1.1.4 REQUIREMENT GENERATION FOR THE ANALYTICAL SUB-SYSTEM (AS)

Using the Analytical Subsystem (AS), the deposited metal onto the electrode is detected and quantified. The top-level requirement with requirement ID (Top_Func_4) presented in **Table 5-1** are decomposed to generate the AS payload sub-system requirement as presentedTable **5**-**2**

Table 5 – 5**:** AS ISRU Payload sub-system level requirement

Requirement ID	Requirement	Requirement source	Requirement type	Requirement description
Sub_A_Func_1	The Analytical Subsystem (AS) Shall demonstrate the ability to detect the type of metal (Iron, Magnesium etc.) deposited onto an electrode	Top_Func_4	Functional	Through the AS the metal deposited onto the electrode can be detected and the type of metal present ascertain. This requirement shall be demonstrated via a practical testing/process
Sub_A_Func_2	The AS Shall demonstrate the ability to quantify the amount of the metal deposited onto the electrode approximately greater than 20% of the original mass of the regolith sample used	Top_Func_4	Functional	Through the AS the metal deposited onto the electrode can be quantify. This requirement shall be demonstrated via a practical testing/process
Sub_A_Desgn_1	The AS system shall fit inside a 1U CubeSat volume	Top_Func_4	Design	Considering the constraint in the volume/size associated with the CubeSat form factor, the AS shall be designed to occupy 1U CubeSat form factor. This requirement shall be demonstrated initially via design and would finally be

Requirement ID	Requirement	Requirement source	Requirement type	Requirement description
				implemented physically to fit into the 1U CubeSat form factor
Sub_A_Desgn_2	The AS components shall be designed to fit on to the top-plate mounting position with ease	Top_Func_4	Design	This requirement shall be demonstrated via design implementation and physical assembly and testing of the system to show that the AS fit on to the top-plate mounting position
Sub_A_Desgn_2	The AS shall be made from material that can be compatible working with sulphuric acid		Design	Sulphuric acid is the reagent used for the leaching process and therefore, the material used in making the EP/WS shall be compatible working with sulphuric acid reagent. This requirement shall be demonstrated initially via design through the selection process from the existing materials compatibility tables and later by testing. The selected material shall be tested to observe the effect of corrosion and material degradation when exposed to the acid reagent for the duration of the

Requirement ID	Requirement	Requirement source	Requirement type	Requirement description
				experiment to determine the unacceptable level.

5.1.1.1.5 REQUIREMENT GENERATION FOR THE SAMPLE ACQUISITION SUB-SYSTEM (SAS)

Using the Sample Acquisition Sub-system (SAS), the sample regolith material is scoop from the surface of the destination C-type NEA and are feed into the RCS. The top-level requirement with requirement ID (Top_Func_5) presented in **Table 5-1** are decomposed to generate the SAS payload sub-system requirement as presented Table 5-2

Table 5 – 6: SAS ISRU Payload sub-system level requirement

Requirement ID	Requirement	Requirement source	Requirement type	Requirement description
Sub_SA_Func_1	The Sample Acquisition Subsystem (SAS) shall demonstrate the ability to scoop and deliver a maximum of 10g of the regolith material into the RCS	Top_Func_5	Functional	This requirement originates from the top-level assumption aiming to place/deliver 10g of the regolith material into the RCS that would be used to achieve the extraction of 2g of the metal. This requirement shall be demonstrated physically.
Sub_SA_Func_2	SAS should fit into a 1U CubeSat form factor	Top_Func_5	Functional	Considering the constraint in the volume/size associated with the CubeSat form factor, the AS shall be designed to occupy 1U CubeSat form factor. This requirement shall be demonstrated initially via design and would finally be implemented physically to fit into the 1U CubeSat form factor
Sub_SA_Func_2	SAS should operate at the soft surface to scoop/deliver < 5mm diameter particle size into the RCS.	Top_Func_5	Functional	This requirement is derived from the top-level assumption of targeting using< 5mm regolith material on the surface. The particle size had a significant effect on the leaching process, with decreasing particle size, the mineral surface area increases and result in an increase in the mineral dissolution.

5.2 THECONCEPT OF CUBESAT COMPATICLE PAYLOADS FOR EARLY ISRU DEMOSTRATION WITHIN THE CRANFIELD SPACE GROUP

Within the Cranfield Space Research group, several ongoing activities are related to the CubeSat compatible payload for the early ISRU demonstration; they include the water electrolysis to separate (oxygen and hydrogen) and metal extraction on destination NEO. Some of the constraints imposed on these activities include:

(1) The payload shall fit within a maximum of 3U CubeSat form factor

(2) The payload processing steps to avoid operating in high temperature (i.e $\geq 100^0$C)

The overall CubeSat system architecture is proposed to comprise of the following subsystem:

- Feedstock acquisition subsystem
- Multiple containers to allow for primary processing of the feedstock
- Collection of primary products from the primary processing
- Secondary processing of primary products and the
- Appropriate sensors and analytical systems to observe and for the quantification of the primary product.

5.2.1 EXTRACTION AND DIOXYGEN AND DIHYDROGEN PRODUCTION FROM WATER-ICE CONTAINING REGOLITH

This co-running research activity within the Cranfield Space Research group (Sitepu, 2020) entails the ISRU demonstration process at a C-type NEA for low-temperature water extraction from water-ice containing regolith and the subsequent electrolysis of the extracted water to produce dioxygen and dihydrogen. The water extraction process architecture comprises of the following subsystem: (1) sample acquisition via counter-rotating brushes/paddles and Archimedes screws, (2) extraction of volatile components via multiple single-use ovens with electrical resistive heating, (3) cold-trapping of evolved condensable

volatiles – primarily water, (4) electrolysis of the trapped water into dioxygen and dihydrogen gas, and (5) analysis of volatiles at various stages of the process with a miniaturise ion-trap mass spectrometer. Figure 5-1 shows the CAD design assembly for the sample acquisition subsystem comprising of counter rotating brushes/paddles and Archimedes screws, extended scissor mechanism and rotatable carousal of five reaction ovens.

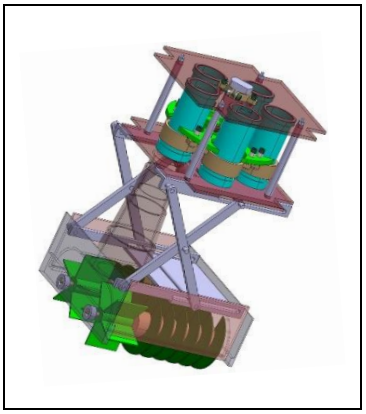


Figure 5-1: CAD design for the sample acquisition subsystem comprising counter rotating brushes/paddles and Archimedes screws, extended scissor mechanism and rotatable carousal of five reaction oven **(Sitepu, 2020)**.

5.3 LEAD TO THE OVERALL PAYLOAD SYSTEM DESIGN

Reference to the top-level requirement generated and classified in section 5.1, the proposed payload for the implementation of the current payload system design comprises of (1) Sample acquisition subsystems (SAS) using the counter-rotating brushes/paddles and Archimedes screws for unconsolidated regolith (2) reaction chamber subsystem (RCS), (3) acid solution delivery and extraction subsystem (ASD&ES), (4) electroplating/wining subsystem (EP/WS) and (5) analytical subsystem (AS) and they appear to agree with the overall proposed CubeSat system architecture presented in section 5.2. Two subsystems relevant to the co-running research activities that entail the ISRU demonstration process at a C-type NEA for low-temperature water extraction appear relevant to this work; they would be re-designed and implemented in the current payload system design. They include: (1) sample acquisition via counter-rotating brushes/paddles

and Archimedes screws will serve the purpose of placing the regolith inside the RCS, (2) the RCS modified to be manufactured out of stainless-steel material will be used for the leaching reaction. Further modification will be carried out on the top-plate to allow for the accommodation of components that will allow handling of liquid leaching solution.

5.3.1 OVERVIEW OF THE PAYLOAD SUBSYSTEM

This section discusses the general overview of the payload subsystem. The overall payload system comprises of (1) sample acquisition subsystem (SAS), (2) reaction chamber subsystems (RCS), (3) acid solution delivery and extraction subsystem (ASD&ES) or the liquid handling subsystem (LHS), (4) the electroplating/wining subsystem (EP/WS) and (5) analytical subsystem (AS). The architecture of the proposed CubeSat compatible with the ISRU demonstration payload system design is as shown in Figure 5-2. These proposed subsystems are discussed in more details in the later section.

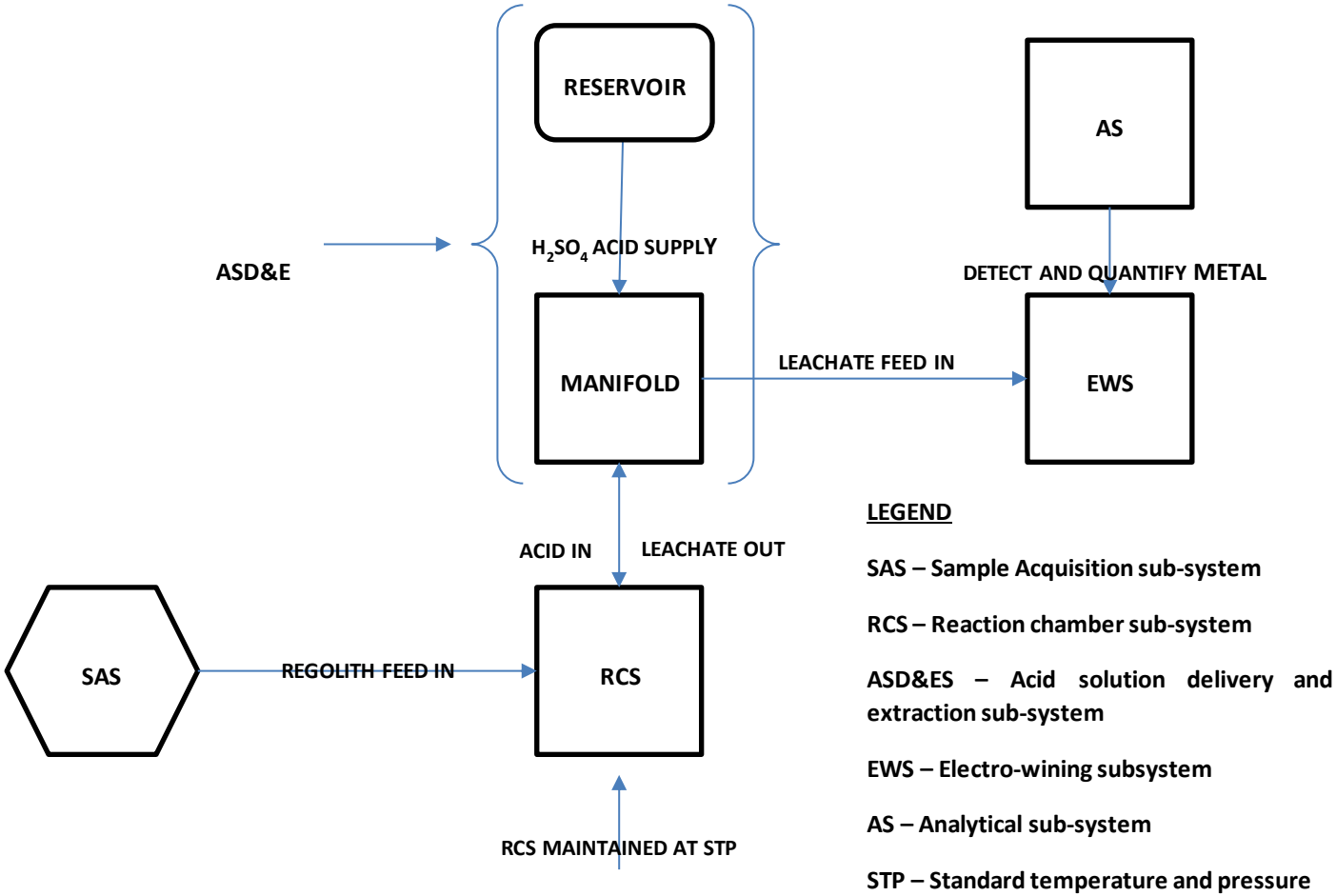


Figure 5-2:. Block diagram representation of the subsystems of the proposed CubeSat compatible ISRU demonstration payload for metal extraction

5.3.1.1 SAMPLE ACQUISITION SUBSYSTEM (SAS)

The SAS mechanism is saddled with the responsibility for collecting regolith samples, delivering the same into the RCS, and performing the hydrometallurgical leaching process. In this research, the sample acquisition method implemented in a co-running CubeSat relevant payload can deliver a maximum of 2g regolith sample mass into the oven is directly adapted. The concept uses two counter-rotating brushes positioned side by side. When enabled, the brushes rotate in opposite directions and collect samples from the surface of the regolith and, through momentum transfer, concentrate the regolith particles through the horn path like connection into the RCS oven and in microgravity.

5.3.1.2 REACTION CHAMBER SUBSYSTEM (RCS)

The RCS mechanism shall be responsible for the efficient interaction between the regolith and sulphuric acid to achieve the leaching process. The version of reaction oven implemented in a co-running CubeSat relevant payload for demonstration of water extraction and comprising five open-ended cylindrical-shaped, based on the initial size, volume, and configuration, appears to be suitable for this project. The RCS is modified to interfacing to solution delivery and removal subsystem. The leaching process is achieved using sulphuric acid; the RCS shall be made from sulphuric acid-resistant material such as stainless steel. Multiple used oven design option is adopted for implementation in the design approach to allow for an aspect of liquid handling and emptying the leftover of the leaching process, cleaning the oven after the extraction of the supernatant, thus allowing the oven system to be re-usable.

5.3.1.3 ACID SOLUTION DELIVERY AND EXTRACTION SUBSYSTEM (ASD&ES)

The standard approach to achieve the metal extraction uses high temperature reactions or electrolysis. The concept of low temperature aqueous acid-based extraction including the use of ASD&ES sub-system is innovative in that it has not been proposed before. The ASD&ES shall be responsible for handling all aspects of solution delivery and extraction into and out of the RCS; the ASD&ES

subsystem is comprised of components such as (a) the valves, (b) pumps, (c) manifolds, (d) reservoirs, (e) tubing connectors and fitting. These components are interconnected, and they interact to establish the ASD&ES that will allow for efficient liquid handling in microgravity. The ASD&ES are operated in two parts, the first part is the delivery of the H_2SO_4 solution from the reservoir into the RCS before the commencement of the leaching process. The second part is the extraction of the supernatant from the RCS after the leaching and transporting it to the electroplating /wining subsystem.

5.3.1.4 ELECTRO PLATING/ELECTRO WINING SUBSYSTEM (EP/WS)

The concept of low temperature aqueous acid-based extraction including the use of EP/WS sub-system is another innovative technique that has not been proposed before. The EP/WS subsystem shall be responsible for electroplating the leached metal ions present in the supernatant onto the working electrode. This version of electrowinning process is implemented using a non-consumable anode such as platinum; the metal ion to be plated is contained in the supernatant. Supernatant rich in metal ion extracted during the leaching process in the reaction oven is transferred to an electrowinning subsystem. The metal ion is electrochemically- reduced and purified onto a suitable electrode. This subsystem (EP/WS) is not included as part of this PhD research work implementation.

5.3.1.5 ANALYTICAL SUBSYSTEM (AS)

The concept of low temperature aqueous acid-based extraction including the use of AS sub-system is yet another innovative technique that has not been proposed before. The AS sub-system aims to achieve the identification and quantification of the metal ion deposited on the working electrode. The anodic stripping voltammetry techniques (ASV) for its versatility is adapted for implementation; the methods are proposed to be implemented using three electrodes working, auxiliary and reference electrode. During the stripping steps, the metal deposited on the electrode earlier during the electrowinning stage is stripped off the electrode using a reversed potential; the current supplied to achieve the stripping

is measured and translated into the quantity of metal ion electro-wined. Three fundamental steps are involved in the AS namely:

- Electroplating the metal ion on the working electrode during the electrodeposition step
- Oxidising the metal from the working electrode during the stripping step and
- Measuring the stripping current as the potential varies

This subsystem (AS) is not included as part of this PhD research work implementation.

5.4 OPERATION CONCEPT FOR THE PAYLOAD SYSTEM DESIGN

In this section, the operational concept of the payload system is briefly discussed. Figure **5-2** presented on page 156 is a block of figures describing the operation concept flow for the ISRU payload system design. The payload system aims to extract metal through the hydrometallurgical leaching process, electroplate the leached metal ions and quantify the metal. The Payload system was assumed to arrive at the target asteroid and securely anchored to the asteroid's surface and in the proper orientation. The payload system operation sequencing starts with using the counter-rotating brushes SAS implemented in a co-running ISRU project (Sitepu, 2020) to deliver ~ 1.5g of fine loose regolith material from the surface of C-type NEA through the lower open-ended part of the reaction oven into the RCS. At the top and bottom ends of the reaction chamber, sealing material is provided to seal the reaction chamber. Delivering the required mass of the regolith into the chamber, the carousel mechanisms rotate the RCS. With the help of the sealing material sliding over the endplates, the regolith is trapped within the RCS. A secured fluid path is established from the reservoir through the manifold and into the RCS. Using the ASD&ES mechanism, H_2S0_4 acid was pumped and delivered into the RCS to leach the regolith. In a microgravity environment, the behaviour of the liquid acid delivered inside the RCS cannot be predicted. To estimate the mass of the regolith scooped into the RCS, the volume of the space occupied by the regolith is measured using the force feedback

sensing mechanism by extending the plunger to compact with the regolith. The plunger distance travel to compact with the regolith is used to estimate the occupied volume inside the RCS and using the regolith material density the equivalent mass of the regolith is estimated. The same mechanism is implemented to ensure that contact between the acid pumped in and the regolith contained inside the RCS has been established for an effective leaching process. At the expiration of the leaching period, the driven mechanism is initialised once again to drive/extend the plunger into the RCS. Sealing is provided with the help of a sealing material in contact with the RCS wall. As the plunger is extended, the waste valve control is switched open to establish a path connecting the RCS and the waste container. The leached metal solution is extracted and transported to the waste container. The extracted acid-metal solution rich in metal ions are transferred to the electrowinning subsystem presumably the waste container. The metal ion through the electrolysis process is reduced and purified onto a suitable working electrode. Finally, using the analytical subsystem the reduced metal onto the electrode is identified and quantified. The anodic stripping voltammetry techniques (ASV) techniques for its versatility is proposed for implementation; the methods are proposed to be implemented using three electrodes working, auxiliary and reference electrodes. During the stripping steps, the metal deposited on the electrode earlier during the electrowinning stage is stripped off the electrode using a reversed potential; the current supplied to achieve the stripping is measured and translated into the quantity of metal ion electro-wined.

5.5 CONCLUSION

In this chapter, the overall payload system design was described. The overall payload system objectives and constraints were defined. The payload system top-level requirements were captured and classified into functional and non-functional requirements. A combination of the top-level requirement generated in agreement with the proposed CubeSat system architecture form a lead to the overall payload system design; five subsystems for the overall system are generated and discussed. The payload operation sequencing was also discussed to give an insight into the system operational flow.

Finally, for this research work, the design has been reduced to the modification of the RCS and the design of the liquid handling subsystem. In the subsequent chapter, the Hydrometallurgical laboratory sulphuric acid leaching experiment on olivine mineral as simulant for C-type NEA will be carried out to further generate additional design requirements for the BB payload system implementation.

6 LABORATORY HYDROMETALLURGICAL SULPHURIC ACID LEACHING OF OLIVINE MINERAL AS THE SIMULANT FOR THE C-TYPE NEAR EARTH ASTEROID (NEA) RYUGU

6.1 INTRODUCTION

In chapter 4, the result of the trade-off study has confirmed the selection of the hydro-metallurgical sulphuric acid leaching process as the potential ISRU process that will be carried forward for implementation in this research work. The selection of the hydro-metallurgical sulphuric acid leaching process was further validated through a sensitivity analysis. Unlike other potential processes that required crushing, grinding and beneficiation, the cost of energy on such process make them expensive, hydrometallurgy leaching process appears to be cheaper, the process has less stages of processing and therefore consume less energy. The hydro-metallurgical acid leaching of mineral ores is a technique for the metal extraction using reagents in aqueous solution for the dissolution of the metal from its ore at lower temperatures, this method was first used for the processing of copper by Rio Tinto in Spain in 1670 (Ambo, 2015).

This chapter aimed to carry out a laboratory-based hydrometallurgical leaching experimental using olivine mineral as a simulant relevant to C-type NEA and sulphuric acid as the leaching reagent to demonstrate/determine how the acid concentration and solid-to-liquid ratio in a state of agitation and non-agitation, at varying leaching duration and at room temperature affect the leaching process. The introduction of solid-to-liquid ratio and the agitation in the hydrometallurgy leaching process is to confirm whether they would have significant influence in the reaction process. The solid-to-liquid volume ratio is expected to potentially provide a balance between the amounts of solid material versus the reagent to achieve an effective leaching reaction/process. while the agitation process is expected to improve contact between the leaching reagent and the regolith material and thereby enhancing the leaching process.

To achieve the selection of leaching reagent for improved metal recovery in the hydrometallurgical leaching process, in-organic acids reagent including H_2SO_4, HCl and HNO_3 were considered. In the leaching of olivine mineral, the H_2SO_4 acid reagent among other acid reagent (H_2SO_4, HCl, $HCLO_4$ and HNO_3) used has shown evidence of maximum metal extraction in decreasing order of H_2SO_4>>HCl>$HCLO_4$ (Ajiboye A. E., 2019). The H_2SO_4 acid reagent was also found to be the common reagent used in the leaching process; they are readily available and cheap too. Finally, H_2SO_4 acid reagent was selected as the most suitable leaching reagent to be used in the leaching process.

The choice of olivine mineral as the regolith simulant relevant to the C-type NEA was informed as result of literature studies carried out. The C-type asteroid was confirmed as the parent body for the carbonaceous chondrite meteorite (CCM), and the CCM family are predominantly olivine and are composed of mainly silicate, oxides, sulphide, organic compounds, and volatiles. Olivine mineral samples in different grain sizes procured from Scan Grit, a UK based mineral company located at Eastfield Road, Immingham was procured and would be used in the experiments to select the appropriate regolith simulant relevant for this experiment.

The equipment used in the leaching processes includes 15ml polypropylene centrifuge tubes (Fisher brand cat.no.-05-539-5) used as proxies for the expected payload reaction containers, Vertical rotatory mixer (Stuart rotator model SB3, with speed range 2 - 40rpm) was used to agitate the reaction mixture inside the centrifuge tubes (or not used when non-agitated reaction is performed) and the laboratory LCD analytical balance digital precision scale with precision at 0.0001g used to measure the mass of reaction tube and mass of reaction tube together with the regolith samples and the thermo fisher scientific Megafuge 16R centrifuge was used for the purpose of enhancing sedimentation of the mixture inside the centrifuge tube to separate the leachate and the sediments (a proxy for the plunger to separate leachate from regolith).

A trial hydrometallurgy leaching experiment was carried out using different particle size ranges of the olivine regolith materials (0.090 – 0.250mm, 0.125 –

0.500mm, 0.180 – 1.000mm and 0.355 – 2.360mm), 1M H_2SO_4 acid reagent in solid-to-liquid volume ratio of 5:5mls for a maximum period of 168hours and in non-agitated state. The outcome of the trial experiment has shown that the particle size has a significant effect on the leaching process and has informed the choice of extra fine grade olivine mineral in grain size range of 0.090 – 0.250mm to be carried forward for further implementation.

Hydrometallurgical experimental design process and the operational method for the experiment were developed and discussed to generate a step-by-step guide in the implementation of the investigation. Different laboratory leaching experiment scenario (initial and repeat laboratory leaching experiment) were carried out to inform the determination of a combination of parameter set that would be used to refine both the payload requirements, payload design, and the payload operations.

The initial and repeat laboratory leaching experiment scenario, each was performed using extra-fine grade olivine mineral regolith samples in the grain size range 0.090 – 0.250mm, multiple sulphuric acid concentration (1M and 5M), variable solid olivine regoliith to fixed liquid acid reagent volume ratio, in both agitation and non-agitation state, and for a total duration of 168hours. The laboratory leaching experiment was carried out inside 15mls centrifuge tubes. The influence of the solid-to-liquid volume ratio, the acid concentration in the leaching experiment and the loss of the acid concentration was checked every 12hours until the expiration of the maximum duration for the leaching period of 168 hours. The leachate was separated from the olivine mineral and will be used in the electro-wining and electrochemical analysis to electroplate, detect, and quantify the leached metal in the future work. The left-over moist olivine mineral is dried. Finally, the weight of the dried mineral was compared with the initial weight of the corresponding olivine mineral before the commencement of the leaching experiment to estimate the mass of the extracted metal that was present in the leachate. Using the same laboratory leaching experimental condition in the initial and repeat experiment, a further experiment scenario including the use of BPB dye indicator solution was also introduced. The BPB dye indicator would eliminate using the litmus test paper, detect the loss of acid concentration/monitor

the pH change by providing the real-time visual colour transition within the required acid pH range. Three different BPB dye solution was prepared with concentrations 2.2mM, 4.4mM and 8.8mM and were all tested. 8.8mM concentration of the BPB dye solution show evidence of deep yellow colour change and we expect to get a better colour transition using the 8.8mM concentration and was therefore selected for this experiment.

6.2 AIMS OF THE EXPERIMENTS

The experimental-work reported in this chapter aimed to demonstrate the effect of acid concentration and solid-to-liquid ratio in a state of agitation and non-agitation for the extraction of metals using olivine mineral as a regolith simulant relevant to C-type NEA and sulphuric acid as the leaching reagent. A further laboratory experiment scenario including the use of BPB dye indicator solution was also aimed at to eliminate using the litmus test paper and monitor the pH change by providing the real-time visual colour transition within the required acid pH range. The results of this could then be used to refine both the payload requirements and the payload design, and payload operations.

6.3 OBJECTIVES OF THE EXPERIMENT

- To study the impact of varying sulphuric acid concentration (1M and 5M) in the olivine mineral leaching process, this will help in determining the required concentration of the reagent to use in the breadboard design implementation and subsequently in the final flight model
- To estimate the required mineral-to-acid volume ratio to be implemented in the bread-board design and the final implementation in the flight model for achieving the maximum extraction and will form a guide in the reaction oven design
- To demonstrate the use of BPB dye indicator solution in the leaching experiment to eliminate using the litmus test paper and to monitor the pH change by providing the real-time visual colour transition within the required acid pH range. To compare the original olivine mineral to the recovered dried sample for any observable differences

6.4 MATERIAL, RE-AGENTS AND THE EQUIPMENT

6.4.1 OLIVINE MINERAL

The choice of the Olivine mineral was a consequence of the literature studies carried out on the mineralogy of the target asteroid (C-type) in Chapter2. The community has a general agreement that the C-type asteroid is the parent body for the carbonaceous chondrite meteorite (CCM). The CCM group members, notably CM and CI, are composed of mainly silicate, oxides, sulphide, organic compounds, and volatiles. The silicate minerals pyroxene, olivine and feldspar are the most abundant mineral in the meteorites, they dominate the stony class of meteorites (Glavin, et al., 2018). The CCM family are predominantly olivine, the olivine mineral is usually forsterite, having more Magnesium than the iron in the CCM (Glavin, et al., 2018). The olivine mineral is cheap, readily available and are also observed to be used in several leaching experiment.

Olivine mineral samples in different grain sizes procured from Scan Grit, a UK based mineral company located at Eastfield Road, Immingham will be used in the experiments to select the appropriate regolith simulant relevant to C-type NEA asteroid Ryugu. The general chemical formula of the olivine mineral is $(Mg, Fe)_2SiO_4$ $(\text{scangrit}, 2021)$ and the chemical composition is as detailed in the Table **6-1**.

Table 6-1: Chemical analysis of Olivine (Mg rich) mineral **(scangrit, 2021)**

Oxide name	**Oxide formula**	**Amount present in (%)**
Silicon oxide	SiO_2	41 - 43
Iron oxide	Fe_2O_3	6 – 8
Magnesium oxide	MgO	47 - 50
Calcium oxide	CaO	0.5 - 1
Aluminium oxide	Al_2O_3	0.4 – 0.5
Titanium oxide	TiO_2	1
nickel oxide	NiO	0.3 – 0.35
Free silica	-	<1

6.4.2 SULPHURIC ACID

A more effective reagent needs to be sought to achieve an improved metal recovery in the hydrometallurgical laboratory leaching process. Possible leaching reagent withing the family of in-organic acids includes H_2SO_4, HCl and HNO_3, (Ajiboye, et al., 2019). H_2SO_4 acid was found to be the common reagent used in the leaching process; they are readily available and cheap (Vračar's, et al., 2003). Also, in another experiment for leaching of olivine mineral, among the acid reagent used, sulphuric acid has shown evidence of maximum metal extraction in decreasing order of H_2SO_4>>HCl>HCLO4 (Ajiboye, et al., 2019). Finally, H_2SO_4 acid was selected as the leaching reagent used in the leaching process. Concentrated Sulphuric acid (98%) procured/obtained from Sigma Aldrich, a UK based chemical company located at Seldon Lane, Poole is the reagent used in preparing the required concentration of the acid used in the leaching process.

A small quantity of the sulphuric acid for the demonstration of the leaching of the space regolith in situ at the destination C-type NEA is imported from the earth. The partly neutralised sulphuric acid resulting from the leaching process, it is unsuitable for re-use. In the future work the project planned the inclusion of sulphuric acid regeneration system that will help in the regeneration of the neutralized sulphuric acid that will be used in the subsequent circle of the leaching process.

6.4.3 EQUIPMENT USED

Disposable 15ml polypropylene centrifuge tubes (Fisher brand cat.no.-05-539-5) procured from Fisher, Loughborough, the UK was used as the reaction containers, Vertical rotatory mixer (Stuart rotator model SB3, with speed range 2 -40rpm) was used to agitate the reaction mixture inside the centrifuge tubes and the laboratory LCD analytical balance digital precision scale with precision at 0.0001g was used to measure the mass of reaction tube and mass of reaction tube together with the samples and the Thermo fisher scientific Megafuge 16R centrifuge was used for the purpose of enhancing sedimentation of the mixture inside the centrifuge tube to separate the leachate and the sediments. As shown in Figure 6-1 Is the setup for initial leaching experiments.

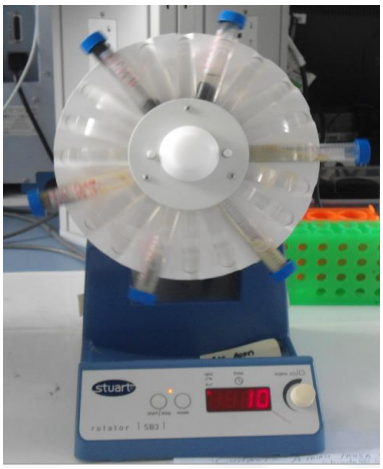


Figure 6-1: setup for the initial leaching experiment

6.5 DESIGN OF HYDROMETALLURGICAL SULPHURIC ACID LEACHING EXPERIMENT OF OLIVINE REGOLITH SIMULANT USING TRIAL EXPERIMENT

This experiment is designed using trial experiment to determine a combination of parameter set that will be carried forward for implementation in the proposed initial and repeat hydrometallurgical sulphuric acid leaching experiment of olivine mineral that would be demonstrated on the bread-board prototype system and eventually on the flight model for the extraction of metal.

6.5.1 TRIAL HYDROMETALLURGICAL SULPHURIC ACID LEACHING EXPERIMENT OF OLIVINE REGOLITH SIMULANT

In the trial leaching experiment, 1M H_2SO_4 acid was initially prepared and used across different particle size ranges of the olivine mineral (0.090 – 0.250mm, 0.125 – 0.500mm, 0.180 – 1.000mm and 0.355 – 2.360mm) procured from Scan Grit a UK based mineral company located at Eastfield Road, Immingham in a solid to liquid volume ratio of 5:5mls. Four centrifuge tubes were used for the trial experiment. To each tube, 5mls of specific olivine mineral was dispensed into, and 5mls of 1M H_2SO_4 acid was added to the four tubes and allowed to react with the olivine mineral contained therein for a maximum period of 168hours. The result of this trial experiment has shown that the particle size had a significant effect on the leaching process, with decreasing olivine mineral particle size, the mineral surface area increases and result in an increase in the mineral

dissolution. The trial experiments informed the choice of extra fine grade olivine mineral in grain size range 0.090 – 0.250mm for further implementation in the hydrometallurgy H_2SO_4 acid leaching experiment.

6.5.2 FURTHER TRIAL HYDROMETALLURGY SULPHURIC ACID LEACHINGEXPERIMENTUSING 0.090 – 0.259MM GRAIN PARTICLES SIZE

A further trial experiment was carried out using 1M H_2SO_4 acid concentration together with the olivine minerals of particle size (0.090 – 0.250mm) in 5:5 solid to liquid volume ratio at room temperature, for a duration of 168 hours and in a non-agitated state. The mineral samples were prepared in three different disposal centrifuge tubes, the olivine mineral + void volumes and the masses of the three samples were measured as shown in Table 6-2. The average bulk density of the olivine mineral was calculated as 1.803g/ml, this would be used in all subsequent experiment. The result outcome of this experiment, the loss of acid concentration, mineral swelling or the volume depletion of the supernatant was observed. The loss of the acid concentration and the mineral expansion were suspected to result from using a lower concentration of the acid and higher volume of the mineral.

Table 6-2: showing the measure olivine mineral +void volume and the measured masses

Material	**Sample 1**	**Sample2**	**Sample3**
Olivine mineral volume (ml)	5	5	5
Olivine mineral measured mass (g)	9.015	9.014	9.015
Olivine mineral calculated bulk density (g/ml)	1.803	1.803	1.803

A second trial experiment was proposed using the same operating condition as in the initial trial experiment with decreasing solid to liquid volume ratio. The proposed decreasing solid-to-liquid volume ratio, it is assumed will potentially provide a balance between the amounts of solid material versus the reagent for an effective leaching process. The result of the second trial, loss of the acid

concentration persists, mineral swelling and the volume depletion of the supernatant was observed to decrease with decreasing solid-to-liquid volume ratio. The challenges associated with the mineral swelling in the leaching process was addressed using the decreasing solid to liquid ratio scenario.

A third trial experiment was proposed using the same condition as in the second trial experiment, and introducing multiple acid concentrations, 1M and 5M sulphuric acid concentration was proposed. The resulting outcome of the third trial experiment was observed to address the problem of acid concentration loss using the 5M acid concentration; the swelling of the mineral was addressed by the decreasing solid to liquid ratio. The higher acid concentration was observed to create a new challenge of mineral consolidation, and the sample could not be re-suspended, this scenario is manifest in the higher solid to liquid ratio and was observed to reduce with decreasing solid-to-liquid ratio.

A fourth trial experiment was proposed using the same condition as in the third trial experiment and using multiple acid concentration (1M and 5M) and in both static and state of agitation. The resulting outcome of the fourth trial experiment was observed to address the problem of acid concentration loss using the 5M acid concentration, the swelling of the mineral was address by the decreasing solid to liquid volume ratio. The challenge associated to the mineral consolidation was observed to be addressed by the mineral agitation and prominent with decreasing solid to liquid ratio. A favourable condition for the leaching process was arrived at, by a combination of using:

- 5M sulphuric acid concentration addresses the problem acid concentration loss
- Decreasing solid to liquid ratio addresses the problem of mineral swelling
- Agitation mechanism addresses the problem of mineral consolidation and enhances the mixing of the reaction mixture

The fourth trial experiment is proposed to be carried forward and be implemented as the final design process in the initial leaching experiment. The summary of the liquid to solid ratio is represented in Table **6**-**3**.

Table 6-3: *Showing the acid to mineral volume ratio used for the experiment*

Material	Sample1	Sample2	Sample3	Sample4	Sample5
Olivine mineral volume (ml)	5	2.50	1.67	1.25	1
Corresponding olivine mineral masses (g)	9.0	4.5	3.0	2.3	1.8
Sulphuric acid volume (ml)	5	5	5	5	5
Solid to liquid volume ratio	5:5	4:5	3:5	2:5	1:5

6.6 DESIGN METHOD FOR THE LABORATORY HYDROMETALLURGAL SULPHURIC ACID INITIAL LEACHING EXPERIMENT ON OLIVINE MINERAL SIMULANT

6.6.1 INTRODUCTION

In this section of the thesis document, the design method for the initial laboratory hydrometallurgical sulphuric acid leaching experiment on the olivine mineral simulant is described. The fourth trial laboratory leaching experiment scenario using multiple acid concentration (1M and 5M), deceasing solid to liquid ratio as illustrated in Table **6-3** in both static and state of agitation and at room temperature and leaching duration of 168hours described in section 6.6.2 was implemented.

6.6.2 DESCRIPTION OF THE EXPERIMENT PROCEDURE

Four different experiments were set up each comprising of five labelled 15mls centrifuge tubes as presented in Table 6 - 4, the leaching process was carried out inside 15mls centrifuge tubes. To each of the centrifuge tube, extra-fine grade olivine mineral samples in the grain size range 0.090 – 0.250mm were dispensed

in the decreasing ratio. Experiment 1&2 are based on 1M H_2SO_4 and experiment 3&4 are based on 5M H_2SO_4 and each in agitation and non-agitation state. 5ml each of 1M and 5M H_2SO_4 was dispensed into each of the 15mls centrifuge tubes samples in experiment 1&2 and experiment 3&4 respectively and allowed to react for a maximum of 168 hours under room temperature. To keep track of the leaching experiment to monitor the influence of the solid to liquid volume ratio and the acid concentration; every 12 hours, each of the sample mixtures was centrifuged to achieve a clear separation between the liquid and solid in the reaction tube. The total volume and individual liquid and solid volume for each test tube content were observed and recorded. The loss of the acid concentration was tested using the litmus test paper, pictures of each sample state are captured for references. The circle of the reaction in both the agitated and non-agitated state for all the samples is repeated for another 12 hours, sample centrifuged, total volume and liquid and solid volume recorded, depletion of acid concentration tested and picture capture. This process continues until the expiration of the maximum duration period of 168 hours. The supernatant was separated from the olivine mineral and intended to be used in the electro-wining and electrochemical analysis to electroplate, detect, and quantify the leached metal. Finally, the moist olivine mineral was dried using an electrically controlled drying oven to remove moisture from them. Each of the recovered moist olivine mineral samples was placed in a labelled petri dish. The weight of each petri dish was recorded, and the dish's weight with the moist olivine mineral was also weighed and recorded. The petri dishes, together with minerals, were placed inside the oven; the oven was set to operate at $50^{O}C$. The mineral drying process was gradual and lasted for about six hours. At the expiration of the six hours, each petri dish containing the dry olivine mineral are weighed over again, the weight of each petri dish is subtracted from the net weight of the dry mineral and petri dish. The weight of the dried mineral was compared with the initial weight of the corresponding olivine mineral before the commencement of the leaching experiment. The mass difference gives an estimate of the mass of the extracted metal that is present in the supernatant.

Table 6- 4: Showing the different experiment and their samples

Experiment	Experiment samples				
Experiment1	S1 - 1	S1 - 2	S1 - 3	S1 - 4	S1 - 5
Experiment2	S2- 1	S2 - 2	S2 - 3	S2 - 4	S2 - 5
Experiment3	S3 - 1	S3 - 2	S3 - 3	S3 - 4	S3 - 5
Experiment4	S4 - 1	S4 - 2	S4 - 3	S4 - 4	S4 - 5

Key/Legend

- S1 – 1 to S1 – 5 represent the five different experiment samples under experiment1
- S2 – 1 to S2 – 5 represent the five different experiment samples under experiment2
- S3 – 1 to S3 – 5 represent the five different experiment samples under experiment3
- S4 – 1 to S4 – 5 represent the five different experiment samples under experiment4

6.6.3 IMPLEMENTATION OF THE INITIAL LABORATORY HYDROMETALLURGICAL SULPHURIC ACID LEACHING EXPERIMENT ON THE OLIVINE MINERAL SIMULANT

The initial laboratory hydrometallurgical sulphuric acid leaching experiment on the olivine mineral simulant was implemented using the design parameters presented in Table 6-4 and following the laid down design method. Observations made during the experiment were captured and recorded. The result of the experiment is presented and described in section 6..6.3.1

Table 6-4: Summary of design parameters used for the initial hydrometallurgical leaching process

Parameter	Conditions
H_2SO_4 acid	1M and 5M
Weight of solid in decreasing order	5 to 1g
Reagent volume	Constant volume (5mL)
Leaching time	168 Hours
Agitation	Both agitate and non-agitate state
Temperature	Standard temperature and pressure (STP)
Particle sizes	Constant range (0.090 – 0.250mm)

6.6.3.1 RESULT AND DISCUSSION OF THE INITIAL LABORATORY HYDROMETALLURGICAL SULPHURIC ACID LEACHING EXPERIMENT ON OLIVINE MINERAL SIMULANT

series of images were captured during the leaching experiment, these images are used to show the variation in the acid concentration loss, mineral expansion and or supernatant/leachate depletion and the mineral colour change as the leaching process progresses. Due to having too many images, for the main section, only the two extremes of the result are presented. The images corresponding to the initial (zero hours) and final (168 hours) phase of the leaching process are shown in **Error! Reference source not found.**. The images are compared to show how the sulphuric acid concentration and the solid-to-liquid volume ratio, over a duration of 168 hours and in both agitation and non-agitation state in the leaching process influence the following parameters:

- Loss of acid concentration

- Supernatant depletion or mineral swelling
- Mineral consolidation
- Mineral loss

The overall photographic results of the initial leaching experiment are presented in Appendix 1.1

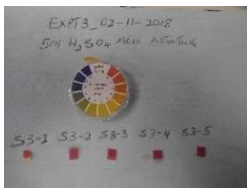
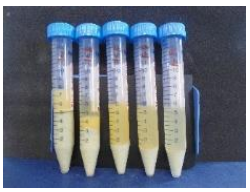
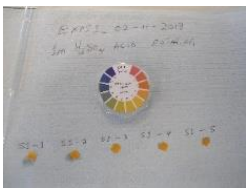
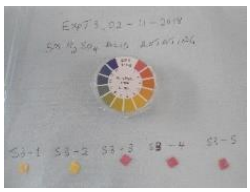
			
			
Expt1, t0 = 0hours	Expt2, t0 = 0hours	Expt3, t0 = 0hours	Expt4, t0 = 0hours
			
			
Expt1, t14 = 168hours	Expt2, t14 = 168hours	Expt3, t14 = 168hours	Expt4, t14 = 168hours

Figure 6-2: Experimental result of the initial hydrometallurgical H_2SO_4 acid leaching of olivine mineral

Legend

- Expt1 - 4 = signifies the experiment numbering from 1 to 4 set of experiment
- t_0 = initial time zero marking the start time/point for the experiment
- t_{14} = final time marking the end time for the experiment

The result outcome of the initial sulphuric acid leaching on the olivine regolith simulant is presented and discussed as follows:

6.6.3.1.1 EFFECT OF SULPHURIC ACIDCONCENTRATION ON SUPERNATANT DEPLETION AND OR MINERAL EXPANSION

The sulphuric acid concentration was observed to impact the supernatant/leachate depletion and or the mineral expansion; as the leaching process progresses, it is evident that the mineral in all the samples across the four experiments are observed to expand. The expansion was observed to be more among samples operated under the higher concentration of the acid and higher solid-to-liquid ratio, consequently, the more supernatant deplete. The summary shown in Table 6-5 indicates the amount of the supernatant in percentage (%) that was depleted across all the samples in the four-experiment set and corresponding to the 168 hours leaching duration. The result indicates that more expansion is recorded among samples with higher acid concentrations and higher solid-to-liquid ratio. In experiments 3 and 4, as shown in Table 6-5, samples S3 – 1 with 5:5 solid-to-liquid ratio and S3 – 5 with 1:5 solid-to-liquid ratio have recorded 100 and 39%, and sample S4-1 with 5:5 solid-to-liquid ratio and S4-5 with 1:5 solid-to-liquid ratio have recorded 54 and 27% maximum supernatant depletion in decreasing solid-to-liquid volume ratio respectively. Among similar samples, the supernatant depletion appears to be more in the agitated samples than the non-agitated samples. Refer to Table 6- 4 for the description of the different experiment and their samples

Table 6-5: Showing Maximum liquid depletion in percentage across the four experiments for the initial laboratory leaching experiment

Maximum Leaching duration (Hours)	**% Maximum liquid depletion in all the samples of the four experiments**				
168	Experiment1 sample using 1M H2SO4 in agitated state				
	S1-1	S1-2	S1-3	S1-4	S1-5
	30	7	16	6	10
	Experiment2 sample using 1M H2SO4 in non-agitated state				
	S2-1	S2-2	S2-3	S2-4	S2-5
	17	7	8	6	8
	Experiment3 sample using 5M H2SO4 in agitated state				
	S3-1	S3-2	S3-3	S3-4	S3-5
	100	100	84	66	39
	Experiment4 sample using 5M H2SO4 in non-agitated state				
	S4-1	S4-2	S4-3	S4-4	S4-5
	54	21	27	26	27

From the summary shown in Table 6-5 the pattern of the supernatant depletion and or mineral expansion across all the samples in the four experiment was shown to decrease with decreasing acid concentration and decreasing solid-to-liquid ratio and specific to similar samples operating under same condition with variation in state of agitation and non-agitation . Sample S1-4 and S2-4 in both experiment 1&2 in agitation and non-agitation state recorded the least supernatant depletion of 6% each, whereas S3-5 and S4-5 in experiment 3&4 in

agitation and non-agitation state recorded the least supernatant depletion of 39% and 27% respectively.

6.6.3.1.2 EFFECT OF SULPHURIC ACID CONCENTRATION ON THE MINERAL CONSOLIDATION

The sulphuric acid concentration was observed to impact on the mineral consolidation. The consolidation of the mineral during the leaching process is a source of concern, it is evident in the recovery of the mineral as shown in The effect of sulphuric acid in leaching out metal from the olivine mineral was studied at room temperature, using particle sizes in the range 0.090 – 0.250mm, at maximum leaching period of 168 hours and across various solid - to - liquid ratio and in both agitated and non-agitated state. Two acid concentration (1M and 5M) were used. The effect of sulphuric acid concentration on the mineral loss is apparent, the mineral mass loss was observed to increase with increasing acid concentration and decreasing solid -to -liquid ratio across all the samples in the four-experiment set. The summary of the leached mineral based on the four different experiment is presented in Table **6-6.** The information presented on Table **6-6,** clearly show that the mineral loss increases with increasing acid concentration from (1M to 5M), decreasing solid-to-liquid and in agitated state.

Table **6-6** at the end of the leaching duration of 168 hours there were no result to show for samples S3 – 1 of experiment 3 and sample S4 – 1 and S4 - 2 in experiment 4 in both agitated and non-agitated state. Due to the higher ratio of the solid-to-liquid the supernatant was depleted completely, the mineral consolidated and cannot be re-suspended, the recovery of the mineral in these sample to estimate the mass loss was not feasible. All the samples in experiments 1 and 2 using the 1M H_2SO_4 concentration in agitated and non-agitated states, were observed not to consolidate; they re-suspend easily throughout the reaction period. In contrast, the mineral consolidation was observed in sample S3-1 and S3-2 of experiment3 and all the samples of experiement4 using the 5M H_2SO_4 concentration and in agitated and non-agitated state respectively., These samples they do not re-suspend with ease and the recovery of some of the samples was not feasible (S3 – 1 and S4 – 1 to S4 – 2 of experiment 3&4 respectively). The higher concentration of the acid used in

all the samples of experiment4 and experiment3 which is five times (x5) higher than those used in samples of experiment1&2 was suspected to be the cause for the mineral consolidation. The consolidation effect was observed to ease out with decreasing solid- to- liquid ratio, this can be attested with the result of sample S3 – 2 through S3 – 5 of experiment3.

6.6.3.1.3 EFFECT OF SULPHURIC ACID CONCENTRATION IN THE MINERAL LOSS

The effect of sulphuric acid in leaching out metal from the olivine mineral was studied at room temperature, using particle sizes in the range 0.090 – 0.250mm, at maximum leaching period of 168 hours and across various solid - to - liquid ratio and in both agitated and non-agitated state. Two acid concentration (1M and 5M) were used. The effect of sulphuric acid concentration on the mineral loss is apparent, the mineral mass loss was observed to increase with increasing acid concentration and decreasing solid -to -liquid ratio across all the samples in the four-experiment set. The summary of the leached mineral based on the four different experiment is presented in Table **6**-**6**. The information presented on Table **6**-**6**, clearly show that the mineral loss increases with increasing acid concentration from (1M to 5M), decreasing solid-to-liquid and in agitated state.

Table 6-6: showing the mass losses corresponding to each sample in each experiment

Samples	**mass loss for experiment1 (g)**	**mass loss for experiment2 (g)**	**mass loss for experiment3 (g)**	**mass loss for experiment4 (g)**
Sample1	0.22	0.22	-	-
Sample2	0.22	0.23	1.42	-
Sample3	0.28	0.26	1.26	0.53
Sample4	0.25	0.23	1.06	0.62
Sample5	0.31	0.28	0.92	0.62

It is important to note that sample1 and samples 1&2 in both experiment 3&4 as presented in Table **6-6**, there is no value to show because the leached mineral have consolidated and cannot be recovered. **Error! Reference source not found.**a represent the result of experiment 1 based on 1M sulphuric acid concentration in agitated state. Vertical rotatory mixer operating at 10rpm was used to agitate/mix the leaching experiment reactant particles and set them in motion and thereby increasing the chances of collision and increasing the rate of reaction. From the result in Figure 6-3a, it is obvious that a maximum of ~17% mass loss corresponding to 0.31g was recorded in the sample extraction result using the least solid to liquid ratio and in agitated state. Figure 6-3b represent the result of experiment 2 based on 1M sulphuric acid concentration in non-agitated/non-mixed state, a maximum of 16% mass loss corresponding to 0.28g was recorded in the sample extraction result using the least solid- to -liquid ratio.

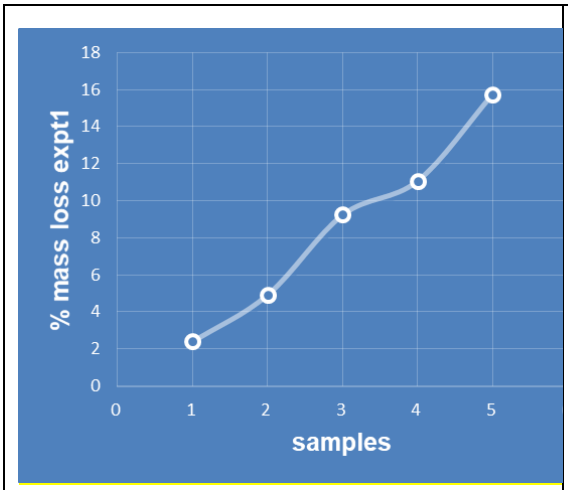


Figure 6 -3a: Represent the %mass loses for experiment 1 using 1M H_2SO_4 acid

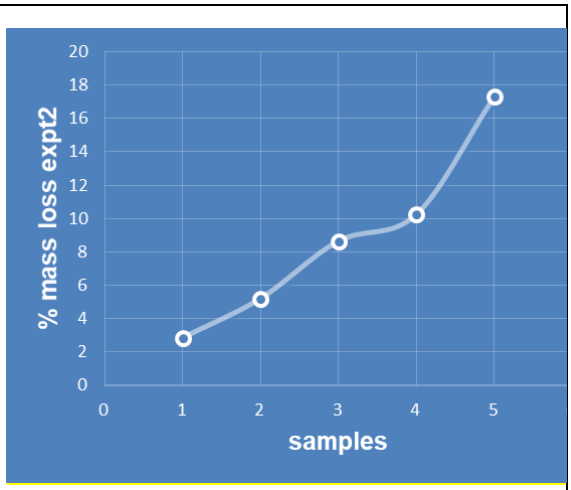


Figure 6 -3b: Represent the %mass loses for experiment 2 using 1M H_2SO_4 acid

Error! Reference source not found.a represent the result of experiment 3 based on 5M sulphuric acid concentration in an agitated state, a maximum of 51% mass loss corresponding to 0.92g was recorded in the sample extraction result using the least solid- to- liquid ratio. **Error! Reference source not found.**b represents the result of experiment 4 based on 5M sulphuric acid concentration in non-agitated state, a maximum of 34.6% mass loss corresponding to 0.62g

was recorded in the sample extraction result using the least solid -to -liquid ratio. It is very conspicuous in the two figures that the value for the percentage mass loss specific to S3-1 and S4-1 to S4-2 for both experiment 3 & 4 respectively was not presented. This is due to the consolidation effect; the supernatant was completely depleted; the mineral was consolidated such that the mineral could not be recovered/re-suspended.

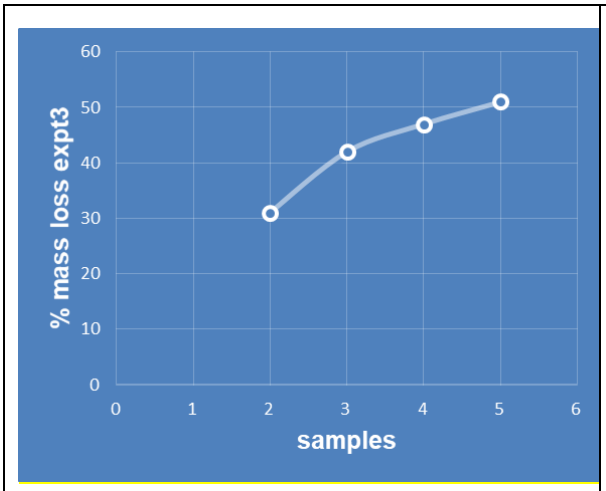


Figure 6 -4a: Represent the %mass loses for experiment 3 using 5M H_2SO_4 acid

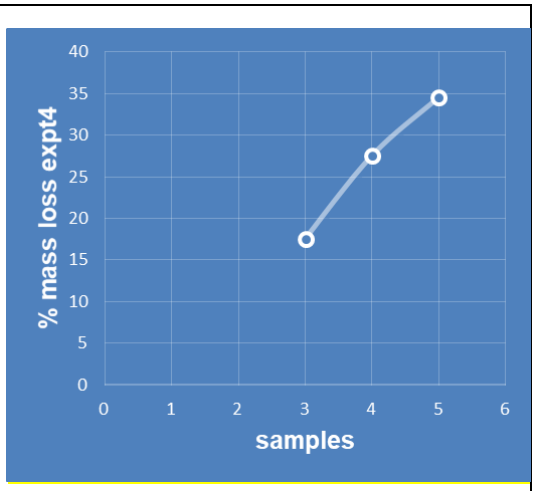


Figure 6 -4b: Represent the %mass loses for experiment 4 using 5M H_2SO_4 acid

The pattern of the mass loss across all the samples in the four sets of experiments is consistent and has shown that more mass loss was recorded among those samples operated in agitated/mixed state, with the decreasing solid-to-liquid ratio and with the highest acid concentration. Experiment 3 - 5 operated in an agitated state is observed to operate in 1:5 solid to liquid ratio state, using 5M H_2SO_4 acid and the highest amount of mass loss in the mineral corresponding to 51% (0.92g) was recorded.

The agitation mechanism is supposedly introduced to improve contact between the sulphuric acid reagent and the regolith material, reducing agglomeration of the reacting mixture and enhancing the leaching process. The result of the laboratory experiment presented in Table 6 - 6 has clearly shown that experiment 3 due to the agitation mechanism and in decreasing solid-to-liquid ratio has recorded higher mass loss.

- The discussion to implement the agitation mechanism in the future BB payload prototype and the flight model is introduced in concluding section of chapter 8 on page 262.
- The possible solution/approach for the implementation of agitation mechanism in the future BB payload prototype and the flight model is introduced in the summary and discussion section relevant to chapter 8 on pages 274 – 275.

6.6.3.1.4 EFFECT OF LOSS OF ACID CONCENTRATION ON THE LEACHING PROCESS

The litmus test paper is used to test the result of the acid concentration loss; the loss of the acid concentration was observed in all the samples in experiment 1&2, in contrast no noticeable loss in the acid concentration was observed in all the samples in experiment 3&4 throughout the leaching duration of 168 hours. Based on the evidence of the litmus paper test result as shown in **Error! Reference source not found.**, the acid concentration loss was observed to be more in the agitated samples than the non-agitated samples. The colour change observed across all the samples in experiment1 and was observed to manifest in sample S2-1 and S2-2 of experiment 2, the acid neutrality was suspected. All the samples in experiments 3&4 appear to maintain lower pH throughout the duration of the experiment, the litmus paper colour change across all the samples in experiment 3&4 throughout the leaching process signal that the acid concentration is still within the acid pH range.

6.6.4 IMPLEMENTATION OF THE REPEAT LABORATORY HYDROMETALLURGICAL SULPHURIC ACID LEACHING EXPERIMENT OF OLIVINE MINERAL SIMULANT

In this section of the thesis a repeat laboratory hydrometallurgical Sulphuric acid leaching experiment of olivine mineral simulant was implemented based on the initial experiment design parameters as shown in The initial laboratory hydrometallurgical sulphuric acid leaching experiment on the olivine mineral simulant was implemented using the design parameters presented in Table 6-4 and following the laid down design method. Observations made during the

experiment were captured and recorded. The result of the experiment is presented and described in section 6..6.3.1

Table **6-4** and following the laid down design method/procedure. The repeat leaching experiment was performed to validate the initial experiment Observations made throughout the experiment were captured and recorded. The result of the experiment is presented in section 6.6.4.1.

6.6.4.1 RESULT AND DISCUSSION OF THE REPEAT LABORATORY HYDROMETALLURGICAL SULPHURIC ACID LEACHING EXPERIMENT OF OLIVINE MINERAL SIMULANT

Images in **Error! Reference source not found.** represent the evidence to show the acid concentration loss, mineral expansion or supernatant depletion and the mineral colour change for the repeat leaching experiment. Due to having too many images, for the main section only the two extremes of the result are presented. The images are compared to show how the Sulphuric acid concentration and the solid-to-liquid ratio in the leaching process influence the following parameters:

- loss of acid concentration
- Supernatant depletion or mineral swelling
- Mineral consolidation
- Mineral loss

The overall photographic results of the repeat leaching experiment are presented in Appendix 1.2

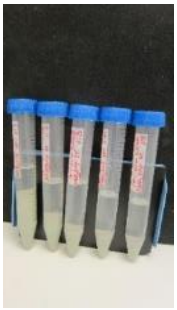
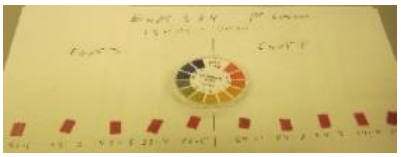
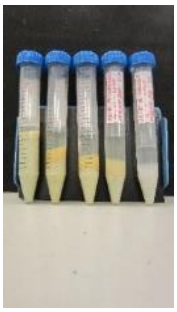
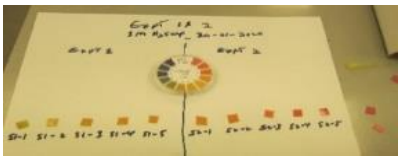
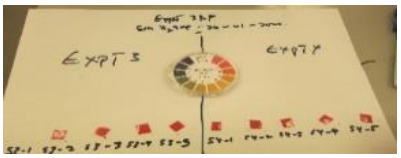
			
			
Expt1, t0 = 0hours	Expt2, t0 = 0hours	Expt3, t0 = 0hours	Expt4, t0 = 0hours
			
			
Expt1, t14 = 168hours	Expt2, t14 = 168hours	Expt3, t14 = 168hours	Expt4, t14 = 168hours

Figure 6-2: Experimental result of the repeat hydrometallurgical H_2SO_4 acid leaching of olivine mineral.

Legend

- Expt1 - 4 = signifies the experiment numbering from 1 to 4 set of experiment,
- t_0 = initial time zero marking the start point for the experiment,

- t_{14} = final time marking the end time for the experiment

The discussion of the result of the repeat leaching experiment discussion is presented as follows:

6.6.4.1.1 EFFECT OF SULPHURIC ACID CONCENTRATION ON SUPERNATANT DEPLETION AND OR MINERAL EXPANSION

The minerals in all the samples across the four experiments were observed to expand. As shown in the initial experiment, the expansion was observed to be more among samples operated under higher acid concentration, and consequently, the more supernatant deplete. The summary shown in Table 6-7 indicates the amount of the supernatant in percentage (%) that was depleted across all the samples in the four-experiment set and corresponding to the 168 hours leaching duration. It is evident in experiment 3 and 4, samples S3 – 1 and S3 – 5 have recorded 100 and 35%, sample S4-1 and S4-5 have recorded 17 and 10% maximum supernatant depletion respectively. Among similar samples, the supernatant depletion appears to be more in the agitated samples than the non-agitated samples.

Table 6-7: Showing the Maximum liquid depletion in percentage based on the four different experiments for the repeat leaching experiment

Maximum Leaching duration (Hours)	**Maximum liquid depletion in (%)**				
168	Experiment1 sample using 1M H2SO4 in agitated state				
	S1-1	S1-2	S1-3	S1-4	S1-5
	33	27	14	7	13
	Experiment2 sample using 1M H2SO4 in non-agitated state				
	S2-1	S2-2	S2-3	S2-4	S2-5
	15	20	7	7	8
	Experiment3 sample using 5M H2SO4 in agitated state				
	S3-1	S3-2	S3-3	S3-4	S3-5
	100	65	76	64	35
	Experiment4 sample using 5M H2SO4 in non-agitated state				
	S4-1	S4-2	S4-3	S4-4	S4-5
	17	21	11	17	10

As it is evident in Table 6-7, the supernatant depletion across all the samples in the four experiment decreases with decrease acid concentration and decreasing solid-to-liquid ratio. The discrepancies in the pattern observed in samples of experiment 1, 2 and 4 can be attributed to higher solid-to-liquid ratio measurement or error in reading and or recording the result, which could have distorted the expected balance. Sample S1-4 and S2-4 in both experiment 1&2 recorded the least supernatant depletion of 7 and 7% respectively, whereas S3-5 and S4-5 in experiment 3&4 recorded 35% and 10% respectively.

6.6.4.1.2 EFFECT OF SULPHURIC ACID CONCENTRATION ON THE MINERAL CONSOLIDATION

The sulphuric acid concentration was observed to impact on the mineral consolidation. All the samples in experiment 1 and 2 using the 1M H_2SO_4 concentration in agitated and non-agitated states, respectively, were observed not to consolidate; they re-suspend easily throughout the reaction period. In contrast, the mineral consolidation was observed in sample S3-1 and S3-2 of experiment3 and all the samples of experiement4 using the 5M H_2SO_4 concentration and in agitated and non-agitated state, respectively they do not re-suspend with ease. The higher concentration of the acid in all the samples of experiment4 and samples S3-1 and S3-2 of experiment3, which is five times (x5) higher than those in samples of experiment1&2 was suspected to be the cause for the mineral consolidation. The consolidation effect was observed to ease out with decreasing solid to liquid ratio.

6.6.4.1.3 EFFECT OF SULPHURIC ACID CONCENTRATION IN THE MINERAL LOSS

The effect of sulphuric acid in leaching out metal from the olivine mineral was studied at room temperature, using particle sizes in the range 0.090 – 0.250mm, at maximum leaching period of 168 hours and across various solid to liquid ratio and in both agitated and non-agitated state. Two acid concentration (1M and 5M) were used. Due to the closedown of the University activities, the process of estimating the amount of mineral loss could not be completed. In the same vein, we suspect the result will likely be in synchrony with the initial leaching experiment's mineral loss.

6.6.4.1.4 EFFECT OF LOSS OF ACID CONCENTRATION ON THE LEACHING PROCESS

The result of the litmus test was carried out; the loss of the acid concentration was observed in all the samples in experiment 1&2 in contrast, no noticeable loss in the acid concentration was observed in all the samples in experiment 3&4 through to the end of the leaching duration of 168 hours. Based on the evidence of the litmus paper test result as shown in **Error! Reference source not found.**, the acid concentration loss rate was observed to be faster in the agitated samples

than the non-agitated samples. The colour change observed across all the samples in experiment1 which was observed to manifest in sample S2-1 and S2-2 of experiment 2, indicates neutrality in the acid content. The colour change formation in the reaction mixture can be attributed to the acid pH tending towards neutral, and the formation of new mineral was suspected [64]. All the samples in experiments 3&4 appear to maintain lower pH throughout the duration of the experiment, the litmus paper colour change across all the samples in experiment 3&4 throughout the duration of the leaching process signal that the acid concentration is still within the acid pH range.

6.6.4.2 DISCUSSION IN RESPECT OF THE INITIAL AND REPEAT LABORATORY METALLURGICAL SULPHURIC ACID LEACHING EXPERIMENT ON OLIVINE MINERAL

Initial leaching experiment was carried out to optimise the result finding and a repeat leaching experiment was performed to validate the first experiment. The result outcome of the initial and repeat experiment appears to agree on how the combination of sulphuric acid concentration and the solid-to-liquid ratio in the leaching process influences loss of acid concentration, supernatant depletion, or mineral swelling, Mineral consolidation, and Mineral loss.

In all the experiment scenario for both the initial and repeat experiment, the loss of the acid concentration in the leaching process was observed and was more conspicuous in the experiment using lower acid concentration. The consequences of acid concentration loss were manifest in experiments 1&2; maximum metal extraction could not be achieved using the lower acid concentration. The scenario can be attested by the mass loss result recorded in experiment 3&4 with higher acid concentration and the same amount of mineral. We expect to maximise the mineral extraction in the flight model implementation, such that enough metals could be available in the supernatant and will be recovered during the electro-winning stage. The mineral expansion or the supernatant depletion in both scenarios (initial and the repeat experiment) was observed; it was more conspicuous among the experiment with higher acid concentration and higher solid-to-liquid ratio and decreases as the solid-to-liquid ratio decrease. Experiments 1&2 appear to have minimal supernatant depletion,

and the acid concentration loss was apparent among the sample of experiments 1&2, and maximum mineral extraction is not feasible. The available options are those of experiments 3&4. But again, all the samples in experiment 4 exhibit consolidation, this scenario will impact the metal recovery process. In the case of samples in experiment 3, the consolidation declines with decreasing solid-to-liquid ratio. Samples S3-5 in both the initial and repeat leaching experiment appear to share common characteristics thus:

- They appear not to lose their acid concentration until the end of the leaching process
- The higher acid concentration with decreasing solid-to-liquid ratio can guarantee maximum mineral extraction during the leaching
- The higher acid concentration with decreasing solid-to-liquid ratio, and in state of agitation, minimal mineral consolidation and minimal supernatant depletion was recorded.
- Sample S3 – 5 in experiment 3 for both initial and repeat experiment have recorded 39% and 35% supernatant depletion respectively.

From the discussion elucidated above, the choice of Sample S3 – 5 operating in higher acid concentration (5M) and with the least solid-to-liquid ratio, and in state of agitation maximum mass loss in the leaching process with minimal loss of acid concentration, minimal depletion of the supernatant and minimal or no mineral consolidation is envisaged. This experimental scenario will impact positively in-flight model implementation.

6.6.4.3 CONCLUSION AND RECOMMENDATION IN RESPECT OF THE INITIAL AND REPEAT LABORATORY METALLURGICAL SULPHURIC ACID REPEAT LEACHING EXPERIMENT ON OLIVINE MINERAL SIMULANT

The laboratory metallurgical sulphuric acid initial leaching experiment was performed, and a repeat experiment was carried out to validate the initial result findings. The result pattern of the two experiments (initial and repeat) has shown that choosing the right combination of the acid concentration and solid-to-liquid ratio is critical in designing the sulphuric acid leaching experiment that can be implemented using the bread board prototype and the eventual implementation

using the flight model. We conclude that the optimal condition for the sulphuric acid leaching of olivine mineral to achieve higher metal extraction from the reaction mixture occurs at 5M H_2SO_4 acid concentration, 1:5 mineral to acid volume ratio and in state of agitation. Experiment 3 scenario specific to sample S3-5 common to both initial and repeat experiment, having mineral to acid volume ratio of 1:5 achieved 51% mineral mass loss, 42% mineral swelling or 39% supernatant depletion and at 168 hours reaction time, at room temperature and in a state of agitation. Table **6-8** is the comparison of mineral percentage loss and mineral swelling across all the sample with 1:5 solid to liquid volume ratio in the four experiments for the initial leaching experiment process.

Table 6-8: showing a comparison of mineral % loss and mineral swelling across all sample of the experiment.

Experiment	Samples	Mineral to acid volume ratio (ml)	Percentage mass loss of mineral (%)	Least percentage mineral swelling (%)
1	S1 - 5	1:5	15.75	16
2	S2 - 5	1:5	17.30	16
3	S3 - 5	1:5	51.00	42
4	S4 - 5	1:5	34.61	29

InTable **6-8**, the data in red corresponding to experiment 1&2 represent the least mineral percentage swelling and those corresponding to experiment 3 represent the maximum percentage mass loss of the mineral.

The pattern of the repeat experiment and those of the initial leaching experiment appear to be similar. This scenario is recommended to be carried forward for the breadboard implementation. It is also worthy to note that in the repeat experiment the metal recovery from the leaching mixture was not concluded due to the closure of the university activities. We are unable to ascertain the recovered metal during the repeat leaching experiment.

6.7 SULPHURIC ACID LEACHING EXPERIMENT OF OLIVINE MINERAL AND USING BPB PH DYE INDICATOR TO MONITOR PH CHANGE AS THE ACID CONCENTRATION REDUCES

6.7.1 INTRODUCTION

In this section of the thesis the sulphuric acid leaching experiment carried out on olivine mineral as demonstrated in the trial and repeat experiment in both sub-sections 6.6.3 and 6.6.4 is replicated using a selected dye indicator. Using the selected dye indicator in the leaching process is proposed to eliminate the use of litmus test paper and to detect the loss of acid concentration and provide real-time visual colour transition within the required acid pH and preparatory to the breadboard prototype demonstration and flight model implementation.

6.7.2 AIMS OF THE EXPERIMENT

This study aims to design sulphuric acid leaching experiment of olivine mineral and using a selected pH dye indicator to monitor the pH change in the acid concentration in the leaching experiment real-time.

6.7.3 OBJECTIVES OF THE EXPERIMENT

- To select an appropriate pH dye indicator suitable for monitoring the pH change within acid concentration range
- Using the selected pH dye indicator to monitor the pH change in the sulphuric acid concentration as the leaching experiment progresses

6.7.4 DESCRIPTION OF THE EXPERIMENT PROCEDURE

The initial and the repeat experiment carried out in subsections 6.6.3 and 6.6 .4 are replicated here using the selected pH dye indicator as an alternative to using the litmus test paper. The selected dye indicator solution is added directly into the leaching mixture prepared inside the centrifuge tube to monitor a real-time visual colour transition as the acid concentration in the leaching process reduces. The entire colour change resulting from the pH change in the leaching process is intended to occur within acidic condition, as the acid concentration

reduces/deplete a colour transition is observed. The use of litmus test paper to monitor the pH as was the case in the initial and the repeat leaching experiment is not feasible in the bread-board prototype demonstration and flight model implementation. Using the pH dye indicator added directly in the leaching process will replace the litmus test paper and provide real-time visual colour transition as the leaching process progresses and within the required acid pH.

6.7.5 PH DYE INDICATOR SELECTION PROCESS

Several pH dye indicator materials as shown in Table 6-9 were identified and studied to select the correct type of pH dye indicator suitable for this experiment. The entire colour transition as an indication of the acid pH change in the leaching process was proposed to occur in acidic conditions to ensure that the result does not drift closer to the neutral state and the pH range of (2.5 – 5.0) maximum was proposed. As shown in Table 6-9 several dye indicators were populated toward selecting the right dye to be implemented in this research work. The dye indicator selection process was based on the following specific characteristics of the pH dye indicator: pH range, maximum absorbance wavelength, molar extinction coefficient, dissociation constant, solubility, and compatibility for use. Among the listed dye indicator in Table 6-9, Bromo Phenol Blue (BPB) dy indicator (pH3.0 – 4.6), Congo (pH3.0 – 5.0) and methyl orange xylene (pH2.9 – 4.6) dye indicator appear to operate within the specified pH range of 2.5 – 5.0. The BPB dye indicator appears to have the maximum absorbance wavelength at the least acid pH as compared to methyl orange xylene and Congo. The precision of absorbance measurement is at best when the absorbance is at highest value closer to one. The Congo dye indicator is also injuries to health and not compatible for use as compared to the BPB dye indicator. For the experiment the BPB dye indicator was selected as the dye indicator to be used.

Table 6-9: summary of dye indicators used in the selection process

Dye MATERIAL NAME	pH RANGE	COLOUR TRANSITION	MAXIMUM ABSORBANCE WAVELENGTH AT STRONGEST ACID pH (nm)	MAXIMUM ABSORBANCE WAVELENGTH AT LEAST ACID pH (nm)	MOLAR EXTINCTION COEFFICIENT AT ACID PHASE (10^{-3} $lmol^{-1}cm^{-1}$)	MOLAR EXTINCTION COEFFICIENT AT BASE PHASE (10^{-3} $lmol^{-1}cm^{-1}$)
Bromophenol blue salt	3.0 – 4.6	Yellow - blue	436	591	58.5	77.8
Bromo-cresol green salt	3.8 – 5.4	Yellow - blue	403	616	8	25
Methyl orange xylene	2.9 – 4.6	Purple - green	270	463	10.8	27
Congo red salt	3.0 – 5.0	Blue - red	479	479	62.6	62.6
Bromo-cresol purple salt	5.2 – 6.8	Yellow - purple	431	590	0.45	1.1
Alizarin red salt	3.8 – 5.4	Yellow - red	445	570	5.15	8.84

6.7.6 PREPARATION OF THE BPB DYE INDICATOR SOLUTION

To prepare the BPB dye indicator solution that will be suitable for our leaching experiment, it is important to get the BPB dye indicator solution in the right concentration. Three different concentration of the BPB dye solution was proposed. The BPB dye indicator solution is prepared using BPB salt and pure ethanol solvent. 0.1g.mol^{-1} each of the BPB dye salt were dissolved in different volumes of the pure ethanol as a solvent corresponding to 33, 67 and 100ml. Three different BPB dye solution was prepared with concentrations 2.2mM, 4.4mM and 8.8mM. These variable concentrations of the BPB solution are used in the leaching process and will help in determining the required concentration of BPB that is best suited for the leaching experiment demonstration. Table 6-10 gives a summary description of the amount of BPB salt and the ethanol solvent used and the concentration obtained.

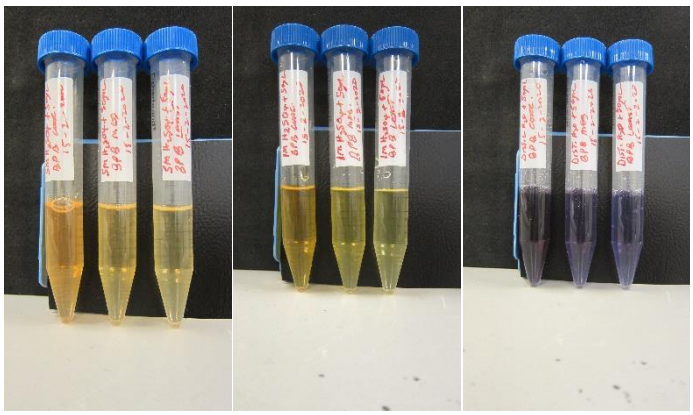
Table 6-10: Showing the volume of ethanol and mass of BPB salt used and the resultant concentration of the BPB solution

parameters	**Sample1**	**Sample2**	**Sample3**
BPB salt mass used (g)	0.1	0.1	0.1
Volume ratio of ethanol used	3:3	2:3	1:3
Corresponding volume of ethanol used (ml)	100	67	33
Concentration of the BPB dye indicator (mM)	2.2	4.4	8.8

6.7.7 INITIAL TESTING OF THE BPB PH DYE SOLUTION

After preparing the BPB pH dye indicator solution, the initial testing of the BPB pH dye indicator solution was carried out to confirm the point at which the colour transition is more visible based on the three samples toward selecting the suitable BPB dye indicator concentration. 1M and 5M of H_2SO_4 acid solution and distilled water were used for the testing to monitor the colour transition. Nine different

samples were prepared in the centrifuge tubes, and three sets each are based on 5ml of 5M H_2SO_4, 5ml of 1M H_2SO_4 and 5ml of distilled water, respectively. 50µL was estimated as the volume BPB dye solution to use for the test. To each of the three samples 50µL equivalent of 2.2, 4.4 and 8.8mM of the BPB dye solution was added. The BPB dye indicator test result as shown in Figure 6-3



Sample1 Sample2 Sample3

Figure 6-3: the BPB dye indicator test result

Legend

Sample1	Test result for different concentration of BPB dye with 5M H_2SO_4
Sample2	Test result for different concentration of BPB dye with 1M H_2SO_4
Sample3	Test result for different concentration of BPB dye with distilled water

6.7.7.1 RESULT FOR THE INITIAL TESTING OF THE BPB DYE INDICATOR SOLUTION

The result for the initial testing of the BPB dye indicator solution, in each set of the three samples:

Using 5M H_2SO_4 acid samples, a deep yellow colour change was observed among the sample with highest concentration of BPB dye (8.8mM). The colour concentration decreases with decreasing BPB dye indicator concentration.

Using 1M H_2SO_4 acid samples, the sample with the highest concentration of BPB dye (8.8mM), a lighter yellow colour change was observed compared to those of the 5M H_2SO_4 acid, and the colour decreases with decreasing BPB dye indicator concentration.

Using distilled water samples, the sample with highest concentration of BPB dye (8.8mM) a deep blue colour change was observed and colour decline with decreasing BPB dye indicator.

6.7.7.2 CONCLUSION IN RESPECT OF THE INITIAL TESTING OF THE BPB DYE INDICATOR SOLUTION

The colour changes in the sample agreed with the expected colour changes, as the BPB dye indicator is tested using acid in 1M and 5M H_2SO_4 and distilled water. Going forward, the 8.8mM concentration of the BPB dye indicator solution shows the evidence of deep yellow colour was selected for use in the hydrometallurgical leaching experiment. We expect to get the best colour transition result using the 8.8mM concentration.

6.7.8 IMPLEMENTATION OF THE LABORATORY HYDROMETALLURGICAL SULPHURIC ACID LEACHING EXPERIMENT ON THE OLIVINE MINERAL SIMULANT AND USING 8.8mM CONCENTRATION BPB pH DYE INDICATOR TO MONITOR COLOUR CHANGE AS THE ACID CONCENTRATION REDUCES

6.7.8.1 INTRODUCTION

In this section of the thesis the hydrometallurgy sulphuric acid leaching experiment on the olivine mineral simulant would be implemented using the 8.8mM concentration of BPB pH dye indicator to monitor the colour change as the acid concentration reduces. The processes implemented on both the initial and the repeat leaching experiment was repeated and to each leaching mixture sample in the experiment 50µL of 8.8mM concentration of the BPB dye indicator solution was added to monitor the colour transition. The result of the experiment is discussed as follows:

6.7.8.2 RESULT AND DISCUSSION OF THE LEACHING EXPERIMENT USING THE BPB DYE INDICATOR TO MONITOR COLOUR CHANGE IN THE LEACHING PROCESS

The result for experiments 1 – 4 using 1M and 5M H_2SO_4 acid concentration respectively for the leaching of olivine mineral simulant and using the BPB dye indicator solution to monitor the colour transition as the acid concentration deplete are presented and discussed thus: in experiment 1&2 using 1M H_2SO_4 acid concentration as evidenced in **Error! Reference source not found.**, the colour transition was visible in the expected manner (from yellow to blue). The result except for the colour presence in the supernatant, in terms of acid concentration loss, mineral expansion or supernatant depletion were observed to conform to those of the initial and repeat experiment using only the reagent and the mineral in the leaching process.

In experiment 3 &4 using 5M H_2SO_4 acid concentration together with the BPB dye indicator, we expect a colour transition from yellow to blue as the acid concentration reduces. As the leaching reaction progresses the BPB dye indicator was observed not to follow the acid concentration colour change pattern. Midway into the leaching process the colour of the pH dye indicator disappears and become colourless. The disappearance of the pH dye indicator colour negates the expected colour transition from yellow to blue as the acid loss its concentration in the leaching process. The leaching experiment result is presented in the **Error! Reference source not found.**

The overall photographic results of the leaching experiment using BPB dye are presented in Appendix 1.3

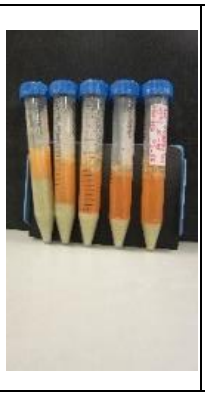
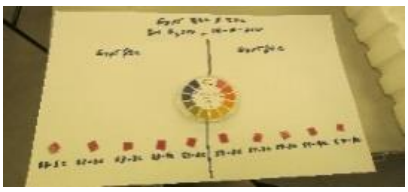
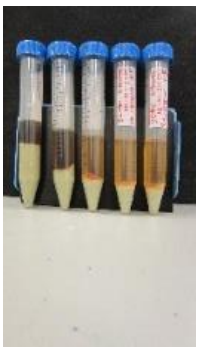
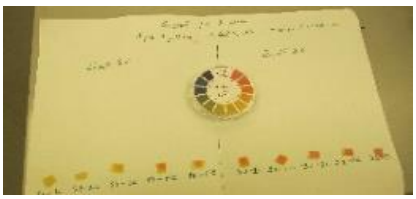
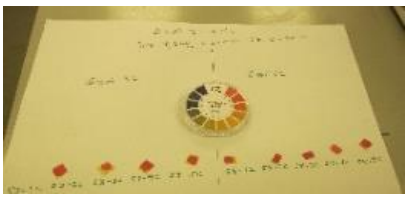
			
			
Expt1, t0 = 0hours	Expt2, t0 = 0hours	Expt3, t0 = 0hours	Expt4, t0 = 0hours
			
			
Expt1, t14 = 168hours	Expt2, t14 = 168hours	Expt3, t14 = 168hours	Expt4, t14 = 168hours

Figure 6-4: result for the sulphuric acid leaching experiment using BPB dye indicator solution to monitor the colour transition

6.7.8.3 CONCLUSION IN RESPECT OF THE IMPLEMENTATION OF THE LABORATORY HYDROMETALLURGICAL SULPHURIC ACID LEACHING EXPERIMENT ON THE OLIVINE MINERAL SIMULANT AND USING 8.8mM CONCENTRATION OF BPB PH DYE INDICATOR

The expected pH dye indicator colour transition was observed in the samples of experiment 1&2, in the case of samples in experiment 3&4 the pH dye indicator colour midway into the leaching reaction disappeared and become colourless. These un-expected behaviour among the samples of experiment 3&4, the acid concentration and or the mineral behaviour in the leaching process was suspected to be the cause. A further experiment to confirm/investigate the cause of the BPB dye indicator colour loss was proposed.

6.8 EXPERIMENT TO INVESTIGATE THE EFFECT OF 1M AND 5M SULPHURIC ACID CONCENTRATION AND DISTILLED WATER ONLY ON 8.8mM BPB DYE INDICATOR

6.8.1 INTRODUCTION

In the previous section, the hydrometallurgical sulphuric acid leaching experiment and using the BPB dye indicator solution to monitor the loss of acid concentration was carried out. The BPB dye indicator behaviour specific to experiment 3&4, the yellow colour was lost, it was observed to change to colourless instead of the expected yellow to blue colour transition as the leaching process progresses. Consequently, a new experiment is proposed to investigate the effect of different concentrations of Sulphuric acid (1M and 5M) and distilled water only on the BPB dye indicator for the duration of the leaching process.

6.8.2 PROCEDURE TO INVESTIGE THE EFFECT OF DIFFERENT CONCENTRATIONS OF SULPHURIC ACID (1M&5M) AND DISTILLED WATER ONLY ON THE BPB DYE INDICATOR

The procedure implemented in the initial testing of the BPB pH dye indicator solution was repeated in this experiment using only the various acid concentration (1M and 5M) and distilled water. Unlike the initial testing experiment of the BPB

pH dye indicator, this experiment was carried out using only 8.8mM BPB dye indicator. Three different samples were prepared in the centrifuge tubes, and to each of the centrifuge tubes 5ml of 5M H_2SO_4, 5ml of 1M H_2SO_4 and 5ml of distilled water was dispensed therein, respectively. To each centrifuge tube containing the acid and distilled water, 50µL of the 8.8mM BPB dye is added to monitor the colour transition. The experiment was monitored for a duration of 168hours. The result of the experiment is shown in Figure **6-5**

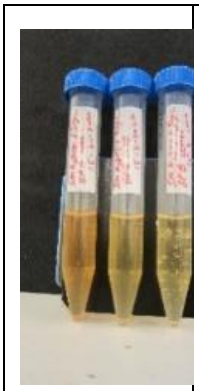
					
S1, t0=0hours	S2, t0=0hours	S3, t0=0hours	S1, t14 = 168hours	S2, t14 = 168hours	S3, t14 = 168hours

Figure 6-5: Result for the effect of 1M&5M acid concentration and distilled water on the 8.8mM BPB dye indicator

Legend

Parameter	Definition
t0 – t14	Signifies the start time and end time for the leaching process
S1	Sample1 using 5ml 5M H2SO4 + 8.8Mm BPB dye
S2	Sample2 using 5ml 1M H2SO4 + 8.8Mm BPB dye
S3	Sample3 using 5ml distilled water + 8.8Mm BPB dye

6.8.3 RESULT AND DISCUSSION FOR THE EXPERIMENT USING BPB DYE INDICATOR WITH ONLY SULPHURIC ACID (1M&5M) AND DISTILLED WATER ONLY

Using the 8.8mM concentration of the BPB dye indicator + distilled water, the same blue colour change was maintained throughout the reaction period, and no loss in the colour of the BPB dye was observed.

Using the 8.8mM concentration of the BPB dye indicator + 1M Sulphuric acid concentration, the same yellow colour change was maintained throughout the reaction period. No loss of colour of the BPB dye was observed.

Using the 8.8mM concentration of the BPB dye indicator + 5M Sulphuric acid concentration, 84hours into the leaching process the yellow colour was observed to disappear and changing to colourless. This colour change negates the expected colour transition from yellow to blue as the acid deplete from 3 - 4.5pH level.

6.9 LEACHING INERT SAND (SILICATE MINERAL) USING SULPHURIC ACID (1M AND 5M) AND DISTILLED WATER TOGETHER WITH 8.8mM BPB DYE INDICATOR TO MONITOR THE COLOUR CHANGE

6.9.1 INTRODUCTION

In this section of the leaching experiment using inert sand in place of the olivine mineral and using both the Sulphuric acid (1M &5M) and the distilled water together with the 8.8mM BPB dye indicator to monitor the colour change was carried. The inert sand is a very stable material and difficult to react with other substances. For this reason, no colour transition in the BPB dye indicator is expected throughout the leaching period of 168hours. This experiment was proposed to investigate the effect of different concentrations of Sulphuric acid (1M and 5M) and distilled water only on the BPB dye indicator and using inert sand in place of the olivine mineral for the duration of the leaching process.

6.9.2 PROCEDURE FOR THE EXPERIMENT TO INVESTIGATE THE EFFECT OF DIFFERENT CONCENTRATIONS OF SULPHURIC ACID (1M&5M) AND DISTILLED WATER ONLY ON THE BPB DYE INDICATOR USING INERT SAND AND SILICATE MINERAL IN PLACE OF OLIVINE MINERAL

Three set of experiment were prepared each containing two centrifuge tube, sample of inert sand obtain from Scan grit a UK company was dispensed into each of the centrifuge tube to a volume of 5ml. To each pair of the centrifuge tube containing the inert sand, 5ml 5M H_2SO_4 was dispensed into pair1, 5ml 1M H_2SO_4 was dispensed into pair2 and 5ml of distilled water was dispensed into pair3 and to each sample 50µL of the 8.8mM BPB dye is added to monitor the colour transition. Each member of the pair is selected and two new groups each of three samples formed. The group1 sample is subjected to the agitation of 10rpm and at room temperature and pressure, the group2 samples are subjected to no agitation at room temperature and pressure, all the samples are leached for 168hours. The result of the investigation is represented thus.

6.9.3 RESULT AND DISCUSSION FOR THE LEACHING EXPERIMENT USING 1M&5M SULPHURIC ACID, DISTILLED WATER AND INERT SAND AND SILICATE MINERAL AND 8.8mM OF THE BPB DYE INDICATOR SOLUTION TO MONITOR THE COLOUR TRANSISTION

Using the distilled water in the leaching of the inert sand and the silicate mineral, the blue colour change was observed to be consistent through the reaction period of 168hours

Using the 1M Sulphuric acid concentration in the leaching experiment of the inert sand and the silicate mineral, the initial yellow colour change was observed to be consistent all through the reaction period.

Using the 5M Sulphuric acid concentration in the leaching experiment of the inert sand and the silicate mineral, the initial yellow colour change was observed to be degraded and turn to colourless, the inert sand and the mineral silicate are observed not to be affected.

6.9.4 CONCLUSION IN RESPECT OF LEACHING EXPERIMENT USING 1M&5M SULPHURIC ACID, DISTILLED WATER AND INERT SAND AND SILICATE MINERAL AND 8.8mM OF THE BPB DYE INDICATOR SOLUTION TO MONITOR THE COLOUR TRANSITION

This experiments investigate the root causes for the BPB dye indicator degradation in the leaching process. The degradation of the BPB dye indicator was observed to happen in the 5M Sulphuric acid concentration and midway into the reaction process. The 1M H_2SO_4 and the distil water do not affect the degradation of the BPB dye indicator solution. Using inert sand and silicate mineral in the leaching process, it was also observed that there was no effect.

The result outcome of the experiment carried out in both section 6.9 and 6.10 of this thesis has established that the degradation of the BPB dye indicator solution from yellow to colourless was as a result of the higher concentration of the sulphuric acid (5M). In the conclusion, to mitigate against the effect of the BPB dye degradation using the sulphuric acid at 5M concentration, the use of an alternative dye material compatible with sulphuric acid or lower version of the acid concentration between 2.5M and 3M of acid concentration was proposed.

6.9.5 DISCUSSION IN RESPECT OF THE INITIAL AND REPEAT EXPERIMENT AND THOSE USING BPB DYE SOLUTION.

The epeat experiment outcome was observed to agree with the result of the initial experiment. A noticeable mineral consolidation and liquid depletion was observed to increase from sample S3-1 through to sample S3-3 in the initial experiment 3 and of the repeat experiment. A similar set of initial experiment were repeated by adding the BPB dye indicator solution to produce a visual colour transition as the acid concentration deplete in the leaching reaction process as against using the litmus test paper. All the samples in experiment 1 and 2 using the different concentration of the BPB dye indicator respond according to the outcome of both the initial and repeat experiment without using the BPB dye indicator. In the case of experiments 3 and 4 using the BPB dye indicator, due to higher concentration of the acid (5M H_2SO_4) and the agitation state, and specific to experiment3, the BPB dye indicate was observed to degrade and changing to colourless. This

colour change differs with the expected colour transition from yellow to blue as the acid concentration deplete. Further investigation into the root cause of the BPB dye indicator solution colour degradation at higher sulphuric acid concentration (5M), it was established that the degradation in BPB dye indicator solution was because of the higher sulphuric acid concentration (5M).

6.10 CONCLUSION

We conclude that the optimum condition for the sulphuric acid leaching of olivine mineral for extraction of metal from the reaction mixture as shown in the initial and the repeat experiment, occurs at 5M H_2SO_4 acid concentration, 168hrs reaction time, 10rpm mixing speed and 1:5 mineral to acid volume ratio. Experiment 3 scenario specific to mineral to acid volume ratio of 1:5 achieved 51% mineral mass loss at 168 hrs reaction time, 10rpm mixing rate and at room temperature this scenario appears to be the best scenario in terms of maximum metal extraction, it is suitable and can be carried forward for the breadboard implementation.

Based on the result outcome of the leaching process using the 8.8Mm BPB concentration, it was concluded that the degradation of the BPB dye indicator solution was caused by the higher concentration of the acid (5M). This observed behaviour is likely to impede the operational performance of the bread board concept and the eventual flight model. To mitigate against this looming challenge, in future work the use of an alternative dye that is stable in 5M H_2SO_4 acid is suggested or lower version of the acid concentration between 2.5M and 3M of acid concentration was proposed.

7 BREADBOARD (BB) PAYLOAD PROTOTYPE DESIGN AND COMPONENTS SELECTION, ASSEMBLY, TESTING AND OPERATIONS

7.1 INTRODUCTION

This Chapter focuses on the design, component selection, assembly, testing and the operations of the BB prototype payload system that will be used to simulate the demonstration of hydrometallurgical leaching process and aspects of liquid handling processes. The BB prototype payload system design will form the basis for informing a future flight model design and implementation in work beyond the current project. The payload system architecture developed in Chapter_5 coupled with the requirements generated from the laboratory leaching experiment, such as the solid to liquid volume ratio, acid concentration, system agitation and the reaction duration informed the BB prototype payload system design and component selection, assembly, testing and operation. The BB prototype payload design was achieved through part designed using CAD software (CATIA V5) and manufactured using the 3D printing and CNC machining techniques and through procurement and using the commercial off the shelf (COTS) hardware. The various prototype components were physically assembled to validate the intended BB prototype payload system design and to simulate the BB demonstration of the hydrometallurgical sulphuric acid leaching experiment and aspects of liquid handling processes. Software code (Arduino Sketches produced in the Arduino IDE) were developed and uploaded onto the hardware to drive the operational sequence of the BB prototype payload system.

7.2 BREADBOARD (BB) PROTOTYPE PAYLOAD DESIGN PROCESS

The hardware's components are partly design using the CAD software (CATIA V5) tool and manufactured using the 3D printer and the CNC machining techniques, other parts were selected and procured from the commercial off the shelf (COTs) components. The COTs components are supposedly cheap and have minimum mass and easy to implement. The CAD software (CATIA V5) designed models are initially 3D printed using the polymer material as a de-risking

approach to justify the CNC machine part production. The modelled part/parts were tested for fitting together and the parts detected not to fit together are adjusted in the CAD software (CATIA V5), printed iteratively and test again and again until the best of fit was identified. The modelled part are categories into 3 parts, namely:

- Those models parts selected and procured directly from the manufacturer (i.e., bipolar stepper motor, solenoid valves, manifolds etc)
- Those models' parts obtained from a co-running project within the space group to extract dioxygen and dihydrogen from water-ice introduced in Chapter_5 and are re-designed and manufactured to suit the project requirement (i.e., RCS, the top plates etc)
- Those part designed and modelled and manufactured by the author (1.e., the liquid handling system)

All these parts are assembled to form the BB prototype system that will be used to simulate the demonstration of hydrometallurgical sulphuric acid leaching of regolith and the liquid handling process. Companies such as Lee company the manufacturers of electro-microfluidic system, Thomson linear actuator, the manufacturers of linear actuator such as a stepper motor, and simply bearing the manufacturers of bearing and seals were among the companies identified and used in the procurement of the COTs hardware's.

7.3 AIMS OF THIS CHAPTER

This chapter aimed to achieve the design and components selection, assembly/manufacture, testing and operations of the BB prototype payload system to simulate the demonstration of hydrometallurgical sulphuric acid leaching experiment and aspect of liquid handling processes.

7.4 OBJECTIVES OF THIS CHAPTER

- To design and manufacture a Liquid Handling System (LHS) that will be used for the delivery and the extraction of liquid to and from the Reaction Chamber System (RCS)
- Perform the hardware components identification and selection for the manufacture of the BB and the LHS payload system

- Assembling of the LHS system with other microfluidic devices to demonstrate the liquid handling operations
- Using the BB prototype to simulate the demonstration of hydrometallurgical sulphuric acid leaching of the olivine mineral as the simulant relevant to C-type NEA Ryugu
- To design the Reaction Chamber Subsystem (RCS) and material selection to be compatible working with sulphuric acid
- To design the top-plate to provide access for the plunger system and other fluidic material into the RCS and provide support, housing, and mounting position.

7.5 OVERVIEW OF THE BREADBOARD (BB) PROTOTYPE PAYLOAD SYSTEM

The BB prototype payload system is designed and developed to simulate the demonstration of hydrometallurgical sulphuric acid leaching of olivine regolith simulant to extract metal-acid solution. In the simulation demonstration using the BB prototype payload system water is used in place of the acid reagent and Bromophenol Blue (BPB) dyed olivine regolith as the simulant to extract BPB dye solution and to determine the extraction efficiency of the system. The system operation shall be compatible working in microgravity. The BB prototype payload system comprises of the following sub-systems:

- Reaction Chamber Sub-systems (RCS) and
- Acid Solution Delivery and Extraction Sub-systems (ASD&ES) or the liquid handling subsystem (LHS)

The RCS is a cylindrical open ended sub-system like the RCS developed for the implementation of dioxygen production and was introduced in Chapter_5. In this work the RCS is designed to allow for interfacing with the supposed liquid handling sub-systems called the acid solution delivery and extraction sub-system (ASD&ES) and since the final flight model is intended to work with sulphuric acid, the parts are manufactured from stainless steel material for its compatibility working with sulphuric acid. The Liquid Handling Subsystem (LHS) is designed to achieve the liquid acid solution delivery from the acid reservoir into the RCS

and the extraction of the liquid acid-metal solution from the RCS to be delivered to the waste container. Three major sub-systems are involved in achieving the task of liquid handling and they includes:

- Liquid supply into the RCS and comprises of several other components namely the reservoir for the liquid storage, the pump to achieve the pumping of the liquid out of the reservoir and into the RCS, the control valve that serve as a switch control to allow/disallow the flow of the pumped liquid from the reservoir into the RCS, the tubing connection that serve as a passage for the liquid and finally a manifold that direct the fluid flow into/out of the RCS.
- The liquid ejection out of the RCS and comprises of other components such as the valve control, tubing, manifold, and the waste container.
- The plunger system and plunger control mechanism (stepper motor with lead screw assembly) that will enable the linear translation of the plunger in/out of the RCS.

The architecture of the BB system for the simulation of the leaching process and aspect of Liquid Handling Sub-system (LHS) and the physically designed and manufactured BB payload system is as presented in Figure 7-1

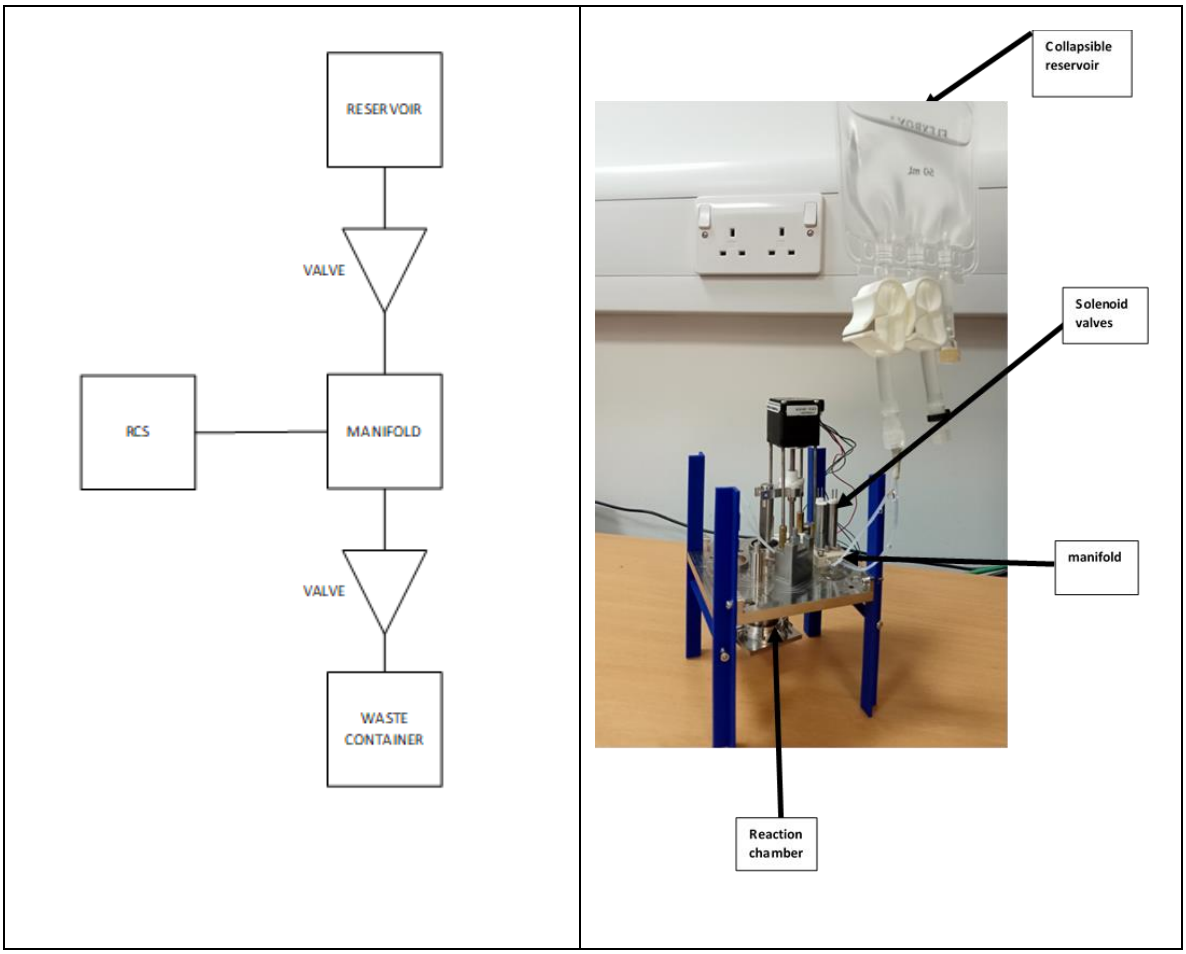


Figure 7-1: From the left the Liquid Handling Sub-system (LHS) architecture and to the right is the designed and manufactured LHS using a combination of polymer and CNC machined parts

7.6 BB PAYLOAD PROTOTYPE SYSTEM DESIGN AND COMPONENTS SELECTION

This section is primarily concerned with the BB prototype system design and component selection that will lead to the BB payload prototype system assembly, testing and operations.

7.6.1 REACTION CHAMBER SUB-SYSTEM (RCS) DESIGN AND MATERIAL SELECTION

The RCS as illustrated in the system architecture introduced in Chapter_5 is one of the critical components used in achieving the BB prototype payload system simulation of the sulphuric acid hydrometallurgical leaching and the aspect of liquid handling. It is a cylindrical open-ended RCS modified to be compatible with

sulphuric acid. The RCS is designed to have 50mm height, 25mm outer diameter and 18mm inner diameter respectively. Based on these design parameters, a single RCS internal volume was estimated at 12.73ml. Sulphuric acid is used as the reagent in the leaching process and is very corrosive, therefore, the choice of material for the implementation of the RCS design is critical. Several materials such as aluminium, titanium, and stainless-steel materials were reviewed. Both aluminium and titanium have poor chemical compatibility with sulphuric acid, stainless-steel material for their compatibility with sulphuric acid were chosen as the material to be used for the RCS design implementation (Bssa, 2021). The most common stainless-steel grades are 304 (L) and 316 (L); they all contain corrosive resistance material such chromium at 18% and 16% respectively (Haihaogroup, 2021). The addition of molybdenum (2 – 3%) in the 316L grades enhances the corrosion resistance properties more than in 304L grades and hence the choice of stainless-steel grade 316L over 304L as the material to be used for this research (Haihaogroup, 2021). Shown in Figure 7-2 to the left and a CNC machined printed version of the RCS to the right is the PLA 3D printed version of the RCS and in the centre is a Catia V5 designed version of a single open-ended reaction chamber.

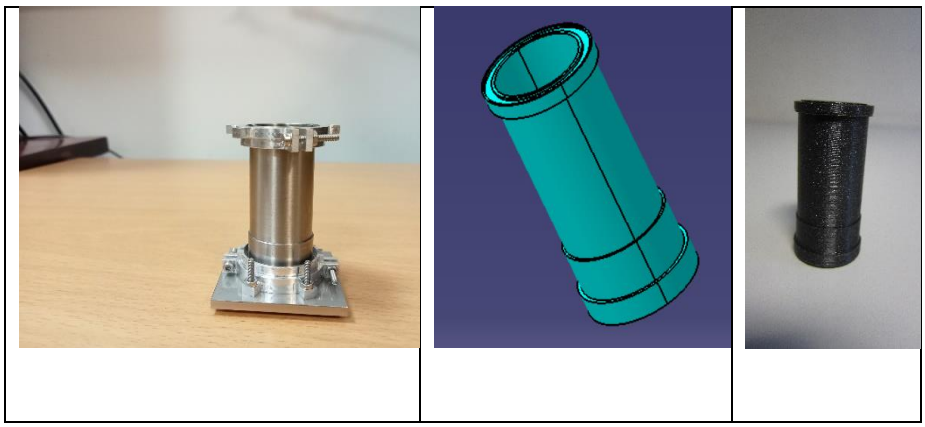


Figure 7-2: To the left and a CNC machined printed version of the RCS, to the right is the PLA 3D printed version of the RCS and in the centre is a Catia V5 designed version of a single open-ended RCS.

7.6.2 TOP PLATE MODIFICATION AND MATERIAL SELECTION

The top plate implemented on CubeSat based ISRU water extraction project as shown first left in Figure 7-3 were adapted and re-designed to enable the accommodation of the liquid handling system (LHS) and the associated system that will ensure efficient interaction between acid solution and the collected olivine regolith. The LHS components comprises of (1) motorised plunger system, (2) the valves control, (3) pumps, (4) manifolds, (5) reservoirs, (6) tubing connectors and fitting and they all serve the purposes such as pumping and switching of acid solution into and the metal-acid solution out of the RCS, provide the liquid storage and flow path within the subsystems. Figure 7-3 shows the original top-plate to the left and the top and rear view of the modified top-plate in the centre and to the right respectively.

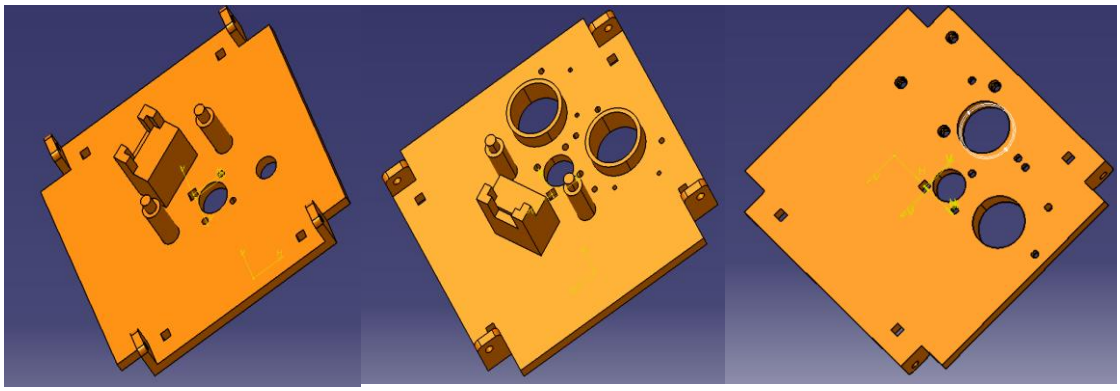


Figure 7-3: To the left represents the initial top plate used in the CubeSat based ISRU water extraction project, middle is the modified top view and to the right is the modified bottom view of the top plate respectively

The modified top plate is made from the stainless-steel materials and as shown in Figure 7-3, they were re-designed to provides:

- Two inlets to provide liquid access point into the RCS and provide support to the plunger on the top-plate surface
- Two mounting positions on the top surface of the top-plate were provided for the base support that plays the dual role of housing the bearings and providing vertical support to the motorised plunger system.

- A mounting position on the top surface of the top-plate is provided for mounting the manifold that connects the valves and pump systems to and from the RCS.
- Two clamping positions on the bottom surface of the top-plate are provided for clamping the RCS.

7.6.2.1 DESIGN OF PLUNGER SUPPORT AND INLET ON THE TOP-PLATE

Two identical plunger guide, inlet and support were designed and provided on the top-plate as shown in Figure 7-4, each having dimension of 10mm depth, 18mm internal diameter and 21mm and outer diameter respectively. The plunger inlet was designed to support, serve as inlet, and to house the plunger head.

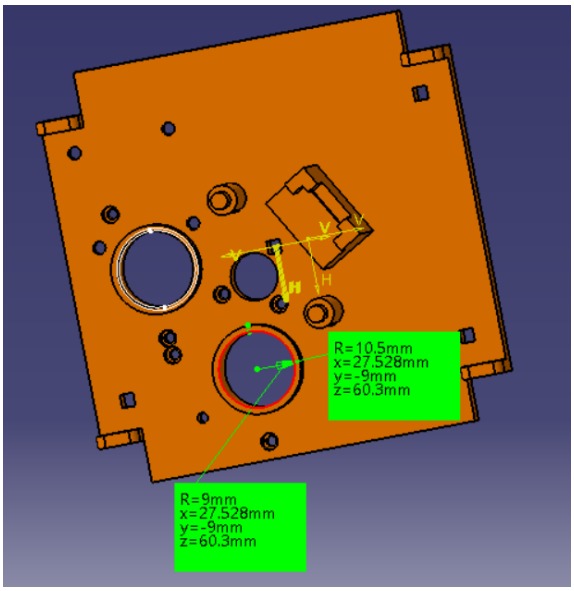


Figure 7-4: Modified top-plate showing the design plunger support position and inlet dimensions

7.6.3 PLUNGER SYSTEM DESIGN AND MATERIAL SELECTION

The plunger system is one of the most important components used for achieving an aspect of the liquid handling and also to ensure efficient interaction between acid solution and the collected regolith samples inside the RCS, they were designed to provide tubing connection that serve as inlet/outlet for liquid into and out of the RCS, provide leak free down/up stroke linear translation with the

internal bore of the RCS using an O ring sealing mechanism. Two plunger system were employed using the linear motorised lead screw assembly, the designed plungers were driven vertically up and down through the cylindrical bore of the RCS to ensure:

- Compression of the reaction mixture inside the RCS to allow for metal-acid solution extraction
- RCS emptying and cleaning to allow for RCS system re-use
- Detection of regolith volume scooped into the RCS
- Detection of Resistance feel that will indicate the acid and regolith have made contact

The mechanism to detect the volume of the regolith scooped into the RCS and the detection for resistance when contact were established between acid regolith will form part of the feature work. The plunger system have direct contact with the sulphuric acid solution and for this reason stainless-steel SS 316 (L) was selected as the material to be used in the plunger system design. Shown in Figure 7-5 are the different images of the plunger system



Figure 7-5: Left to the right the Catia V5 designed plunger, PLA 3D printed versions of the plunger and CNC machined version of the plunger.

7.6.3.1 THE PLUNGER SYSTEM SIZING

The two identical plungers are designed to be of equal length about 65.7mm and diameter of 9mm, at the narrow upper end of the plungers a depression of 6.5mm length, 6mm diameter and 3mm and depth respectively were created to provide a holding support for the extended arm from the lead screw system assembly. the bottom end of the plunger is designed such that it has a total thickness of 7mm, outer diameter of 17.75mm, a groove was design to house the O ring

material that contact the internal wall lining of the RCS to provide sealing. The two plungers differ only, one has hole to connect the RCS with the manifold through a tubing and the other completely seal for achieving the emptying of the regolith remnant from the RCS to allow for the RCS re-use. Figure 7-6 shows the dimension of the plunger system.

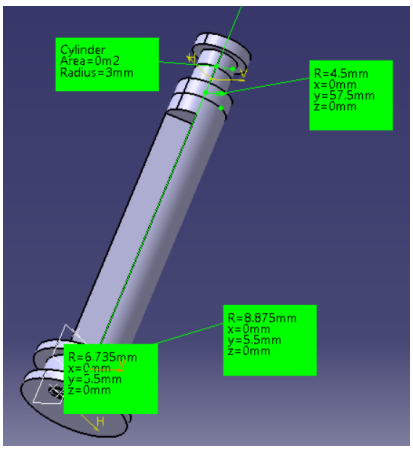


Figure 7-6: Designed plunger, the plunger arm support and plunger head dimensions

7.6.4 MOTORISED LEAD SCREW LINEAR ACTUATOR SYSTEM DESIGN AND MATERIAL SELECTION

To achieve the up and down linear translational motion of the plunger mechanisms a bi-directionally operated motorised lead screw linear actuator assembly to linearly drive the plunger in and out of the RCS to enable the acid solution delivery and the metal-acid solution extraction to and from the RCS is required. The motorised system were designed and selected on the basis of the estimated force required to compressed and drive the plunger through a stroke bore depth of 50mm. Constraint by mass and volume in the CubeSat system under consideration, directly coupled lead screw stepper motor reduce the number of components and also reduce the overall footprint and this is convenient for our application. The coupled lead screw motorised system assembly comprises of stepper motor, lead screw and lead nut. The plunger support/compression arm, bearings and system base support provide additional support to the operation of the motorised lead screw assembly. The stepper motor rotate and actuate a lead screw that linearly translate a load attached to

the lead nut. The motor rotating screw assembly actuator has the following unique features:

- Coupled directly to the lead screw and thereby eliminating the coupler and reducing the overall footprint
- Have reduced number of components and therefore reduced assembly length and this is quite beneficial for the implementation of our design

The Catia model of the bipolar stepper motor and the motorised lead screw linear actuator system assembly is shown in Figure 7-7

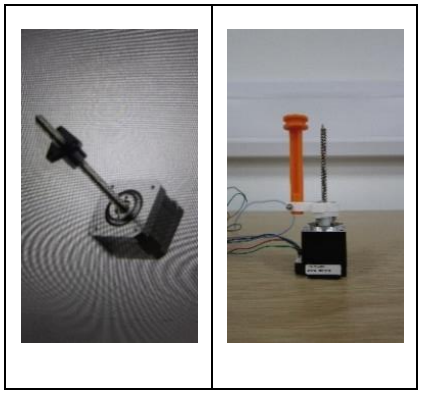


Figure 7-7: Left to right the Catia model of the stepper motor assembly, physical version of the stepper motor with mounted plunger attached to the support arm

7.6.4.1 STEPPER MOTOR DESIGN AND SELECTION

To design the type of stepper motor used as the driving mechanism for the plunger system, parameters such as the plunger compression force required to drive the plunger within the RCS need to be determine. It is assumed that the system operates within standard temperature and pressure (STP) condition, estimating the plunger compression force, RCS internal pressure of 1bar (100,000N-m^2) (Energy-Education, n.d.) was assumed and the RCS internal area was calculated at 3.34 x $10^{-4}m^2$ and a resultant plunger compressional force of 33.4N was calculated.

Factoring an assumed lead screw efficiency of e = 0.35 and the lead value of 1mm (10^{-3}m) (motorised-lead-screw, n.d.) and using the Equation 12, motor torque of approximately 0.016N-m was calculated. Equation 12: Represent the motor torque equation

$$Torque = f_T * \left(\frac{l}{2\pi e}\right)$$ **Equation 12**

Where, f_T = total compression force, L= lead screw lead (mm),
e= lead screw efficiency, π = 3.143

The combination of compressional force of $33.4N$ and motor torque of ~0.016N-m suggest that ML08 Motorised Lead Screw linear actuator manufactured by Thomson linear motion (Thomson, n.d.), has motor length of 29.5mm, maximum lead screw length of 102mm and a recommended maximum thrust 44N can conveniently sufficed for the BB prototype payload system design implementation.

The system external and frictional forces are not factored in calculating the compressional force on the plunger; to ensure the effective and efficient operation of the plunger system a higher motorised linear system that will accommodate these variables is consider for the BB design implementation. ML11 Motorised Lead Screw linear actuator (Thomson, n.d.) with near double the maximum thrust will be more than enough for the plunger system breadboard implementation.

ML11 Motorised Lead Screw linear actuator stepper motor operating within 80 – 95N maximum thrust, with motor length of 32 - 44mm and achieving 200 steps per revolution is recommended. As shown in Table 7-1, three motorised lead screw linear actuator motor system that met these requirements were identified and are listed together with their specification.

Table 7-1*: showing the three different NEMA11 motorised lead screw linear actuator stepper motor*

Motor specifications	**Motor model**		
	11A051 (Thomson, n.d.)	**11-2105 (dingsmotionUSA, n.d.)**	**11E2105 (dings, n.d.)**
Torque (N-m]	0.066	0.046	0.55
Voltage (V)	3.85	4.5	4.55
Current (A)	0.51	0.50	0.50
Resistance (Ω)	7.54	9.1	9.1
Power (W)	1.96	2.25	2.28
Motor mass (g)	110	250	400
Motor steps per revolution	200	200	200
Motor length (mm)	32	34	33.5
Motor maximum thrust (N)	89	130	-

As shown in Table 7-1, three NEMA 11 motorised lead screw linear actuator stepper motor from three different manufacturers were identified and compared. NEMA 11 stepper motor linear actuator (model 11A051) from Thomson linear motion appears to provide the maximum torque of 0.066N-m, consume less power of 1.96W and has the least mass of $\sim 110g$ and coupled with the least motor length was selected to be implemented in this research work

7.6.4.2 LEAD SCREW OPTION AND LEAD SCREW NUT ASSEMBLY

Based on the type of stepper motor selected for the implementation of our design, NEMA 11 stepper motor from Thomson linear motion uses integrated 4mm

diameter lead screw, having a lead of 1mm (the advance of the nut along the length of the screw per revolution) and travelling 0.005mm per full step and achieving 200 steps per revolution. The specification of the lead screw option in metric unit is as shown In Table 7-2.

Table 7-2*: the chosen lead screw specification* **(Thomson, n.d.)**

Screw code	Motor type	Lead screw diameter (mm)	Screw lead (mm)	Travel/step (mm)
M04-01	ML11	4	1	0.005

7.6.4.2.1 THE LEAD SCREW SIZING

The lead screw originally of length 102mm cannot fit into the CubeSat envelop length of 100mm. For the benefit of this work, the CubeSat envelop length was relaxed by 20%. A simple excel iteration was set up to estimate the sizing of the lead screw and is presented in **Appendix 2.1**. Parameters such as the maximum stroke length, length of lead screw nut and the motor length were considered to arrive at total lead screw length of 74mm excluding the motor length.

7.6.4.3 PLUNGER ARM SUPPORT

The plunger arm support is designed to be compatible and attached to the lead screw nut on the motor assembly side and to the plunger on the plunger side. The arm provide horizontal support to the plunger and linearly translate the plunger up and down when the motor is actuated and through the linear translation of the lead nut. The catia V5 model and the PLA 3D printed version of the plunger arm support are shown in Figure 7-8

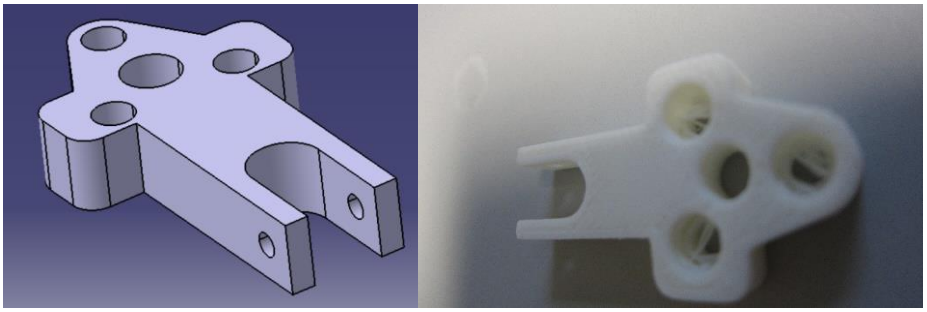


Figure 7-8: left to right showing *catia V5 model and the PLA 3D printed version of the plunger arm support*

Figure2-6 shows the designed plunger arm support and together with the dimensions of the leadscrew mounting position, 3 identical holes for strapping/screwing the screw nut lead with the arm support and the plunger holding position.

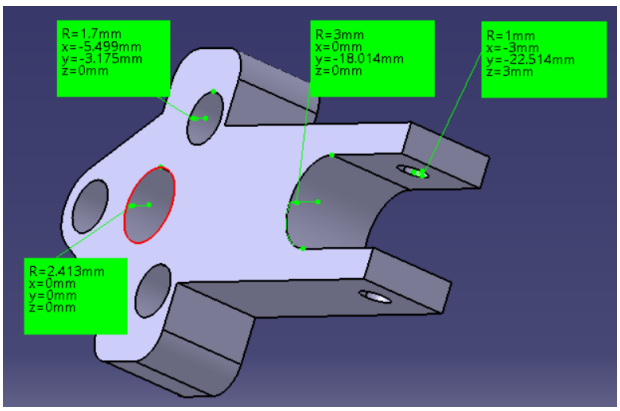


Figure 7-9: Designed plunger arm support showing the dimension of the screw lead support, screw lead nut screwing position and the plunger support

7.6.4.4 BEARING SELECTION AND LEAD SCREW MACHINING

The lead screw assembly in vertical linear translation generates both radial and axial loads and requires a means of support to absorb the effect of these loads components and to prevent the lead screw from buckling. Unlike the roller bearings that are designed to handle heavy load, the ball bearing is designed to handle small amount of weight and therefore compatible with our design application. Flange ball bearing for its ability to handle both radial and axial loads and provide support for a shaft that runs perpendicular to the bearing mounting

surface are selected for implementation in our design. Deep groove flange ball bearing with combined radial/axial thrust and compatible with the designed base support is selected and MF63ZZ model was procured from Simple bearing UK company. The lead screw machining to fit into the flange ball bearing groove was carried out in the Cranfield University workshop. The lead screw machining dimensions together with the corresponding flange ball bearing dimension were shown in Table 7-3

Table 7-3: Ball bearing specification and the lead screw machining data

Lead screw diameter (mm)	Flange ball bearing specifications in (mm)				Lead screw cutting dimension in (mm)	
	OD	ID	W	Bearing Trade No.	Lead screw machined OD	Lead screw machined width
4	6	3	2.5	MF63ZZ	3	2.5

Legend

OD	Flange ball bearing outer diameter
ID	Flange ball bearing internal diameter
W	Flange ball bearing width

7.6.4.5 STEPPER MOTOR AND FLANGE BALL BEARING BASE SUPPORT DESIGN

The stepper motor and flange ball bearing base support were designed to house and provide support to the MF63ZZ flange ball bearing housing the floating side of the lead screw. The system base support was designed based on the stepper motor dimension and the volume envelop of the system base support is dimensioned $(28 \times 28 \times 3)\text{mm}^3$ and with a nutch on one side to fit-in with the outer diameter of the plunger head mounting position. At the four corners of the system base support, position/holding point for the vertical motor support are provided. The stepper motor base support design and stepper motor base

support assembled with the MF63ZZ flange ball bearing mounted in position are shown in Figure 7-10 respectively.

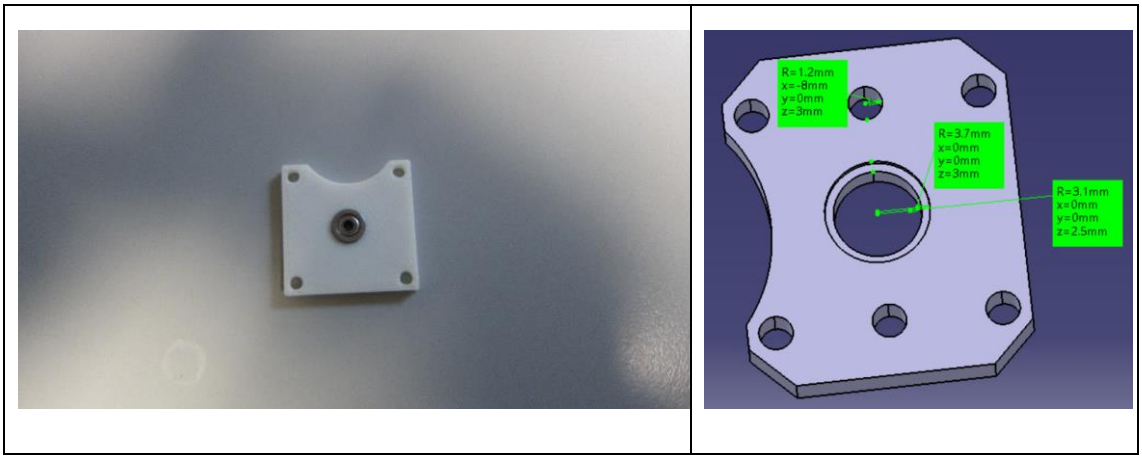


Figure 7-10: Left to right showing the stepper motor-based support assembled with the flange ball bearing and the designed base support showing the dimensions

7.6.4.6 MOTOR VERTICAL SUPPORT DESIGN

The motor vertical support designed to connect the stepper motor to the base support and also provide additional structural stability within the system. There are four identical vertical support connecting the stepper motor at the four corners of the stepper motor and originating from four edges of the bearing base support. The vertical support has a total length of 71.64mm and outer diameter of 4mm. To the bottom end of the vertical support a hollow is created through which the support is screwed to the topplate base support, the hollow has a diameter of 2.5mm and a depth of 5mm. The top end diameter of the vertical support is reduced to 1.8mm and a point end of 4.7mm length was created to fit and lock with the motor holes to provide a secured vertical support to the motor. Shown in Figure 7-11 is the stepper motor vertical support design

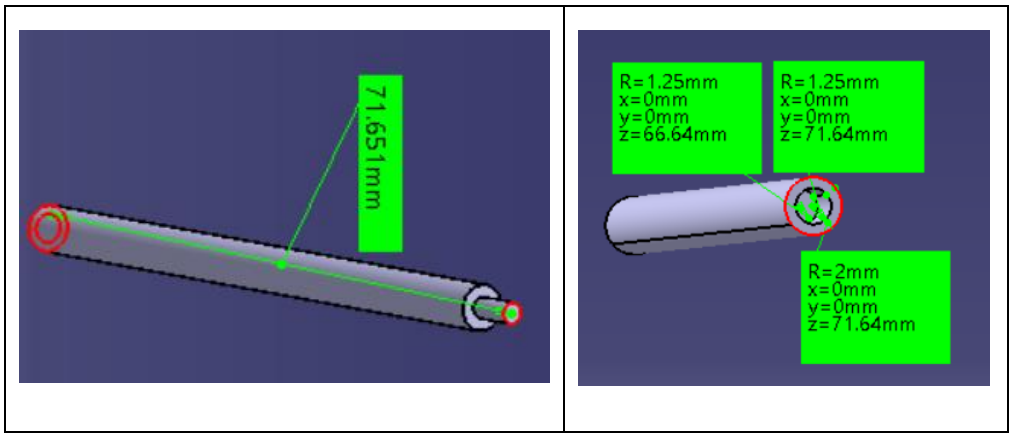


Figure 7-11: Left to right showing the stepper motor designed vertical support with the various dimensions

7.6.5 DESIGN OF SEALING MECHANISM AND MATERIAL SELECTION

To ensure an effective leaching process a leak free and internally pressurised RCS design must be ensured. Sealing materials in contact with RCS wall and at the top and bottom ends of the RCS are required to seal the RCS to eliminate the leakages and ensure the smooth sliding along the wall of the RCS and over the end of the top and bottom plates during plunger reciprocating motion and carousel mechanism rotation of the RCS respectively.

In this research work the Parker O ring standard handbook for its wealth of information about the properties of the most important sealing elastomers material was majorly used as guide for designing and selection of the seal material. To achieve an effective internal dynamic/reciprocating sealing mechanism; considering the RCS cylindrical bore of internal diameter of 18mm the corresponding O ring nominal cross section (CS) proposed is 2.54/2.69mm (Min/Max) and a corresponding groove width of 3.81/4.04mm was calculated using the standard 1.5*(O ring CS). At higher compression on the O ring material beyond 40%, defective O ring was difficult to avoid and at 25% or less compression of the O ring material, the defect is virtually eliminated (ORD5700, n.d.). For this design 15% (0.15) compression of the O ring material was assumed and the O ring piston groove diameter was calculated at 15.68mm. The O ring gland depth was estimated at 2.16mm, piston groove depth at 2.10mm. From the

piston groove diameter and assuming an O ring stretch of 3% (0.03), the O ring internal and outer diameter were calculated at 15.21mm 20.29mm respectively. To accommodate a groove of width 3.81mm by a height (depth) 2.10mm the top plate thickness was modified to 10mm.

To satisfy the Aerospace Recommended Practice (ARP-1231) for gland design, elastomeric O-ring seals general considerations were implemented. The gland fill ratio (ratio of the O ring cross sectional area and groove cross sectional area) should be approximately 65% and not be larger than 85%.

- Using the MINMAX CS of 2.54/2.69mm and the groove width and depth of 3.81/4.04mm and 2.16mm respectively, the gland fill ratio of 64/67% was calculated.
- Factoring the effect of thermal expansion on both the groove and the elastomer O ring material the new calculated value for the gland fill ratio is 65/75%
- In both situations the O ring is smaller than the groove they fit in; the gland fill ratio is far less than 85%. Satisfying this design consideration, no shearing failures on the O ring due to force increase is envisage.

The dimension of the top and bottom mounting position for the elastomer O ring material is like the one used on the reaction oven in the water extraction project discussed in Chapter_5. This elastomer O ring will be adapted in this research. The specification of the designed elastomer O ring material is as shown in Table1-4:

Table 7-4: showing the specifications of the designed elastomer O ring

Elastomer O ring specifications	**Corresponding value**
Cross section (CS) mm	2.54
Internal diameter (ID) mm	15.21
Outer diameter (OD) mm	20.29

7.6.5.1 O RING MATERIAL SELECTION

Identifying the specification of the elastomer O ring material of interest and designing the housing for the O ring material it is equally important to select the

elastomer rubber material that will be compatible with both the environment and material it will interact with. Several O ring materials where subjected to the selection criteria based on the following maximum consideration, the calibrated C-type NEA temperature range of (-43^{0}C to 150^{0}C) (okada, et al., 2017), 10% sulphuric acid concentration, at 1atmosphere pressure and material hardness. Fluorocarbon (Viton) elastomer rubber material meets these criteria and qualifies as the material of choice with the following specifications:

- Fluorocarbon (Viton) offer excellent chemical resistance to all grade of sulphuric acid and has temperature operating range -50^{0}C to 204^{0}C (Easternseals, n.d.).

The Figure 7-12 is a chart describing the choice of the O ring material based on the material hardness and pressure, obtained from ORD5700 Parker O ring handbook (ORD5700, n.d.):

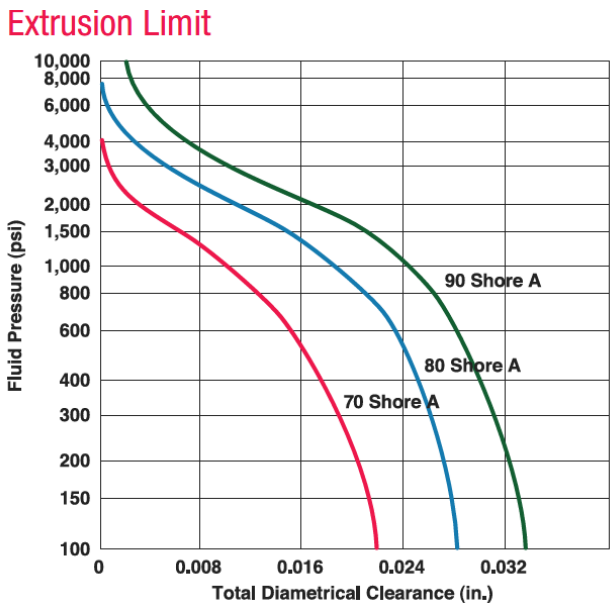


Figure 7-12: a chart for elastomer material hardness and pressure selection **(ORD5700, n.d.)**

From the earlier design information, the system internal pressure is ~ 230Psi and the diametrical gap clearance were 0.056mm (0.022inches). The extrusion limit of the O rings under pressure is determined by the size of the diametrical clearance gap and the hardness of the O ring material; it's can be seen from the chart in Figure 7-12 that the intersection point between the sealed pressure and

diametrical clearance falls to the left of material hardness curve with 70A. Fluorocarbon elastomer O ring material with hardness 70A is best suited for this design and are shown in Figure 7-13 and Fluorocarbon elastomer (FKM) material for its superior mechanical strength, excellent chemical resistance and excellent thermal resistance was chosen as the rubber/sealing material to use.



Figure 7-13*:* Left to right showing images of the designed and selected Elastomer O ring and the one implemented in the production of dioxygen project.

Appendix 3.1 Present an iteration for estimating the plunger head design based on the RCS internal diameter and the O ring sizing.

7.6.6 ACID RESERVOIR DESIGN AND MATERIAL SELECTION

The reservoir for storing the acid is designed based on the total volume of the 5 RCS proposed to be used in the project implementation. Based on a single RCS height of 50mm and internal diameter of 18mm, the volume was estimated at 12.73ml the total volume including 25% safety factor was estimated at ≈ 100ml. A collapsible reservoir having volume 100ml and made from PTFE polymer material and compatible with all grades sulphuric acid solution (Cplabsafety, n.d.) was proposed to be used as the sulphuric acid storage system. shown in Figure 7-14 is a sample collapsible reservoir and assembled with a tubing connector.



Figure 7-14: showing the collapsible reservoir assembled with a double ended fitting MINISTAC tubing

7.6.7 MANIFOLD SELECTION

The manifold was used to integrate fluidic components and consolidate fittings and tubing in a fluidic circuit. For this work, the manifold is selected to provide connection to the acid reservoir, pump system, solenoid valves, tubing, and fittings with reduced system complexity and to be compatible working with sulphuric acid. The manifold interconnect and simplify valve and other components mounting to achieve efficient and effective liquid channelling between the various components in the fluidic system. The bonding techniques is best suited for the manufacture of the manifold and the process involves machining channels, holes and shape in the plastic layer and then bonding them together to create a three-dimensional fluid path in a single manifold component. The post bonding machining create the valve fixing, connector and other fittings. The choice of the plastic material for building the manifold is critical. Different plastic material for the manufacture of manifold including Acrylic (PMMA), Ultem (PEI) plastic, and Polycarbonate thermoplastic are studied. The Polycarbonate thermoplastic material for its compatibility with Sulphuric acid and high temperature resistance is selected as the material of interest with the following properties.

- B^1 rating very good with minor effect at 10 – 75% H_2SO_4 (Cplabsafety, n.d.)

A PLA 3D printed version of the manifold was manufactured and a de-risking component and eventually a miniature 3way isolation manifold manufactured

from Polycarbonate thermoplastic meet this requirement and was procured from the lee components company for used in this research work. The PLA 3D printed version, CAD design version of the manifold and the physical version manifold with mounted valves are shown in Figure 7-15:

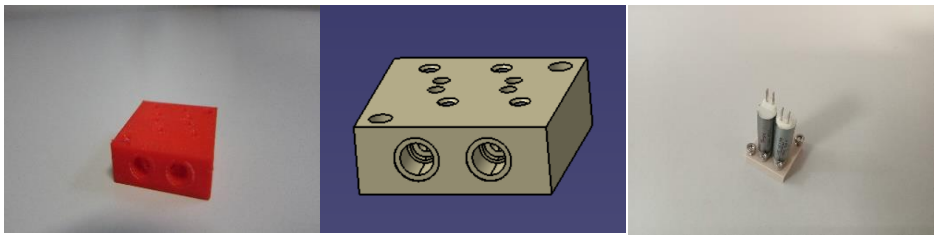


Figure 7-15: Left to the right is the PLA 3D printed version of the manifold, a Catia V5 model of the manifold and the physical manifold assembled with valves control

7.6.8 SOLENOID VALVE (SV) SELECTION

A solenoid valve is a device that provide a switching function in a fluidic system, and they operate in two distinct states; when the coil is activated by an electrical current (Normally open state) and when the valve is resting without electricity (Normally close state). For this design a single three stage SV was proposed to serve the purpose of isolation and connection to the waste container and the reservoir respectively. Constrained by size, mass and cost, a three stage SV compatible with the CubeSat form factor was not feasible. A compact LFN SV manufactured by the Lee components company that are cheap, adaptable on a simple manifold, readily available and can be driven with a simple design and built transistor circuit was proposed to take the place of the three stage SV valve. 2 flange type LFNA1250125H (leeco, n.d.) SV was procured and are to be independently operated by a design and built transistor circuit to control the flow of liquid from the reservoir into the RCS and the ejection of the liquid from the RCS into the waste container and are all interconnected through the manifold. The flange type LFNA1250125H for ease of mounting on the manifold was selected. The LFN type solenoid valves figures and the specification are as shown in Figure 7-16 and Table 7-5 respectively



Figure 7-16: showing the LFN flange type solenoid valves mounted on a manifold **(leeco, n.d.)**

Table 7-5: Listing the specification of the LFN SV **(leeco, n.d.)**

Specification	**Value**
Voltage (V)	12
Driving current	75mA
Internal volume (µl)	13
Power (mW)	900
Operated pressure (psig)	30
LOHM rate	2500
Weight (g)	6
2 way normally close design	-
Chemically inert	-
Have zero dead volume	-
Wetted material	FKM

The LFNA1250125H SV is originally designed to operate as a normal SV and required an additional special SV drive circuit configured to enable it operating as latching SV with the following benefits:

- Continuous opening of the SV with lower holding voltage
- Reduced coil temperature and
- Reduced power consumption

Maximum spike voltage of 20Vdc and recommended spike duration of 25ms an average of 900mW power was consumed using the special SV drive circuit. The SV drive circuit is used to spike and hold drive circuit to achieve enhance response time and reduce the average power. From table above, using:

- Hold voltage 5Vdc a power consumption of 160mW was arrived at
- 75 – 90% power consumption was recorded and
- Reduced coil temperature of 38^0C as against the maximum of 66^0C was recorded.

7.6.9 PUMP SELECTION

The pump is one of the most important parts used in the liquid handling processes, the pump system is designed to deliver a precise volume of the re agent from the reservoir through the SV and into the RCS for the purpose of achieving the leaching process. During the pump selection process in addition to performance of the pump, connector types, hardware size and weight are also considered as the parameters for the selection process. Micro Positive displacement pump (PDP) for its ability to trap a fixed volume of fluid and discharging same volume of fluid, also unlike other types of pumps they produce same flow at a given RPM irrespective of the discharge pressure. The PDP pump is designed such that at all-time they are operated simultaneously with the SV at the discharge side of the pump to avoid possible line burst and the pump and valve damage. The normally closed fixed volume and chemically inert PDP pumps manufactured by the lee microfluidic for its light weight and operation compatibility with the SV are considered. The comparison on the three types of fixed volume solenoid driven PDP pumps from lee components were shown on Table 7-6.

Table 7-6: specification of different types of pumps for selection

Pump characteristics	**LPM Pump (leeco, n.d.)**	**LPL Pump (leeco, n.d.)**	**LPG Pump (leeco, n.d.)**
Dispense volume range (µL)	25	50	175
Power consumed (W)	1.5	2	7
Voltage consumption (Vdc)	12	12	12
Operating frequency (Hz)	5	2	5
% Accuracy	± 15	± 6	± 10
Wetted material	PEEK/FKM	PEEK/FKM	PEEK/FKM

LPLA1250650L PDP SV pump type suitable for use as either soft press on tubing or manifold mounting appears to be suitable for our design implementation and was chosen. The PDP SV pump is designed to dispense 50 µL and achieve a pumping accuracy $\pm 6\%$ and consuming 2W of power and the pump has a total size of 75mm. The LPLA1250650L PDP SV pump was quite very expensive and was not included in the implementation of the breadboard prototype. For the BB prototype implementation, the liquid reservoir was directly connected to the RCS through a tubing connector and switched using the reservoir valve control. The manifold stand between the waste valve, the reservoir valve, and the RCS, whenever the SV controlling the liquid flow from the reservoir is switch on, the manifold isolates the waste valve control, connect the reservoir valve and due to gravity effect allow the liquid flow from the reservoir into the RCS.

7.6.10 TUBING AND FITTING MATERIAL SELECTION

The smallest tubing and fitting materials in terms of the tube diameter and fitting end sizes that will be compatible with the manifold fitting ends and compatible with the fittings end on the plunger and compatible working with sulphuric acid were required in the design and selection process. For this project and due to the miniature nature of the fitting ends on the manifold and the lack of the necessary

tools to prepare the fitting system; we appear to be constraint to using the standard tubing with two fitting ends readily assembled. So far, the 062 Minstac fitting system manufactured by the Lee Microfluidic Company is the only fittings system that appears to meet our design requirement with the following features:

- The tubing is made from PTFE thermoplastic material that is compatible with all grades of sulphuric acid
- The tubing has the smallest tubing size with minimum external and internal tube diameter of 1.57mm and less 1mm respectively
- The smallest fitting end uses 0.138 – 40UNF type of fitting end and translating into 3.5mm thread head diameter and 0.635mm pitch
- The fitting assembly provide a reliable leak proof system

7.7 ELECTRICAL/ELECTRONIC SUPPORT SYSTEM IN THE BREADBOARD (BB) PROTOTYPE PAYLAOD SYSTEM DESIGN

The electrical/Electronic support system in the BB prototype payload system design are additional support to the mechanical systems of the BB prototype payload system that support/drive the operations of the solenoid valves (SV) and the stepper motor for liquid handling and the plunger control respectively. The electrical and electronic support system required in this project to complement the mechanical systems include:

- Transistor circuit design and components selection and building to control the switching operations of the solenoid valves (SV) that will allow/disallow the liquid flow into and out of the RCS
- Hardware components selection, integrations, and coding to enable the stepper motor operation in a forward and reverse stepping sequence to achieve the plunger linear translation IN/OUT of the RCS

7.8 OVERVIEW OF THE DRIVE CIRCUIT FOR THE CONTROL OF THE SV AND THE STEPPER MOTOR CONTROL FOR THE ACTUATION OF THE PLUNGER

To achieve the implementation of the BB prototype payload system design, the electrical/electronic support systems are required to complement. In section 7.6.3, the plunger system has been designed and selected as the medium that will drive the operation of the liquid handling system. Also, in section 7.6.8, the SV has been selected as the medium through which the liquid flow into and out of the RCS is control. This section will design the drive circuit for the control of the SV and the stepper motor control for the actuation of the plunger

7.8.1 THE DRIVE CIRCUIT FOR THE CONTROL OF THE SV

The SV with a part No. LFNA1250125H is an integral part of the liquid handling system of the BB prototype payload system selected and described in section 7.6.8 and will be used in this project to perform the function of switching control of the liquid flow into and out of the RCS. The SV specification as presented in Table 7-5 of section 7.6.8, the switching control of a single SV is activated by an electrical current equivalent to 0.075A (75mA). The generation and supply of the load current to drive the SV will require the design and manufacture of a simple transistor circuit containing series of components that help in managing the proper flow of charge. These series of components together with their values are identified for the implementation of the proposed transistor circuit design. The critical components that drive the circuit design includes the transistor acting like a switch to control the switching of the SV load current and a voltage regulator that will provide constant 5V dc output voltage to drive the gate of the switching transistor. Other standard components that support the circuit design are the Zener diode connected in parallel with the SV to protect the transistor from any self-generated back electro-motive-force (emf), push button switch plays the role of switching ON/OFF to allow the passage of 5V dc constant supply from the output of the voltage regulator to drive the gate of the transistor, jumper wires that interconnect the various components in the design and a breadboard onto which the design electronics circuit are created and for test or demonstration purposes.

7.8.2 TRANSISTOR SWITCHING CIRCUIT DESIGN AND COMPONENTS SELECTION

In designing the transistor switching circuit and component selections, several switching devices such as the relays and transistors have been considered. The relay switching device is not suitable as a possible option in the implementation of the switching circuit design; the relay due to their electromechanically nature they are less reliable compared to the transistors, they occupy larger spaces, they are heavier in mass and costlier too (Arrow, n.d.).

In the transistor options, two families of the transistors exist namely the Bipolar Junction Transistor (BJT) and the Field Effect Transistors (FET). The BJT and FET are two different types of semiconductors and they differ measuredly in their working principles; the BJT is current controlled devices because the output collector emitter voltage is controlled by the input base current while FET is voltage-controlled devices because the input gate voltage controlled the output drain voltage (Elprocus, n.d.).

7.8.2.1 BIPOLAR JUNCTION TRANSISTOR (BJT)

The Bipolar Junction Transistors (BJT) are basically NPN and PNP. The NPN or PNP denote the BJT transistor arrangement/configuration. In the formation of the NPN transistors, N-type region having a high electron concentration (-ve) and the P-type having a high hole concentration (+ve) are place side by side to form a NP-junctions semiconductor material called a diode. Two NP-junctions are connected sharing a P terminal and NPN transistor is formed (Abdelhalim Z & Abdelhalim, 2000). The NPN transistor has the P-type silicon as the base and sand witched between two pieces of N-type collector and emitter. The PNP transistor arrangement is the reverse of the NPN.

7.8.2.2 FIELD EFFECT TRANSISTORS (FET)

Field Effect Transistors (FET) such as IGFET and JFET. The junction field effect transistor (JFET) is available in two polarities (N-channel and P-channel) and consist of N-type silicon with P-type regions electrically connected to form the gate (NXP, 1993). JFET operation is based on reverse biasing the PN junction

between the gate and channel to control the channel width and hence the current flow from the drain to the source (NXP, 1993). The Insulated Gate Field Effect Transistor (IGFET) they operate in the same manner as JFET, but they have gate terminal that is electrically isolated from the conductive channel, a good example of IGFET is the Metal Oxide Semi-Conductor Field Effect Transistor (MOSFET) (NXP, 1993).

7.8.2.3 TRANSISTOR SELECTION

Both BJT and FET can be used as switches or amplification devices in electronic circuits. The FET are slightly more expensive than the BJT type of the transistors, the FET transistor are selected in preference to BJT given the following reasons (rfwireless, n.d.)

- FET have faster switching time than the BJT
- FET consumed less power compared to the BJT
- FET has better heat stability as compared to the BJT
- FET are smaller compared to BJT
- FET has less noise as compared to BJT

Within the FET family, MOSFET they are easier to manufacture and are more widely used than the JFET. The MOSFET can also operate in either the depletion or in enhancement mode compared to the JFET that operate only in the depletion mode. The MOSFET transistor within the FET family is selected over the JFET for implementation in this project

7.8.2.4 MOSFET SWITCHING TRANSISTOR PART NO. IRF640N

MOSFET transistor with the part No. IRF640N was selected as a switching transistor for the implementation of the switching control of the SV, it is a fast-switching transistor, operate within the temperature range of (-55 to 175^0C) and has maximum drain to source voltage (V_{DSS}) = 200V, and maximum drain current (I_D) = 18A (Apogeeweb, n.d.). Shown in Figure 7-17 is the IRF640N MOSFET transistor.



Figure 7-17: IRF640N MOSFET transistor **(Apogeeweb, n.d.)**

7.8.2.5 DESIGN AND SELECTION OF A DC VOLTAGE REGULATOR

To permit the switching of 12V dc source voltage to induce the operation of the SV, a combination of a voltage regulator supplying a low and constant dc voltage to drive the gate operation of the MOSFET transistor is required. From the specification sheet of the selected MOSFET transistor, the threshold voltage (V_{TH}) of IRF640N MOSFET switching transistor is a positive value between 2 - 4V minimum to maximum (Apogeeweb, n.d.). To efficiently drive/switch the transistor to allow the flow of the drain current (I_D) across the drain (D) and source (S) of the MOSFET transistor, the voltage across the gate and source (V_{GS}) must be made appropriately greater the threshold voltage ($V_{GS} > V_{TH}$).

Considering the threshold voltage (V_{TH}) of IRF640N MOSFET switching transistor at the maximum value (4V dc), to efficiently drive/switch the transistor the condition provide that the gate-source (V_{GS}) must be made appropriately greater the threshold voltage ($V_{GS} > V_{TH}$) must be made.

- Therefore, assuming the maximum threshold voltage of the transistor 4V dc, a minimum of constant 5V dc output from the voltage regulator is required to drive the gate of the MOSFET transistor.
- To estimate the input voltage to a dc voltage regulator, we consider the minimum input voltage should be the output voltage added by a value of three.
- To have a voltage of 5V dc output from the voltage regulator a minimum input voltage of 8V is sufficient and a 12V input can be very convenient.
- A 12V dc input voltage regulator available in the Cranfield Space Group Laboratory will be used as the feed in supply of the selected voltage regulator.

7.8.2.5.1 POWER VOLTAGE REGULATOR (5V DC OUTPUT) PART NO L7805C IC

Power voltage regulator with part No. L7805C IC will conveniently provide 5V dc output voltage to drive the gate of the IRF640N MOSFET switching transistor. L7805C IC power voltage regulator can support output current in the range of 5mA – 1A, support input voltage range of 7 – 18V dc and can output 4.9V dc minimum, 5V dc typical and 5.1V dc maximum output voltages respectively (components101, n.d.). Shown in Figure 7-18 is the 7805IC dc voltage regulator and Figure 7-19 showing the main driving components on the breadboard.



Figure 7-18 : 7805 dc voltage regulator **(components101, n.d.)**

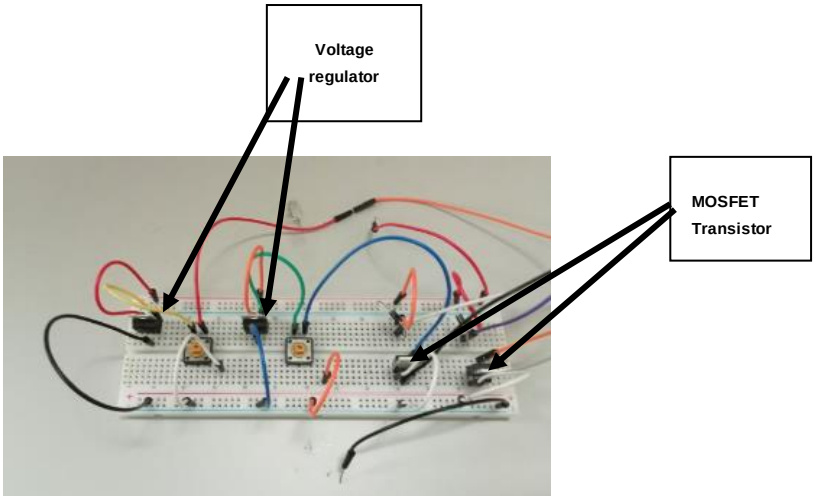


Figure 7-19: Breadboard components mounting showing the circuit driving components MOSFET transistor and the voltage regulator

7.8.3 SIMPLE TRANSISTOR CIRCUIT CONCEPT OF OPERATION

This section described the operational concept of the designed and manufactured MOSFET transistor circuit. The transistor acting as a switch aims to drive the switching of the SV to control the liquid flow into and out of the RCS. Several

components make up the transistor circuit; Setting up the components and establishing the connection on the breadboard a 12V dc power supply is switched on to serve as the input supply to the dc voltage regulator, the dc voltage regulators process the 12V dc to output a constant 5V dc that will switch/drive the gate of the MOSFET transistor to allow the passage of the driving current across the SV as the system load, a switch placed between the dc Voltage regulator and the transistor gate play the role of switching/isolating the constant 5V dc to the gate of the MOSFET transistor to switch ON/OFF the SV load. The jumper wires are used in interconnecting the system components. The SV is an inductive load, and a Zener diode is placed in parallel with the SV load to protect the MOSFET transistor against the effect of self-generated electro-motive force (emf).

The simple transistor circuit design and built on a breadboard comprises of:

- 2LFN SV independently control each by a MOSFET transistor acting as a switch
- 12v dc power supply that provide voltage supply to the input of the voltage regulator (7812C)
- 2 voltage regulators (7812C) each supplying a constant 5v input voltage to the switching MOSFET transistor
- 2 MOSFET transistor each controlling the switching of the LFN SV
- 2 switch controls used to alternate the switching of the 5v to the MOSFET transistor
- Breadboard and jumper wires

The designed and built transistor circuit and interconnecting the SV, tubing and the reservoir is shown Figure 7-20.

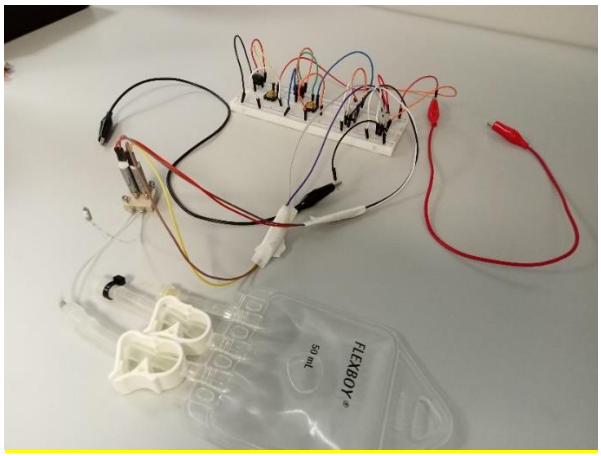


Figure 7-20a: An assembly of the transistor circuit together with the SV and the collapsible reservoir

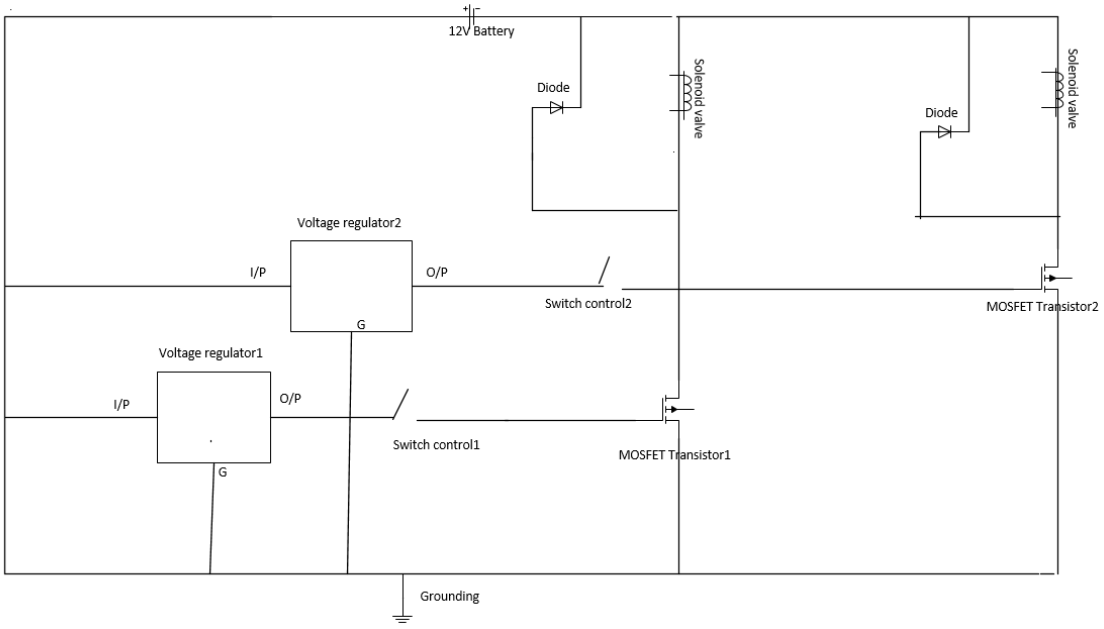


Figure 7-20b: Represent a simple Visio schematic that represent a two stage SV switching control

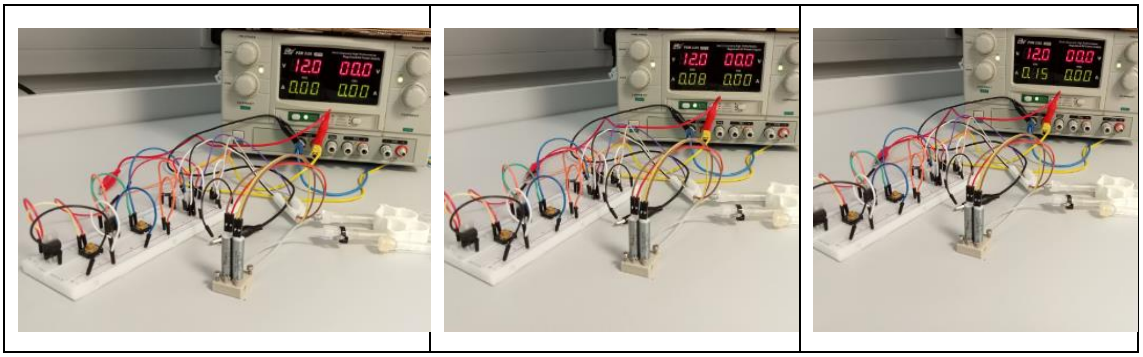
7.8.4 GROUND TESTING OF THE SV SWITCHING CONTROL USING THE IRF640N TRANSISTOR SWITCHING CIRCUIT

The ground testing of the SV switching control using the MOSFET transistor switching circuit was performed successfully and the process and result of the ground testing was described below and was also illustrated in Figure 7-21

- The first figure from the left the MOSFET transistor circuit was set up and connected to 12V dc voltage supply, no load current induced across circuit to drive the load, hence zero current flow was recorded on the display panel of the 12V dc voltage supply.
- The second figure in the centre, the MOSFET transistor circuit was set up and connected to 12V dc voltage supply, one MOSFET transistor was switched on and load current was induced across the circuit to drive the operation of a single SV, a maximum of 80mA load current was observed to flow as illustrated on the display panel of the 12V dc voltage supply.

- The third figure on the right, the MOSFET transistor circuit was set up and connected to the voltage supply of 12V, two MOSFET transistor were switched on and load current was induced across the circuit to drive the operation of both the two SV, a maximum of 150mA load current was observed to flow as illustrated on the display panel of the 12V dc voltage supply.

Figure 7-21: On the left is the transistor switch with no load current induced, in the middle



with load current induced to operate a single SV and to the right with induced load current to operate two SV.

Legend describing Figure 7-21

Figure on the left	MOSFET transistor does not switch on and no-load current induced across circuit to drive the load, hence zero current flow was recorded on the display panel of the 12V dc voltage supply.
Figure in the middle	A single MOSFET transistor was switched on and load current was induced across the circuit to drive the operation of a single SV, hence 80mA load current flow was recorded on the display panel of the 12V dc voltage supply.

Figure on the right	Two of the MOSFET transistor were simultaneously switched on and load current was induced across the circuit to drive the operation of the two SV, hence 150mA load current flow was recorded on the display panel of the 12V dc voltage supply

7.8.5 STEPPER MOTOR CONTROL FOR THE LINEAR ACTUATION OF THE PLUNGER IN/OUT OF THE RCS

To simulate the supply of reagent (sulphuric acid) and the extraction of the metal acid solution into and out of the RCS, a mechanism that will enable the linear translation of the plunger into and out of the RCS is required. Chapter_7, Section 7.6 the bipolar stepper motor was selected as suitable for the linear translation of the plunger mechanism into and out of the RCS. In this section hardware components selection, integrations, and coding to enable the stepper motor operation in a forward and reverse stepping sequence, speed control and micro-stepping to achieve the plunger linear translation IN/OUT of the RCS will be described

The following hardware's working together were identified to achieve the desire task driving the stepper motor and are described in detail below.

- Arduino Uno board
- V4.2 version of the easy driver controller
- Variable dc power supply,
- NEMA11 bipolar stepper motor coupled together with the linear actuator system and a laptop system.
- Breadboard
- USB cable and
- Jumper wires

7.8.5.1 ARDUINO HARDWARE AND SOFTWARE

The Arduino hardware is an open-source microcontroller used for constructing and programming electronic devices (Louis, 2016). For the implementation of this work 5 digital Input/Out pins Arduino hardware are required to interface the motor driver controller and to achieve the motor functions control. The Arduino

Uno board R3 has 14 digital I/O pins, 6 out of which are pins used to provide Pulse width modulation (PWM) output and is quite suitable for this work (spiceman, n.d.); the Arduino Uno board was selected for this aspect of the project implementation. The Arduino Uno board is shown in Figure 7-22



Figure 7-22: An Arduino Uno board **(spiceman, n.d.)**

7.8.5.2 STEPPER MOTOR DRIVER/CONTROLLER SELECTION

Stepper motor drivers interface the Arduino Uno board on one side and the bipolar stepper motor on the other. The controller supply power to the stepper motor and they also provide the switching control, stepping sequence and clock pulses received from the Arduino Uno to determine the step rates. The stepper motor driver selection can be influenced by factors such as power output, speed, micro stepping, cost, and size in terms of weight and volume. In the selection criteria, three types of drivers have been identified and analysed as shown in Table 7-7:

Table 7-7: List of different types of driver controllers for a selection process

Motor specification	**Motor types**		
	A4988 (robotpark, n.d.)	**DRV 8825 (pololu, n.d.)**	**Easy driver (Sparkfun, n.d.)**
Micro stepping	Up-to 1/16	Up-to 1/32	Up-to 1/8
Voltage range	8 – 35 (V)	8.2 – 45 (V)	8 – 35 (V)
Current range	1 – 2 (A)	1 – 2.5 (A)	1 – 2 (A)
Maximum Power (W)	70	98	70
Weight	1.8g	1.6g	1.6g
Cost	$5.95	-	$5.45

The easy driver compared to the other two types of drivers has minimal micro-stepping and by extension decrease mechanical noise and reduces resonance problem, they consume less power, they are smaller in terms of mass and volume, they are cheaper, also they are versatile and readily available. The easy driver hardware was selected for use in this project to provide the bipolar stepper motor the switching control, stepping sequence and clock pulses to determine the step rates.

7.8.5.2.1 EASY DRIVER BOARD SELECTION AND DESCRIPTION

The easy driver board is designed based on A3967 IC and enables to drive bipolar stepper motor of different wire configurations and work with either 3.3V or 5V systems. The easy driver is designed to operate at variable current stages and can drive up to about 750mA per phase of a bi-polar stepper motor and has two setting of micro-stepping (MS1 and MS2). V4.2 version of the easy driver is quite versatile and work with either 3.3V or 5V system, has variable current stages and has twos settings of micro-stepping (MS1 and MS2). The V4.2 version of easy driver board is used for the implementation of this design and the pin description of the board are as shown in Figure 7-23:

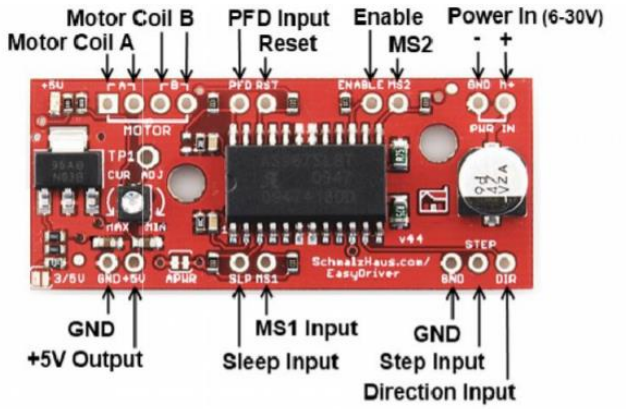


Figure 7-23: An easy driver board **(Sparkfun, n.d.)**

7.8.5.3 CONNECTING THE EASY DRIVER WITH ARDUINO UNO BOARD

The communication between the Arduino and the easy driver boards are achievable using digital I/O pins with pulse wide modulation (PWM). The critical pins on the easy driver identified and used are the STEP, DIRECTION, ENABLE

and MS1 and MS2, and the corresponding I/O pins (4, 5, 6, 8 and 9) on the Arduino with PWM capabilities are identified and are cross connected with using jumper wires. The pins cross connection between the Arduino board and the Easy driver board are as shown in Table **7-8** and the physical breadboard interconnection between the Arduino board and the Easy driver board is presented in Figure 7-24.

Table 7-8: Showing the pins cross connections between the Arduino and Easy driver boards **(Sparkfun, n.d.)**

Arduino board pins connection point	Easy driver pins connection point
Pin 4	MS1
Pin 5	MS2
Pin 6	ENABLE
Pin 8	DIR
Pin 9	STP

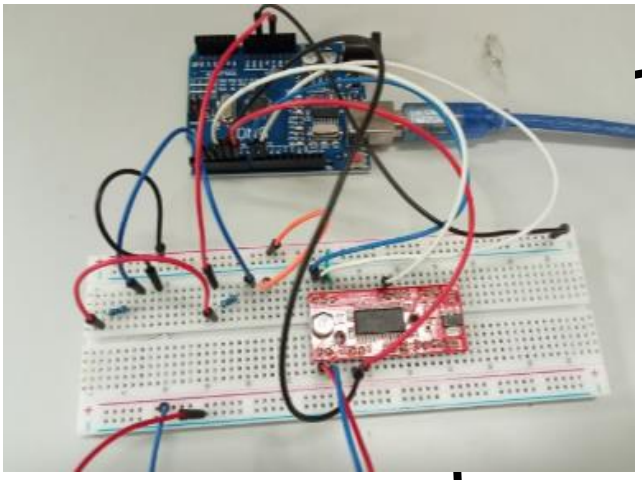


Figure 7-24: Physical breadboard interconnection between the Arduino board and the Easy driver board

7.8.6 CODE WRITING, CODE UPLOADING, AND THE SYSTEM TESTING

After setting-up the various hardware on the breadboard and establishing the jumper wire interconnection as shown in Table **7-8** and physically on Figure 7-24, the code written to enable the precise control of the stepper motor to move the plunger linearly into RCS and return it to a pre-determine starting point is presented in Figure 7-25 were uploaded onto the Arduino interface and to communicate with the Easy driver.



Figure 7-25: written code to control the linear transition of the stepper motor into RCS and out of the RCS

7.8.6.1 INTERPRETATION OF THE UPLOADED CODE

In the first section of the code called the void setup

- The pins connection between the Arduino Uno board and the easy driver controller are defined as presented in Table **7-8**

- The pins functions are declared and were set as output and put them to the proper logic levels to begin driving the motor.

In the second section of the code called the main loop or (void loop)

- Open communication between the Arduino Uno board and the Easy driver was established through the serial ports
- The Easy driver continuously scan the serial ports for input and compare the inputs to the four possible functions of the stepper motor and execute them. The four possible stepper motor functions include:
    - Driving the stepper motor forward
    - Driving the stepper motor in reverse
    - Forward and reverse
    - Micro stepping the stepper motor and

In this project we are interested in two of the stepper motors functions to drive the stepper motor in forward and reverse order to precisely control the plunger linear motion into RCS and returning it to a pre-determine starting point and the micro-stepping.

7.8.7 STEPPER MOTOR STEPPING USING ARDUINO IDE TO CONTROL THE PLUNGER LINEAR TRANSLATION TO A PRE-DETERMINE HEIGHT/DEPTH AND CORRESPONDING TO DISPLACED VOLUME

The RCS is calibrated in terms of volume displacement, considering the diameter of the cylindrical shaped RCS and the linear retraction height of the of the plunger relative to the stepper motor pre-determined stepping. The overall internal volume of the cylindrical shaped RCS at 50mm height and the internal diameter of 18mm correspond to 12.73mls. Approximately 6mls of the internal volume of the RCS is estimated to be the volume that will accommodate both the water and the regolith in a volume ratio of 1:5 and for the demonstration of the extraction process. Therefore $\approx$ 25mm is estimated as the displacement height or the plunger head marked extension start point into the RCS to displace the 6ml equivalent volume. During the simulation of liquid handling process the solid to

liquid ratio of 1:5ml implemented in Chapter_6 experiment to be used, 5ml of the liquid volume will be pumped into the RCS and to react with 1ml (1.3g) regolith.

7.8.8 MICRO-STEPPING THE BIPOLAR STEPPER MOTOR

The micro-stepping of the stepper motor is determined by the combination of the state of the MS pins, as shown in the truth table by changing the setting for one of the MS pins, the micro-step state is determined. For this work, the stepper motor is operated in full step and therefore achieving improve torque and speed performance. In a full step stepper motor operation, 200steps required per revolution (360^0), a step angle therefore correspond to 1.8^0. Micro-step truth table combination is presented in Table 7-9

Table 7-9: Truth table showing the combination of micro-step state **(Sparkfun, n.d.)**

MS1	MS2	Micro-step state
L	L	Full step
H	L	Hall step
L	H	Quarter step
H	H	Eight steps

7.8.9 GROUND DEMOSTRATION OF THE STEPPER MOTOR MOTION IN FORWARD AND REVERSE DIRECTION

The Arduino board, easy driver controller board and the other component for driving the stepper motor were assembled to demonstrate the ground testing of the stepper motor linear translations of the plunger is shown in Figure 7-26. The ground testing of the stepper motor functionality using the Easy Driver controller and instigated by the Arduino control command was carried out successful, the components properly set-up and when a closed circuit was established the stepper motors functions to drive the stepper motor in forward and reverse order to precisely control the plunger linear motion into RCS was achieved. It can be observed on the display screen of the Dc voltage regulator shown in Figure 7-26

that because of the stepper motor operations, 170mA current flow with a voltage drop of 4.5V dc and in both directions was achieved.

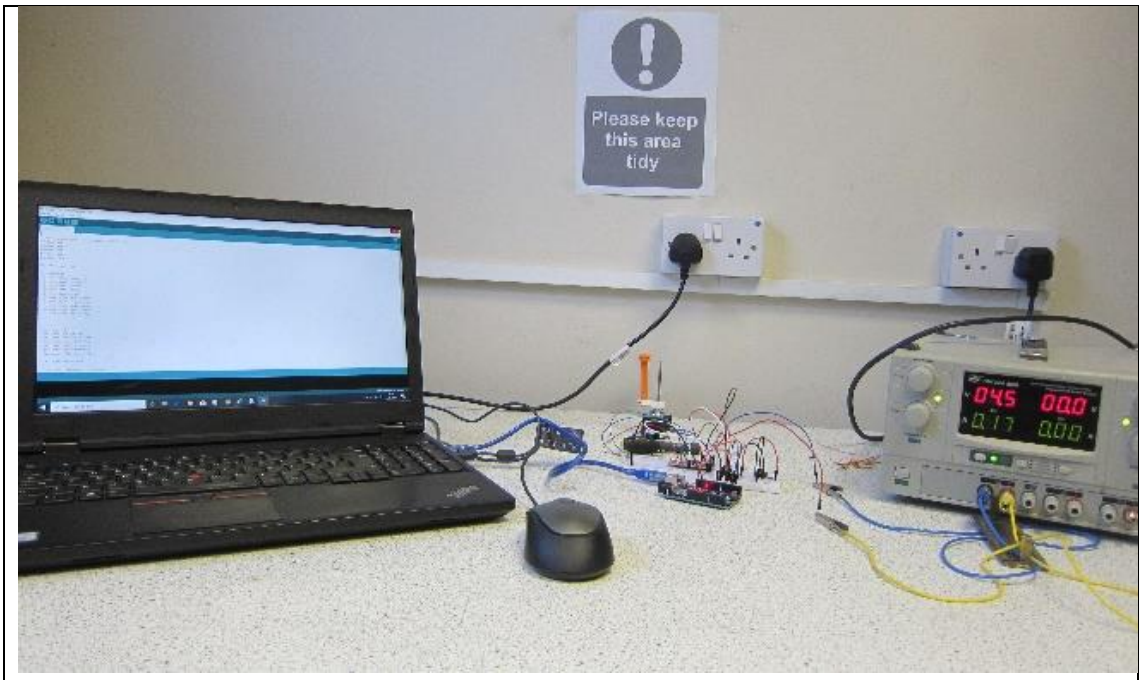


Figure 7-26: Assembly of Arduino and Easy driver board interfacing other components (the Dc voltage power source, and the laptop)

Legend

Stepper motor operations	On the display screen of the voltage supply, the stepper motor operations consumed 170mA of current flow with a voltage drop of 4.5V dc and in both direction

7.9 OVERALL BB PROTOTYPE SYSTEM ASSEMBLY, TESTING AND DEMOSTRATION OF OPERATION

In this section the electrical/electronic system designed and selected in section 7.8 of Chapter_7 (the stepper motor assembly and the SV control system) were integrated together with the BB payload system mechanical components and were tested for the demonstration of the plunger linear extension and retraction

into/out of the RCS on one side and the liquid flow control on the other side using the SV control system.

7.9.1 BB PROTOTYPE SYSTEM ASSEMBLY

The electrical/electronic support system together with the BB payload prototype mechanical components were assembled to build a complete BB prototype payload system as shown Figure 7-27. The assembled BB prototype was tested for the demonstration of the plunger linear extension and retraction into/out of the RCS on one side and the liquid flow control on the other side using the SV control system. Shown in Figure 7-27 to the left is 3D machined, in the centre is designed model using the Catia tool and to the right is 3D printed version of the built BB prototype.

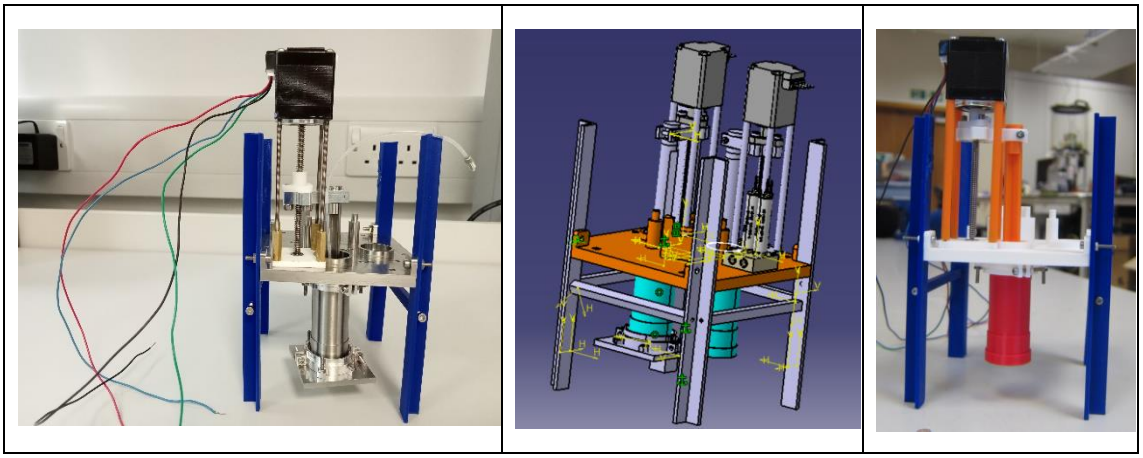


Figure 7-27 : To the left is 3D machined, in the centre is designed model and to the right is 3D printed and built BB prototype

7.9.1.1 BB PROTOTYPE SYSTEM TESTING AND OPERATION FOR THE DEMOSTRATION OF THE PLUNGER SYSTEM EXTENSION AND RETRACTION INTO/OUT OF THE RCS USING THE STEPPER MOTOR SYSTEM AND AN ASPECT OF LIQUID HANDLING USING THE SV CONTROL SYSTEM

The BB prototype payload system assembled as shown in Figure 7-27 are powered from a 12V dc voltage source to achieve their operations. The stepper motor operation to linearly extend and retract the plunger in /out of the RCS and the aspect of liquid handling using the SV control system was designed to operate

simultaneously and to commences at a pre-determine plunger head height (25mm above the bottom of the RCS).

The system operation is described thus:

- At the pre-determine plunger head height, 25mm above the bottom of the RCS, Initially the stepper motor is switched on simultaneously together with the waste valve control to extend/drive the plunger into the RCS and at the same time to de-pressurise the RCS.
- At the pre-determine travelled depth into the RCS, the stepper motor was put on hold and the delay function between direction (DIR) change over period allow for:
    - Isolating the waste valve control to dis-allow the de-pressurisation of the RCS
    - Switching on the reservoir valve control such that, in the reverse direction linear motion to retract the plunger creating head space and due to gravity effect liquid from the reservoir flow into the RCS to fill it to the predetermine retraction height.
    - Assuming that the leachate was collected inside the waste container during the extension of the plunger into the RCS, the change over time would allow for the replacement of the waste container.
    - The filling and emptying time of the RCS is captured using a digital stopwatch and was recorded, and will be used in estimating the liquid flow rate into/out of the RCS
- In the second phase of the plunger extension into the RCS, the stepper motor together with the waste valve control were switched on simultaneously and as the plunger extends into the RCS, liquids were expelled through the control waste valve and collected inside a waste container
- The process of the plunger extension and retraction into and out of the RCS was performed three (3) times to ensure repeatability.

7.9.1.2 RESULT FOR DEMOSTRATING THE OPERATIONS OF THE BB PROTOTYPE SYSTEM

The initial ISRU BB payload system was produced, the stepper motor and the SV control demonstration carried out to achieve an initial operation and testing were performed and the following result was recorded.

- The demonstration of the bipolar stepper motor operations in forward and reverse motion to achieve the plunger extension and retraction into/out of the RCS was performed successful.
- The SV valves controlled with the designed and manufactured transistor circuit were successfully and independently switched ON and OFF to indicate the opening and closing of the valve control to allow the in-flow/out-flow of liquid into and out of the RCS.
- The overall BB prototype system assembly successfully demonstrate the extension/retraction of the plunger system into/out of the RCS and as well as the SV control to allow the in-flow/out-flow of liquid into and out of the RCS.

In the overall, the BB prototype payload system operations to enable communication among the various system components to achieve the desire task of performing stepper motor operation to demonstrate the plunger system extension and retraction into/Out of the RCS and using the SV control mechanism to demonstrate an aspect of liquid handling has been achieved. The BB prototype system is now ready for the implementation of the BPB dye solution extraction.

7.10 CONCLUSION

The overall payload system hardware design, components selection and assembly for the BB prototype payload system development was performed. The developed BB payload testing and operations to control the linear translation of the plunger system in/out of the RCS and the opening and closing of the SV control was successfully carried out in this chapter.

The initial demonstration of the BB prototype payload system testing/operation performed in this chapter was carried out under the influence of gravity, as the plunger system is linearly retracted and the SV controlling the reservoir are switched open the liquid inside the reservoir flow with ease into the RCS. In a microgravity environment where liquid behaviour cannot be predicted, to ensure the liquid flow into the RCS a spring-loaded flexible reservoir will be included to maintain a constant overpressure to squeeze the collapsible reservoir. In the subsequent chapter, the assembled BB prototype system will be used to simulate the demonstration hydrometallurgical acid leaching of regolith and the aspect of liquid handling process.

8 USING THE DESIGNED AND MANUFACTURED BREADBOARD PAYLOAD PROTOTYPE TO SIMULATE DEMOSTRATION OF THE HYDROMETALLURGY SULPHURIC ACID LEACHING OF THE OLIVINE MINERAL AND ASPECT OF LIQUID HANDLING

8.1 INTRODUCTION

The BB payload prototype was designed, manufactured, and the mechanical and fluidic operation without leaching was tested in Chapter_7. This chapter of the thesis document aimed to simulate the demonstration of the hydrometallurgy leaching experiment and the aspect of liquid handling using the designed and manufactured BB payload prototype system in a non-agitated state only. The demonstration of the static extraction (non-agitation) using the BB payload prototype was carried-out to established if the earlier tube-based acid reagent extractions performed in chapter 6 could be replicated. Similarly, two additional hydrometallurgy leaching experiment using the 15mls plastic centrifuge in both agitation and non-agitation states was also simulated. The whole idea is to compare the outcome of the two additional simulated leaching experiments with those performed using the designed and manufactured BB payload prototype to further establish the significance or otherwise of the agitation mechanism.

The significance of agitation in the leaching experiment has been established from chapter 6, at this stage of the demonstration we could not use the agitation components on the BB payload prototype because the agitation mechanism was not included in the initial BB payload prototype design. A mechanism to implement agitation in the future BB payload prototype and the flight model that would be compatible with operation on an asteroid surface in microgravity would be develop.

In chapter 6 laboratory leaching experiment, sulphuric acid was used to demonstrate the leaching process. The sulphuric acid is substituted with water and the olivine regolith simulant with BPB dyed olivine regolith simulant to

simulate the demonstration of the leaching process in the current experiments. The substitution was informed due to local health and safety reasons (issue with access to “chemical” laboratories versus “engineering laboratories / workshops”). The extension period allowed to finish the PhD research work was coming to an end and at the time the chemical laboratories were closed due to Covid-19 related issues. Using chemical such as sulphuric acid is not allow in the engineering laboratories/workshop and therefore, a proxy had to be developed for simulating the removal of materials from the solid phase (of olivine) into the liquid phase. A Bromophenol Blue (BPB) dye was dried onto the olivine regolith simulant and then the BB payload prototype was used to demonstrate the “extraction” of the dye from the regolith using water as the substitute for the acid.

This latter study was required to demonstrate the simulated leaching protocol of extracting dried BPB dyed on the surface of olivine particles using water (as a proxy for hydrometallurgy sulphuric acid leaching of metal ions from the olivine regolith materials). Parameters such as solid-to-liquid ratio of 1:5 with the corresponding solid mass equivalent to 1.3g/1ml and liquid volume equivalent of 5mls were replicated all through the experiments. The solid-to-liquid ratio as was identified in the tube-based acid extraction to be critical in designing the leaching process, they provide a balance between the amounts of solid material versus the reagent used to achieve an effective leaching reaction/process.

In addition to all the equipment used in the initial and repeat hydrometallurgy leaching experiment in chapter 6, more other equipment used in the present simulated leaching experiment includes the BB payload prototype designed, manufactured, and tested in chapter 7 and the UV- Vis spectrophotometer. The UV-Visible spectrophotometer is used to compute/measure the maximum absorbance for each of the extracted BPB solution and together with the molar absorption coefficient the concentration of the BPB solution was determined using the Beer’s Lambert law. Finally, the average amount of BPB extracted for each experiment in moles is compared with the initial amount of BPB used in the extraction (dried onto regolith) in moles to arrive at the average extraction efficiency for each of the three experiments. The most significant parameter that

influences the average extraction efficiency for each of the three different simulated leaching experiments set would be determined.

8.2 AIMS OF THE EXPERIMENT

This experiment aims to simulate the demonstration of hydrometallurgy sulphuric leaching of BPB dyed olivine mineral and an aspect of liquid handling process using the design and manufactured BB prototype payload system in non-agitated state and including two additional extraction experiment using the 15mls plastic centrifuge in both agitation and non-agitation states to extract BPB solution dissolved from BPB dyed olivine mineral prepared using 3 different concentrations of the BPB dye. The UV-Visible spectrophotometer is used to compute the maximum absorbance for each of the extracted BPB solution and together with the molar absorption coefficient the concentration of the BPB solution was determined using the Beer's Lambert law.

The extraction efficiency for each of the extracted BPB solution was estimated by comparing the concentration of the extracted BPB solution with the initial concentration of the BPB solution used to determine the most significant parameter that influences extraction efficiency for each of the three different simulated leaching experiments set would be determined.

8.3 OBJECTIVES OF THE EXPERIMENT

- Using the BB payload prototype to simulate the hydrometallurgy sulphuric acid leaching of the olivine mineral in a non-agitated state
- Using the BB payload prototype to simulate the demonstration of an aspect of liquid handling process through the supply and extraction of liquid into and out of the RCS
- Using the 15mls plastic centrifuge tubes to simulate the hydrometallurgy sulphuric acid leaching of the olivine mineral in both agitation and non-agitation states and to compare their result with those performed using the BB payload prototype

- Using the UV-Visible spectrophotometer configured at 590nm wavelength and within the alkaline range to determine the maximum absorbance of BPB solution extracted from the RCS
- Using the Beer's Lambert law equation to determine the concentration of BPB dye present in the extracted solution
- Estimate the extraction efficiency of the BPB dye by comparing the extracted BPB solution with the initial concentration of the BPB solution used

8.4 MATERIAL, RE-AGENT AND EQUIPMENT USED

8.4.1 OLIVINE MINERAL

In subsection_6.4.1 the olivine mineral procured from Scan Grit a UK based mineral company located at Eastfield Road, Immingham was discussed extensively. In this Chapter, extra fine grade olivine mineral samples in the grain size range 0.090 – 0.250mm used in both the initial and repeat leaching experiments in chapter 6 as a regolith simulant relevant to C-type NEA asteroid Ryugu was replicated. BPB DYE SOLUTION

In subsection 6.7.2 the selection and preparation process of BPB solution of 3 different concentrations was discussed. The BPB dye was readily available and was used as an acid pH depletion indicator in the hydrometallurgy sulphuric acid leaching of the olivine mineral in Chapter_6. 2.2mM, 4.4mM and 8.8mM initial concentration of the BPB solution was used to prepare the diluted BPB solution dried onto the olivine mineral regolith.

8.4.2 DISTILLED WATER

The distilled water used as the reagent in place of the sulphuric acid to dissolve the BPB dried on to the olivine regolith mineral during the BB payload prototype simulation of the extraction experiment and those using the 15mls plastic centrifuge tubes was obtained through a purification process by recovering the steam of a boiling water through condensation.

8.4.3 EQUIPMENT USED

The BB prototype designed and built in Chapter_7 will be used to simulate the demonstration of the leaching process and an aspect of liquid handling process in a non-agitated state. Disposable 15ml polypropylene centrifuge tubes (Fisher brand cat.no.-05-539-5) was used as the reaction containers for the samples that will be subjected to non-agitation and agitation state, Vertical rotatory mixer (Stuart rotator model SB3, with speed range 2-40rpm) was used to agitate the reaction mixture inside the centrifuge tubes and the laboratory analytical balance digital precision scale with a precision at 0.0001g was used to measure the mass of reaction tube and mass of reaction tube together with the samples. The UV-Visible spectrophotometer DU-730 manufactured by Beckman Coulter Incorporated configured at a reading wavelength of 590nm that correspond to the wavelength of maximum absorbance of 0.981AU for a BPB solution in the alkaline form and that has a molar extinctions coefficient of 75000 $M^{-1}cm^{-1}$ (Merck, n.d.)

8.5 EXPERIMENT DESIGN METHODOLOGY TO SIMULATE THE DEMOSTRATION OF THE EXTRACTION OF THE BPB SOLUTION FROM THE BPB DYED OLIVINE MINERAL DISSOLVED IN WATER

This experiment is designed to simulate the demonstration of the extraction of the BPB solution from the BPB dyed olivine regolith mineral dissolved in water. The experiment is carried out in a non-agitated state using the BB payload prototype designed and manufactured in Chapter_7 and including two additional extraction experiment using the 15mls plastic centrifuge in both agitation and non-agitation states to extract BPB solution dissolved from BPB dyed olivine mineral prepared using 3 different concentrations of the BPB dye $(8.94 * 10^{-6},\ 4.47 * 10^{-6}, 2.23 * 10^{-6})\ moles$. The solid to liquid volume ratio of 1:5 implemented in the leaching experiment of Chapter_6 is carried forward and implemented in the extraction experiment. 1ml of the BPB dyed olivine regolith corresponding to 1.3g together with 5ml of water was used for the extraction experiment. Presented in Table 8-1 are the summary of the design parameters used for each of the extraction experiment.

Table 8-1: Parameters for the experiment

Parameter	Conditions
Reagent volume (water)	5ml (Constant volume)
Volume of the BPB dyed olivine regolith	1ml
Mass of corresponding BPB dyed olivine regolith	1.3g
Different extraction duration	60, 30 and 15 minutes
amount of BPB dye in mole used per 1.3g of the olivine regolith (moles)	$(8.94 * 10^{-6}, 4.47 * 10^{-6}, 2.23 * 10^{-6})\ moles$

Three sets of experiments were prepared and based on two variables (the amount of the BPB solution dried onto the olivine regolith in moles and the duration of the extraction process) as presented in Table 8-1. Each of the three-experiment set would be replicated three times and each replica is performed in nine batches, in a combination of three batches each based on specific amount of BPB solution $(8.94 * 10^{-6}, 4.47 * 10^{-6}, 2.23 * 10^{-6})$ per moles and each are allocated extraction time of 60, 30 and 15minutes respectively. In total twenty-seven batches per extraction experiment and eighty-one batches for the three-extraction experiment was carried out. The three set of experiment that will be carried out comprises:

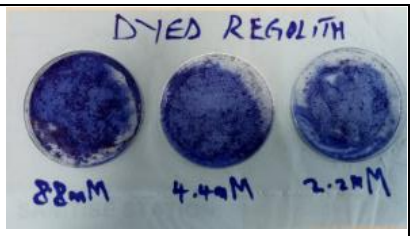
- Extraction experiment of the BPB solution using the Breadboard prototype with no agitation
- Extraction experiment of the BPB solution using 15ml plastic centrifuge tube with no agitation
- Extraction experiment of the BPB solution using 15ml plastic centrifuge tube with agitation using the vertical rotary mixer.

8.5.1 PREPARATORY STEPS FOR CREATING THE BPB DYED OLIVINE REGOLITH

Three different concentrations of the BPB solution prepared in subsection 6.7.6 corresponding to (8.8, 4.4 and 2.2mM) were the initial concentration of the BPB solution used to prepare the diluted version of the BPB solution dried onto the olivine regolith simulant. 5ml each of the different concentration of the initial BPB solution is the volume used to $create\ the\ \ amount\ of\ the\ BPB\ solution\ corresponding\ to$ $(4.4 * 10^{-5}, 2.2 * 10^{-5}, 1.1 * 10^{-5})$ in moles used to dye the olivine regolith simulant in a solid-to-liquid volume ratio of 5:5ml. 5mls of the olivine regolith simulant corresponding to 6.4g each were dispensed into three labelled centrifuge tubes and to each of the tubes $5ml$ of initial BPB solution in different concentration was added. The mixture in each tube was shaken thoroughly to ensure proper dying of the olivine regolith. The resulting mixture inside the tubes were emptied into three labelled petri dish and allowed to dry under room temperature. Shown in Figure 8-1 are the wet and the dry version of the BPB dyed olivine regolith



Wet version of the BPB dyed olivine regolith



Dry version of the BPB dyed olivine regolith

Figure 8-1: To the left is the wet version of the BPB dyed olivine regolith and to the right is the dry version of the BPB dyed olivine regolith

The dried BPB dyed olivine regolith simulant are stored in three labelled containers and ready for the demonstration of the extraction process. The amount of BPB dyed olivine regolith used in each of the extraction experiment is 1.3g and the amount of the BPB solution dried onto each 1.3g of the regolith correspond to $(8.94 * 10^{-6}, 4.47 * 10^{-6}, 2.23 * 10^{-6} moles)$ $and\ will\ be\ used\ for\ the\ extraction.$

8.6 EXTRACTION EXPERIMENT PROCESS OF THE BPB SOLUTION USING THE BB PAYLOAD PROTOTYPE WITH NO AGITATION

The BB payload prototype designed and built in Chapter_7 is used in this experiment to simulate the demonstration of the sulphuric acid leaching process and an aspect of liquid handling that entails the supply and extraction of liquid into and out of RCS. The experiment is performed in triplets to ensure repeatability. Solid-to-liquid volume ratio of 1:5ml (1.3g/5ml) as suggested in the leaching experiment demonstrated in Chapter_6 was implemented. Each of the extraction experiment using the BB prototype is performed in three replica (1-1, 1-2 and 1-3), each replica has nine batches, and each three batches are based on specific amount BPB solution dried on the olivine regolith mineral and at three different extraction time (60, 30 and 15minutes).

In batch1 extraction, 1.3g of olivine regolith simulant dried with initial amount of the BPB solution used in extraction (dried onto regolith) corresponding to $8.94 * 10^{-6}\ moles$ was dispensed inside the BB payload prototype RCS and the plunger replaced to seal the RCS airtight and having other components of BB payload prototype re-assembled. For the BB prototype payload description refer to subsection_7.9.1.2. The bipolar stepper motor operation is initiated in the forward direction to depressurise the inside of the RCS. The plunger is linearly extended inside the RCS and the transistor drive circuit is simultaneously switched-on to control the opening of the waste valve through which trapped liquid/air inside the RCS is expelled. At the pre-determined plunger extension depth inside the RCS the stepper motor motion was stopped to initiate a reverse motion after a pre-determined delay period, and the waste valve control is isolated. Pumping of the liquid into the RCS is achieved by linearly retracting the plunger out of the RCS; the bipolar stepper motor is operated in reverse direction to linearly retract the plunger out of the RCS to a pre-determined height and the transistor drive circuit is simultaneously switched-on to control the opening of the reservoir valve, and due to gravity effect liquid (water) in-flow into the RCS from the reservoir. The time delay function provided for switching between the plunger extension and retraction into and out of the RCS, allow enough time for:

- The isolation of waste or the reservoir valve

- Opening of the reservoir or the waste valve and
- Replacement of the waste container

Once the stepper motor stopped at the pre-determine retraction height, the motor is switch-off and the reservoir control valve is isolated, the pumped-in liquid (water) mix and react with BPB dyed olivine regolith simulant in a non-agitation state for the next 60minutes to extract the BPB dye dried onto the regolith. At the expiration of the 60minutes, the stepper motor operation is initiated once again to extend the plunger into the RCS and simultaneously the waste valve control is switched-on to allow the out-flow of the extracted BPB solution that will be collected in the waste container (a 15mls centrifuge tube). The above procedure is repeated for the extraction experiment replica (1-2&1-3) and each allocated extraction duration of 30 and 15minutes respectively. The round of the experimental procedure described above is repeated twice for each of the batches to ensure repeatability. Subsequently, another 1.3g of olivine regolith simulant dried with initial amount of the BPB solution corresponding to ($4.47 * 10^{-6}$, $2.23 * 10^{-6}$) moles are dispensed into the RCS, the round of the experimental procedure described above is performed and is repeated twice for each set of experiment to ensure repeatability. Sample simulation of the BB payload prototype BPB solution extraction is presented in Figure 8-2.

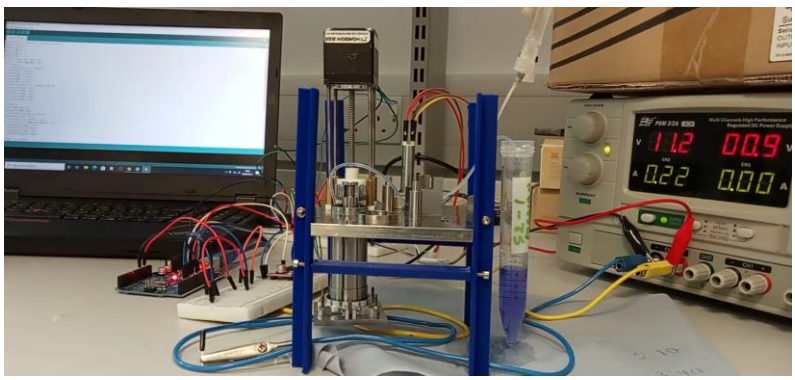


Figure 8-2: sample simulation of the BB payload system extraction experiment

At the expiration of each extraction experiment, the data for BPB solution collected in the waste container are recorded and will be used in determining:

- The maximum absorbance of each extract using the UV- Visible spectrophotometer configured at 590nm wavelength.
- Using the Beer's Lambert equation to compute the concentration of the BPB in the diluted extraction solution for each extract in molar (M)
- Compute the concentration of the BPB in the undiluted extraction solution for each extract using the dilution factor in molar (M)
- Determine the total amount of BPB solution extracted from the BPB dyed regolith for each extract in (moles)
- Calculate the extraction efficiency for each extract by comparing the total amount of the BPB solution extracted from the dyed olivine regolith in (moles) to the initial amount of the BPB dye dried onto the regolith in (moles)

8.6.1 MEASURING THE MAXIMUM ABSORBANCE FOR THE EXTRACTED BPB SOLUTION USING THE BB PAYLOAD PROTOTYPE

The BPB solution extracted during the experiment using the BB payload prototype were collected in the labelled 15ml plastic centrifuge tubes. The UV-Vis spectrophotometer was used to measure the maximum absorbance for each of the extracted BPB solution. Higher absorbance value was recorded for each BPB solution extracted; dilution factor was used to arrive at the corresponding maximum absorbance in the range of 0.981AU at 590nm wavelength. For the first extraction experiment (Replica1-1), the result for the BB prototype payload extraction experiment without agitation using different amount of the BPB solution in (Moles), at different extraction duration and including the dilution factor is present in Figure 8-3.

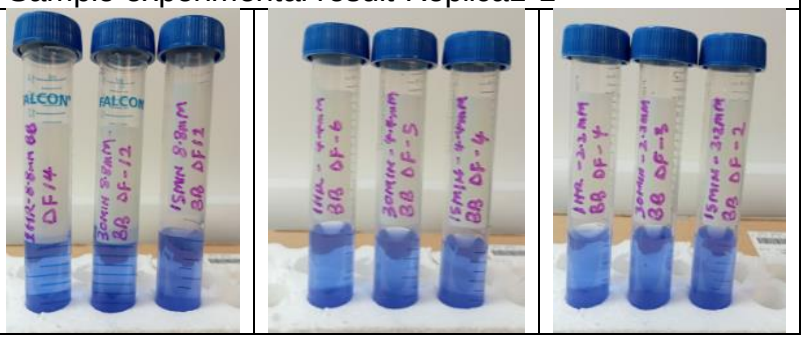
Samples	Sample experimental result Replica1-1
Result for the BB samples without agitations at different extraction duration and including the dilution factor	

Figure 8-3: Represent sample extraction experimental result for Replica1-1

8.6.2 COMPUTING THE CONCENTRATION OF THE BPB USING THE BEER'S LAMBERT EQUATION

Using the Beer's Lambert equation, the constant cuvette path length (1cm), constant molar extinction coefficient of ($75000 M^{-1}cm^{-1}$) and the computed maximum absorbance for each of the extracted BPB solution were used to compute:

- The concentration of BPB solution in diluted extracted solution
- The dilution factor for each of the sample was multiplied with the concentration of the BPB solution in diluted state to arrive at the concentration of the BPB blue solution in the undiluted extraction solution.
- The volume of the extracted BPB solution for each sample was multiplied with the concentration of the BPB in undiluted extraction solution to arrive at the total amount of the BPB solution extracted from the BPB dyed olivine regolith for each sample.
- Finally, the total amount of the BPB solution extracted from the BPB dyed olivine regolith for each sample was compared with the initial amount of BPB dried onto the olivine regolith to compute the extraction efficiency for each extracted sample.

The above procedure was repeated for the extraction experiment (Replica1-2 and Replica1-3). The extraction efficiency for the 3 replicas was averaged to determine the average extraction efficiency and finally, the extraction efficiency standard deviation was computed. A summary result for the extraction

experiments in three replicas is presented Table 8-2 and the overall result is presented in **Appendix 4.1**

Table 8-2: A summary result for the extraction experiments in three replicas using the BB payload prototype

Initial amount of BPB used in the extraction (dried onto regolith) (moles) *10^{-6}	Duration for the extraction (minutes)	Dilution factor of extraction solution to allow valid OD measurement	Total amount of BPB extracted from dyed olivine for replica1-1 (moles) * 10^{-7}	Extraction efficiency for replica1-1	Total amount of BPB extracted from dyed olivine for replica1-2 (moles) * 10^{-7}	Extraction efficiency for replica1-2	Total amount of BPB extracted from dyed olivine for replica1-3 (moles) * 10^{-7}	Extraction efficiency for replica1-3	Average extraction efficiency	Extraction efficiency std dev
8.94	60	14	8.48	9.5	8.37	9.4	8.30	9.3	9.4	0.10
8.94	30	12	7.26	8.1	7.18	8.0	6.76	7.6	7.9	0.30
8.94	15	12	7.23	8.1	7.00	7.8	6.75	7.6	7.8	0.27
4.47	60	6	3.61	8.1	3.43	7.7	3.41	7.6	7.8	0.26
4.47	30	5	2.99	6.7	2.80	6.3	2.80	6.3	6.4	0.25
4.47	15	4	2.38	5.3	2.27	5.1	2.23	5.0	5.1	0.18
2.23	60	4	2.39	10.7	2.37	10.6	2.29	10.2	10.5	0.25
2.23	30	3	1.76	7.9	1.75	7.8	1.66	7.4	7.7	0.24
2.23	15	2	1.34	6.0	1.16	5.2	1.10	4.9	5.3	0.55

Legend/description of components

- Column1 represent the initial amount of the BPB used in the extraction experiment (dried onto the regolith) in moles
- Column2 represent the corresponding duration for each extraction experiment in minutes
- Column3 represent the dilution factor used for each of the extracted solution to achieve the required concentration of the BPB in undiluted state
- Values in red colour in columns 4, 6 and 8 represent the total amount of BPB extracted from dyed olivine for the three replicas in (moles)
- Values in blue in columns 5, 7 and 9 represent the extraction efficiency for three replicas in extraction experiment1. The extraction efficiency for each member of the replica experiment is arrived at by taking the ratio of the total amount of BPB extracted from dyed olivine for each replica to the Initial amount of BPB used in the extraction (dried onto regolith)
- Values in orange colours in column 10 represent the average extraction efficiency for the three replicas in experiment1.

8.6.3 EXPERIMENT1 RESULT USING BB PAYLOAD PROTOTYPE FOR THE BPB SOLUTION EXTRACTION IN A STATIONARY/NON-AGITATED STATE

Presented in Table **8**-**2** is a summary result for the extraction experiments in three replicas using the BB payload prototype. The total amount of the BPB solution extracted for the three replicas, and the corresponding extraction duration taken from using the BB payload prototype in stationary state are presented in **Error! Reference source not found.** and Table **8**-**2**.

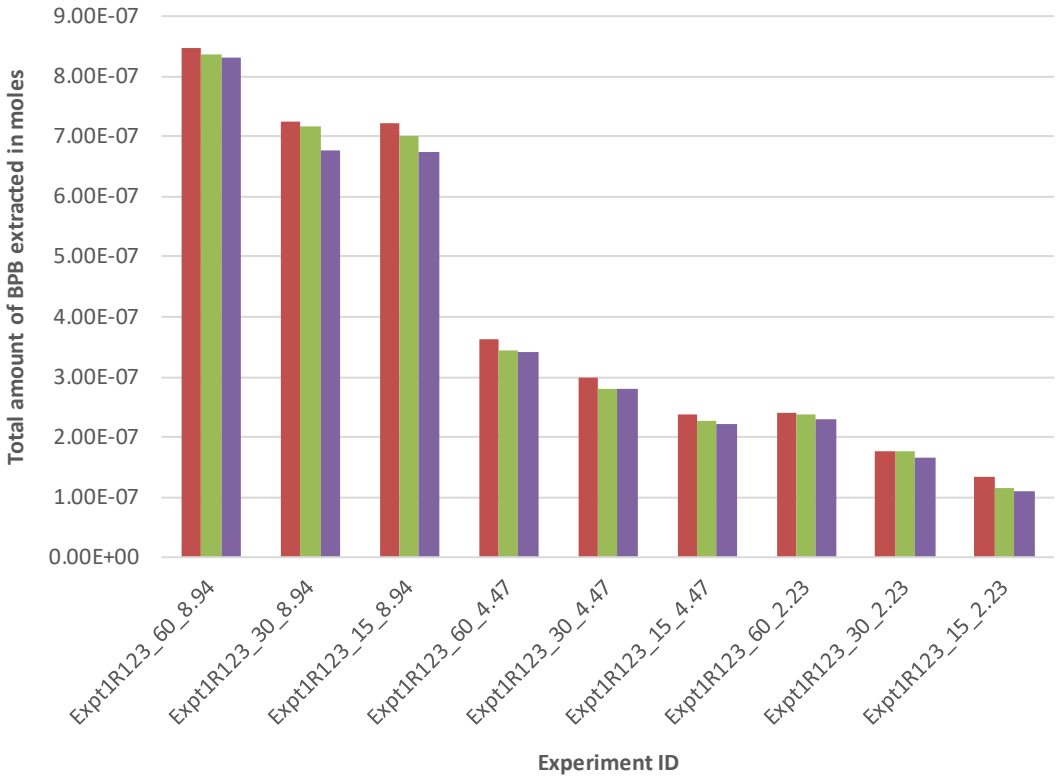


Figure 8-4: Experiment1 BPB extraction result based on using the BB payload prototype and including the replicas

Describing the codes presented along the X-axis, each of the code comprises of three variables. Let consider the first code on the left of the bar plot along the X-axis (Expt1R123_60_8.94), the description is illustrated in **Error! Reference source not found.**

Table 8-3: Interpreting the codes along the x-axis of the bar plot

Expt1R123 denote Experiment1 replica 1,2 and 3
60 denote the duration of the extraction experiment
8.94 denote the Initial amount of BPB dried onto the olivine regolith
Value on the Y axis represent the BPB extraction value in moles

NB: The code interpretation pattern as presented in **Error! Reference source not found.** applies to all other codes in the bar chart plot.

8.6.3.1 DESCRIPTION OF THE EXPERIMENT RESULT USING THE BB PAYLOAD PROTOTYPE IN STATTIONARY/NON-AGITATED STATE

$8.94 \times 10^{-6} moles$ amount of BPB solution was dried onto the olivine regolith, the experiment was carried out at three different extraction duration of 60, 30 and 15minutes and in three experiment replicas. The average amount of the BPB solution extracted for each leaching duration corresponds to $8.38 \times 10^{-7}, 7.06 \times 10^{-7}\ and\ \ 6.99 \times 10^{-7}\ in\ moles$ across the three replicas and the corresponding extraction efficiency of 9.4, 7.9 and 7.8 was obtained.

$4.47 \times 10^{-6} moles$ amount of BPB solution was dried onto the olivine regolith, and the experiment carried out at three different extraction duration of 60, 30 and 15minutes across three experiment replicas. The average amount of the BPB solution extracted for each leaching duration corresponds to $3.48 \times 10^{-7}, 2.86 \times 10^{-7}\ and\ \ 2.29 \times 10^{-7}\ in\ moles$ and across the three experiment replicas. The corresponding extraction efficiency of 7.8, 6.4 and 5.1 was obtained.

$2.23 \times 10^{-6} moles$ amount of BPB solution was dried onto the olivine regolith, and the experiment carried out at three different extraction duration of 60, 30 and 15minutes across three experiment replicas. The average amount of the BPB solution extracted for each leaching duration corresponds to $2.35 \times 10^{-7}, 1.72 \times 10^{-7}\ and\ \ 1.20 \times 10^{-7}\ in\ moles$ and across the three experiment replicas. The corresponding extraction efficiency of 10.5, 7.7 and 5.4 was obtained.

8.7 EXTRACTION EXPERIMENT PROCESS OF THE BPB SOLUTION USING 15ML PLASTIC CENTRIFUGE TUBE WITH NO AGITATION

The extraction experiments were set up in three replicas (2-1, 2-2 & 2-3) to ensure repeatability; each of the extraction experiment replica comprises of nine labelled 15mls centrifuge tube inside which the extraction was carried-out in a non-agitation state. The centrifuge tubes are arranged into three batches and each comprising of three tubes are held inside the tube rack.

Experiment extraction based on replica 2-1, batch1, 1.3g of the olivine regolith simulant dried with $8.94 * 10^{-6} moles\ of\ BPB\ dye$ are dispensed into the tubes, batch2, 1.3g of the olivine regolith simulant dried with $4.47 * 10^{-6} moles\ of\ BPB\ dye$ are dispensed into the tubes and batch3, 1.3g of the olivine regolith simulant dried with $2.23 * 10^{-6}$moles of BPB dye are dispensed into the tubes. 5ml of water was dispensed into each tube in the three batches and the mixture allowed to react for a specific time interval without agitation. The three tubes in each batch are allocated extraction time of 60, 30 and 15minutes respectively. At the expiration of each extraction time, the tubes in each batch having same extraction time are collected, the BPB solution from the mixture in each tube was then separated from the olivine regolith and kept in new labelled centrifuge tubes and will be used in determining the maximum absorbance of each extract using the UV- Visible spectrophotometer configured at 590nm wavelength.

8.7.1 MEASURING THE MAXIMUM ABSORBANCE FOR THE EXTRACTED BPB SOLUTION USING THE 15MLS PLASTIC CENTRIFUGE TUBE WITH NO AGITATIONBB PAYLOAD PROTOTYPE

The extraction experiment using 15ml plastic centrifuge tube with no agitation, the operating conditions are the same as those of extraction experiment using the BB payload prototype. Using the UV- Visible spectrophotometer configured at 590nm wavelength and factoring the dilution factor the maximum absorbance for each of the extracted BPB solution was calculated in the range of 0.981AU. Figure 8-5 represent the result for the extraction experiment of (Replica2-1) using 15ml plastic centrifuge tube with no agitation at different extraction duration and including the dilution factor.

Samples	Sample experimental result Replica2-1		
Result for the stationary samples without agitation at different extraction durations and including the dilution factor			

Figure 8-5: Represent sample extraction experimental result for Replica2-1

8.7.2 COMPUTING THE CONCENTRATION OF THE BPB USING THE BEER'S LAMBERT EQUATION

Using the Beer's Lambert equation, the constant cuvette path length (1cm), constant molar extinction coefficient (75000$M^{-1}cm^{-1}$) and the computed maximum absorbance for each of the extracted BPB solution were used to compute:

- The concentration of BPB solution in diluted extracted solution for each sample
- The concentration of the BPB blue solution in the undiluted extraction solution for each sample.
- The total amount of the BPB extracted from the BPB dyed olivine regolith for each sample
- The extraction efficiency for each extracted sample.

The experiment extraction procedure based on replica 2-1 described in this section are replicated for experiment replica 2 – 2 and replica 2 - 3 and the corresponding data recorded. The average extraction efficiency for the 3 replicas was determine and finally, the extraction efficiency standard deviation was computed. A summary result for the extraction experiments in three replicas is presented in Table 8-4 and the overall result is presented in **Appendix 4.2**

Table 8-4: A summary result for the extraction experiments using the 15ml centrifuge tubes in three replicas and non-agitated

Initial amount of BPB used in the extraction (dried onto regolith) (moles) *10^{-6}	Duration for the extraction (minutes)	Dilution factor of extraction solution to allow valid OD measurement	Total amount of BPB extracted from dyed olivine for replica1-1 (moles) * 10^{-7}	Extraction efficiency for replica2-1	Total amount of BPB extracted from dyed olivine for replica1-2 (moles) * 10^{-7}	Extraction efficiency for replica2-2	Total amount of BPB extracted from dyed olivine for replica1-3 (moles) * 10^{-7}	Extraction efficiency for replica2-3	Average extraction efficiency	Extraction efficiency std dev
8.94	60	14	8.48	9.5	8.37	9.4	8.42	9.4	9.4	0.06
8.94	30	12	7.18	8.0	7.16	8.0	7.17	8.0	8.0	0.01
8.94	15	12	7.07	7.9	7.01	7.8	7.12	8.0	7.9	0.06
4.47	60	6	4.16	9.3	4.13	9.2	4.17	9.3	9.3	0.06
4.47	30	5	2.93	6.6	2.90	6.5	2.92	6.5	6.5	0.04
4.47	15	4	2.27	5.1	2.30	5.1	2.28	5.1	5.1	0.03
2.23	60	4	2.90	13.0	2.90	13.0	2.92	13.1	13.0	0.05
2.23	30	3	2.27	10.2	2.25	10.1	2.26	10.1	10.1	0.03
2.23	15	2	1.68	7.5	1.67	7.5	1.68	7.5	7.5	0.02

Legend/description of components

- Column1 represent the initial amount of the BPB used in the extraction experiment (dried onto the regolith) in moles
- Column2 represent the corresponding duration for each extraction experiment in minutes
- Column3 represent the dilution factor used for each of the extracted solution to achieve the required concentration of the BPB in undiluted state
- Values in red colour in columns 4, 6 and 8 represent the total amount of BPB extracted from dyed olivine for the three replicas in (moles)
- Values in blue in columns 5, 7 and 9 represent the extraction efficiency for three replicas in extraction experiment1. The extraction efficiency for each member of the replica experiment is arrived at by taking the ratio of the total amount of BPB extracted from dyed olivine for each replica to the Initial amount of BPB used in the extraction (dried onto regolith)
- Values in orange colours in column 10 represent the average extraction efficiency for the three replicas in experiment1.

8.7.3 EXPERIMENT2 RESULT USING THE 15MLS CENTRIFUGE TUBES FOR THE BPB SOLUTION EXTRACTION IN A NON-AGITATED STATE

Presented in Table **8-4** is a summary result for the extraction experiments in three replicas using the 15mls centrifuge tubes. The total amount of the BPB solution extracted for the three replicas, and the corresponding extraction duration taken from using the 15mls centrifuge in non-agitated state are presented in **Error! Reference source not found.**.

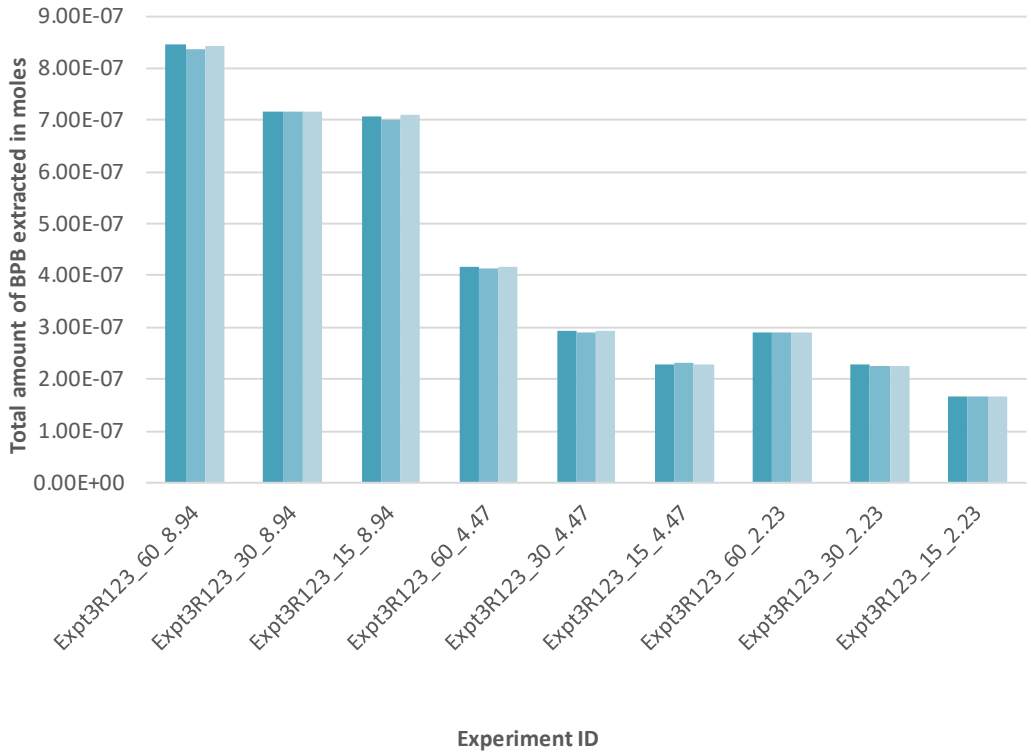


Figure 8-6: Experiement2 BPB extraction result using 15mls centrifuge tubes in non-agitated state

8.7.3.1 DESCRIPTION OF THE EXPERIMENT RESULT USING THE 15MLS CENTRIFUGE TUBE IN NON-AGITATED STATE

$8.94 \times 10^{-6} moles$ amount of BPB solution was dried onto the olivine regolith, the experiment carried out at three different extraction duration of 60, 30 and 15minutes and in three experiment replicas. The average amount of the BPB solution for each leaching duration extracted corresponds to $8.42 \times 10^{-7}, 7.17 \times 10^{-7}\ and\ 7.07 \times 10^{-7}\ in\ moles$ and across the three replicas and the corresponding extraction efficiency of 9.4, 8.0 and 7.9 was also obtained.

$4.47 \times 10^{-6} moles$ amount of BPB solution was dried onto the olivine regolith, the experiment carried out at three different extraction duration of 60, 30 and 15minutes and across three experiment replicas. The average amount of the BPB solution extracted for each leaching duration corresponds to $4.15 \times 10^{-7}, 2.92 \times$

10^{-7} and 2.29×10^{-7} $in\,moles$ and across the three experiment replicas and the corresponding extraction efficiency of 9.3, 6.5 and 5.1 was also obtained.

$2.23 \times 10^{-6} moles$ amount of BPB solution was dried onto the olivine regolith and the experiment carried out at three different extraction duration of 60, 30 and 15minutes and across three experiment replicas. The average amount of the BPB solution extracted for each leaching duration corresponds to 2.90×10^{-7}, 2.26×10^{-7} and 1.68×10^{-7} $in\,moles$ and across the three experiment replicas and the corresponding extraction efficiency of 13.1, 10.1 and 7.5 was also obtained.

8.8 EXTRACTION EXPERIMENT PROCESS OF THE BPB SOLUTION USING 15ML PLASTIC CENTRIFUGE WITH AGITATION USING THE VERTICAL ROTARY MIXER

This experiment was carried out in 15ml plastic centrifuge tubes, and the number of samples is like/similar to those in the 15mls plastic centrifuge tube in non-agitation state. The centrifuge tubes are arranged into three batches and each comprising of three tubes.

Experiment extraction based on replica 3-1, batch1, 1.3g of the olivine regolith simulant dried with $8.94 * 10^{-6} moles\ of\ BPB\ dye$ are dispensed into the tubes, batch2, 1.3g of the olivine regolith simulant dried with $4.47 * 10^{-6} moles\ of\ BPB\ dye$ are dispensed into the tubes and batch3, 1.3g of the olivine regolith simulant dried with $2.23 * 10^{-6}$moles of BPB dye are dispensed into the tubes. 5ml of water was dispensed into each tube in the three batches and the mixture allowed to react for a specific time interval without agitation. The three tubes in each batch are allocated extraction time of 60, 30 and 15minutes respectively and are subjected to agitation using the vertical rotary mixer set at 10rpm. The introduction of the slow mixing speed at 10rpm is to enable a room for comparison with the result of extraction experiment using the BB payload and those using the 15mls centrifuge tubes and at non-agitating state. The tubes are mounted on the vertical rotary mixer as shown in Figure 8-7 .



Figure 8-7: plastic centrifuge tubes agitated using the vertical rotary mixer

At the expiration of each extraction time, the tubes in each batch and with same extraction time are collected, the BPB solution from the mixture in each tube was then separated from the dyed olivine regolith and kept in new labelled centrifuge tubes and to be used in determining the maximum absorbance of each extract using the UV-Visible spectrophotometer configured at 590nm wavelength.

8.8.1 MEASURING THE MAXIMUM ABSORBANCE FOR THE EXTRACTED BPB SOLUTION USING THE 15MLS PLASTIC CENTRIFUGE TUBE WITH WITH AGITATION USING THE VERTCAL ROTARY MIXER

Using the UV- spectrophotometer configured at 590nm wavelength and factoring the dilution factor the maximum absorbance for each of the extracted BPB solution was calculated in the range of 0.981AU. For the first extraction experiment (Replica3-1), the result for the BB extraction experiment (Replica3-1) without agitation at different extraction duration and including the dilution factor is presented in Figure 8-8.

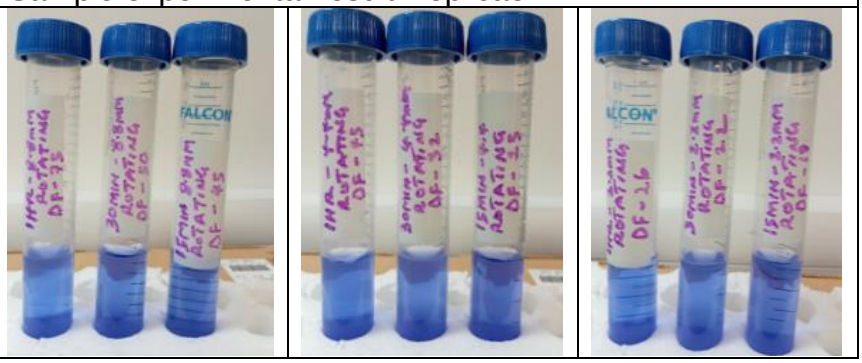
Samples	Sample experimental result Replica3-1
Result for the rotating samples with agitation at different extraction durations and including the dilution factor	

Figure 8-8: Represent sample extraction experimental result for Replica1-1

8.8.2 COMPUTING THE CONCENTRATION OF THE BPB USING THE BEER'S LAMBERT EQUATION

Using the Beer's Lambert equation, the constant cuvette path length (1cm), constant molar extinction coefficient (75000) and the computed maximum absorbance for each of the extracted BPB solution were used to compute:

- The concentration of BPB solution in diluted extracted solution for each sample
- The concentration of the BPB blue solution in the undiluted extraction solution for each sample.
- The total amount of the BPB extracted from the BPB dyed olivine regolith for each sample
- The extraction efficiency for each extracted sample.

The experiment extraction procedure based on replica 3-1 described in this section are replicated for experiment replica 3 – 2 and replica 3 - 3 and the corresponding data recorded. A summary result for the extraction experiments in three replicas is presented in Table 8-5 and the overall result is presented in **Appendix 4.3**

Table 8-5: A summary result for the extraction experiments using the 15ml centrifuge tubes in three replicas and agitated

Initial amount of BPB used in the extraction (dried onto regolith) (moles) *10^{-6}	Duration for the extraction (minutes)	Dilution factor of extraction solution to allow valid OD measurement	Total amount of BPB extracted from dyed olivine for replica1-1 (moles) * 10^{-6}	Extraction efficiency for replica2-1	Total amount of BPB extracted from dyed olivine for replica1-2 (moles) * 10^{-6}	Extraction efficiency for replica2-2	Total amount of BPB extracted from dyed olivine for replica1-3 (moles) * 10^{-6}	Extraction efficiency for replica2-3	Average extraction efficiency	Extraction efficiency std dev
8.94	60	75	4.60	51.5	4.52	50.6	4.56	51.1	51.1	0.5
8.94	30	50	3.06	34.2	2.93	32.8	3.00	33.5	33.5	0.7
8.94	15	45	2.77	31.0	2.57	28.8	2.65	29.7	29.8	1.1
4.47	60	45	2.71	60.7	2.62	58.7	2.67	59.7	59.7	1.0
4.47	30	32	1.86	41.6	1.87	41.9	1.88	42.1	41.9	0.2
4.47	15	25	1.54	34.5	1.43	32.1	1.49	33.3	33.3	1.2
2.23	60	26	1.56	70.0	1.58	70.5	1.57	70.3	70.3	0.3
2.23	30	22	1.36	60.8	1.32	58.9	1.34	59.9	59.9	0.9
2.23	15	19	1.13	50.6	1.14	51.2	1.14	51.0	50.9	0.3

Legend/description of components

- Column1 represent the initial amount of the BPB used in the extraction experiment (dried onto the regolith) in moles
- Column2 represent the corresponding duration for each extraction experiment in minutes
- Column3 represent the dilution factor used for each of the extracted solution to achieve the required concentration of the BPB in undiluted state
- Values in red colour in columns 4, 6 and 8 represent the total amount of BPB extracted from dyed olivine for the three replicas in (moles)
- Values in blue in columns 5, 7 and 9 represent the extraction efficiency for three replicas in extraction experiment1. The extraction efficiency for each member of the replica experiment is arrived at by taking the ratio of the total amount of BPB extracted from dyed olivine for each replica to the Initial amount of BPB used in the extraction (dried onto regolith)
- Values in orange colours in column 10 represent the average extraction efficiency for the three replicas in experiment1.

8.8.3 EXPERIMENT3 RESULT USING THE 15MLS CENTRIFUGE TUBES FOR THE BPB SOLUTION EXTRACTION IN AN AGITATED STATE USING THE VERTCAL ROTARY MIXER

Presented in Table 8-5 is a summary result for the extraction experiments in three replicas using the 15mls centrifuge tubes. The total amount of the BPB solution extracted for the three replicas, and the corresponding extraction duration taken from using the 15mls centrifuge in agitated state are presented in Figure **8-9**

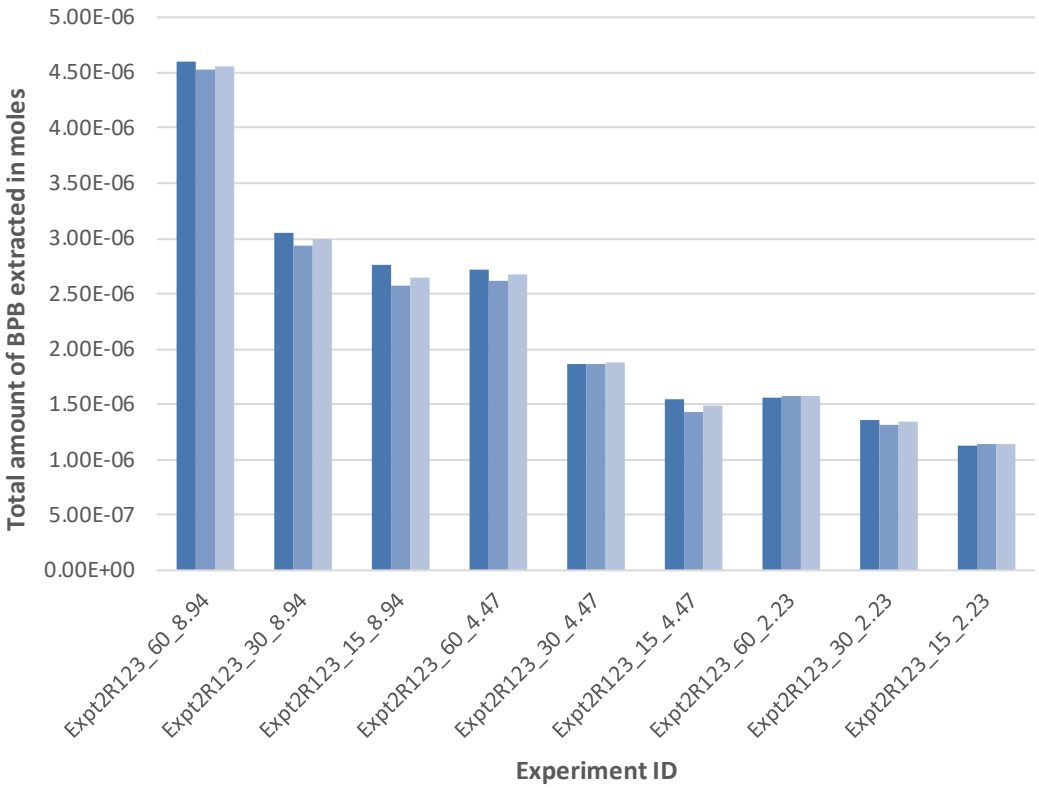


Figure 8-9: Experiement3 BPB extraction result using 15mls centrifuge tubes in agitated state

8.8.3.1 DESCRIPTION OF THE EXPERIMENT RESULT USING THE 15MLS CENTRIFUGE TUBE IN AGITATED STATE USING THE VERTCAL ROTARY MIXER

$8.94 \times 10^{-6} moles$ amount of BPB solution was dried onto the olivine regolith, and the experiment carried out at three different extraction duration of 60, 30 and 15minutes and in three experiment replicas. The average amount of the BPB solution extracted for each leaching duration corresponds to $4.56 \times 10^{-6}, 3.0 \times 10^{-6}\ and\ 2.66 \times 10^{-6}\ in\ moles$ and across the three replicas and the corresponding extraction efficiency of 51.1, 33.5 and 29.8 was also obtained.

$4.47 \times 10^{-6} moles$ amount of BPB solution was dried onto the olivine regolith, and the experiment carried out at three different extraction duration of 60, 30 and 15minutes and across three experiment replicas. The average amount of the BPB solution extracted for each leaching duration corresponds to $2.67 \times 10^{-6}, 1.87 \times 10^{-6}\ and\ 1.49 \times 10^{-6}\ in\ moles$ and across the three experiment replicas and the corresponding extraction efficiency of 59.7, 41.9 and 33.3 was also obtained.

$2.23 \times 10^{-6} moles$ amount of BPB solution was dried onto the olivine regolith and the experiment carried out at three different extraction duration of 60, 30 and 15minutes and across three experiment replicas. The average amount of the BPB solution extracted for each leaching duration corresponds to $1.57 \times 10^{-6}, 1.34 \times 10^{-6}\ and\ 1.14 \times 10^{-6}\ in\ moles$ and across the three experiment replicas and the corresponding extraction efficiency of 70.3, 59.9 and 50.9 was also obtained.

8.9 COMPARISON OF THE EXPERIMENTS RESULT

In this section the result of the various experiment carried out are compared, the extraction efficiency for each of the three experiments are established to determine the value of final product output achieved in an extraction process across the three experiments. The result would further inform the choice of an extraction leaching process to be carried forward for implementation in the ISRU payload flight model.

8.9.1 COMPARING THE RESULT OF EXPERIMENT1 USING THE BB PAYLOAD PROTOTYPE IN NON-AGITATED STATE TO THOSE OF EXPERIMENT2 USING 15MLS CENTRIFUGE TUBE IN NON-AGITATED STATE

The information in column 1&2, 4&5 in Table **8-6** represent the average BPB solution extraction and the average BPB solution extraction efficiency for Experiement1 using the BB payload prototype and Experiment2 using the 15mls centrifuge tubes both in a non-agitated state. The results for the two experiments (Experiment1 & Experiment2) are compared, they appear to be similar with an insignificant difference. The differences in column 7&10 of Table **8-6** represent the insignificant differences between:

- The result of the BPB solution extraction for Experiment1 and those of Experiment2
- The result of the BPB solution extraction efficiency for Experiment1 and those of Experiment2

8.9.2 COMPARING THE RESULT OF EXPERIMENT1 USING THE BB PAYLOAD PROTOTYPE IN NON-AGITATED STATE TO THOSE OF EXPERIMENT2 USING 15MLS CENTRIFUGE TUBE IN NON-AGITATED STATE

The information in column 1&3, 4&6 in Table **8**-**6** represent the average BPB solution extraction and the average BPB solution extraction efficiency for Experiement1 using the BB payload prototype in a non-agitated state and Experiment3 using the 15mls centrifuge tubes in agitated state. The results for the two experiments (Experiment1 & Experiment3) are compared, they appear to be de-similar with a very significant difference. The differences in column 8&11 of Table **8**-**6** represent the significant differences between:

- The result of the BPB solution extraction for Experiment1 and those of Experiment3
- The result of the BPB solution extraction efficiency for Experiment1 and those of Experimewnt3

8.9.3 COMPARING THE RESULT OF EXPERIMENT2 USING THE 15MLS CENTRIFUGE TUBE IN NON-AGITATED STATE TO THOSE OF EXPERIMENT3 USING 15MLS CENTRIFUGE TUBE IN AGITATED STATE

The information in column 2&3, 5&6 in Table **8**-**6** represent the average BPB solution extraction and the average BPB solution extraction efficiency for Experiement2 using the 15mls centrifuge tube in non-agitated state and Experiment3 using the 15mls centrifuge tubes in agitated state. The results for the two experiments (Experiment2 & Experiment3) are compared, they appear to be de-similar with a very significant difference. The differences in column 9&12 of Table **8**-**6** represent the significant differences between:

- The result of the BPB solution extraction for Experiment2 and those of Experiment3
- The result of the BPB solution extraction efficiency for Experiment2
- and those of Experimewnt3

Presented in Figure 8-10 is a plot representing the distribution of the average BPB solution extraction result for Experiment 1 – 3.

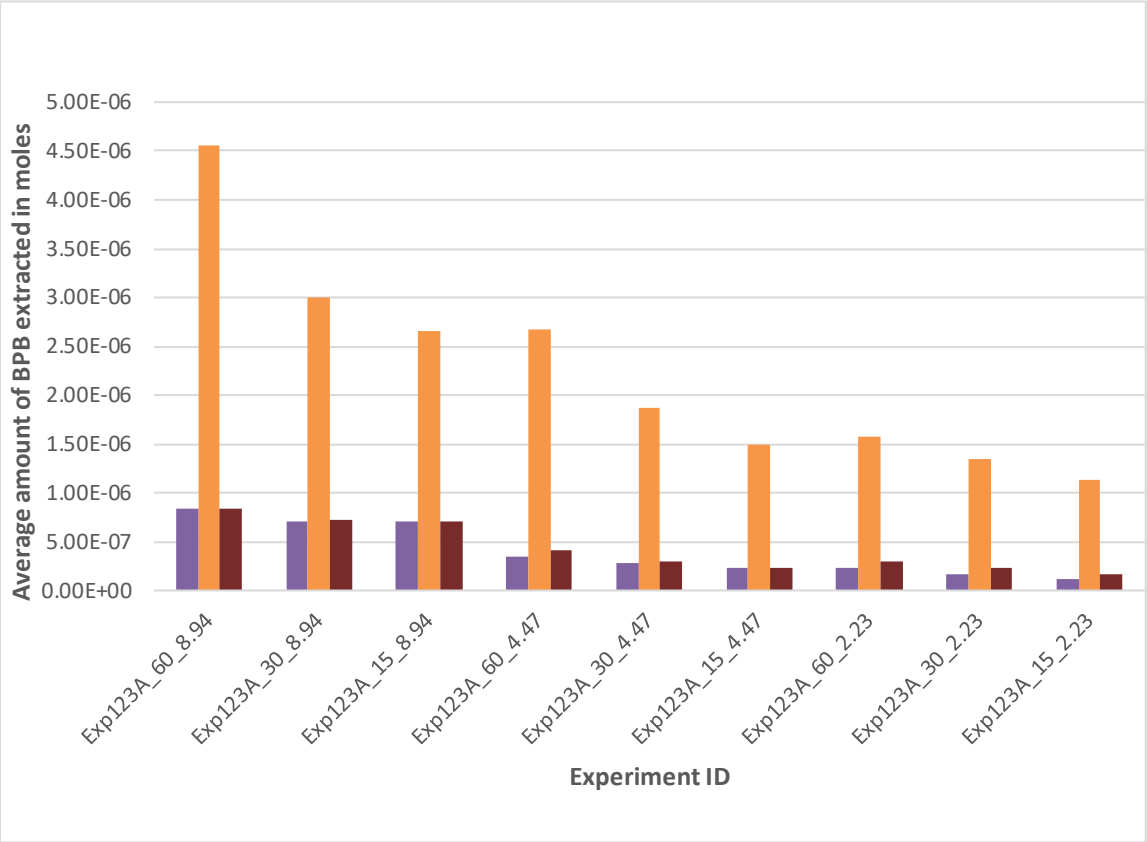


Figure 8-10: Experiment1-3 average BPB extraction result

Table 8-6 present the distribution for the average amount of BPB solution extracted, the average extraction efficiency and the corresponding difference of the BPB solution extracted and the average extraction efficiency across the experiment1-3

Table 8-6: Showing the average amount of BPB solution extracted, the average extraction efficiency and the corresponding difference of the BPB solution extracted and the average extraction efficiency across the experiment1-3

Average BPB solution extraction across Expt1-3			**Average BPB solution extraction efficiency across Expt1-3**			**Differences in the BPB solution extraction across Experiment1-3**			**Differences in the BPB solution extraction efficiency across Expt1-3**		
BBEA (10^{-7}) moles	CTEA_NA (10^{-7}) moles	CTEA_A (10^{-6}) moles	BBEA_EE (%)	CTEA_NA_EE (%)	CTEA_A_EE (%)	BBEA - CTEA_NA 01^{-7} mole	CTEA_A – BBEA 01^{-6} mole	CTEA_A - CTEA_NA 01^{-6} mole	BBEA_EE - CTEA_NA_EE (%)	CTEA_A_EE - BBEA_EE (%)	CTEA_A_EE - CTEA_NA_EE (%)
8.38	8.42	4.56	9.40	9.40	51.10	0.04	3.72	3.72	0.10	41.70	41.70
7.06	7.17	3.00	7.90	8.00	33.50	0.11	2.30	2.28	0.10	25.60	25.50
6.99	7.07	2.06	7.80	7.90	29.80	0.08	1.36	1.35	0.10	22.00	21.90
3.48	4.15	2.67	7.80	9.30	59.70	0.67	2.32	2.26	0.15	51.90	50.40
2.86	2.92	1.87	6.40	6.50	41.90	0.06	1.58	1.58	0.10	35.50	35.40
2.29	2.29	1.49	5.10	5.10	33.30	0.00	1.25	1.26	0.00	28.20	28.20
2.35	2.90	1.57	10.50	13.00	70.30	0.55	1.34	1.28	2.50	59.80	57.30
1.72	2.26	1.34	7.70	10.10	59.90	0.54	1.17	1.11	2.40	52.40	49.80
1.2	1.68	1.14	5.40	7.50	50.90	0.48	1.02	1.00	2.10	45.50	43.40

Legend

BBEA	Breadboard extraction average
CTEA_NA	Centrifuge tube extraction average _ non-agitated
CTEA_A	Centrifuge tube extraction average _ agitated
BBEA_EE	Breadboard extraction average _ extraction efficiency
CTEA_NA_EE	Centrifuge tube extraction average _ non-agitated _ extraction efficiency
CTEA_A_EE	Centrifuge tube extraction average _ agitated _ extraction efficiency

As presented in Table **8**-**6** , the average amount of BPB solution extracted, the average extraction efficiency, the corresponding difference of the BPB solution extracted, and the average extraction efficiency across the experiment1-3 were compared.

The average result of the replicas of experiment1 and experiment2 using the BB payload and the 15mls centrifuge tubes in a non-agitated state and across the samples appears to be consistent with one another. The average result of the replicas of experiment3 in an agitated state across the samples is significantly higher than those of experiment1 and experiment2 using the BB payload and the one using the centrifuge tubes both in non-agitated.

8.10 DISCUSSION OF THE BPB SOLUTION EXTRACTION EXPERIMENTS RESULT BASED ON THE THREE (3) DIFFERENT EXPERIMENT CARRIED OUT

Table **8**-**6** and Figure **8**-**10** present both the data based and pictorial bar chart result of the amount of the BPB solution extracted in moles and the corresponding BPB solution extraction efficiency in percentage for the three different experiments carried out. In Figure **8**-**10**, three different colours (purple, orange

and brown) presented in bar chat represent the average result of the amount of the BPB solution extracted in moles as follows:

- The purple colour bar chart represents the distribution of the amount of the BPB solution extracted in moles for Experiment1 using the BB payload prototype in non-agitated state
- The brown colour bar chart represents the distribution of the amount of the BPB solution extracted in moles for Experiment2 using the 15mls centrifuge tube in non-agitated state
- The orange colour bar chart represents the distribution of the amount of the BPB solution extracted in moles for Experiment3 using the 15mls centrifuge tube in an agitated state

From the bar chat distribution shown in Figure **8**-**10** the purple and brown colour represent the result of the BPB solution extraction for experiment1 and experiment2 both in non-agitated state. It is obvious from the bar chart plot result, the two result (purple and brown) they appear to be similar with a very insignificant differences of $4.0 * 10^{-9}\ to\ 6.7 * 10^{-8}\ moles$ minimum/maximum value across column 7 on Table **8**-**6**. The orange colour represents the result of the BPB solution extraction for experiment3 in agitated state. Comparing the orange colour to the purple and the brown colours in the bar chart plot they appear to be greatly dissimilar with a very significant difference of $1.0 * 10^{-6}\ to\ 3.72 * 10^{-6}\ moles$ minimum/maximum value across both column 8&9 on Table **8**-**6**. The experiment variables, the amount of the BPB solution dried on to the olivine regolith in moles, the duration of the extraction process, and the state of agitation, these variables are observed to impact in the BPB solution extraction across all the three sets of experiment carried out as follows:

The trend of the result across all the three experiment appears to be consistent. Presented in Table 8-6, columns 1, 2 & 3 represent the average amount BPB solution extracted in moles, and columns 4, 5 & 6 represent the average extraction efficiency in percentage. Across the columns top to bottom, the higher the Initial amount of BPB used in the extraction (dried onto regolith) in moles and the longer the duration of the extraction, the amount of the BPB solution

extracted, and the extraction efficiency increases. The trend continues to decline as the Initial amount of BPB used in the extraction (dried onto regolith) in mole and the duration of the extraction declined

The impact of the amount of the BPB solution extracted, and the extraction efficiency appears to be more significant among the samples in experiment3 using the 15mls centrifuge tubes in agitated state. Column 3&6 in Table **8-6** represent the BPB solution extraction and the extraction efficiency result for experiment3. The BPB solution extraction result is $3.72 * 10^{-6}\ moles$ maximum and $1.0 * 10^{-6}$ mole minimum across column 3 top to bottom are much greater than those across column 1&2 of experiment 1&2 on Table **8-6**. The extraction efficiency result present across column 6 for experiment3 top to bottom is x5 greater than those present across column 4&5 of experiment1&2. All the three experiment share common parameters (concentration of the BPB solution used and the solid-to-liquid ratio). Unlike experiment 1&2 both operating in a non-agitated state, experiment3 stand out to includes the agitation mechanism. The higher BPB solution extraction and extraction efficiency values recorded for experiment3 can be attributed to the influence of the agitation mechanism.

8.11 CONCLUSION

The BPB solution extraction experiment (as a replacement for the extraction using sulphuric acid given the inability to use the acid due to local health and safety issues) was performed in three different approaches (1) using the designed and manufactured BB payload prototype in a non-agitated state, (2) using the 15mls centrifuge tubes in non-agitated and (3) using the 15mls centrifuge tubes in an agitated state. Each of the experiments was replicated three times. The resulting patterns of experiment1 and experiment2 appear to be similar and consistent. The result of the BPB solution extraction and the extraction efficiency of experiment3 is significantly higher compared to those of experiment1 and experiment2 and across the experimental samples. The common variables shared by the three different experiment includes the Initial amount of BPB used in the extraction (dried onto regolith) in moles, the duration for extraction process and the solid-to-liquid ratio (1ml of solid-to-5ml of liquid). In experiment3, it can be concluded that the higher BPB solution extraction and the higher extraction

efficiency recorded are attributed to the state of agitation. The summary of the significant differences in the BPB solution extraction and the extraction efficiency result between experiment3 & experiment1 and between experiment3 & experiment2 are presented in Table **8-7**

Table 8-7: Showing the significant differences in the extraction result and the corresponding equivalent in percentage

Extraction result differences between experiment3 and experiment1 (moles) *10^{-6}	**Extraction result differences between experiment3 and experiment2 (moles) *10^{-6}**
4.56 (81.62%)	3.72 (81.54%)
2.30 (76.50%)	2.28 (76.10%)
1.36 (66.10%)	1.35 (65.68%)
2.32 (87.00%)	2.26 (84.46%)
1.58 (84.71%)	1.58 (84.40%)
1.26 (84.63%)	1.26 (84.63%)
1.31 (83.00%)	1.28 (81.53%)
1.17 (87.00%)	1.11 (83.11%)
1.02 (89.00%)	1.00 (85.26%)

It is clear in the sulphuric acid leaching simulation result under this chapter that the BPB dye extraction process is much more efficient using the agitation mechanism. The immediate future work should be to replicate the dried dye extraction in agitated state using the originally intended acid extraction of metal ions from olivine. To achieve this task a protocol or mechanism to implement agitation in the future BB payload and the flight model that would be compatible with operation on a C-type NEA Ryugu surface in microgravity need to be developed. the possible approach to implement agitation in the future BB payload

prototype and the flight model is discussed further in chapter 9, the summary and discussion section of chapter 8.

.

9 SUMMARY AND DISCUSSION, CONCLUSIONS, AND FUTURE WORK

9.1 IINTRODUCTION

This chapter concludes the PhD work on the research topic, toward the design and manufacture of a CubeSat relevant mission payloads for demonstrating aspects of In-Situ Resource Utilisation (ISRU) on a C-type Near Earth Asteroid (NEA). Relevant research work carried out are discussed, summarised, the achievement recorded, recommendations and future work are discussed in this chapter.

9.2 SUMMARY AND DISCUSSION

In this PhD research work an initial study to design a 3U CubeSat payload for demonstrating aspects of *In Situ* Resource Utilisation (*ISRU)* to extract metals through hydrometallurgical sulphuric acid leaching of olivine mineral as the simulant present on a C-type NEA has been completed. The research summary and discussion for each chapter of the thesis is presented.

The introduction section (chapter 1) in this project presents/described the research background that dwelled around three core components that constitutes this research work (the concept of In Situ Resource Utilisation (ISRU) technology, destination for demonstration of the ISRU process and the interplanetary CubeSat technology). The research gap was developed that dwelled on the non-existence within the ISRU communities of a miniature ISRU demonstration payload in CubeSat form factor that will use the regolith to extract metal as a de-risking technology. Three research questions were formulated that would address the research gap developed, these research question includes which is the possible Earth-based ISRU techniques, is it possible to scale down the identified possible Earth-based ISRU techniques and what is the suitable location to perform the ISRU experiment on, and what is the potential resource available. The aims and objectives of the project was defined and followed by the step-by-step methodology for realising the defined project objectives.

A literature survey was conducted in chapter 2 to study the three core components introduced in the research background (the concept of ISRU technology, destination for demonstration of the ISRU process and the interplanetary CubeSat technology). A general knowledge of the asteroid was reviewed to give the researcher a better understanding of their position within the solar system and what they are made up in terms of the mineral composition. The C-type NEA family due to their presence <1.3AU within the Sun proximity/vicinity and the availability of abundant resources such as hydrocarbon, volatiles, and metals among others, they were identified as potential flight opportunities/destinations and was selected for further scrutiny. Furthermore, the mineral composition of the asteroid was analysed to establish the relationship between C-type asteroids to the carbonaceous chondrite (CC) meteorite. The C-type asteroids are presumed parent's bodies of the CC meteorite and the commonest meteorite are the CI and CM meteorite. Relevant ISRU processes such as Mars Oxygen ISRU Experiment (MOXIE) tagged the Mars rover 2020 presently in Mars to demonstrate the ISRU process to produce oxygen using the Martian carbon dioxide and Regolith and Environment Science and Oxygen and Lunar Volatile Extraction (RESOLVE) a demonstration of lunar Resource Prospector Mission (LRPM) in a lunar analogue at Hawaii on the slope of Mauna Kea were identified and reviewed to give the researcher an insight into the techniques and operational process of the ISRU technology. A general CubeSat technology was reviewed and the Interplanetary CubeSat missions such as MarCO, COPINS and Bio-sentinel were also reviewed to examine key missions' drivers such as the CubeSat system architecture design, power requirement, the CubeSat form factor and many more.

The result of the literature review has provided knowledge on the current state of the ISRU process, the CubeSat technology, and the destination C-type NEA. This knowledge was used as the basis for developing the project background and subsequently, tailoring the choice of an ISRU process that can be demonstrated on a C-type NEA that will be compatible with the interplanetary CubeSat technology.

Chapter 3 work is about answering the research question that dwelled on determining a suitable location in which to perform an ISRU experiment via CubeSat mission demonstration payload. Earlier in chapter 2, the C-type NEA was selected as the potential destination for the demonstration of the ISRU process that is compatible with the CubeSat technology. A database made up 28 potential C-type NEAs from among which a target destination could be selected was created from a combination of NHATS and the Asterank databases. An initial filtering process was performed over the C-type NEA created database, the number of the C-type NEA was reduced to 5 potential targets including 101955 Bennu, 162173 Ryugu JU3, 2008EV5, 1989ML and 2005YU55. A trade off study was conducted over these potential targets, and C-type NEA 162173 Ryugu JU3 emerged the winner. The result of a sensitivity analysis carried out further confirm the emergence of the C-type NEA Ryugu as the winner.

162173 Ryugu JU3 a C-type NEA emerged as the destination for the demonstration of the ISRU process to extract metal. Since the ISRU payload is in CubeSat size, assumptions were made to say that if the chosen destination were to be the Lunar body such as the Moon, the deep gravitational well present there-in will affect the CubeSat payload operations. The CubeSat would be required to have a massive amount of force to decelerate during entry, descent, and landing. Due to the very shallow gravity well present on the surface of Ryugu, a small amount of force is required to counter the effect of the shallow gravity well on the CubeSat during entry, descent, and landing. In terms of available resources, the asteroids, and the Moon both are focused on regolith resources. Regarding mission opportunities, currently, missions to asteroids are not as popular as those to Moon but with the successful return of the sample return missions by Hayabusa 2 back to earth and the expected return of the recently concluded OSIRIS-REx missions to Bennu in 2023, the composition of the asteroid will be enhanced and validated and will open opportunities for space communities to explore ISRU mission on asteroids. An additional indication that the asteroids might be the next most targeted location soon is the private sectors picking interest in performing the ISRU process on asteroids to mine precious metals.

Chapter 4 answer's the research question that dwelled on selecting the possible Earth-based ISRU techniques that will be compatible working within CubeSat form factor to demonstrate the ISRU process on the identified target location. Seven (7) well established Earth-based ISRU processes were identified as potential processes for considerations and multi criteria analysis techniques was used to achieve the selection process. According to a set of evaluation criteria a trade-off study was conducted to compare the 7 selected ISRU processes to limit the number of options to those with highest score and toward selecting the potential process. Process P7 (the hydrometallurgical Sulphuric acid leaching process on olivine mineral and including electrochemistry) emerged the overall winner with the highest overall weighted score of 71.00 point, followed by process P2 and P3 each with 64.40 and 63.00 point respectively. Further sensitivity check was conducted to validate the ranking order, and three methodologies were applied. The result of the sensitivity check based on method 1&2 was consistent, and the initial winning sequence of P7, P2 and P3 was maintained and the margin across all the winning alternatives is insignificant. The sensitivity check based on the method3; the order of the scoring was observed to conflict with those of method 1&2, the winning sequence was P6, P7 and P4. In the conclusion P7, having emerged as the winner during the trade-off study and has withstood the sensitivity analysis in method 1&2, process P7 was finally selected as the leading alternative to be carried forward for implementation in this research work.

Comparing the favoured process with the other contending ISRU regolith utilization processes (thermal reduction, vapor phase pyrolysis, molten oxide electrolysis, and the sulphuric acid reduction process) only the sulphuric acid reduction process appears to be another suitable process for implementation using the CubeSat payload concept. The other processes due to their higher operating temperatures >800^{0}C and with some of them having system complexity, they are not compatible working within the CubeSat concept. The sulphuric acid reduction process shares the same system complexity as the favoured process, the degree of the sulphuric acid temperature associated with the sulphuric acid reduction process compared to the favoured process is higher. The favoured process stands out to have the least power, energy, and operates

at room temperature with the following corresponding values 2KJ, 1w and 273k as against the sulphuric acid reduction process.

Chapter 5 answer's partly the research question that dwelled on scaling down the Earth-based ISRU techniques into a miniature demonstration payload in the CubeSat form factor. The overall payload system design was described, the overall payload system objectives and constraints are defined, and the payload system top-level requirements were captured and classified into the functional and non-functional requirements. Several assumptions and limitations associated to the CubeSat technology, the location for demonstration of the ISRU process and the ISRU method inform the generation of the top-level system requirement, and the design concept for the ISRU payload system. A combination of the top-level requirement generated in agreement with the proposed CubeSat system architecture form a lead to the overall payload system design that comprises of 5 sub-systems to includes (Sample acquisition sub-system, Reaction chamber sub-system, Liquid handling sub-system, Electro winning sub-system and Analytical sub-system. It is assumed that each of the sub-system takes a 1U CubeSat unit volume.

This research work has been reduced to the design and manufacture of the RCS and the top-plate system, and the design and manufacture of the leaching and liquid handling sub-system. 3U CubeSat volume budget was proposed to accommodate the reduced ISRU payload and in accordance with the CubeSat powers system requirement, a standard 3U CubeSat has a maximum power budget in the range of 7 – 20W. Therefore, a standard 3U CubeSat power consumption shall not be >20W. In the final analysis, the inclusion of the electrochemical BB system (electro-winning and analytical sub-systems) in future work will enable the manufacture of a complete end-to-end BB system that will inform the final flight model.

Chapter 6 was reduced to the design of a laboratory hydrometallurgical leaching experiment that help in determining a combination of parameter sets that will be carried forward for demonstration on the bread-board system and eventually the flight model for the extraction of metal. The outcome of the initial and final

laboratory hydrometallurgical leaching experiments are in agreement, an optimum condition for the sulphuric acid leaching of olivine mineral for extraction of metal from the reaction mixture occurs at 5M H_2SO_4 concentration, 168hrs reaction time, 10rpm mixing speed, and 1:5 mineral to acid volume ratio. In another set of laboratory hydrometallurgical leaching experiment carried out Bromo-Phenol Blue (BPB) dye was introduced in the leaching experiment to eliminate using the litmus paper, detect the loss of acid concentration by providing the real-time visual colour transition from yellow to blue and within the required acid pH range. Despite recording the optimal condition for the leaching experiment achieved in the initial and final experiment, the expected colour transition from yellow to blue using the BPB dye solution could not happen. The BPB dye solution degrades and change from yellow to colourless instead of from yellow to blue colour transition. The result of an investigation to confirm the sources of the degradation of the BPB solution, 5M sulphuric acid concentration was confirmed to be the cause. To mitigate against this looming challenge, in the future work, the use of lower version of the sulphuric acid (2 – 3M) or using an alternative dye indicator that is stable in 5M H_2SO_4 acid is suggested.

Four different laboratory hydrometallurgical leaching experiment was carried out, Experiment 1&2 are based on 1M H_2SO_4 and experiment 3&4 are based on 5M H_2SO_4 and each in agitation and non-agitation state, at room temperature and at leaching duration of 168hours. The overall outcome of the experiments carried out has confirmed that acid concentration, state of agitation and solid-to-liquid ratio, they have significant influence in the leaching reaction process. Using multiple sulphuric acid concentration (1M and 5M) and similar solid-to-liquid ratio was observed to have significant impact in the laboratory hydrometallurgical sulphuric acid leaching of olivine mineral. The experiment using the 1M acid concentration and similar solid-to-liquid ratio was observed to experience loss of acid concentration and mineral swelling, while those experiments using the 5M acid concentration and similar solid-to-liquid ratio are only affected by the mineral swelling and consolidation. The introduction of decreasing solid-to-liquid ratio, the challenges associated with the mineral swelling was observed to decline across all the experiments. The introduction of an agitation system across all the

leaching experiment has eliminated the challenges associated with the mineral consolidation. In the overall, the 5M sulphuric acid concentration has eliminated the challenges associated to acid concentration loss, decreasing solid-to-liquid volume ratio has provided a balance between the amounts of solid material versus the reagent used and thereby eliminated the challenges associated with the mineral swelling. In the same vein the agitation process has improve contact between the leaching reagent, eliminated the mineral consolidation and thereby enhancing the leaching process. Favourable condition/parameters for the leaching process of 5M H_2SO_4 concentration, in state of agitation and 1:5 solid-to-liquid ratio was arrived at. The combination of these parameter set would be used to refine both the payload requirements, payload design, and the payload operations.

Chapter 7 discuss the Breadboard (BB) payload prototype system design, component selection, assembly, testing the mechanical and the liquid handling aspect of the operations was instigated. The critical components of BB payload prototype systems comprise of the Reaction Chamber Sub-systems (RCS), the system top-plate and the Liquid Handling Sub-systems (LHS). The RCS and the top-plate were designed to allow for interfacing with the LHS called the Acid Solution Delivery and Extraction Sub-systems (ASD&ES), while the LHS was designed and built to achieve the liquid acid solution delivery from the acid reservoir into the RCS and the extraction of the liquid acid-metal solution from the RCS to be delivered to the waste container. The payloads hardware's components are partly design using the CAD software (CATIA V5) tool and manufactured using the 3D printer and the CNC machining techniques, other parts were selected and procured from the commercial off the shelf (COTs) components. These payloads hardware components includes: The plunger system and plunger control mechanism (stepper motor with lead screw assembly) that will enable the linear translation of the plunger in/out of the RCS, the reservoir for the liquid storage, the pump to achieve the pumping of the liquid out of the reservoir and into the RCS, the control valve that serve as a switch control to allow/disallow the flow of the pumped liquid from the reservoir into the RCS, the tubing connection that serve as a passage for the liquid, the manifold that direct

the fluid flow into/out of the RCS and the waste container used to receive the extracted solution.

All the hardware components are design to be compatible working with sulphuric acid. A single open-ended RCS was designed to have an estimated internal volume at 12.73ml. The top plate was designed to enable the accommodation of the LHS and other associated system such as the plunger system that will ensure efficient interaction between acid solution and the olivine regolith material inside the RCS. Two inlets access point into the RCS to provide support to the plunger on the top-plate surface were provided, the plunger system provide tubing connection that serve as inlet/outlet for liquid into and out of the RCS and also provide leak free down/up stroke linear translation with the internal bore of the RCS. A groove was provided at bottom head of the plunger to house the O ring material that contact with the internal wall lining of the RCS to provide sealing. Other two mounting position on the top surface of the top-plate were provided; one for the base support that plays the dual role of housing the bearings and providing vertical support to the motorised plunger system and another mounting position for the manifold that connects the valves and pump systems to and from the RCS and finally two clamping positions on the bottom surface of the top-plate are also provided for clamping the RCS. A linear motorised lead screw assembly was designed; ML11 Motorised Lead Screw linear actuator stepper motor operating within 80 – 95N maximum thrust force, was selected to drive the plunger systems vertically up and down through the cylindrical bore of the RCS to enable the acid solution delivery and the metal-acid solution extraction to and from the RCS.

To achieve a leak free and internally pressurised RCS system, sealing materials in contact with RCS wall and at the top and bottom ends of the RCS were used. Fluorocarbon (Viton) elastomer rubber material with excellent chemical resistance to all grade of sulphuric acid and has temperature operating range of -50^0C to 204^0C was selected as the elastomer material to be used as the sealing mechanism. Based on a single RCS volume estimated at 12.73ml the total reservoir volume including 25% safety factor was estimated at ≈ 100ml. A collapsible reservoir having volume 100ml and made from PTFE polymer material

and compatible with all grades sulphuric acid solution was proposed to be used as the sulphuric acid storage system. A single three stage solenoid valve (SV) was proposed to serve the purpose of isolation and connection to the waste container and the reservoir respectively. Constrained by size, mass and cost, a three stage SV compatible with the CubeSat form factor was not feasible and two (2) compact LFN SV manufactured by the Lee components company was selected and procured to replace the three stage SV valve and a Micro Positive displacement pump (PDP) for its ability to trap a fixed volume of fluid and discharging same volume of fluid was selected for implementation. Due to the miniature nature of the fitting ends on the manifold we are constrained to using the standard tubing with two fitting ends readily assembled. 062 Minstac fitting system with the tubing made from PTFE thermoplastic material compatible with all grades of sulphuric acid and manufactured by the Lee Microfluidic Company was selected and procured for implementation in this research work. The manifold made from Polycarbonate thermoplastic material for its compatibility with sulphuric acid and high temperature resistance was selected to provide the inter-connection to the acid reservoir, pump system, solenoid valves, tubing, and fittings with reduced system complexity.

Additional electrical/electronic system was designed to drive the mechanical systems operations of the BB prototype payload system. A transistor switching system was proposed to control the operation of the SV and a MOSFET transistor with IRF640N number for their ease to manufacture and are more widely used than the JFET was selected as a switching transistor for the implementation of the switching control of the SV. A combination of the Arduino Uno and easy driver controller hardware's in conjunction with a written code working together was used to drive the operations of the bipolar stepper motor to achieve the linear translation of the plunger mechanism into and out of the RCS. It is worthy to note that for the BB prototype design implementation, the liquid reservoir was directly connected to the RCS through two tubing connectors separated by a manifold and switched using the reservoir valve control.

Finally, the initial ISRU BB payload system has been successfully produced and assembled and the initial mechanical testing and the liquid handling aspect of the operation were performed. The designed BB payload system for leaching and liquid handling manufactured comprises of (RCS, valves, manifold, tubing, and connectors, motorized leadscrew linear actuators, electrical/electronic system designed to drive the mechanical systems operations of the BB prototype payload system, and the modified top-plates). All these components that made up the RCS, the LHS and the top plate arrangement, they are arranged to occupy 3U equivalent volume of the CubeSat. The overall ISRU BB payload system in addition to designed BB payload prototype and including the remaining sub-system (electroplating/wining subsystem (EP/WS), and analytical subsystem (AS)) to achieve the completion of an end-to-end BB system are expected to fit into the 5U volume of the CubeSat budgeted.

Due to high cost, the micro positive displacement pump proposed for this project design implementation was not included. For the BB payload prototype demonstration, the pumping of the liquid influenced due to gravity. The collapsible reservoir was positioned vertically, once the controlled valve is switch on, due to the influence of gravity the liquid flows. To implement the liquid flow control in microgravity, the collapsible reservoir is compressed upon to force the liquid flow out once the controlled valve is switch open.

Chapter 8, aimed to simulate the demonstration of the hydrometallurgy leaching experiment and the aspect of liquid handling using the designed and manufactured BB payload prototype system in a non-agitated state only. In addition to the simulation demonstration using the BB payload prototype, two other tube-based hydrometallurgy leaching experiment in both agitation and non-agitation states was also simulated. The outcome of the tube-based simulated leaching experiments with those performed using the designed and manufactured BB payload prototype are (1) to established if the earlier tube-based acid reagent extractions performed in chapter 6 could be replicated, (2) to further establish the significance or otherwise of the agitation mechanism in the leaching process.

The successful simulation of the hydrometallurgy leaching experiment using the designed and manufactured BB payload in Chapter_8 is an early indication of the project feasibility. Testing the system in microgravity/vacuum environment to clarify the BB payload system feasibility must be performed. The extraction result pattern of experiment1 and experiment2 they appear to be consistent with one another. The extraction result of experiment3 is significantly higher in terms of (amount of BPB extracted in moles and the extraction efficiency) compared to those of experiment1 and experiment2. Experiment3 using 15mls centrifuge tubes in an agitated state have recorded more BPB solution extraction that translated to higher extraction efficiency. From the pattern of the result, it is evident that the amount of the BPB solution dried onto the olivine regolith, the duration of the extraction process and agitation state impact significantly in the BPB solution extraction process. The amount of the BPB solution dried onto the olivine regolith and the duration of the extraction process applies across all the sets of experiments carried out. The agitation state was only specific to Experiment3 that is tube-based.

Since the BPB dye solution extraction will be carried out in space and using the designed and manufactured BB payload prototype. As it is evident in Experiment3, the agitation state has further influenced the BPB solution extraction. The inclusion of the agitation system in the BB payload system is necessary, it would further enhance the BPB dye solution extraction as was the case in Experiment3. The emerging challenge is that due to the miniature nature of the intended BB payload prototype system (CubeSat based), the implementation of the current agitation system demonstrated in the laboratory on the BB payload prototype using the vertical rotatory mixer is not feasible. The implementation of the laboratory-based agitation mechanism using the vertical rotatory mixer in space is difficult due to absence of gravity, the behaviour of the liquid mixture to achieve the proper mixing cannot be certain

The already existing plunger mechanism present in the BB payload prototype that was successfully tested for the aspect of liquid handling (the supply and extraction of liquid into/out-off the RCS) is the possible solution to use as a

potential means of agitating the leaching process in the microgravity space. One way to achieve the agitation of the leaching process in the microgravity space, over the pre-determined leaching duration, the plunger mechanism is continuously driven up/down the RCS to agitate the reaction mixture as the leaching process progresses. The continuous plunger mechanism up/down stroke inside the RCS have the potential to create some sort of turbulence to agitate the reaction mixture.

The question on what if the fluid boils, the chances of the liquid boiling within the RCS envelop in microgravity is not envisage for the following reasons: When the regolith material from the surface of the C-type NEA is scooped into the RCS and sealed to get the regolith material trapped inside. At the time when the regolith material is trapped inside the RCS, a vacuum of low pressure is created within the internal space of the RCS. As explained by the Gay-Lussac's, that the pressure is directly proportional to its temperature at constant volume. We therefore assume that due to the low pressure inside the RCS internal space the internal temperature is also low. Opening the control valve of the acid reagent reservoir, the liquid acid reagent is injected/pumped the first time into vacuum low-pressure/low-temperature RCS internal space to leach the regolith. Initially the liquid acid reagent boils and then pressurised the inside of the RCS and quickly get stable. With the existence of low pressure and low temperature inside the RCS, In the low-pressure phase the liquid acid reagent would want to boil, and in lower temperature state the liquid acid reagent would want to freeze. Due to the combination of low temperature/low-pressure within the RCS environment the liquid acid reagent state cancels out and quickly stably.

On the question can the setup be radiation-hardened? The simple answer is that the setup cannot be radiation hardened. The expected BB payload prototype mechanical components such as the (RCS, plungers' system etc) and the chemical used in the leaching process, they are not expected to degrade, they are considered low risk and do not require any radiation hardening. All electronics components are susceptible to radiation damage and required to be made resistant to damage through radiation hardening. Therefore, standard techniques

are implemented as design solution toward mitigating the effect of radiation hardening on the electronic components.

9.3 FINAL CONCLUSION

The process of the design and manufacture of a CubeSat relevant mission payloads for demonstrating aspects of In-Situ Resource Utilisation (ISRU) on a C-type Near Earth Asteroid (NEA) has been concluded. A follow up to the description of the project background and the research gap in the ISRU communities, the literature review toward selecting the most compatible target location and the ISRU technique for metal extraction in a CubeSat scenario implementation was conducted. As a result of the trade-off studies carried out, the C-type NEA 162173 Ryugu JU3 and the hydrometallurgical Sulphuric acid leaching experiment on olivine mineral + electrochemistry has emerged the winners and were further validated through a sensitive analysis. A set of requirements are generated and in agreement with the proposed CubeSat system architecture the overall payload system design was achieved. This project has been reduced to the design of the RCS and the system top-plate, and the design of the leaching and the liquid handling sub-system.

The result of the hydrometallurgical sulphuric acid leaching experiments (both initial and repeat) the acid concentration, solid-to-liquid ratio, in the state of agitation were identified as the critical parameters that influences the leaching process the most. 5M H_2SO_4 acid concentration, 1:5 mineral to acid volume ratio and in state of agitation are the optimal condition to achieve higher metal extraction in the leaching process.

The BB payload prototype was designed and manufactured. The assembled BB payload system was mechanically tested, and the liquid handling operation was performed to indicate the usefulness of the process. In the final analysis the BB payload prototype system in a non-agitated state together with two additional leaching experiment using the 15mls plastic centrifuge tubes in both agitation and non-agitation states was simulated. The simulated experiment has established that the earlier tube-based leaching experiment can be replicated and the significant of the agitation mechanism in the leaching process was also

confirmed. Therefore, the use of the plunger mechanism as a potential means through which the reaction mixture in the leaching process get agitated is feasible. The future work would require the inclusion and testing of the plunger mechanism operating as an agitation mechanism in the context of the BB payload prototype.

9.4 FUTURE WORKS

The future work section describes the next steps to take after the completion of the on-going project that will increase the technology readiness level (TRL) of the CubeSat-like ISRU payload. The future work is broken into three components namely, the immediate term future work, medium term future work and the long term (towards payload flight implementation) term future work.

9.4.1 IMMEDIATE TERM FUTURE WORK

This section introduces those aspect of the PhD work that were initially planned, due to time challenged they were not implemented, or they have been improvised. The immediate team future work is a direct lead from the current work.

9.4.1.1 INCLUSION OF AGITATION MECHANISM

In both the sulphuric acid leaching experiment carried out in Chapter_6 and the BPB solution extraction demonstrated in Chapter_8 using the BB payload system, it was obvious significant leaching/BPB solution extraction was recorded in the state of agitation. In the future work the BB payload prototype system shall be designed to include the agitationmechanism or protocol that will agitate the RCS sub-system to achieve the optimal leaching /result.

The implementation of the laboratory-based agitation mechanism using the vertical rotatory mixer in space is difficult due to absence of gravity. Therefore, the existing plunger mechanism present in the BB payload prototype that was successfully tested for the aspect of liquid handling (the supply and extraction of liquid into/out-off the RCS) is considered as the possible solution to use as a means of agitating the leaching process in space. One way to achieve the

agitation of the leaching process in space, over the pre-determined leaching duration, the plunger mechanism is continuously driven up and down the RCS to agitate the reaction mixture by repeatedly pushing the same volume of extraction liquid into the RCS and withdrawing it so that the liquid with flow into and around the regolith and therefore increasing the extraction efficiency.

9.4.1.2 INCLUSION OF HEATING ELEMENT

The flight model is intended to operate in the C-type NEA Ryugu space environment with the varying environmental temperature. The inclusion of the heating element strapped around the RCS will help balance the RCS internal temperature with the environment. The RCS designed and developed by a Ph.D. co-researcher for the extraction of Oxygen from ice water includes a resistive heating element/strap and will be adapted (Sitepu, 2020).

9.4.1.3 INCLUSION OF PARTICLES FILTERS

The liquid passages such as the valves and the connector head implemented in the BB payload system over time will be prone to blockage by the metal particles contained inside the acid-metal solution and during the extraction process. The inclusion of a particle filter in the immediate term future version of the BB payload prototype will limit/eliminate the challenges of the particle residue blocking the filters and the other liquid passages.

9.4.1.4 INCLUSION OF ALTERNATIVE pH INDICATOR DYE MATERIAL THAT WILL BE STABLE IN 5M H_2SO_4 ACID

Using Bromophenol blue (BPB) dye in the leaching experiment to detect the loss of sulphuric acid concentration through the real-time visual colour transition from yellow to blue and within the required acid pH range. The colour degradation of the BPB dye indicator was observed using the 5M Sulphuric acid concentration. To mitigate against this looming challenge, in future work the use of an alternative dye that is stable in 5M H_2SO_4 acid is suggested.

9.4.1.5 INCLUSION OF FORCE FEEDBACK SENSING MECHANISM THAT WILL ESTIMATE THE MASS/VOLUME OF REGOLITH COLLECTED INSIDE THE RCS

The behaviour of the liquid acid and the regolith materials delivered inside the RCS cannot be predicted when the BB payload system is operated in the presence of a microgravity environment. The leaching experiment to be implemented inside the RCS is designed to be implemented in a solid-to-liquid volume ratio of 1:5ml and the corresponding mass of the solid is equivalent to 1.3g. To estimate the mass of the regolith scooped into the RCS, the volume of the space occupied by the regolith is measured using the force feedback sensing mechanism by extending the plunger to compact with the regolith. The plunger distance travel to compact with the regolith is used to estimate the occupied volume inside the RCS and using the regolith material density the equivalent mass of the regolith is estimated. The same mechanism is implemented to ensure that contact between the acid pumped in and the regolith contained inside the RCS has been established for an effective leaching process.

9.4.1.6 INCLUSION OF AN AUTOMATED TRANSISTOR SYSTEM SWITCHING CONTROL AND THE SWITCHING INTERVAL

The switching control of the waste valve and the reservoir valve implemented in the BB payload system was achieved manually using a push button. In the near future implementation, the valve control switching shall be automated.

9.4.1.7 INCLUSION OF PUMPING MECHANISM IN THE FORM OF A SPRING-LOADED FLEXIBLE RESERVOIR

During the BB testing/operation due to the gravity effect liquid inside the reservoir flow with ease once the control valves are switched open. Testing within a microgravity environment and for the fact that the liquid behaviour cannot be predicted. To ensure the liquid flow in microgravity a spring-loaded flexible reservoir to maintain a constant overpressure is required to squeeze the collapsible reservoir and to allow the flow of liquid.

9.4.2 MEDIUM TERM FUTURE WORK

The medium-term future works is next after the immediate term future work, it is the aspect of the future work that need to be demonstrated in the next generation of the development towards the final payload.

9.4.2.1 THERMAL VACUUM TESTING

Most of the ISRU payload system parts and structures are made from a single material (stainless steel). largely, we do not expect a mismatch in the coefficient of thermal expansion of the material. Thermal vacuum testing is required on the payload system and will help in predicting and forecasting the performance of various materials at vacuum environment of the destination asteroid. The thermal vacuum testing chambers provide a clean, temperature-controlled, high vacuum environment for testing high-tech products in space simulated (vacuum) conditions. Thermal vacuum testing has been employed since the beginning of the U.S. space program as a way of mitigating risk and preparing for the extreme temperatures encountered at the orbit.

9.4.2.2 EARTH BASED MICROGRAVITY TEST

This kind of test is carried out inside a near zero-gravity facility to allow the payload system components experience a condition of near weightlessness. The payload system is subjected to free fall using drops towers or parabolic flight; for a drop tower, the drop tube/chamber is evacuated thereby reducing the aerodynamic drag on the free-falling payload to a microgravity value for typically a few single seconds. The drop tower produces 10^{-6}g and under less than 5s, a catapult operation based on the drop tower reaches up to 9s of microgravity time. Parabolic flight facilities produce a low gravity value in the range 10^{-2} g to 10^{-3} g and provides low gravity up to 25s duration. Unlike parabolic flight, the drop tower does not allow human intervention. The parabolic flight with its associated advantage over the drop tower appears to be potentially the most feasible to perform this demonstration.

9.4.2.3 INCLUSION OF THE SULPHURIC ACID REGENERATION SYSTEM

The leaching process will require importing small quantities of sulphuric acid for the initial leaching of the space regolith in situ. After the sulphuric acid has performed its function in the leaching process, it becomes partly neutralized and will contain multiple impurities, such as organics and metals, making it unsuitable for immediate re-use. In the intermediate future work, the inclusion of a sulphuric acid regeneration system that will help in the regeneration of the neutralized sulphuric acid from the metal-acid solution that will be used in the subsequent circle of the leaching process will be considered,

9.4.3 LONG TERM FUTURE WORK (TOWARD PAYLOAD FLIGHT IMPLEMENTATION)

This aspect of the future work is demonstrated once the Immediate-term and medium-term future work have been sufficiently studied and implemented and will result in the inclusion of the final payload in the mission.

9.4.3.1 INCLUSION OF THE DESIGN AND MANUFACTURE OF ELECTROCHEMICAL BB PAYOLAD SYSTEM AND TOWARD ACHIEVING THE FORMATION OF ELEGANT BB SYSTEM

In Chapter_5 the overall proposed payload comprises of 5 sub-systems, this research work implementation has been reduced to the Breadboard (BB) payload prototype design and manufacture for the demonstration of hydrometallurgical acid leaching of regolith and the aspect of the liquid handling process. The long-term future work will entail the development of the electrochemical BB system that includes (electro-winning and analytical sub-systems). These developed BB systems are then assembled into a complete end-to-end BB system called the elegant BB system that will inform the flight model design, manufacture, testing, and validation. Since the direction of ISRU related activities has shown that asteroid mining has become less favoured and Lunar activities have greatly increased, the CubeSat spacecraft ISRU payload design and implementation will focus on the Lunar body application.

REFERENCES

Abdelhalim Z, A. & Abdelhalim, Z. A., 2000. *The bipolar transistors, theory and basic applications.* First edition ed. Cairo (Ain Shams): Faculty of Engineering Ain Shams University.

Ahrens, T. J., 2013. *Global Earth Physic: A handbook of physical constants.* s.l.:American geophysical union.

Ajiboye, A. . E. et al., 2019. Extraction of Copper and Zinc from Waste Printed circuit board. *Recycling,* 27 08.4(3).

Ambo, A. I., 2015. *Chemical investigation of leaching and electrochemical behaviour of sensor-based.* Exeter: Exeter University.

Apogeeweb, n.d. *apogeeweb.net.* [Online]
Available at: https://www.apogeeweb.net/circuitry/irf640n-mosfet-datasheet-equivalent-pinout.html
[Accessed 24 11 2021].

Arrow, n.d. *arrow.com.* [Online]
Available at: https://www.arrow.com/en/research-and-events/articles/relays-vs-transistors-choosing-the-best-tool-for-the-job
[Accessed 17 10 2021].

Badescu, V., 2013. Asteroids Prospective energy and material resources. In: V. Badescu, ed. *Asteroids .* s.l.:springer, p. 689.

Bahill, A. T. & Madni, A. A., 2017. *Tradeoff Decisions in System Design.* 1 ed. s.l.:springer.

Berk p., et al., 2010. Hydrous mineralogy of CM and CI chondrites from infrared spectroscopy and their relationship with low albedo asteroids. *Geochimica et Cosmochimica Acta,* 74(16), pp. 4881-4892.

Bischoff, A. et al., 1993. Paired Renazzo-type (CR) carbonaceous chondrites from the Sahara. *Geochimica et Cosmochimica Acta,* 04, 57(7), pp. 1587-1603.

Braukmüller, N. et al., 2018. The chemical composition of carbonaceous chondrites: Implications for volatile element depletion, complementarity and alteration. *Geochimica et Cosmochimica Acta,* 15 10, Volume 239, pp. 17-48.

Briggs, A., 2021. *www.earthsky.org.* [Online] Available at: https://earthsky.org/space/what-is-the-asteroid-belt/

Browning, L. . B., McSween , H. Y. & Zolensky, M. E., 1996. Correlated alteration effects in CM carbonaceous chondrites. *Geochimica et Cosmochimica Acta,* 07, 60(14), pp. 2621-2633.

Bssa, 2021. *bssa.org.uk.* [Online] Available at: https://bssa.org.uk/bssa_articles/selection-of-stainless-steels-for-handling-sulphuric-acid-h2so4/
[Accessed 13 09 2021].

Carsten, S., Hamilton A, J., Fray J, D. & Crawford A, I., 2012. The production of oxygen and metal from lunar regolith. *Planetary and space science,* 12, 74(1), pp. 49-56.

Chang, C. et al., 2017. Asteroid spin-rate studies using large sky-field surveys. *Geoscience letters,* 06 09.17(4).

Choe, W. et al., 2010. Compositions and taxonomy of 15 unusual carbonaceous chondrites. *Meteoritics and planetary science,* 28 07, 45(4), pp. 531-554.

Clark L, D., Keller W, B. & Kirkland A, J., 2009. *Field Test Result of the PILOT Hydrogen Reduction Reactor..* Pasadena, California, s.n., p. 157.

Clark, B. . E., Binzel, R. P., Cloutis, E. & Howell's, E. . S., 2011. Asteroid (101955) 1999 RQ36: Spectroscopy from 0.4 to 2.4 μm and meteorite analogs. *Icarus,* 12, 216(2), pp. 462-475.

Clark, B. E. et al., 2010. Spectroscopy of B-type asteroids: Subgroups andmeteorite analogs. *Geophysical Research Journals,* 10 06.115(E6).

components101, n.d. *components101.com.* [Online] Available at: https://components101.com/ics/7805-voltage-regulator-ic-pinout-

datasheet
[Accessed 14 11 2021].

Cplabsafety, n.d. *calpaclab.com.* [Online] Available at: https://www.calpaclab.com/teflon-ptfe-compatibility/ [Accessed 09 09 2021].

Curerri, P. et al., 2006. *Process demostration for lunar In Situ Resource Utilisation-Molten magma electrolysis,* s.l.: NASA trs.

DeMeo, F. . E. & Carry, B., 2014. Solar system evolution from compositional mapping of the asteroid belt. *nature,* 24 01, Volume 505, pp. 629-634.

dings, n.d. *motioncontrolproducts.com.* [Online] Available at: https://www.motioncontrolproducts.com/wp-content/uploads/2018/08/Hybrid-stepper-motor-ballscrew-linear-actuator-REV20180129.pdf
[Accessed 10 03 2019].

dingsmotionUSA, n.d. *dingsmotionusa.com.* [Online] Available at: https://dingsmotionusa.com/nema-11-linear-actuators [Accessed 15 03 2019].

Easternseals, n.d. *easternseals.co.uk.* [Online] Available at: https://www.easternseals.co.uk/materials/viton-fkm-fpm-fluorocarbon/#:~:text=Viton%C2%AE%20has%20excellent%20resistance,set%2C%20and%20good%20mechanical%20properties.
[Accessed 11 08 2021].

education, e., n.d. *energyeducation.ca.* [Online] Available at: https://energyeducation.ca/encyclopedia/Standard_conditions_for_temperature_and_pressure
[Accessed 03 10 2020].

Edward, S., 2007. Chondrites and the Protoplanetary Disk: Chondrites and Their Components. *Earth and planetary science,* 30 01, 35(1), p. 577–620.

Elprocus, n.d. *elprocus.com.* [Online] Available at: https://www.elprocus.com/difference-between-bjt-and-fet/#:~:text=The%20acronym%20of%20the%20BJT,stands%20for%20Field%20Effect%20Transistor.&text=The%20major%20difference%20between%20BJT%20and%20FET%20is%20that%20in,and%20minority%20charge%20carriers%20flo
[Accessed 17 08 2021].

Eric, C., Pomeroy R, B., Banks S, I. & Alexis, B., 2007. *Vacuum Pyrolysis and Related ISRU Techniques.* s.l., AIP Publishers.

Eugene, J., 1990. Chemical analyses of meteorites: A compilation of stony and iron meteorite analyses. *Meteoritics and planetary science,* 12, 25(4), pp. 323-337.

Fagan, A. L. & Neal, C. . R., 2016. A new lunar high-Ti basalt type defined from clasts in Apollo 16 breccia 60639. *Geochimica et Cosmochimica Acta,* 15 01, Volume 173, pp. 352-372.

Ferrari, F. et al., 2015. *The Asteroid Impact Mission: Consolidated Mission Analysis and Scientific Payload Operations at Binary Asteroid Didymos.* s.l., s.n.

Fornasier, S., Lazzarin, M., Barbieri, C. & Barucci, M. A., 1999. Spectroscopic comparison of aqueous altered asteroids with CM2 carbonaceous chondrite meteorites. *Astronomy and astrophysics,* 11 02, Volume 135, pp. 65 - 73.

Fujiwara, A., Kawaguchi, A., Yeomans, D. K. & Abe, M., 2006. The Rubble-Pile Asteroid Itokawa as Observed by Hayabusa. *science,* 02 06, 312(5778), pp. 1330-1334.

Glavin, D. P. et al., 2018. The Origin and Evolution of Organic Matter in Carbonaceous Chondrites and Links to Their Parent Bodies. *Primitive Meteorites and Asteroids,* pp. 205-271.

Gotame, R. C., 2020. *www.physicsfeed.com.* [Online] Available at: https://physicsfeed.com/post/moxie-converts-carbon-dioxide-usable-oxygen/

Grier, J. A. & Rivkin , A. S., 2018. Airless bodies of the inner solar system: Understanding the Process Affecting Rocky, Airless Surfaces. In: *Airless bodies of the inner solar system.* s.l.:Lunar and planetary institutes, p. 293.

Gustafson, R., White's, B. C. & Fidler's, M., 2011. *2010 Field Demonstration of the Solar Carbothermal Regolith Reduction Process to Produce Oxygen.* Orlando, Florida, Aerospace research central.

Haihaogroup, 2021. *thepipefitting.com.* [Online] Available at: https://thepipefitting.com/the-difference-between-304-304l-316-316l-steel-materials.html

Heid H, t. et al., 2000. *CubeSat: A new generation of picosatellite for education and industry low-cost space experimentation..* s.l., semantic scholars.

Howard, K. T., Alexander, C. M., Schrader, D. L. & Dyl, K. A., 2015. Classification of hydrous meteorites (CR, CM and C2 ungrouped) by phyllosilicate fraction: PSD-XRD modal mineralogy and planetesimal environments. *Geochimica et Cosmochimica Acta,* 15 01, Volume 149, pp. 206-222.

Irhoma , I. O. & Sansom, C., 2017. CSP assessment in comparison to other electricity generation options using multi-criteria decision analysis (the Libyan case). *IJEIT,* 01.6(7).

Jarosewich, E., 1990. Chemical analyses of meteorites - A compilation of stony and iron meteorite analyses. *Meteoritics,* 25 12, 25(4), pp. 323-337.

John, M., 2006. *Production of Lunar Oxygen Through Vacuum Pyrolysis,* Goerge washington: s.n.

Kambezidis, H. D., 2012. The solar resources. In: A. Sayigh, ed. *Comprehensive Renewable Energy .* s.l.:Elsevier, pp. 27-84.

Keller, H. U. et al., 2010. E-Type Asteroid (2867) Steins as Imaged by OSIRIS on Board Rosetta. *Science,* 08 01, 327(5962), pp. 190-193.

Kronrod, E. V., Kronrod, V. & Nefedyev's, Y. A., 2018. Geochemical constraints for the bulk composition of the Moon. *Geochemistry International,* 12, 483(1), pp. 1475-1479.

L'vov, B. . V., 2000. Mechanism of carbothermal reduction of iron, cobalt, nickel and copper oxides. *Thermochimica Acta,* 28 09, 360(2), pp. 109-120.

Lalvani, S. B. et al., 2004. Reduction of iron oxide in carbon monoxide atmosphere—reaction controlled kinetics. *Fuel Processing Technology,* 15 11, 86(1), pp. 33-47.

leeco, n.d. *theleeco.com.* [Online] Available at: https://www.theleeco.com/resources/download/?gl=PDF.nsf/LookUpPublic/LFNA1250125H?OpenDocument
[Accessed 09 10 2021].

Lefèvre, F. et al., 2008. Heterogenous chemistry in the atmosphere of Mars. *nature,* 21 08, Volume 454, pp. 971-975.

Lewis, B. et al., 2014. *BioSentinel: Monitoring DNA Damage Repair Beyond Low Earth Orbit on a 6U Nanosatellite.* s.l., s.n.

Louis, L., 2016. Working Principle of Arduino and Using it as a Tool for Study and Research. *International Journal of Control, Automation, Communication and Systems (IJCACS),* 04, Volume 1, p. 9.

Lucy, 2018. *lucy.swri.edu.* [Online].

Martins, S., 2017. *www.sciencing.com.* [Online] Available at: https://sciencing.com/distance-affect-solar-radiation-planet-receives-2341.html

McAdam, M. M., Sunshine, J. M., Howard, K. T. & McKoy, T. M., 2015. Aqueous alteration on asteroids: Linking the mineralogy and spectroscopy of CM and CI chondrites. *Icarus,* Volume 245, pp. 320-332.

Merck, n.d. *www.sigmaaldrich.com.* [Online] Available at: https://www.sigmaaldrich.com/GB/en/search/bromophenol-blue-product-datasheet?focus=products&page=1&perPage=30&sort=relevance&term=bromophenol%20blue%20product%20datasheet&type=product [Accessed 24 11 2021].

Michalevsky, Y. & Winetraub, Y., 2017. *SpaceTEE: Secure and Tamper-Proof Computing in Space using CubeSats.* s.l., s.n., pp. 27-32.

Mohapatra, N. C., 2020. The gravitational force of the heavier celestial body is directly proportional to the product of the mass and acceleration of the lighter celestial body. *Global scientific Journal,* 10.8(10).

Moore, P., 2005. Asteroids beyond the main belt. In: *SOLAR SYSTEM | Asteroids, Comets and Space Dust.* s.l.:Elsevier, pp. 220-227.

Nanosatsdatabase, 2022. *www.nanosats.eu.* [Online] Available at: https://www.nanosats.eu/

NASA, 2019. *www.nasa.gov.* [Online] Available at: www.nasa.gov/osiris-rex

NASA, 2021. *www.nasa.gov.* [Online] Available at: https://www.nasa.gov/feature/ames/nasa-s-biosentinel-team-prepares-cubesat-for-deep-space-flight [Accessed 15 06 2021].

NASA, 2021. *www.nasa.gov.* [Online] Available at: https://www.nasa.gov/press-release/nasa-s-perseverance-mars-rover-extracts-first-oxygen-from-red-planet

NASA, n.d. *www.solarsystem.nasa.gov.* [Online] Available at: https://solarsystem.nasa.gov/missions/mars-cube-one/in-depth/# [Accessed 15 05 2020].

Nasajpl, n.d. *www.cneos.jpl.nasa.gov.* [Online] Available at: https://cneos.jpl.nasa.gov/about/neo_groups.html

NEARShoemaker, 1996. *www.nssdc.gsfc.nasa.gov.* [Online] Available at: https://nssdc.gsfc.nasa.gov/planetary/near.html

Nelson , M. . L., Britt , D. T. & Lebofsky, . L. A., 1993. Review of asteroid compositions. *astrophysics data system,* pp. 493 - 522.

newsportng, 2021. *www.newspotng.com.* [Online].

NXP, 1993. *nxp.com.* [Online] Available at: https://www.nxp.com/docs/en/application-note/AN211A.pdf [Accessed 07 11 2021].

okada, T. et al., 2017. Thermal Infrared Imaging Experiments of C-Type Asteroid 162173 Ryugu on Hayabusa2. *space science review,* Volume 208, pp. 255-286.

ORD5700, n.d. *www.parker.com.* [Online] Available at: https://www.parker.com/Literature/O-Ring%20Division%20Literature/ORD%205700.pdf [Accessed 07 03 2019].

Ostrowski, D. . R., Lacy, C., Gietzen's, K. . M. & Sears's, D. W., 2011. IRTF spectra for 17 asteroids from the C and X complexes: A discussion of continuum slopes and their relationships to C chondrites and phyllosilicates. *Icarus,* 04, 212(2), pp. 682-696.

Paz, A. et al., 2013. *RESOLVE OVEN Field Demonstration Unit for Lunar Resource Extraction.* Dallas, Texas, s.n.

pololu, n.d. *www.pololu.com.* [Online] Available at: https://www.pololu.com/product/2982/specs [Accessed 15 11 2021].

rfwireless, n.d. *www.rfwireless-world.com.* [Online] Available at: https://www.rfwireless-world.com/Terminology/BJT-vs-FET.html [Accessed 11 11 2021].

robotpark, n.d. *robotpark.com.* [Online] Available at: http://www.robotpark.com/A4988-Stepper-Motor-Driver [Accessed 09 11 2021].

ROOMSJA, 2016. *www.room.eu.com.* [Online] Available at: https://room.eu.com/search?q=rover+payload

Rosetta, 2021. *www.sci.esa.in.* [Online] Available at: https://sci.esa.int/web/rosetta/-/47389-21-lutetia

Ruzicka, A., Snyder, G. A. & Taylor, L. . A., 2001. Comparative geochemistry of basalts from the moon, earth, HED asteroid, and Mars: implications for the origin of the moon. *Geochimica et Cosmochimica Acta,* 15 03, 65(6), pp. 979-997.

scangrit, 2021. *www.scangrit.co.uk.* [Online] Available at: https://www.scangrit.co.uk/wp-content/uploads/2018/06/Olivine-TDS-2017.pdf
[Accessed 31 12 2021].

Schoolcraft, J., Klesh, . A. & Werne, T., 2016. *MarCO: Interplanetary Mission Development on a CubeSat scale.* Daejeon, Korea , s.n.

Schwandt, C., Hamilton, J. A., Fray, D. . J. & Crawford, I. A., 2012. The production of oxygen and metal from lunar regolith. *Planetary and space science,* 12, 74(1), pp. 49-56.

science, N., 2021. *www.solarsystem.nasa.gov.* [Online] Available at: https://solarsystem.nasa.gov/asteroids-comets-and-meteors/overview/

Shepard, M. K., 2015. *Asteroids: Relics of Ancient Time.* Pennsylvania: Cambridge University Press.

Sibille L, et al., 2010. *Performance testing of molten regolith electrolysis with transfer of molten material for the production of oxygen and metal on the moon.* Orlando, Florida, NASA Technical Reports Server.

Sitepu, E., 2020. *CubeSat compatible payload to demostrate In-Situ Resource Utilisation (ISRU) at Near Earth Asteroid (NEA).* Cranfield(Bedford-Bedfordshire): Cranfield University.

Smith, E. . D., Szidarovszky, F., Karnavas, W. . J. & Bahill, A. T., 2008. Sensitivity Analysis, a Powerful System Validation Technique. *Cybernetics and Systemics,* 2(1), pp. 39-56.

Sparkfun, n.d. *learn.sparkfun.com.* [Online] Available at: https://learn.sparkfun.com/tutorials/easy-driver-hook-up-guide/all [Accessed 09 11 2021].

spiceman, n.d. *spiceman.net.* [Online] Available at: https://spiceman.net/arduino-uno/ [Accessed 24 11 2021].

Taylor A, L. & Carrier D, W., 1993. Oxygen production on the Moon: AN Overview and Evaluation. *Astrophysics data system,* p. 69–108..

Thomson, n.d. *thomsonlinear.com.* [Online] Available at: www.thomsonlinear.com [Accessed 10 03 2019].

Tilman S., D. B. T. J., 2014. *Encyclopedia of the Solar System.* 3 ed. s.l.:Elsevier.

Vračar's, R. . Ž., Vučković's, N. & Kamberović, Ž., 2003. Leaching of copper(I) sulphide by sulphuric acid solution with addition of sodium nitrate. *Hydrometallurgy,* 70(1-3), pp. 143-151.

Wagner, D., Devisme, . O., Patisson, F. & Ablitzer , D., 2006. *A laboratory study of the reduction of Iron oxides by hydrogen.* San Diego, s.n., pp. 111-120.

Weisberg M.K, 2018. Meteorites. *Encyclopedia of Geochemistry.*

Weisberg, M. K., Mckoy, T. K. & Krot, N. T., 2006. Systematics and Evaluation of Meteorite Classification. *Meteorites and the Early Solar System,* pp. 19-52.

Wong, A., 2018. *www.cnbc.com.* [Online] Available at: https://www.cnbc.com/2018/05/15/mining-asteroids-could-be-worth-trillions-of-dollars.html

Yutchi, T., Watanabe, S., Millikin, R. E. & Sujita, S., 2019. *Hayabusa2: Successful touchdown and scientific findings for Ryugu.* Houston, s.n.

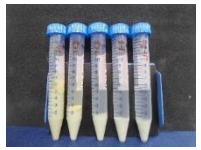
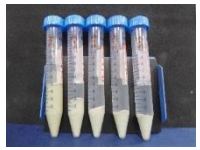
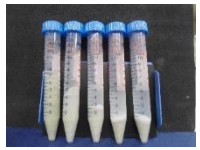
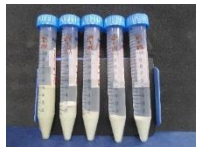
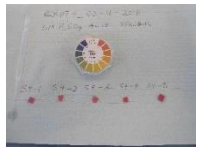
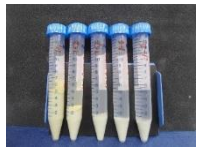
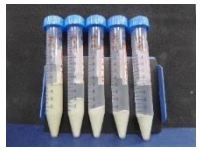
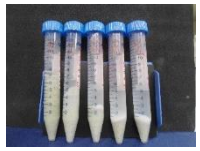
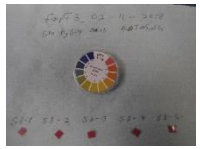
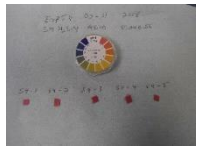
Ziffer, J. E., Licandro, J., Campins's, H. & Walker's , M. E., 2011. Near-infrared spectroscopy of primitive asteroid families. *Icarus,* 06, 213(2), pp. 538-546.

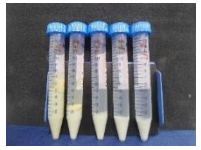
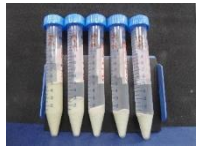
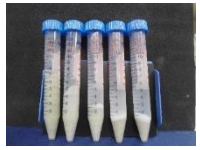
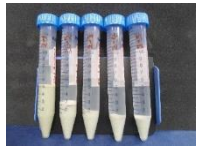
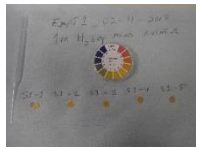
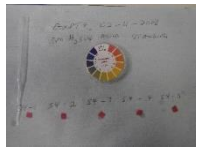
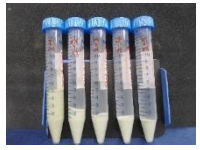
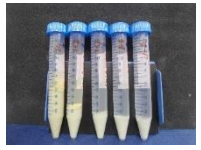
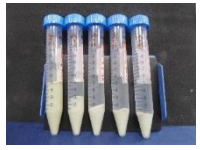
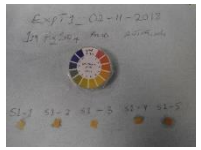
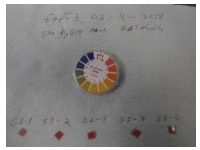
Appendix 1. Representation of Photographic evidence of the sulphuric acid leaching experiment

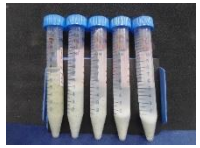
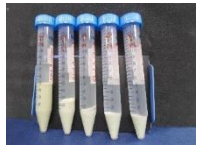
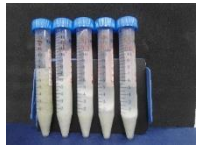
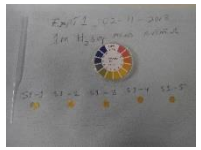
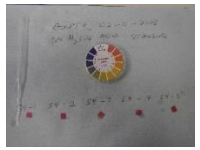
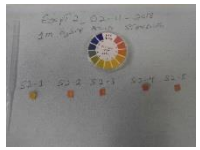
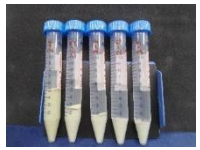
Appendix1.1: Present the complete photographic images captured during the initial leaching experiment.

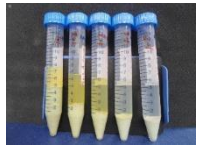
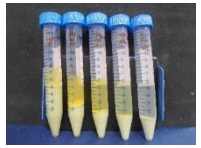
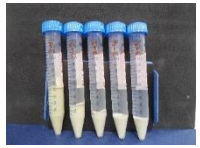
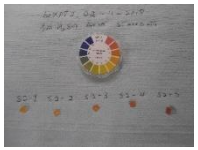
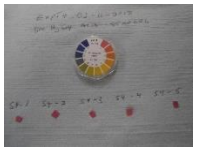
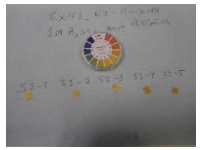
- The initial leaching experiments were performed in four different groups each comprising of five labelled 15mls centrifuge tubes as presented in **Appendix 1.1**
- To each of the centrifuge tubes per experiment, olivine mineral regoliths were dispensed in the decreasing volume ratio of 1-5
- Experiments 1&2 are based on 1M H_2SO_4 and experiments 3&4 are based on 5M H_2SO_4 and each is in agitation and non-agitation state respectively.
- 5ml of 1M and 5ml of 5M H_2SO_4 were dispensed into each of the groups in experiments 1&2 and experiments 3&4 respectively
- The leaching process was allowed to react for a maximum of 168 hours under room temperature.
- The influence of the solid to liquid volume ratio and the acid concentration in the leaching process was monitored; every 12 hours each of the sample mixtures were tested for the loss of the acid concentration using the litmus test paper, and pictures of each sample state are captured for references.
- This process continues until the expiration of the maximum duration of 168hours.
- As presented in **Appendix 1.1**, all the samples in experiment1 at the maximum leaching duration of 168hours the liquid are observed to change from colourless to yellow. This result due to the depletion of the 1M H2SO4 acid. This is not the case with the higher acid concentration of 5M.
- The maximum leaching duration at which the highest acid concentration depletion was recorded informed the choice of 168hours as the maximum leaching duration.

Appendix 1.1: Complete photographic images captured during the initial leaching experiment

							
							
Expt1, t1 = 12hours	Expt2, t1 = 12hours	Expt3, t1 = 12hours	Expt4, t1 = 12hours	Expt1, t2 = 24hours	Expt2, t2= 24hours	Expt3, t2 = 24hours	Expt4, t2 = 24hours
							
							
Expt1, t3= 36hours	Expt2, t3 = 36hours	Expt3, t3 = 36hours	Expt4, t3 = 36hours	Expt1, t4 = 48hours	Expt2, t4 = 48hours	Expt3, t4 = 48hours	Expt4, t4 = 48hours

							
							
Expt1, t5 = 60hours	Expt2, t5 = 60hours	Expt3, t5 = 60hours	Expt4, t5 = 60hours	Expt1, t6 = 72hours	Expt2, t6 = 72hours	Expt3, t6 = 72hours	Expt4, t6 = 72hours
Complete photographic images captured during the initial leaching experiment continue…							
							
							
Expt1, t7 = 84hours	Expt2, t7 = 84hours	Expt3, t7 = 84hours	Expt4, t7 = 84hours	Expt1, t8 = 96hours	Expt2, t8 = 96hours	Expt3, t8= 96hours	Expt4, t8 = 96hours

							
							
Expt1, t9 = 108hours	Expt2, t9 = 108hours	Expt3, t9 = 108hours	Expt4, t10= 108hours	Expt1, t10 = 120hours	Expt2, t10 = 120hours	Expt3, t10 = 120hours	Expt4, t10= 120hours
							
							
Expt1, t11 = 132hours	Expt2, t11= 132hours	Expt3, t11 = 132hours	Expt4, t11= 132hours	Expt1, t12= 144hours	Expt2, t12= 144hours	Expt3, t12 = 144hours	Expt4, t12 = 144hours
Complete photographic images captured during the initial leaching experiment continue…							

							
							
Expt1, t13 = 156hours	Expt2, t13 = 156hours	Expt3, t13 = 156hours	Expt4, t13 = 156hours	Expt1, t14 = 168hours	Expt2, t14 = 168hours	Expt3, t14 = 168hours	Expt4, t14 = 168hours

Appendix1.2: Present the complete photographic images captured during the repeat leaching experiment.

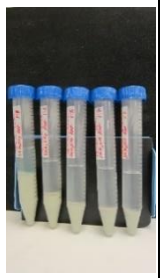
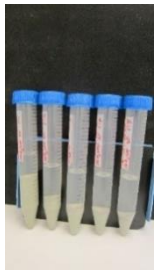
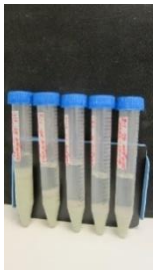
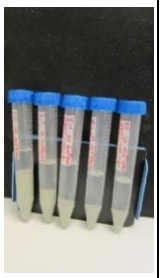
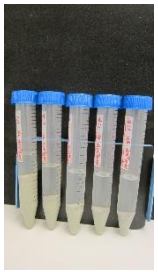
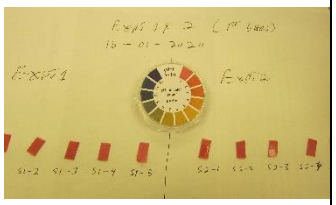
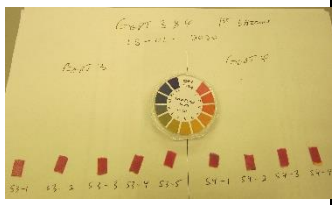
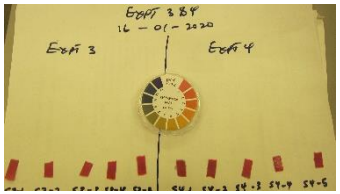
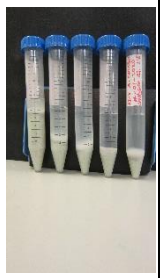
The procedures/methods implemented in the initial sulphuric acid leaching experiment was replicated in the repeat experiments to ensure repeatability and to determine a combination of parameters that will enhance the leaching/metal extraction that will be carried forward for a demonstration on the breadboard system.

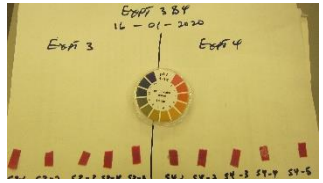
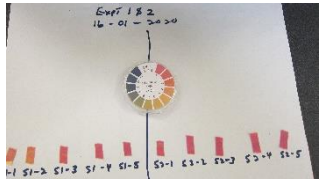
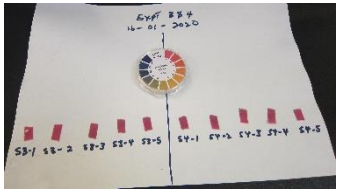
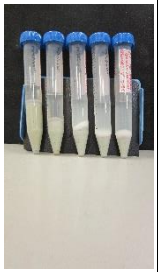
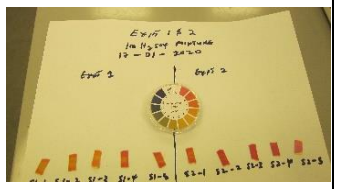
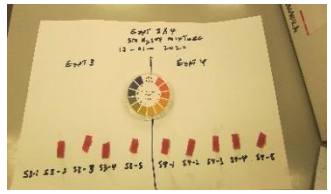
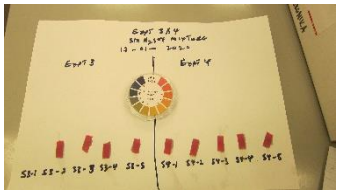
The initial and repeat experiment was performed to optimize and validate the leaching experiment using variables such as 1M and 5M sulphuric acid concentration, solid-to-liquid ratio, in the state of agitation, and non-agitation, for 168hours and at room temperature.

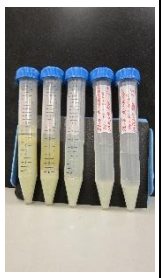
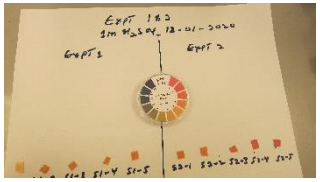
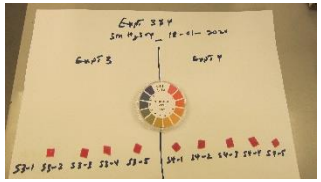
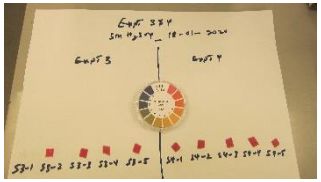
The complete Photographic result presented in both **Appendixes 1.1 & 1.2** are compared to show how the Sulphuric acid concentration and the solid-to-liquid volume ratio in the leaching process influence the effect of (1) loss of acid concentration, (2) mineral swelling, (3) Mineral consolidation and (4) Mineral loss on the metal extraction across the experiments carried out.

The optimal condition to achieve higher metal extraction from the reaction mixture occurs at 5M H_2SO_4 acid concentration, 1:5 mineral to acid volume ratio (1g/5ml), for 168hrs reaction time, and in state agitation speed, and 51% mineral mass loss was achieved.

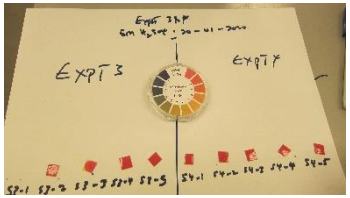
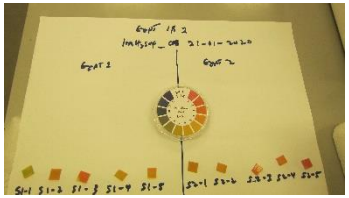
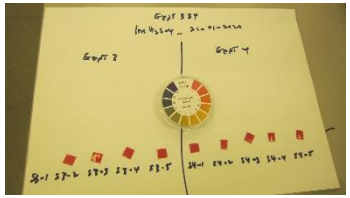
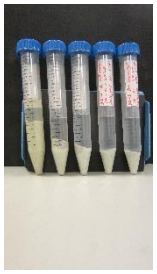
Appendix 1.2: Repeat sulphuric acid leaching experiment of olivine mineral result

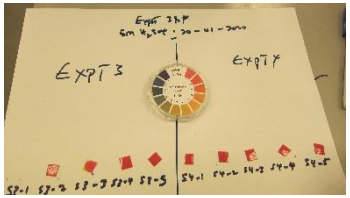
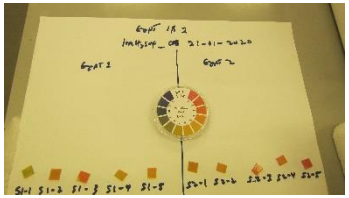
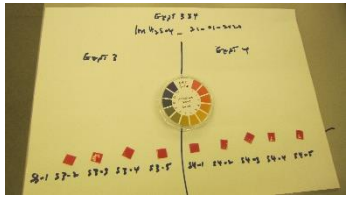
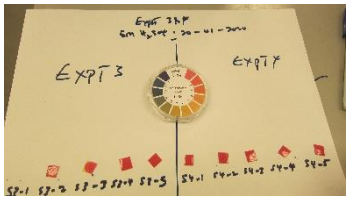
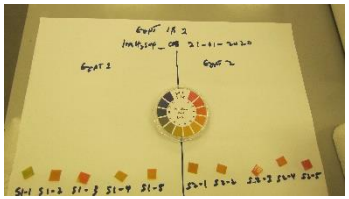
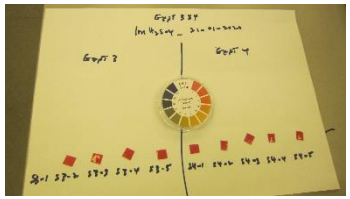
							
							
Expt1, t1 = 12hours	Expt2, t1 = 12hours	Expt3, t1 = 12hours	Expt4, t1 = 12hours	Expt1, t2 = 24hours	Expt2, t2= 24hours	Expt3, t2 = 24hours	Expt4, t2 = 24hours
							

							
Expt1, t3= 36hours	Expt2, t3 = 36hours	Expt3, t3 = 36hours	Expt4, t3 = 36hours	Expt1, t4 = 48hours	Expt2, t4 = 48hours	Expt3, t4 = 48hours	Expt4, t4 = 48hours
Repeat sulphuric acid leaching experiment of olivine mineral result continue…							
							
							

Expt1, t5 = 60hours	Expt2, t5 = 60hours	Expt3, t5 = 60hours	Expt4, t5 = 60hours	Expt1, t6 = 72hours	Expt2, t6 = 72hours	Expt3, t6= 72hours	Expt4, t6 = 72hours
							
							
Expt1, t7 = 84hours	Expt2, t7 = 84hours	Expt3, t7 = 84hours	Expt4, t7= 84hours	Expt1, t8 = 96hours	Expt2, t8= 96hours	Expt3, t8 = 96hours	Expt4, t8= 96hours

Repeat sulphuric acid leaching experiment of olivine mineral result continue…

							
							
Expt1, t9 = 108hours	Expt2, t9= 108hours	Expt3, t9 = 108hours	Expt4, t9 = 108hours	Expt1, t10 = 120hours	Expt2, t10= 120hours	Expt3, t10= 120hours	Expt4, t10 = 120hours
							

							
Expt1, t11 = 132hours	Expt2, t11 = 132hours	Expt3, t11 = 132hours	Expt4, t11 = 132hours	Expt1, t12= 144hours	Expt2, t12= 144hours	Expt3, t12 = 144hours	Expt4, t12 = 144hours
Repeat sulphuric acid leaching experiment of olivine mineral result continue…							
							
							

Expt1, t13= 156hours	Expt2, t13= 156hours	Expt3, t13= 156hours	Expt4, t13= 156hours	Expt1, t14 = 168hours	Expt2, t14= 168hours	Expt3, t14= 168hours	Expt4, t14 = 168hours

Legend

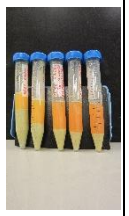
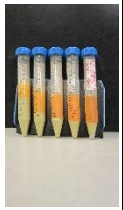
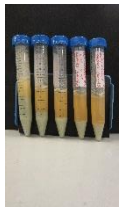
Expt and t represent the experiment number and the experiment duration

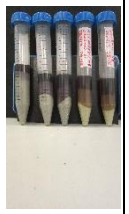
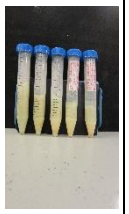
Appendix1.3: Present the complete photographic images captured during the leaching experiment including Bromophenol blue (BPB) dye to eliminate using the litmus paper, detect the loss of acid concentration, and provide the real-time visual colour transition from yellow to blue and within the required acid pH range.

The procedures/methods implemented in the initial and repeat sulphuric acid leaching experiment was replicated in these experiments, except for the introduction of the use of BPB dye solution.

The expected colour change from yellow to blue could not be achieved among the 5M H_2SO_4 acid concentration. The BPB dye solution degrades and changes to colourless. To mitigate against this looming challenge, in future work the use of an alternative dye that is stable in 5M H_2SO_4 acid is suggested.

Appendix 1.3: Complete photographic images captured during the leaching experiment using BPB dye

CBPB 8.8mM				MCBPB 4.4mM				LCBPB 2.2mM			
											
Expt1, t1 = 12hours	Expt2, t1 = 12hours	Expt3, t1 = 12hours	Expt4, t1 = 12hours	Expt1, t1 = 12hours	Expt2, t1= 12hours	Expt3, t1 = 12hours	Expt4, t1 = 12hours	Expt1, t1 = 12hours	Expt2, t1= 12hours	Expt3, t1 = 12hours	Expt4, t1 = 12hours
											
Expt1, t2= 24hours	Expt2, t2= 24hours	Expt3, t2= 24hours	Expt4, t2= 24hours	Expt1, t2 = 24hours	Expt2, t2 = 24hours	Expt3, t2 = 24hours	Expt4, t2 = 24hours	Expt1, t2 = 24hours	Expt2, t2 = 24hours	Expt3, t2 = 24hours	Expt4, t2 = 24hours

											
Expt1, t3 = 36hours	Expt2, t3 = 36hours	Expt3, t3 = 36hours	Expt4, t3 = 36hours	Expt1, t3 = 36hours	Expt2, t3 = 36hours	Expt3, t3 = 36hours	Expt4, t3 = 36hours	Expt1, t3 = 36hours	Expt2, t3 = 36hours	Expt3, t3 = 36hours	Expt4, t3 = 36hours

Legend

Expt and t represent the experiment number and the experiment duration

CBPB represent concentrated bromophenol blue solution at 8.8mM

MBPB represent medium bromophenol blue at 4.4mM

LBPB represent least bromophenol blue at 2.2mM

Appendix 2. Present Iteration to estimate the sizing of the leadscrew by relaxing the CubeSat envelope to increase by 20%

The iteration as presented in **Appendix 2.1** is performed to estimate the sizing of the motorised lead screw assembly together with other attachment that can fit into the CubeSat envelop and be able to perform the desire functions.

Parameters such as the maximum stroke length, length of lead screw nut were considered to arrive at total lead screw length of 74mm excluding the motor length.

ML11 motorised lead screw linear actuator stepper motor with the following specifications was chosen as the motor assembly to use

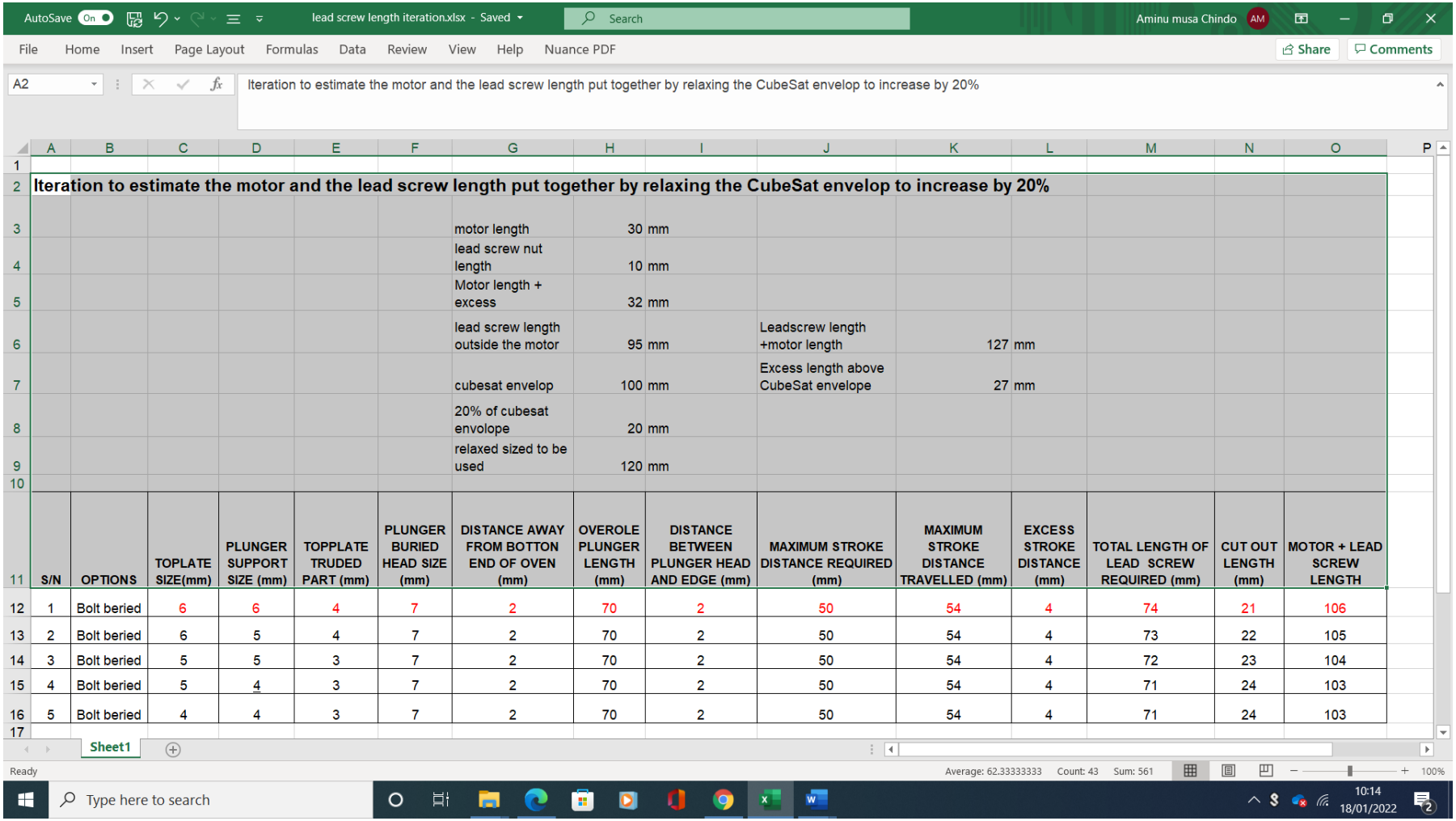
- Linear actuator stepper motor length 32mm
- Lead screw overall length 102mm
- Linear actuator stepper motor maximum thrust 80 – 95N

The initial iteration has shown that the sizing of the linear actuator stepper motor assembly together with other part cannot fit into the CubeSat envelop.

to achieve the design and manufacture of breadboard system to demonstrate the leaching and liquid handling process, the CubeSat envelop was relaxed to increase by 20%.

As presented in **Appendix 2.1**, the iteration with the Motor + lead screw total length of 106mm was arrived at.

Appendix 2.1: Iteration to estimate the motor and leadscrew length put together



AutoSave On | lead screw length iteration.xlsx - Saved | Search | Aminu musa Chindo AM

File Home Insert Page Layout Formulas Data Review View Help Nuance PDF | Share | Comments

A2 | Iteration to estimate the motor and the lead screw length put together by relaxing the CubeSat envelop to increase by 20%

Iteration to estimate the motor and the lead screw length put together by relaxing the CubeSat envelop to increase by 20%

						motor length	30	mm							
						lead screw nut length	10	mm							
						Motor length + excess	32	mm							
						lead screw length outside the motor	95	mm	Leadscrew length +motor length	127	mm				
						cubesat envelop	100	mm	Excess length above CubeSat envelope	27	mm				
						20% of cubesat envolope	20	mm							
						relaxed sized to be used	120	mm							

S/N	OPTIONS	TOPLATE SIZE(mm)	PLUNGER SUPPORT SIZE (mm)	TOPPLATE TRUDED PART (mm)	PLUNGER BURIED HEAD SIZE (mm)	DISTANCE AWAY FROM BOTTON END OF OVEN (mm)	OVEROLE PLUNGER LENGTH (mm)	DISTANCE BETWEEN PLUNGER HEAD AND EDGE (mm)	MAXIMUM STROKE DISTANCE REQUIRED (mm)	MAXIMUM STROKE DISTANCE TRAVELLED (mm)	EXCESS STROKE DISTANCE (mm)	TOTAL LENGTH OF LEAD SCREW REQUIRED (mm)	CUT OUT LENGTH (mm)	MOTOR + LEAD SCREW LENGTH
1	Bolt beried	6	6	4	7	2	70	2	50	54	4	74	21	106
2	Bolt beried	6	5	4	7	2	70	2	50	54	4	73	22	105
3	Bolt beried	5	5	3	7	2	70	2	50	54	4	72	23	104
4	Bolt beried	5	4	3	7	2	70	2	50	54	4	71	24	103
5	Bolt beried	4	4	3	7	2	70	2	50	54	4	71	24	103

Sheet1 | Ready | Average: 62.33333333 Count: 43 Sum: 561 | 100%

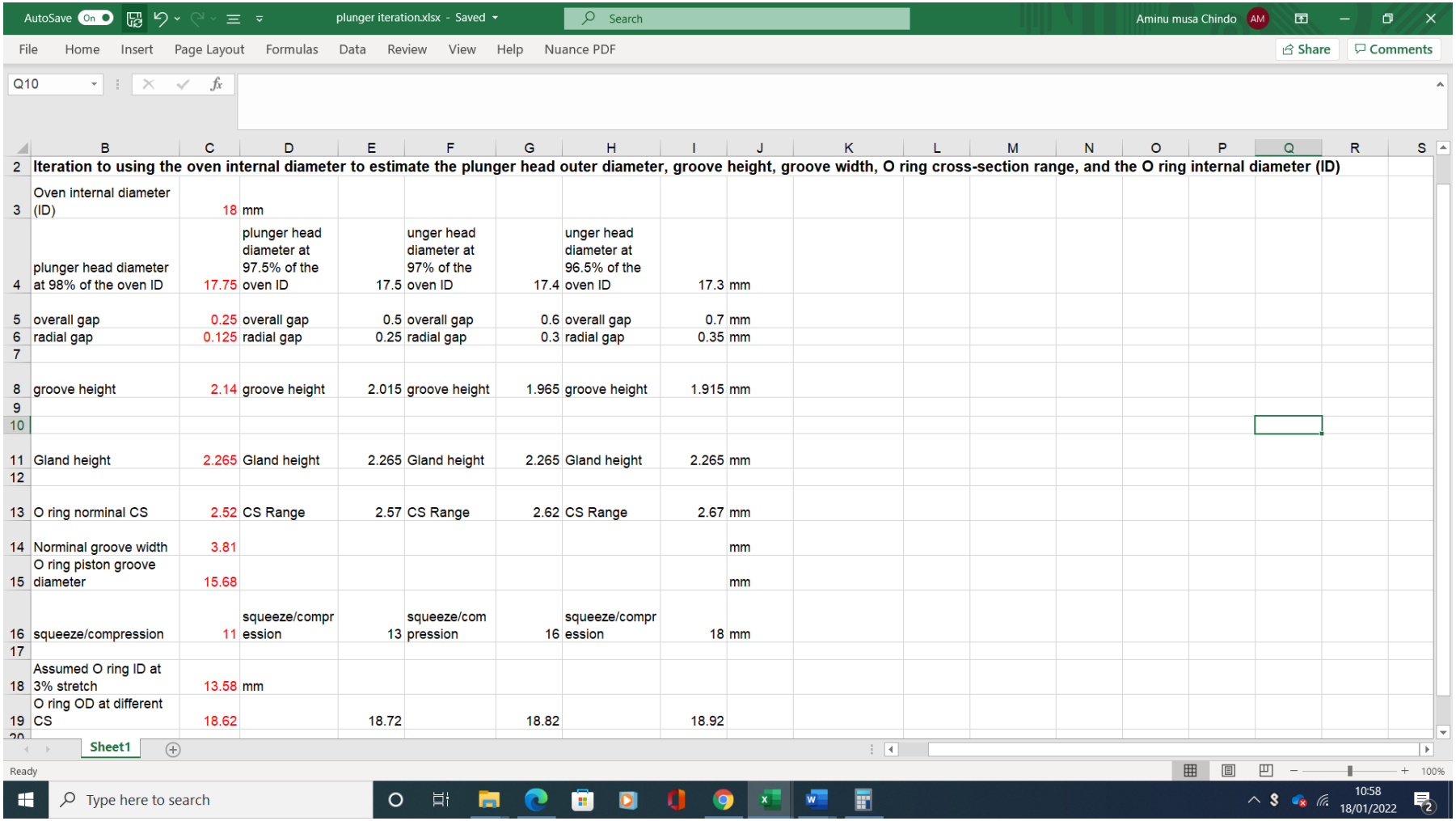
Type here to search | 10:14 18/01/2022

Appendix 3. Represent Iteration to estimate the plunger and the O ring specifications/dimension

Appendix 3.1 Present the iteration to estimate the plunger head outer diameter (OD) based on the RCS internal diameter (ID) of 18mm and the O ring sizing.

- Assuming 98% of the RCS ID, the plunger head diameter was estimated at 17.64mm and the radial gap of 0.18mm was arrived at.
- Getting the right radial gap between the plunger head OD and the RCS ID to ensure a leak-free and smooth sliding of the chosen O ring material
- Based on the 18mm ID of the RCS, an O ring nominal cross-section of 2.52/2.69mm (MIN/MAX) was proposed.
- Using the standard formula 1.5*(O ring CS), the O ring nominal groove width of 3.81/4.04mm was estimated
- assuming 15% (0.15) compression of the O ring material the O ring piston groove diameter was calculated at 15.68mm.
- O ring gland depth was estimated at 2.27mm and the piston groove depth arrive at 2.14mm
- Considering the piston groove diameter, 3% (0.03) stretch of the O ring material was considered, and the O ring internal diameter (ID) and outer diameter (OD) of 13.58mm and 18.62mm was arrived at.
- The top plate thickness was modified to 10mm to accommodate the plunger head with groove of width 3.81mm by a height (depth) 2.14mm.

Appendix 3.1: Iteration to estimate the plunger and the O ring specifications/dimension



plunger iteration.xlsx - Saved

	B	C	D	E	F	G	H	I	J
2	**Iteration to using the oven internal diameter to estimate the plunger head outer diameter, groove height, groove width, O ring cross-section range, and the O ring internal diameter (ID)**								
3	Oven internal diameter (ID)	18	mm						
4	plunger head diameter at 98% of the oven ID	17.75	plunger head diameter at 97.5% of the oven ID	17.5	unger head diameter at 97% of the oven ID	17.4	unger head diameter at 96.5% of the oven ID	17.3	mm
5	overall gap	0.25	overall gap	0.5	overall gap	0.6	overall gap	0.7	mm
6	radial gap	0.125	radial gap	0.25	radial gap	0.3	radial gap	0.35	mm
7									
8	groove height	2.14	groove height	2.015	groove height	1.965	groove height	1.915	mm
9									
10									
11	Gland height	2.265	Gland height	2.265	Gland height	2.265	Gland height	2.265	mm
12									
13	O ring norminal CS	2.52	CS Range	2.57	CS Range	2.62	CS Range	2.67	mm
14	Norminal groove width	3.81							mm
15	O ring piston groove diameter	15.68							mm
16	squeeze/compression	11	squeeze/compression	13	squeeze/compression	16	squeeze/compression	18	mm
17									
18	Assumed O ring ID at 3% stretch	13.58	mm						
19	O ring OD at different CS	18.62		18.72		18.82		18.92	

Appendix 4. Represent the leaching experiment using the BPB dye indictor

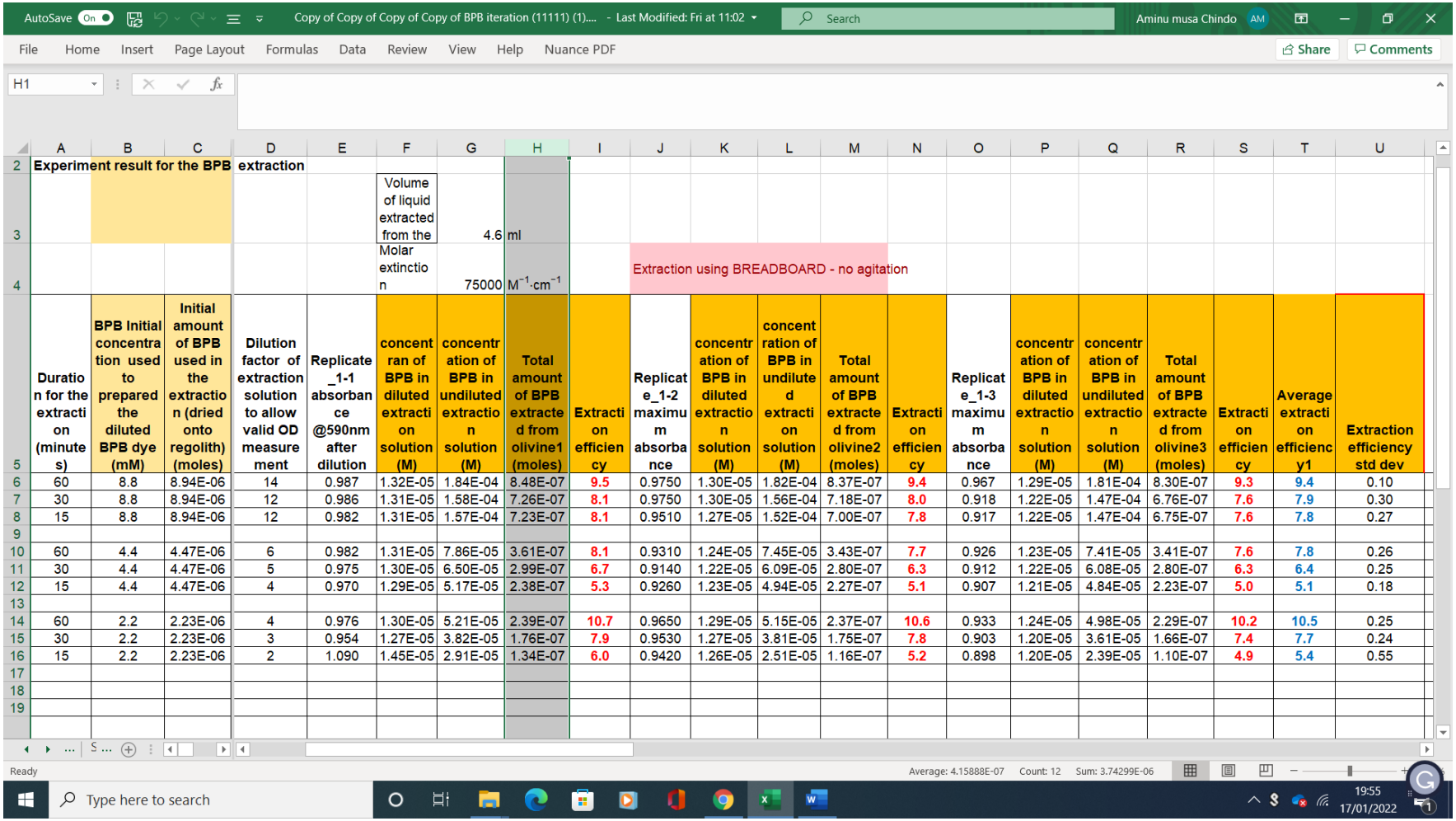
Appendix 4.1 through 4.3 present the extraction result of the leaching experiment using the BPB dye indicator and based on:

- Using the BB payload system in the non-agitated state
- Using the 15mls centrifuge tubes in non-agitated state and
- Using the 15mls centrifuge tubes in agitated state

In the resulting outcome of the BPB solution extraction experiment, it was observed that the variables (the amount of the BPB solution dried onto the olivine regolith and duration of the extraction process) impact the BPB solution extraction across all the sets of experiments carried out.

- The impact appears to be more significant among the samples in experiment3 using the 15mls centrifuge tubes in an agitated state, higher extraction yield was achieved.
- The results of experiement1 using the BB payload prototype and those of Experiment2 using the 15mls centrifuge tubes in a non-agitated state, appear to be similar with slightly in-significant differences.
- The result for experiement3 using 15mls centrifuge tubes in the agitated state with those of Experiment1 and Experiement2 using the BB payload prototype and the 15mls centrifuge tubes in the non-agitated state respectively. A very significant difference was observed in terms of the extraction.

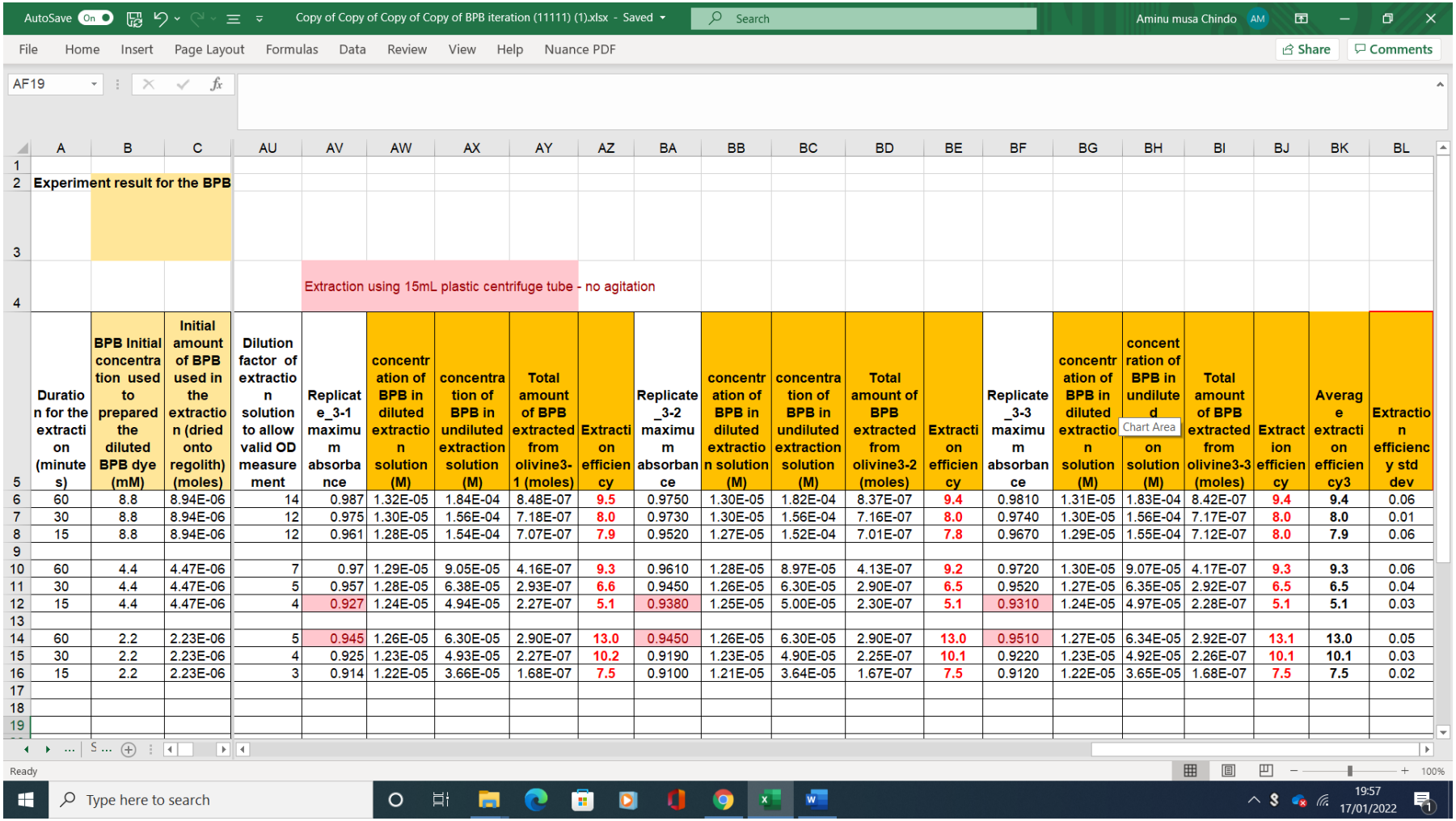
Appendix 4.1: BPB Leaching extraction result using the breadboard in non-agitated state



Experiment result for the BPB extraction

					Volume of liquid extracted from the	4.6	ml													
					Molar extinction	75000	$M^{-1} \cdot cm^{-1}$		Extraction using BREADBOARD - no agitation											
Duration for the extraction (minutes)	BPB Initial concentration used to prepared the diluted BPB dye (mM)	Initial amount of BPB used in the extraction (dried onto regolith) (moles)	Dilution factor of extraction solution to allow valid OD measurement	Replicate_1-1 absorbance @590nm after dilution	concentran of BPB in diluted extraction solution (M)	concentration of BPB in undiluted extraction solution (M)	Total amount of BPB extracted from olivine1 (moles)	Extraction efficiency	Replicate_1-2 maximum absorbance	concentration of BPB in diluted extraction solution (M)	concentration of BPB in undiluted extraction solution (M)	Total amount of BPB extracted from olivine2 (moles)	Extraction efficiency	Replicate_1-3 maximum absorbance	concentration of BPB in diluted extraction solution (M)	concentration of BPB in undiluted extraction solution (M)	Total amount of BPB extracted from olivine3 (moles)	Extraction efficiency	Average extraction efficiency1	Extraction efficiency std dev
60	8.8	8.94E-06	14	0.987	1.32E-05	1.84E-04	8.48E-07	9.5	0.9750	1.30E-05	1.82E-04	8.37E-07	9.4	0.967	1.29E-05	1.81E-04	8.30E-07	9.3	9.4	0.10
30	8.8	8.94E-06	12	0.986	1.31E-05	1.58E-04	7.26E-07	8.1	0.9750	1.30E-05	1.56E-04	7.18E-07	8.0	0.918	1.22E-05	1.47E-04	6.76E-07	7.6	7.9	0.30
15	8.8	8.94E-06	12	0.982	1.31E-05	1.57E-04	7.23E-07	8.1	0.9510	1.27E-05	1.52E-04	7.00E-07	7.8	0.917	1.22E-05	1.47E-04	6.75E-07	7.6	7.8	0.27
60	4.4	4.47E-06	6	0.982	1.31E-05	7.86E-05	3.61E-07	8.1	0.9310	1.24E-05	7.45E-05	3.43E-07	7.7	0.926	1.23E-05	7.41E-05	3.41E-07	7.6	7.8	0.26
30	4.4	4.47E-06	5	0.975	1.30E-05	6.50E-05	2.99E-07	6.7	0.9140	1.22E-05	6.09E-05	2.80E-07	6.3	0.912	1.22E-05	6.08E-05	2.80E-07	6.3	6.4	0.25
15	4.4	4.47E-06	4	0.970	1.29E-05	5.17E-05	2.38E-07	5.3	0.9260	1.23E-05	4.94E-05	2.27E-07	5.1	0.907	1.21E-05	4.84E-05	2.23E-07	5.0	5.1	0.18
60	2.2	2.23E-06	4	0.976	1.30E-05	5.21E-05	2.39E-07	10.7	0.9650	1.29E-05	5.15E-05	2.37E-07	10.6	0.933	1.24E-05	4.98E-05	2.29E-07	10.2	10.5	0.25
30	2.2	2.23E-06	3	0.954	1.27E-05	3.82E-05	1.76E-07	7.9	0.9530	1.27E-05	3.81E-05	1.75E-07	7.8	0.903	1.20E-05	3.61E-05	1.66E-07	7.4	7.7	0.24
15	2.2	2.23E-06	2	1.090	1.45E-05	2.91E-05	1.34E-07	6.0	0.9420	1.26E-05	2.51E-05	1.16E-07	5.2	0.898	1.20E-05	2.39E-05	1.10E-07	4.9	5.4	0.55

Appendix 4.2: BPB Leaching extraction result using the 15mls plastic centrifuge tube in non-agitated state

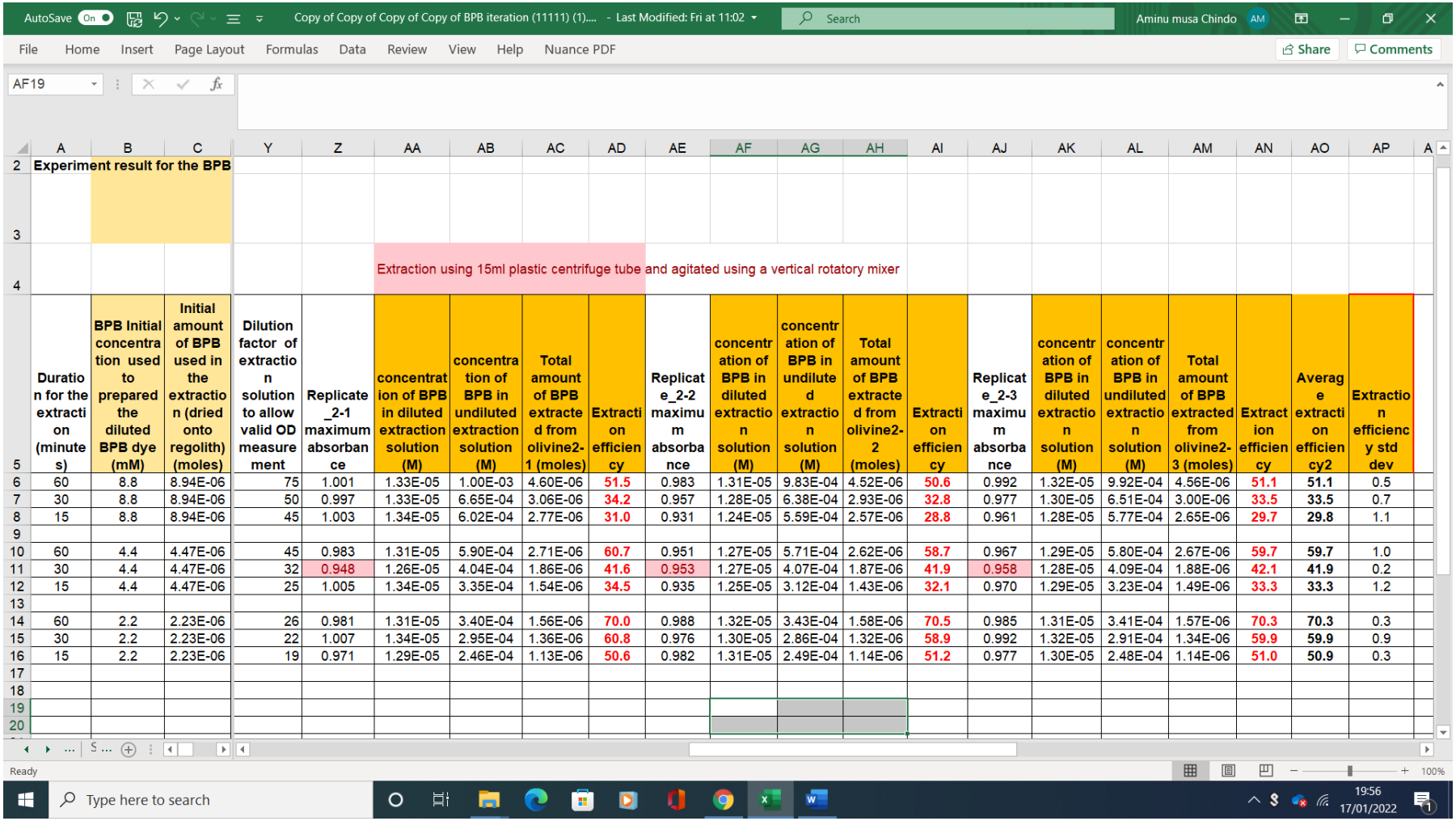


Experiment result for the BPB

Extraction using 15mL plastic centrifuge tube - no agitation

Duration for the extraction (minutes)	BPB Initial concentration used to prepared the diluted BPB dye (mM)	Initial amount of BPB used in the extraction (dried onto regolith) (moles)	Dilution factor of extraction solution to allow valid OD measurement	Replicate_3-1 maximum absorbance	concentration of BPB in diluted extraction solution (M)	concentration of BPB in undiluted extraction solution (M)	Total amount of BPB extracted from olivine3-1 (moles)	Extraction efficiency	Replicate_3-2 maximum absorbance	concentration of BPB in diluted extraction solution (M)	concentration of BPB in undiluted extraction solution (M)	Total amount of BPB extracted from olivine3-2 (moles)	Extraction efficiency	Replicate_3-3 maximum absorbance	concentration of BPB in diluted extraction solution (M)	concentration of BPB in undiluted solution (M)	Total amount of BPB extracted from olivine3-3 (moles)	Extraction efficiency	Average extraction efficiency3	Extraction efficiency std dev
60	8.8	8.94E-06	14	0.987	1.32E-05	1.84E-04	8.48E-07	9.5	0.9750	1.30E-05	1.82E-04	8.37E-07	9.4	0.9810	1.31E-05	1.83E-04	8.42E-07	9.4	9.4	0.06
30	8.8	8.94E-06	12	0.975	1.30E-05	1.56E-04	7.18E-07	8.0	0.9730	1.30E-05	1.56E-04	7.16E-07	8.0	0.9740	1.30E-05	1.56E-04	7.17E-07	8.0	8.0	0.01
15	8.8	8.94E-06	12	0.961	1.28E-05	1.54E-04	7.07E-07	7.9	0.9520	1.27E-05	1.52E-04	7.01E-07	7.8	0.9670	1.29E-05	1.55E-04	7.12E-07	8.0	7.9	0.06
60	4.4	4.47E-06	7	0.97	1.29E-05	9.05E-05	4.16E-07	9.3	0.9610	1.28E-05	8.97E-05	4.13E-07	9.2	0.9720	1.30E-05	9.07E-05	4.17E-07	9.3	9.3	0.06
30	4.4	4.47E-06	5	0.957	1.28E-05	6.38E-05	2.93E-07	6.6	0.9450	1.26E-05	6.30E-05	2.90E-07	6.5	0.9520	1.27E-05	6.35E-05	2.92E-07	6.5	6.5	0.04
15	4.4	4.47E-06	4	0.927	1.24E-05	4.94E-05	2.27E-07	5.1	0.9380	1.25E-05	5.00E-05	2.30E-07	5.1	0.9310	1.24E-05	4.97E-05	2.28E-07	5.1	5.1	0.03
60	2.2	2.23E-06	5	0.945	1.26E-05	6.30E-05	2.90E-07	13.0	0.9450	1.26E-05	6.30E-05	2.90E-07	13.0	0.9510	1.27E-05	6.34E-05	2.92E-07	13.1	13.0	0.05
30	2.2	2.23E-06	4	0.925	1.23E-05	4.93E-05	2.27E-07	10.2	0.9190	1.23E-05	4.90E-05	2.25E-07	10.1	0.9220	1.23E-05	4.92E-05	2.26E-07	10.1	10.1	0.03
15	2.2	2.23E-06	3	0.914	1.22E-05	3.66E-05	1.68E-07	7.5	0.9100	1.21E-05	3.64E-05	1.67E-07	7.5	0.9120	1.22E-05	3.65E-05	1.68E-07	7.5	7.5	0.02

Appendix 4.3: BPB Leaching extraction result using the 15mls centrifuge tube in agitated state



Experiment result for the BPB

Extraction using 15ml plastic centrifuge tube and agitated using a vertical rotatory mixer

Duration for the extraction (minutes)	BPB Initial concentration used to prepared the diluted BPB dye (mM)	Initial amount of BPB used in the extraction (dried onto regolith) (moles)	Dilution factor of extraction solution to allow valid OD measurement	Replicate_2-1 maximum absorbance	concentration of BPB in diluted extraction solution (M)	concentration of BPB in undiluted extraction solution (M)	Total amount of BPB extracted from olivine2-1 (moles)	Extraction efficiency	Replicate_2-2 maximum absorbance	concentration of BPB in diluted extraction solution (M)	concentration of BPB in undiluted extraction solution (M)	Total amount of BPB extracted from olivine2-2 (moles)	Extraction efficiency	Replicate_2-3 maximum absorbance	concentration of BPB in diluted extraction solution (M)	concentration of BPB in undiluted extraction solution (M)	Total amount of BPB extracted from olivine2-3 (moles)	Extraction efficiency	Average extraction efficiency2	Extraction efficiency std dev
60	8.8	8.94E-06	75	1.001	1.33E-05	1.00E-03	4.60E-06	51.5	0.983	1.31E-05	9.83E-04	4.52E-06	50.6	0.992	1.32E-05	9.92E-04	4.56E-06	51.1	51.1	0.5
30	8.8	8.94E-06	50	0.997	1.33E-05	6.65E-04	3.06E-06	34.2	0.957	1.28E-05	6.38E-04	2.93E-06	32.8	0.977	1.30E-05	6.51E-04	3.00E-06	33.5	33.5	0.7
15	8.8	8.94E-06	45	1.003	1.34E-05	6.02E-04	2.77E-06	31.0	0.931	1.24E-05	5.59E-04	2.57E-06	28.8	0.961	1.28E-05	5.77E-04	2.65E-06	29.7	29.8	1.1
60	4.4	4.47E-06	45	0.983	1.31E-05	5.90E-04	2.71E-06	60.7	0.951	1.27E-05	5.71E-04	2.62E-06	58.7	0.967	1.29E-05	5.80E-04	2.67E-06	59.7	59.7	1.0
30	4.4	4.47E-06	32	0.948	1.26E-05	4.04E-04	1.86E-06	41.6	0.953	1.27E-05	4.07E-04	1.87E-06	41.9	0.958	1.28E-05	4.09E-04	1.88E-06	42.1	41.9	0.2
15	4.4	4.47E-06	25	1.005	1.34E-05	3.35E-04	1.54E-06	34.5	0.935	1.25E-05	3.12E-04	1.43E-06	32.1	0.970	1.29E-05	3.23E-04	1.49E-06	33.3	33.3	1.2
60	2.2	2.23E-06	26	0.981	1.31E-05	3.40E-04	1.56E-06	70.0	0.988	1.32E-05	3.43E-04	1.58E-06	70.5	0.985	1.31E-05	3.41E-04	1.57E-06	70.3	70.3	0.3
30	2.2	2.23E-06	22	1.007	1.34E-05	2.95E-04	1.36E-06	60.8	0.976	1.30E-05	2.86E-04	1.32E-06	58.9	0.992	1.32E-05	2.91E-04	1.34E-06	59.9	59.9	0.9
15	2.2	2.23E-06	19	0.971	1.29E-05	2.46E-04	1.13E-06	50.6	0.982	1.31E-05	2.49E-04	1.14E-06	51.2	0.977	1.30E-05	2.48E-04	1.14E-06	51.0	50.9	0.3